DAC 62389

DEVELOPMENT OF A SYSTEM FOR BIAXIAL PRESTRESSING BRITTLE MATERIALS

SEPTEMBER 1968

Prepared under Contract No. NAS8-21083
for
National Aeronautics and Space Administration
Marshall Space Flight Center
Huntsville, Alabama

DAC 62389

DEVELOPMENT OF A SYSTEM FOR BIAXIAL PRESTRESSING BRITTLE MATERIALS

SEPTEMBER 1968

By

L. B. GRESZCZUK, R.J. MILLER AND W.C. NETTER
McDonnell Douglas Astronautics Company-Western Division
Santa Monica, California

Prepared under Contract No. NAS8-21083
for
National Aeronautics and Space Administration
Marshall Space Flight Center
Huntsville, Alabama

PREFACE

This Final Report was prepared by the McDonnell Douglas Astronautics Company - Western Division (MDAC-WD), Santa Monica, California, under Contract No. NAS 8-21083, entitled "Development of a System for Biaxial Prestressing Brittle Materials." The program is being monitored by National Aeronautics and Space Administration, Marshall Space Flight Center, V. F. Seitzinger, Project Engineer. The program was under the technical management of Mr. L. B. Greszczuk--Project Director. The personnel participating in this program were Messrs. R. J. Miller, W. C. Netter, D. D. Losee, T. T. Sakurai, C. T. Powers, V. L. Freeman, and H. Leggett who has advised on various aspects of material development.

ABSTRACT

Experimental and theoretical studies were performed on strengthening of ceramics with discontinuous fibers. Strengthening of chemically consolidated zirconia with discontinuous tungsten fibers, graphite (Thornel 40) fibers, and sapphire as well as silicon carbide whiskers, was investigated experimentally. Addition of SiC whiskers gave highest increase in strength of zirconia at room and elevated temperatures. A 7.4-weight-percent of SiC whiskers increased the room-temperature average flexure strength of ZrO_2 from 4,000 psi to 5,700 psi, at 2,000°F, the strength increased from 165 psi to 1,600 psi. The SiC-whisker-strengthened matrix was characterized for mechanical and physical properties at room and elevated temperatures. Analytical tradeoff studies were performed on strength of prestressed, whisker-strengthened zirconia. Flexure and tensile specimens, uniaxially prestressed with tungsten cables, were fabricated and tested at room and elevated temperatures. The response of uniaxially prestressed ceramic to thermal shock and thermal cycling was also evaluated and compared to non-prestressed matrix. A theory has been developed for predicting the stresses in biaxially prestressed cylindrical structures subjected to external loading and thermal environment. Equations and an analytical approach for estimating the strength of such structures were developed. Biaxially prestressed cylinders were then designed, fabricated, and tested. Four types of tests were performed on cylindrical specimens: (1) hoop tensile tests at room temperature (1:0 stress ratio); (2) biaxial tensile tests at room temperature (1:2 stress ratio); hoop tensile tests at 2000°F (1:0 stress ratio); high-velocity ballistic impact tests. The strengths of biaxially prestressed cylinders tested in hoop tension and biaxial tension at room temperature, and in hoop tension at elevated temperature, were 9,350 psi, 10,970 psi and 4,740 psi, respectively. The test data on uniaxially and biaxially prestressed specimens were evaluated and correlated with theory.

CONTENTS

FIGURES

TABLES

Section 1
INTRODUCTION

The properties that make ceramics desirable as structural materials for elevated temperature applications are their high melting points, high compressive strengths, good strength retention at high temperatures, and excellent resistance to oxidation. The undesirable properties of ceramics for anticipated high-temperature aerospace application, such as nose tips, leading edges, body surfaces, nozzle components, heat shields, and permanent external thermal protective coatings for spacecraft and manned re-entry vehicles, are their low tensile strengths and poor resistance to impact, vibration, and thermal shock. If ceramics are to be utilized in the above-cited applications, their undesirable properties must be overcome or circumvented, and advantage must be taken of their desirable characteristics. It is the need to overcome these major weaknesses that has led to research on strengthening of ceramics by means of metal fibers, whiskers, and mechanical and thermal prestressing.

Experimental and theoretical studies on uniaxial prestressing of ceramics with high-strength wires have been conducted at McDonnell Douglas Astronautics Company - Western Division (MDAC-WD) under contract NAS 7-429 (Reference 1-1). During this initial effort, analytical methods were developed for predicting the behavior of prestressed ceramics, and an experimental procedure was developed for inducing uniaxial prestress. In essence, the concept consisted of internally prestressing, in compression, a ceramic matrix with continuous wires, while processing at low temperatures. The ceramic matrix was chemically consolidated at from 400°F to 600°F, thus eliminating the degradation of metal reinforcing usually associated with the high processing temperatures of conventional ceramics. The ceramic slurry was cast around pretensioned filaments and

cured in place. After the ceramic was cured and removed from the mold, release of the pretensioned filaments induced a compressive stress in the ceramic. This increased the tensile load-carrying ability of the ceramic, since to fail the ceramic in tension, the induced compressive forces had to be overcome first.

In the present effort additional strengthening of the ceramic was achieved through addition of SiC whiskers to the ceramic, and prestressing the resultant matrix with continuous filaments. Moreover, methods were developed for biaxial prestressing of complex configurations, such as cylinders. Prior to fabricating biaxially prestressed cylinders, analytical studies were conducted on the factors governing the induced prestress as well as on the strength of resultant configurations. An extensive test program was conducted on the properties of non-prestressed, SiC-whisker-strengthened ZrO_2 and on uniaxially prestressed, SiC-whisker-strengthened ZrO_2. Data were obtained on flexure and tensile strengths at room and elevated temperatures, as well as on thermal expansion, thermal shock, and thermal cycling. The biaxially prestressed cylindrical specimens were tested in hoop and biaxial tension at room temperature, in hoop tension at 2,000°F, and under high-velocity ballistic-impact loading.

The program was divided into two phases to provide continuity of material development and evaluation, analytical studies, and biaxial prestressing.

1.1 PHASE I - MATERIAL STRENGTHENING

A literature survey was conducted on strengthening of the ceramic matrix through addition of whiskers and short, discontinuous fibers. During this survey, pertinent information was also gathered on the properties of candidate reinforcing materials. The matrix selected for experimental work was chemically consolidated zirconia. Strengthening of ZrO_2 with graphite (Thornel) fibers, tungsten fibers, silicon carbide fibers, and sapphire whiskers was then investigated. The optimum fiber-strengthened matrix was then characterized at ambient and elevated temperatures to obtain mechanical properties such as flexure, shear and tensile strengths, and Young's modulus. In addition, thermal expansion, apparent porosity,

apparent specific gravity, bulk density, and true density were determined. Analytical tradeoff studies were then conducted on uniaxially prestressed, whisker-strengthened ZrO_2. Prestressed specimens were then designed, fabricated, and tested at room and elevated temperatures. In addition to obtaining flexure and tensile strength data, the response of prestressed specimens to thermal shock and thermal cycling was also investigated.

1.2 PHASE II - BIAXIAL PRESTRESSING

A continuous survey of available literature was conducted for the duration of the program relative to the current technology on methods of prestressing ceramic materials. Mechanical and thermal methods of inducing biaxial prestress in ceramic cylindrical configurations were investigated. The methods which were considered included shrink-fitting of metal bands onto ceramic cylinders, circumferential and axial prestressing of cylinders, and helical winding of cylinders with filaments under high tension. The last technique was chosen as a means of inducing biaxial prestress in cylindrical specimens. In addition, analysis methods for predicting the prestress in, and the strength of, biaxially prestressed cylinders were developed. Employing the results of Phase I and the analysis developed in Phase II, tradeoff studies on factors affecting the strength of cylinders were conducted. Biaxially prestressed cylinders were then designed, fabricated, and tested in uniaxial hoop tension and biaxial tension. The uniaxial hoop strength was obtained at room and elevated temperatures. The experimental data on the biaxially prestressed cylinders were compared with the theoretically predicted results. In addition to the above tests, high-velocity ballistic-impact tests were also performed.

1.3 REFERENCES FOR SECTION 1

1-1. L. B. Greszczuk, and H. Leggett. Development of a System for Prestressing Brittle Material. Douglas Aircraft Company, Missile and Space Systems Division, Santa Monica, California, Final Report, prepared under contract No. NAS 7-429, August 1967.

Section 2
GENERAL CONSIDERATIONS OF FIBER-STRENGTHENED CERAMICS

2.1 LITERATURE SURVEY ON FIBER-REINFORCED CERAMICS

Numerous filaments and whiskers exist which can be used to increase the strength of ceramics. To establish the best manner of strengthening the ceramics with whiskers and fibers, a literature survey has been conducted on the most recent work performed in this area. The results of this survey were used in the selection of several candidate reinforcing materials for strengthening the chemically consolidated zirconia. The calcia-stabilized zirconia was phosphate-bonded, and cured at a temperature of 600°F. Prior to performing any experimental work on fiber-strengthened zirconia, analytical studies were performed on the required properties of the fibers to produce crack-free ceramics, on the effect of porosity on the strength of fiber-strengthened ceramics, and on the effect of fiber alignment on the strength of fiber-ceramic composites.

Five factors must be considered when choosing filamentary materials for strengthening brittle matrixes:

1. Modulus of elasticity.
2. Relationship between the coefficients of thermal expansion of the constituents.
3. Fiber aspect ratio.
4. Bonding between fibers and matrix.
5. Maximum temperature at which the fibers can be utilized.

In order for the fibers to carry a significant load, their modulus of elasticity must be higher than that of the matrix. Harmon (Reference 2-1) has found that high-strength filament material must have a modulus of elasticity at least twice that of the matrix.

Harris, et al. (Reference 2-2) state that an inorganic, fiber-reinforced matrix will not be as brittle as an unreinforced matrix because the fibrous form of a ceramic material is more resilient than the bulk material. Furthermore, the phosphate matrix has more plastic behavior than is normally encountered in ceramic materials (Reference 2-3). For the ceramics which require high-temperature processing, the coefficient of thermal expansion of the matrix must be equal to or lower than, that of the fiber. This criterion is an important consideration during cooling of the composite. If the coefficient of thermal expansion of the ceramic is greater than that of the fiber, cracking of the ceramic may take place upon cooling of the composite.

The aspect ratio (length of the fiber divided by the fiber diameter) for an inorganic composite should be greater than 10:1 (Reference 2-1). This ratio is required to be large enough to minimize the shear stresses between the fiber and the matrix at the ends of the fiber, and to develop the load-carrying ability of the fiber (Reference 2-4).

Transfer of stress from matrix to fiber can occur only if there is a bond between the two components. Harris, et al. (Reference 2-5) state that a poor fiber-matrix bond results in low shear resistance. Heating of ceramic composite materials develops shear stresses that can cause failure of the fiber-matrix bond. Efforts to obtain chemical bonds may be limited by reactions that destroy the fibrous structure. Ebner (Reference 2-6) found that silicon carbide and graphite were more resistant to attack by fluorine and hydrogen fluoride at high temperatures than other refractories, such as alumina or zirconia. The majority of the applications for ceramics as load-bearing elements of systems will require oxidation resistance. Woodburn and Lynch (Reference 2-7) have demonstrated that phosphates provide oxidation resistance to carbon-containing materials. Hence, filamentary materials made of silicon carbide or graphite should not be limited by reactions with the matrix, but there is the possibility that alumina fibers may be adversely affected by the matrix.

Fibrous materials are available in polycrystalline form, referred to as fibers, and as single crystals, referred to as whiskers. The greater strength of the whiskers versus that of fibers is because of the absence of grain boundaries, dislocations, impurities, imperfections, and voids (Reference 2-8).

The literature on inorganic composites reinforced with fibers is limited, and the majority of the work is on metal matrices. This literature survey only considered studies utilizing ceramic matrixes.

R. Singleton, D. Miller, and A. Wallace (Reference 2-9) reinforced mullite ($2\ SiO_2 \cdot 3\ Al_2O_3$) with 20-volume-percent tungsten or molybdenum wire. The wire was 50 microns in diamter, cut into 1,500-micron lengths, thus giving a length-to-diameter ratio (ℓ/d) of 30. The coefficient of thermal expansion from room temperature to 1,832°F for tungsten, molybdenum, and mullite were 2.55, 3.33 and 2.89 x 10^{-6} in./in. per °F, respectively. The composite mixture was hot-pressed in vacuum to 98 percent of the theoretical density. The mullite was formed from silica and alumina. At room temperature, the average flexure strength for unreinforced mullite was 12,000 psi, for a molybdenum-mullite system 22,700 psi, and for a tungsten-mullite system 23,400 psi.

Harris, Sales, and Corbett (Reference 2-10) found that the addition of silicon carbide whiskers to the silica matrix of a filament-wound inorganic composite did not provide an increase in tensile strength; however, they found that the shear strength increased 122 percent.

Results of bending tests performed by Bortz (Reference 2-11) on a ceramic composite fabricated with 20-volume-percent molybdenum wire and 80-volume-percent petalite ($Li_2O \cdot A\ell_2O_3 \cdot 8SiO_2$) revealed that the composite was 50 percent stronger than the unreinforced petalite body. The ceramic had a coefficient of thermal expansion of 0.11 x 10^{-6} in./in.°F. The modulus of elasticity of the ceramic was 18 x 10^6 psi, while that of metal was 46 x 10^6 psi. The petalite body was 90-weight-percent petalite and 10-weight-percent kaolin. The petalite was ball milled with the kaolin, 2-mil-diameter

by 1/8-inch-long molybdenum wires were added to the batch in the ball mill, following which milling was continued. The mixture was hot pressed at 2,408°F and at 3,000 psi. The results of the flexure test are given in Figure 2-1, where it may be noted that the area under the stress-strain curve for the reinforced body was 400 percent greater than the unreinforced body.

Tinklepaugh, Goss, and Hoskyns (Reference 2-12) studied the flexural properties of electrical porcelain-tungsten fiber systems. The body was hot pressed at a temperature of 2,360°F. The thermal expansion of the ceramic was up to 30 percent greater than that of tungsten at temperatures above 600°F. The ceramic failed at the same load whether it was reinforced or not, but the fibers held the composite together as the load was increased. The ultimate load at which the composite failed was much higher than the load required to cause failures of the ceramic. Failure of the composite occurred when the fibers pulled out. One composite containing 20-volume-percent chopped tungsten fibers failed at a flexure stress of 28,460 psi; one without reinforcement failed at a flexure stress of 4,780 psi. The tungsten wires were 0.002-inch diameter by 0.125-inch long. Some additional experimental results obtained from Reference 2-12 are shown in Figure 2-2, where the flexure strength of tungsten-fiber-reinforced ceramic is plotted as a function of fiber-volume fraction.

In conjunction with the work on fiber-reinforced ceramics, mention should also be made of the experimental work of Fisher and Hodson (Reference 2-13). Their work involved making tungsten-fiber-reinforced SiC, TaC, B_4C, TiC, HfC and ZrC. These composites were intended for nozzle applications, and were produced by hot pressing. Of the six carbides listed above, SiC, TaC and B_4C were found to react extensively with the metal phase and, therefore, were eliminated as candidate materials for nozzles. The remaining three carbides were found to form a good metallurgical bond with the tungsten fibers. It was found that although the fibers react with the ceramics, detrimental interactions could be avoided by controlling the processing conditions.

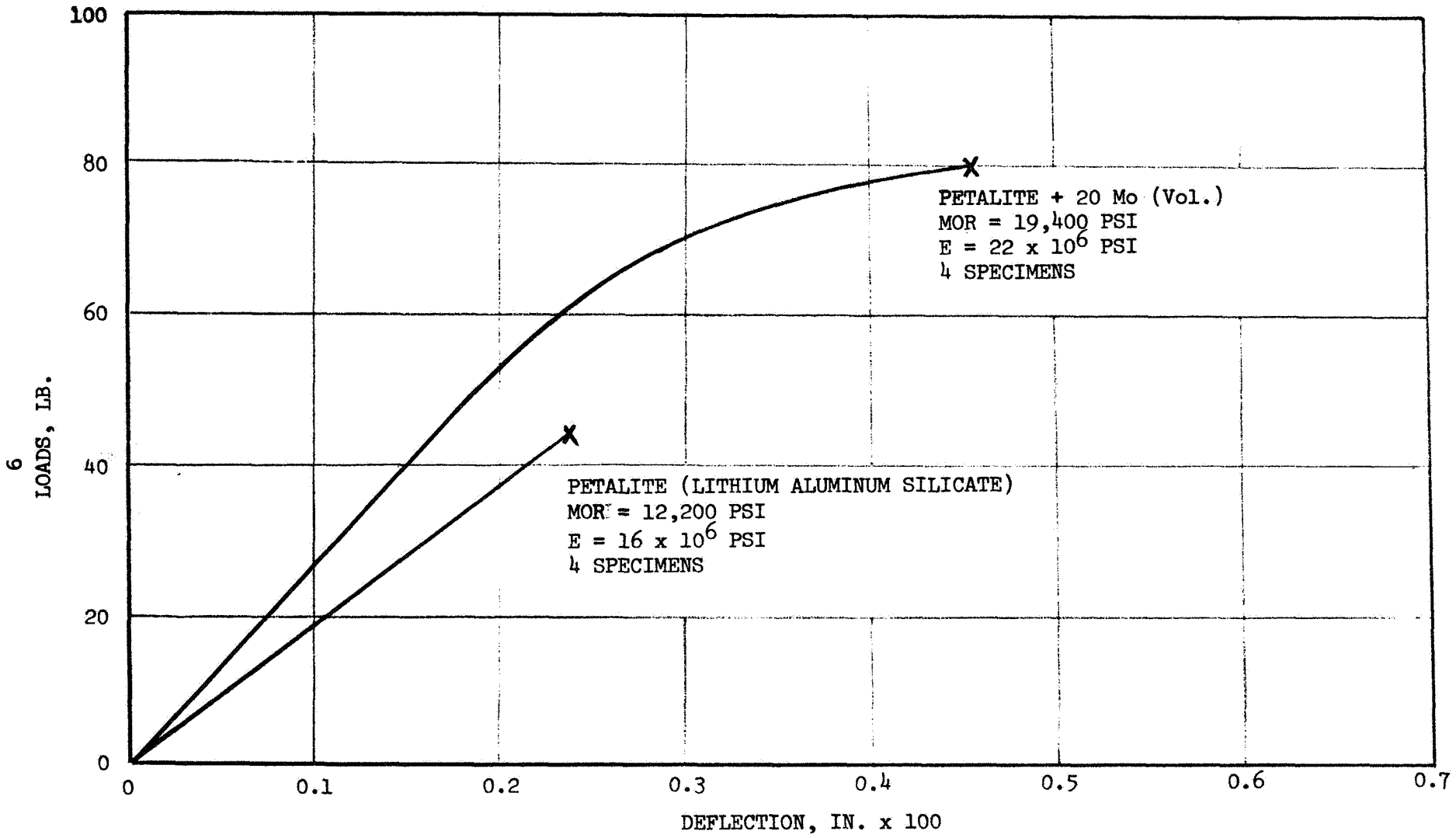

Figure 2-1. Load-Deflection of Petalite Bodies (Reference 2-11)

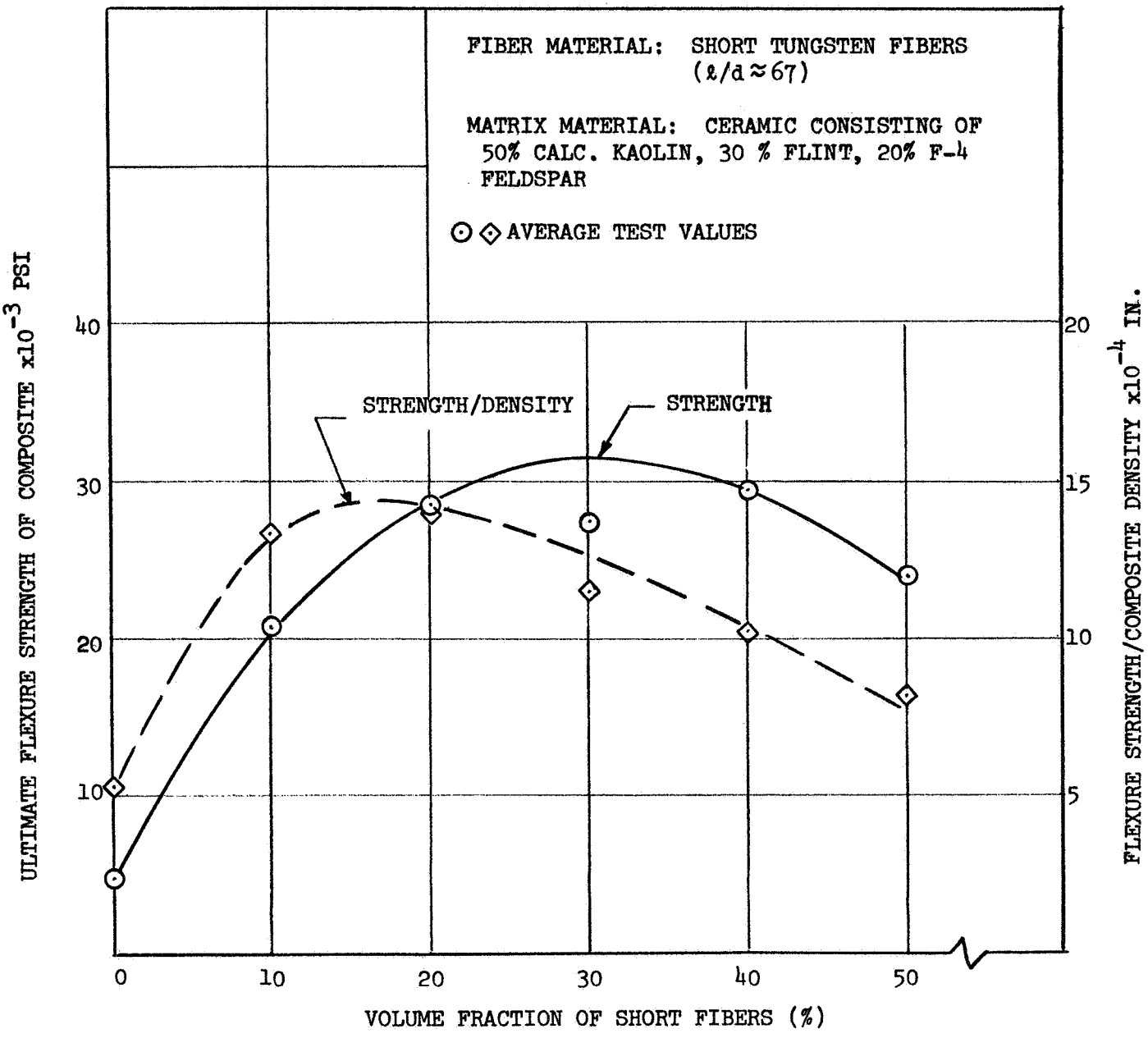

Figure 2-2. Flexure Strength of Fiber Strengthened Ceramic (Ref 2-12)

Levy (Reference 2-14) points out that the factors which appear to restrict the reinforcing of ceramics with refractory metals are:

1. Reactions between metal and ceramic phase.
2. Contamination of either phase by foreign elements.
3. Lack of sintering of ceramic because of presence of the metal during heating.

The work of Baskin, Arenberg and Handwerk (Reference 2-15) involved reinforcing thoria with fibers of mild steel, stainless steel 430, molybdenum, niobium, Zircaloy-2, and zirconium. The compacts were produced by hot pressing at a temperature of 2, 732°F at a pressure of 2, 500 psi. The samples were subjected to thermal shock test which consisted of heating the specimens to 1, 832°F and quenching in mercury. Of the various composites tested, molybdenum-fiber-reinforced thoria exhibited the best resistance to repeated thermal shock. It was also found that thin fibers were more effective than thicker ones. The mechanism of improving thermal cycling behavior was primarily a mechanical one, rather than a modification of physical properties. The presence of ductile metal fibers served both as a crack-inducing and crack-confining mechanism which served to prevent catastrophic failure. It is noted in Reference 2-15 that the micro and macro cracks in the matrix ceramic, if properly controlled by a strong metal reinforcement network, are actually an advantage. The advantages attributable to the presence of cracks are as follows (Reference 2-14):

1. High residual stresses induced in the ceramic during processing are relieved.
2. High stresses generated by thermal gradients acting over long distances are prevented.
3. Crack sensitivity of the body is reduced by the presence of a multitude of already built-in cracks. The existing cracks essentially stop crack propagation.
4. The modulus of elasticity is reduced.
5. The ability of the composite to move elastically or plastically under the influence of the applied stresses is made possible by the segmenting of the ceramic blocks.

The mechanism of crack formation in fiber-reinforced ceramics is further discussed by Swica, Hoskyns, Goss, Connor, and Tinklepaugh (Reference 2-16), and by Levinson (Reference 2-17).

In addition to the work contained in the references cited above, a comprehensive review of the work on fiber-strengthened ceramics, and reinforced ceramics in general, is given by Levy (Reference 2-14), Boland and Walton (Reference 2-18), Walton and Corbett (Reference 2-19), and Carroll-Porczynski (Reference 2-20). The first reference is of particular importance to the present work, for it is the only work which describes chemically bonded ceramics. Most of the other references deal with hot-pressed materials.

In Reference 2-14, Levy describes a concept for producing a reinforced ceramic, whereby an aluminum phosphate-bonded alumina is reinforced with stainless steel corrugated strip. Such a composite was intended for ramjet combustion chamber applications. An extension of this concept to wing leading edge configurations has been made by substituting a molybdenum wire mesh precoated with a pack cementation covering for the corrugated stainless steel strip. These components have successfully withstood several 20-minute cycles of exposure up to 3,500°F. The above concept was further extended to higher operating temperature through the use of phosphate-bonded zirconia as the matrix material. Chromia was added to zirconia to increase the workability and emittance of the material. The resultant ceramic matrix was incorporated into a reinforced-ceramic coating system which consisted of corrugated strip-reinforcement of molybdenum alloy (0.010-inch thick by 0.125-inch wide), resistance welded to a base metal substrate of 0.5 percent Ti molybdenum alloy sheet. The surfaces of the molybdenum were plasma-sprayed with chromium to facilitate resistance welding, and to protect the material against oxidation. The welded assembly was covered with a vitrified coating for the purpose of further increasing the oxidation resistance of molybdenum. According to Levy (Reference 2-14), the resultant system exhibited excellent resistance to thermal shock, and withstood a steep thermal gradient through its thickness without any apparent damage to the composite.

Additional references on fiber-strengthened and reinforced ceramics are given in the Bibliography.

2.2 CANDIDATE FIBER AND WHISKER REINFORCING MATERIALS AND THEIR PROPERTIES

The physical and thermophysical properties of various fibers and whiskers, which appear as potential candidates for reinforcing the chemically bonded zirconia, are given in Table 2-1. Table 2-2 shows the rating of the various fibers and whiskers in terms of relative potential. This parameter takes into account the filament tensile strength, density, and the cost of the fibers (or whiskers), which dictates the practicability of using a particular reinforcing material. For comparison purposes, stainless steel is also included in Table 2-2.

From the results given in Table 2-2, it is quite obvious that silicon carbide whiskers have the highest relative potential. Carbon/graphite and tungsten appear quite attractive for elevated temperature applications. Alumina whiskers appear promising because of their high strength. The materials cited above have coefficients of thermal expansion sufficiently close to those of chemically bonded zirconia so that cracking of the matrix would be minimized.

2.3 ANALYTICAL STUDIES ON FIBER-STRENGTHENED CERAMICS

Analytical studies were conducted to gain an understanding of factors affecting the strength of fiber-reinforced ceramics. These studies included determination of the required properties of fibers to minimize, or possibly avoid, cracking of the ceramic; the strength of fiber-reinforced ceramic as affected by porosity; the relationship between porosity and fiber-volume fraction, and the effect of fiber alignment.

2.3.1 Required Fiber Properties for a Crack-Free Ceramic

When a ceramic matrix, such as chemically bonded zirconia, is reinforced with short fibers or whiskers, and the composite is then subjected to an elevated temperature, cracking of the ceramic will take place if a proper

Table 2-1

AVAILABILITY OF HIGH-TEMPERATURE* FILAMENTARY MATERIALS

Filament Type	(2-21)** Melting or Softening Point °C	°F	(2-21) Density (ρ) gm/cc	lb/in.^{3}	(2-21) Tensile Strength (σ), 10^3 psi	(2-21) Specific Strength $(\sigma/\rho)\ 10^{-6}$ in.	(2-21) Young's Modulus (E) 10^6 psi	Specific Modulus $(E/\rho)\ 10^7$ in.	(2-21) σ/E Ratio	(2-22) Coefficient of Thermal Expansion at 20°C x 10^{-6} °C	°F	(2-21) Approximate Cost ($/lb)	(2-21) Typical Cross-Sectional Dimensions, (microns)
Fibers													
Silica	1,660	3,020	2.19	0.079	850	10.8	10.5	13.3	0.081	0.40	0.22	30	35
Alumina	2,040	3,700	3.15	0.114	300	2.6	25	21.9	0.012	6	3.33	N/A	N/A
Zirconia	2,650	4,800	4.84	0.175	300	1.7	50	28.6	0.006	5.6(2-24)	3.1(2-24)	N/A	N/A
Graphite(2-26) (Thornel 40)	3,650	6,600	1.50	0.054	350	6.5	40	74.1	0.088	2.5(2-24)	1.4(2-24)	500	7
Boron nitride	2,980	5,400	1.90	0.069	200	2.9	13	18.8	0.015	7.7(2-24)	4.3(2-24)	175	7
Tungsten	3,400	6,150	19.4	0.697	580	0.8	59	8.5	0.010	4.6(2-22a)	2.55(2-22a)	710	13
Rhenium	3,180	5,756	21.0	0.759	290(20 mil)(2-25)	0.5	68	9.0	0.004	6.7	3.70	16,000	120
Molybdenum	2,620	4,750	10.2	0.369	320	0.9	52	14.1	0.006	4.9(2-23a)	2.72(2-23a)	630	25
75 W/25 Re	3,120	5,648	19.6	0.710	475(10 mil)(2-25)	0.7	N/A	N/A	N/A	N/A	N/A	4,200	76
Whiskers													
Alumina	2,040	3,700	3.96	0.143	3,000	21.2	62	43.4	0.048	6-9	3.33-5.0	2,700-12,000	3-10
Boron carbide	2,450	4,440	2.52	0.091	2,000	21.9	70	76.9	0.028	4.5	2.50	N/A	N/A
Silicon carbide	2,690	4,870	3.18	0.115	3,000	26.1	70	60.8	0.043	5.9	3.17	250	1- 3
Silicon nitride	1,900	3,450	3.18	0.115	2,000	17.4	55	47.8	0.036	2.5(2-24)	1.4(2-24)	N/A	N/A
Graphite	3,650	6,600	1.66	0.60	2,845	47.4	102	170.0	0.028	4	2.22	N/A	N/A
BeO(2-27)	2,570	4,660	2.85	0.103	1,900	18.4	50	48.5	0.038	8-13	4.4 -7.2	113,000	3-10
Matrixes													
Zirconia										3.6(2-28)	2.0(2-28)		
Alumina										5.4(2-28)	3.0(2-28)		

*For application at 2, 500°F and above.

**The numbers in parentheses denote references.

a - Denotes wire.

N/A Not Available.

Table 2-2

RELATIVE POTENTIAL FOR CONTINUOUS AND DISCONTINUOUS REINFORCING FILAMENTS

Filament Type	Average Ultimate Tensile Strength σ_{uts} (lb/in.^{2}) (x 10^3)	Density ρ (lb/in.^{3})	Approximate Cost, C ($/lb)	Relative Potential* $\sigma/\rho C$ (in.-lb/$)	Melting or Softening Temperature (°F)
Continuous					
Stainless Steel	600	0.280	50	42,800	2,500
Boron Nitride	200	0.069	175	16,600	5,400
Carbon/Graphite	350	0.054	500	13,000	6,600**
Silicon Carbide	400	0.125	2,100	1,520	4,870
Molybdenum	320	0.369	630	1,376	4,732
Tungsten	580	0.697	710	1,171	6,138
75 Tungsten/25 Rhenium	475	0.710	4,200	159	5,640
Rhenium	290	0.759	16,000	24	5,752
Discontinuous					
Silicon Carbide	3,000	0.115	250	104,300	4,870
Silicon Nitride	800	0.115	1,350	5,150	3,450
Alumina	3,000	0.143	12,000	1,750	3,700
Beryllium Oxide	1,900	0.103	113,000	163	4,630
Graphite	2,845	0.060	Not Available	- -	6,600**
Boron Carbide	2,000	0.091	Not Available	- -	4,400

*The higher the value of (σ/ C), the greater the potential
** Sublimes

relationship does not exist between the elastic properties and coefficients of thermal expansion of the two materials. The optimum relationship between the properties of the constituents can be established by considering the problem of multiaxial thermal residual stresses in a composite consisting of a solid cylinder imbedded in a material with different elastic properties (Figure 2-3).

For small fiber-volume fractions of the reinforcements, the interaction of stresses from adjacent filaments will be negligible; therefore, the solution of the problem will be similar to that for two, thick, concentric cylinders. This solution is similar to that given in Reference 2-28, except that the thermal effects are included here.

For a thick-walled cylinder subjected to internal and external pressures, as well as axial stress, and a temperature ΔT (Figure 2-4), the solution for the radial displacement, u, and the axial strain, ϵ_z, is

$$u_m = \frac{1-\nu_m}{E_m}\left(\frac{p_a a^2 - p_b b^2}{b^2 - a^2}\right) r + \frac{1+\nu_m}{E_m}\left(\frac{a^2 b^2}{r}\right)\left(\frac{p_a - p_b}{b^2 - a^2}\right)$$

$$- \frac{\nu_m}{E_m}\sigma_{zm} r + \alpha_m \Delta T r \qquad (2\text{-}1)$$

$$\epsilon_{zm} = \frac{1}{E_m}\left[\sigma_{zm} - 2\nu_m\left(\frac{p_a a^2 - p_b b^2}{b^2 - a^2}\right)\right] + \alpha_m \Delta T r \qquad (2\text{-}2)$$

where ν is Poisson's ratio, E is the modulus of elasticity, α is the coefficient of thermal expansion, and ΔT is the difference between initial, T_o, and final, T_f, temperatures,

$$\Delta T = T_f - T_o$$

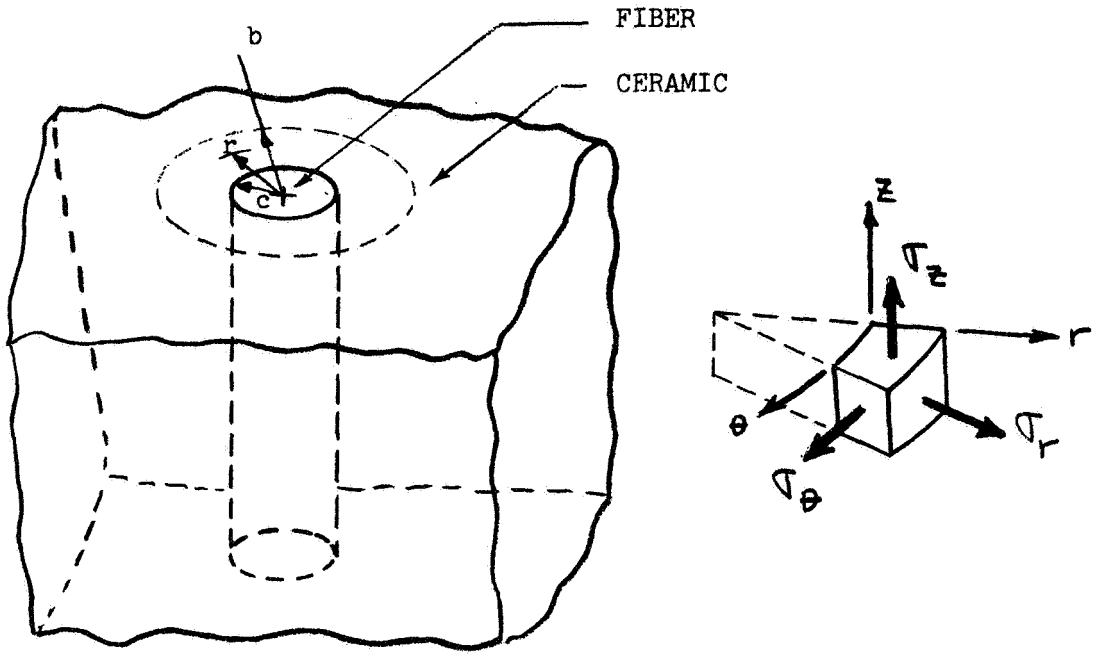

Figure 2-3. Model for Investigating Thermal Residual Stresses

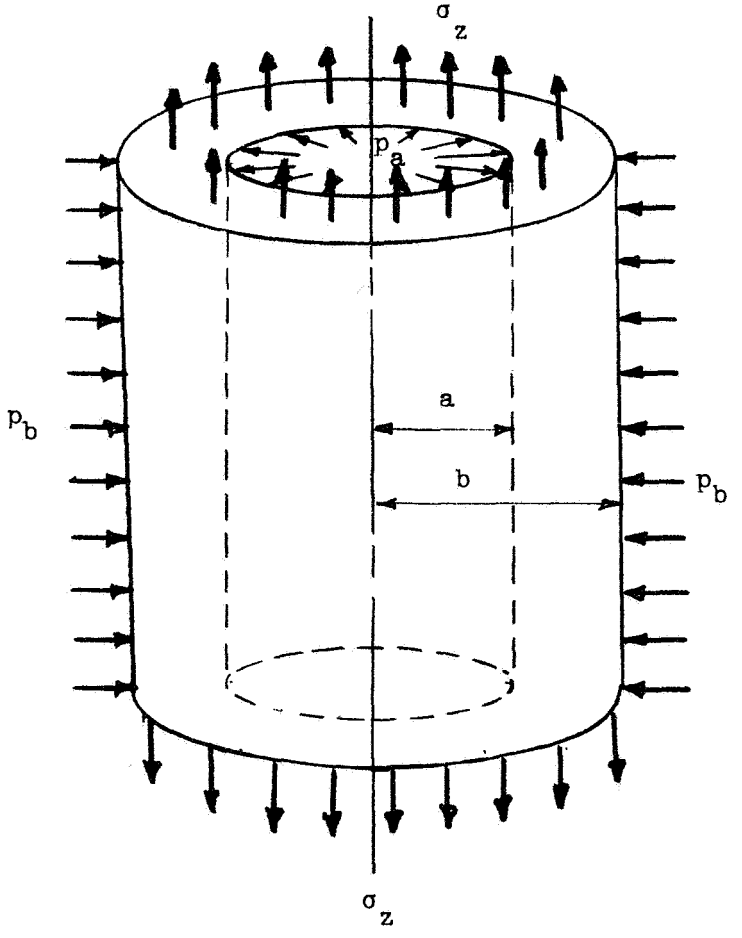

Figure 2-4. Thick Cylinder Under Multiaxial Loading

The problem under consideration (Figure 2-3) can now be solved with the aid of the above equations, if appropriate equations of equilibrium and compatibility are established. These equations require that at

$$r = c, \quad u_c = u_f$$

and also that

$$\left.\begin{aligned} r = c, \quad \sigma_{rc} &= \sigma_{rf} = -p \\ \epsilon_{zc} &= \epsilon_{zf} \\ \sigma_{zc}\,(b^2 - c^2) &= -\sigma_{zf} c^2 \end{aligned}\right\} \quad (2\text{-}3)$$

where p is the interface pressure, and the subscripts c and f denote the ceramic and filaments, respectively. From Equations 2-1 and 2-2 the radial displacement and the axial strain for the fiber at r = c (see Figure 2-3) are

$$\left.\begin{aligned} u_f &= \frac{1-\nu_f}{E_f}(-p)\,c - \frac{\nu_f}{E_f}\,\sigma_{zf}\,c + \alpha_f \Delta T c \\ \epsilon_{zf} &= \frac{1}{E_f}\left[\sigma_{zf} - 2\nu_f\,(-p)\right] + \alpha_f \Delta T \end{aligned}\right\} \quad (2\text{-}4)$$

Similarily, the radial displacement for the ceramic at r = c, and also the axial strain, is:

$$\left.\begin{aligned} u_c &= \frac{1-\nu_c}{E_c}\left(\frac{pc^2}{b^2-c^2}\right)c + \frac{1+\nu_c}{E_c}\left(\frac{cb^2 p}{b^2-c^2}\right) - \frac{\nu_c}{E_c}(\sigma_{zc})c + \alpha_c \Delta T c \\ \epsilon_{zc} &= \frac{1}{E_c}\;\sigma_{zc} - 2\nu_c\left(\frac{pc^2}{b^2-c^2}\right) + \alpha_c \Delta T \end{aligned}\right\} \quad (2\text{-}5)$$

Combining Equations 2-3, 2-4, and 2-5, and solving for p and σ_{zf} yields

$$p = \frac{(\alpha_f - \alpha_c)E_f E_c (1-k)\Delta T\left[(1+\nu_f)(1-k)E_c + (1+\nu_c)kE_f\right]}{\left\{E_f\left[(1+k)+(1-k)\nu_c\right] + (1-\nu_f)(1-k)E_c\right\}\left[E_c(1-k)+E_f k\right] - 2\left[\nu_f(1-k)E_c + \nu_c k E_f\right]^2} \tag{2-6}$$

$$\sigma_{zf} = -\left\{\frac{(\alpha_f - \alpha_c)E_c E_f (1-k)\Delta T + 2p\left[\nu_f(1-k)E_c + \nu_c k E_f\right]}{E_c(1-k) + E_f k}\right\} \tag{2-7}$$

and, finally, at r = c, the stresses are

$$\sigma_{zc} = -\sigma_{zf}\left(\frac{k}{1-k}\right) \tag{2-8}$$

$$\sigma_{rc} = \sigma_{rf} = -p \tag{2-9}$$

where, for convenience, k denotes fiber-volume fraction

$$k = \frac{\pi c^2}{\pi b^2} \tag{2-10}$$

The circumferential stress in the ceramic of r = c is

$$\sigma_{\theta c} = \left(\frac{1+k}{1-k}\right) p \tag{2-11}$$

Equations 2-6 through 2-11 may be used to establish the properties required of the fibers to prevent the ceramic cracking when it is cooled from the processing temperature to room temperature, or heated to a use temperature greater than the processing temperature.

It is apparent from the above equations that the stresses caused by differences in the coefficients of thermal expansion of the two materials can be reduced by minimizing the difference $(\alpha_f - \alpha_c)$. Indeed, these stresses will be identically equal to zero at any temperature, if $(\alpha_f - \alpha_c)$ at that temperature is equal to zero. If the properties of the ceramic material are known, it is possible to solve by trial and error for the properties of the fibers to attain a crack-free composite. Although this is a straightforward process,

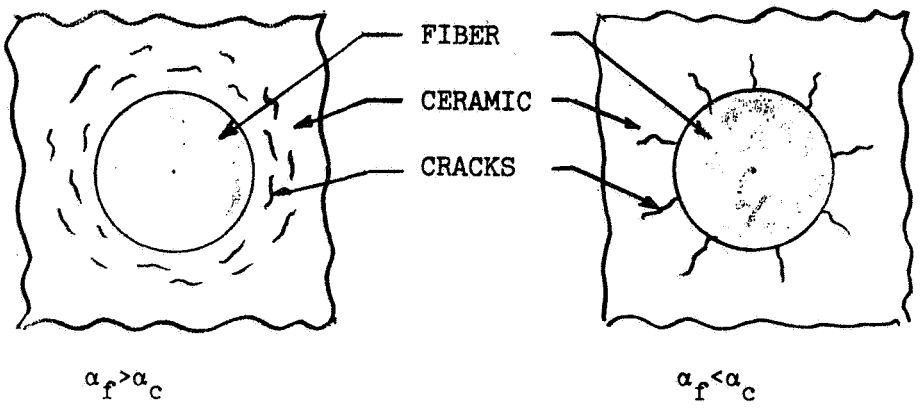

(a) Ceramic cracking during cooling, ($T_f < T_0$, ΔT negative).

T_0 = CONSOLIDATION TEMPERATURE

T_f = USE TEMPERATURE

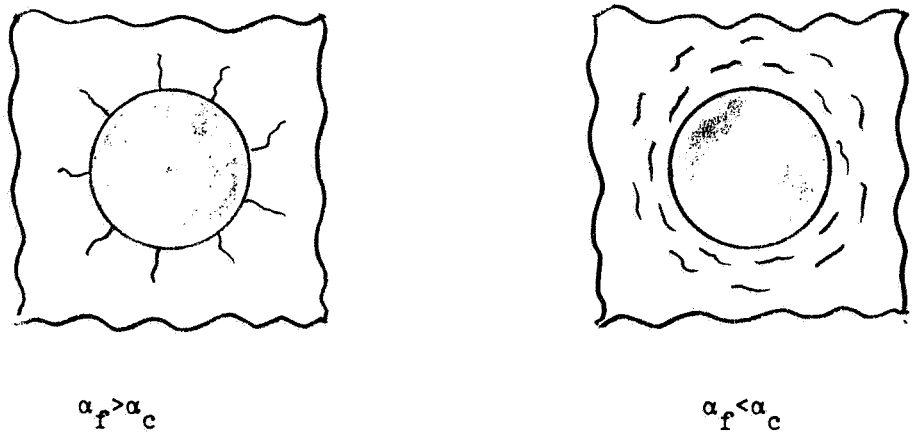

(b) Ceramic cracking during heating ($T_f > T_0$, ΔT positive).

Figure 2-5. Conditions Under Which Ceramic Cracking Occurs

it is rather cumbersome in view of the complexity of the equations for the residual thermal stresses. The procedure can, however, be simplified by making some simplifying assumptions.

2.3.2 Required Fiber Properties for ZrO_2 Matrix

Since, in the present concept, the volume fraction of the fibers will be small, say, $k < \pm 20$ percent, the fibers will be far apart. For this condition, it is justifiable to assume that the stresses around the fiber are identical to those that would exist around a single fiber imbedded in an infinite matrix. To obtain the stresses corresponding to this condition, it is necessary to let $b \rightarrow \infty$, which essentially requires that $k \rightarrow 0$. Setting $k = 0$, and solving for σ_{rc} and $\sigma_{\theta c}$, yields

$$\sigma_{\theta c} = -\sigma_{rc} = \frac{(\alpha_f - \alpha_c)\, E_f\, E_c\, (1+\nu_f)\, \Delta T}{(1+\nu_c)E_f + (1-\nu_f)E_c - 2\nu_f^2 E_c} \qquad (2\text{-}12)$$

Since the matrix (chemically bonded zirconia) has been selected and its properties α_c, E_c, and σ_c are known as a function of temperature (Reference 2-28), one can solve for the fiber properties, E_f and α_f, so that no cracking of the reinforced ceramic takes place when it is subjected to elevated temperatures. In view of the lack of information on the variation of ν_f and ν_c with temperature, it will be assumed that these properties remain constant with temperature.

Since the compressive strength of ceramics is generally much higher than their tensile strength, the tensile residual thermal stress will be the critical parameter. From Equation 2-12 it is quite obvious that ceramic cracking will occur under four conditions. These are illustrated in Figure 2-5. For the case of a weak bond between the fibers and ceramic, failure at the interface will occur, rather than circumferential cracking. Cracking under any of the four conditions shown in Figure 2-5 can be avoided if a reinforcement with appropriate properties is selected. These properties can be obtained from the following equation:

$$\alpha_f = \alpha_c \pm \sigma_c \frac{(1+\nu_c)E_f + (1-\nu_f)E_c - 2\nu_f^2 E_c}{(1+\nu_f)E_f E_c \Delta T} \qquad (2\text{-}13)$$

It is apparent from the above equation that the bounds for the coefficient of thermal expansion of the fiber can be established to prevent ceramic cracking. Typical results are illustrated in Figures 2-6 and 2-7 wherein are shown the bounds within which α_f has to fall in order to prevent cracking of the chemically bonded zirconia. Properties of zirconia obtained from flexure (Reference 2-28) were used to arrive at the results shown in Figure 2-6, while Figure 2-7 is based on properties of zirconia obtained from tension tests (Reference 2-28). Since the bounds for α_f are rather insensitive to E_f (Figure 2-6), Figure 2-7 shows only the results for the case when $E_f \gg E_c$. Thus, to obtain a crack-free, fiber-reinforced ceramic, α_f at any temperature has to fall within the shaded area of the curve.

2.3.3 Tailor-Made Fiber Properties

In the previous section it was established that the strength of fiber-reinforced ceramics is influenced strongly by the coefficient of thermal expansion of the fibers. If fibers cannot be found whose coefficients of thermal expansion fall within the allowable bounds illustrated in Figures 2-6 and 2-7, the fibers can be tailor made by adding a layer of another material. The properties of tailor-made fibers may be made to fall within the required bounds by using such a procedure. The expression for the coefficient of thermal expansion of the coated fibers may readily be derived from equations given in Section 2.3.1. The thermal properties of the coated fibers will depend on the coefficients of thermal expansion and Young's moduli of the fibers and the coating, on Poisson's ratios of the constituents, and on their volume fractions. Some typical results are shown in Figure 2-8, which also shows the coefficient of thermal expansion, in the radial direction, of a composite fiber (coated fiber) as a function of the coefficient of thermal expansion of the coating material, and the volume fraction of the constituents. Of the various constituent properties that influence the coefficient of thermal expansion of a composite fiber, the coefficient of thermal expansion of the coating material has the greatest influence. Varying the modulus of elasticity of the coating, or its Poisson's ratio, does not have much influence on the coefficient of thermal expansion of the composite fiber.

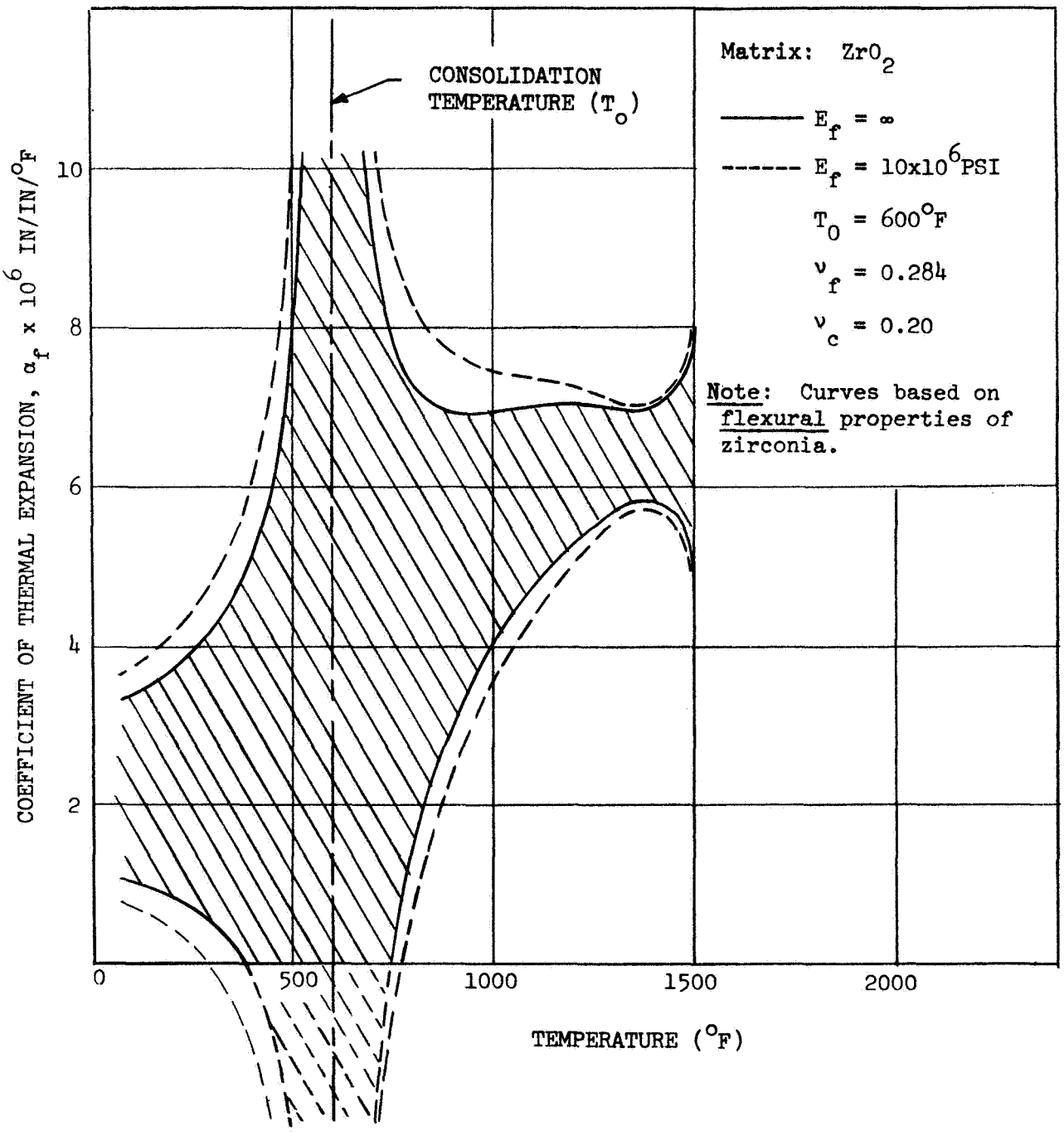

Figure 2-6. Upper and Lower Bounds for the Required Coefficients of Thermal Expansion of the Fibers (Based on Flexure Data).

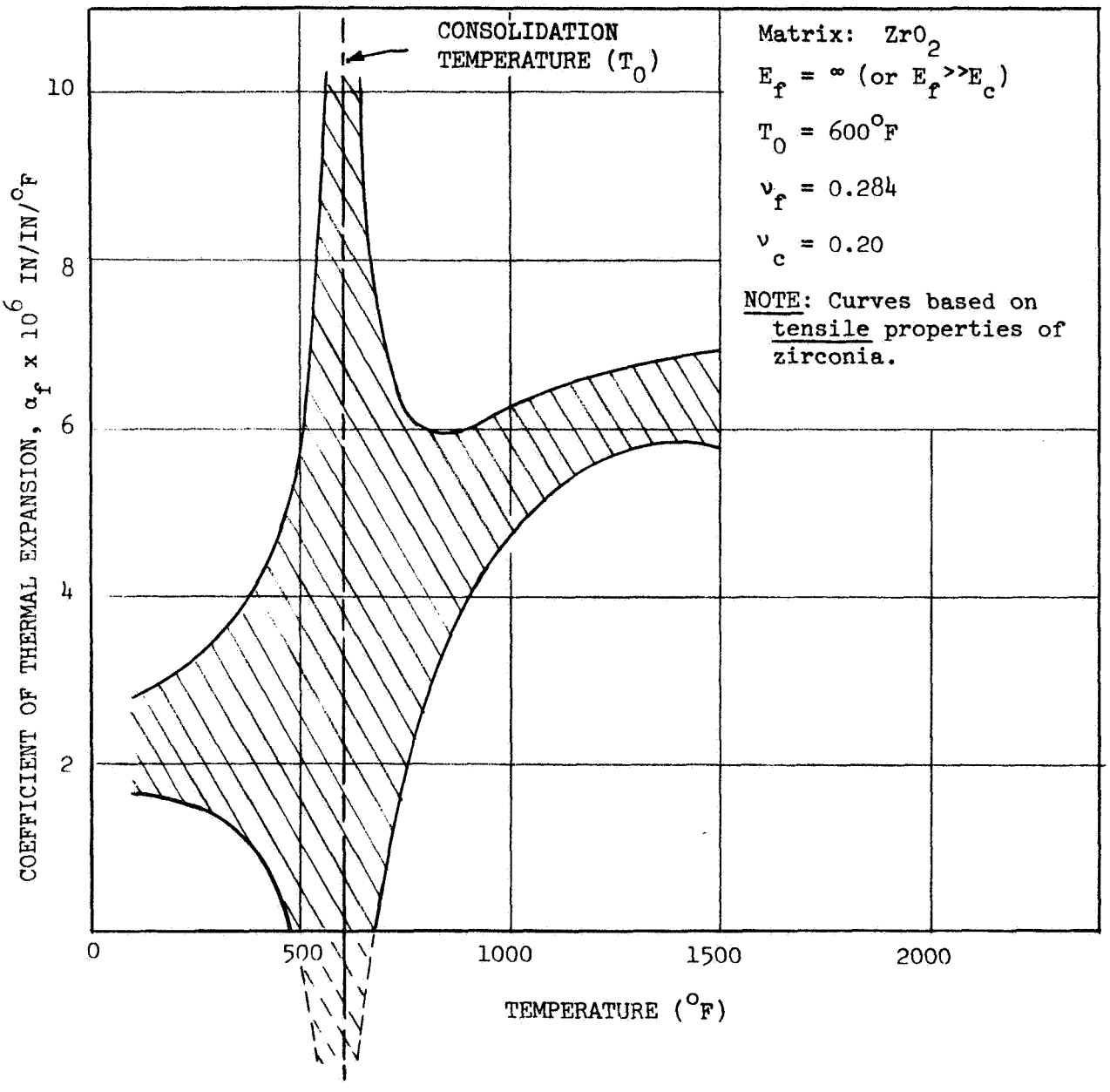

Figure 2-7. Upper and Lower Bounds for the Required Coefficients of Thermal Expansion of the Fibers (Based on Tensile Data)

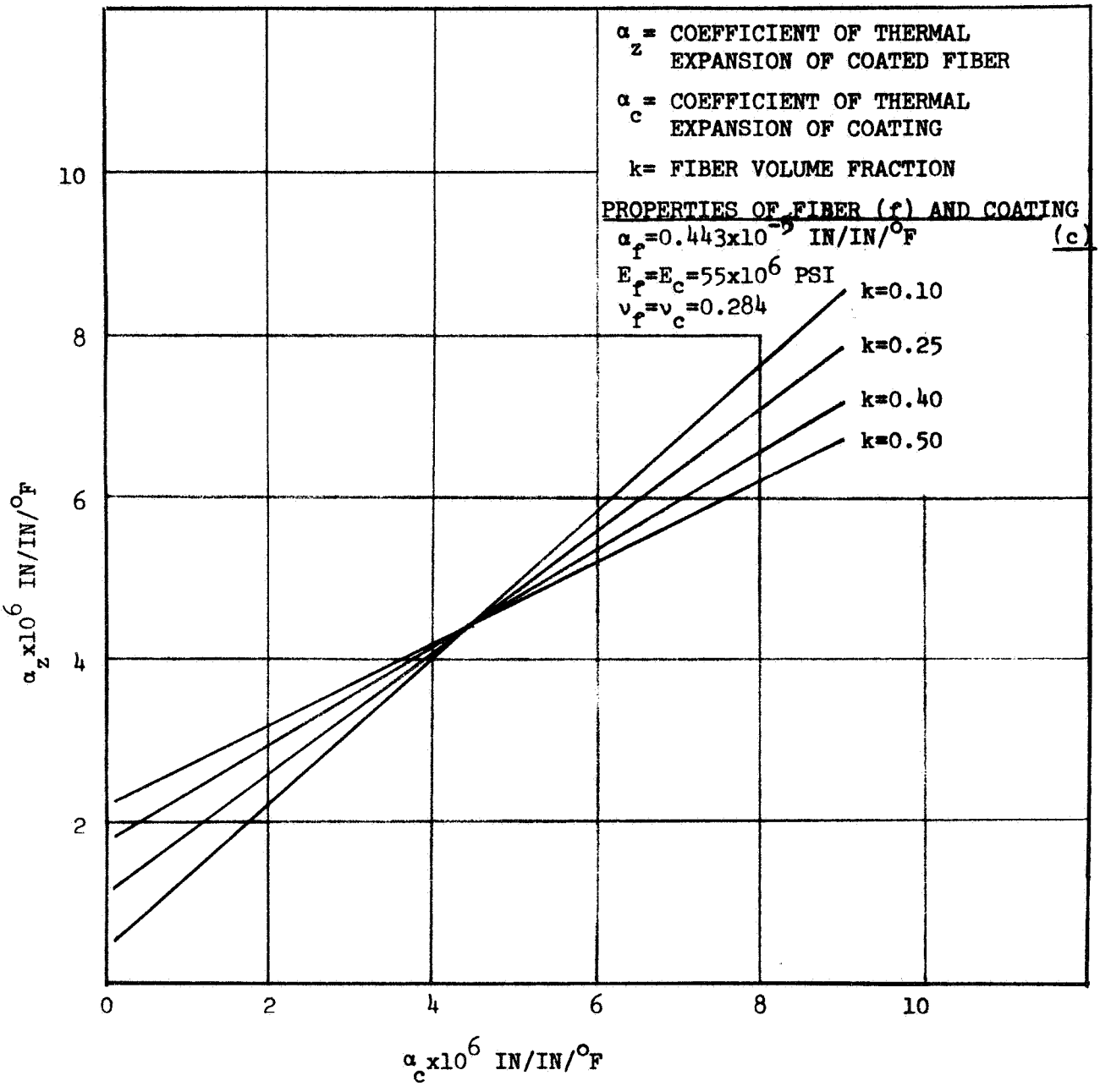

Figure 2-8. Coefficient of Thermal Expansion of Coated Fiber as a Function of the Coefficient of Thermal Expansion of the Coating.

2.3.4 Effect of Porosity on the Strength of Fiber-Reinforced Ceramics

The experimental work of Swica, Hoskyns, Goss, Connor, and Tinklepaugh (Reference 2-16) on the strength of tungsten-fiber-reinforced ceramics has shown that the strength of composites does not increase continuously with increasing fiber content, but reaches an optimum value at a rather low fiber volume (≈30 percent). Composites with volume fractions higher than this value showed marked decreases in strength. Similar results were found in some of the preliminary in-house work conducted at MDAC-WD on the strength of chemically bonded zirconia reinforced with silicon carbide whiskers. Preliminary theoretical studies in this area, based in part on the work of Reference 2-29, indicate that this behavior can be explained by accounting for porosity. As the fiber volume fraction increases, so does the porosity (Reference 2-12). There are two types of porosity: (1) pores which occupy volume and can be measured, and (2) zero-volume pores consisting of fibers which have not formed a bond with the ceramic, and therefore act as pores. It is reasonable to expect that as the fiber volume fraction increases, so does the percent of unbonded fibers. Assuming that the increase in volume fraction of pores is proportional to the increase in the volume fraction of fibers, the following equation has been established for the tensile strength of fiber-reinforced ceramic containing pores:

$$\overline{\sigma} = \left[1 - \frac{\pi}{4}\left(\frac{6\eta k_f}{\pi}\right)^{2/3}\right]\left[\beta \sigma_f k_f + \sigma_c(1-k_f)\right] \qquad (2\text{-}14)$$

where σ_f is the strength of the fibers, σ_c is the strength of the ceramic, k_f is the fiber volume fraction, η is the ratio of the volume of pores divided by the fiber volume fraction ($\eta = k_p/k_f$) and β is a parameter which accounts for nonalignment of the fibers (or their random distribution), strength degradation of the fibers due to fabrication, presence of fibers shorter than the critical length, and other similar factors. In arriving at the above equation it was assumed that the pores are spherical (Reference 2-29) and that the aspect ratio of most of the fibers is large enough so that they act as continuous fibers. Typical results based on Equation 2-14 and experimental results obtained from Reference 2-12 are shown in Figure 2-9. Strength of

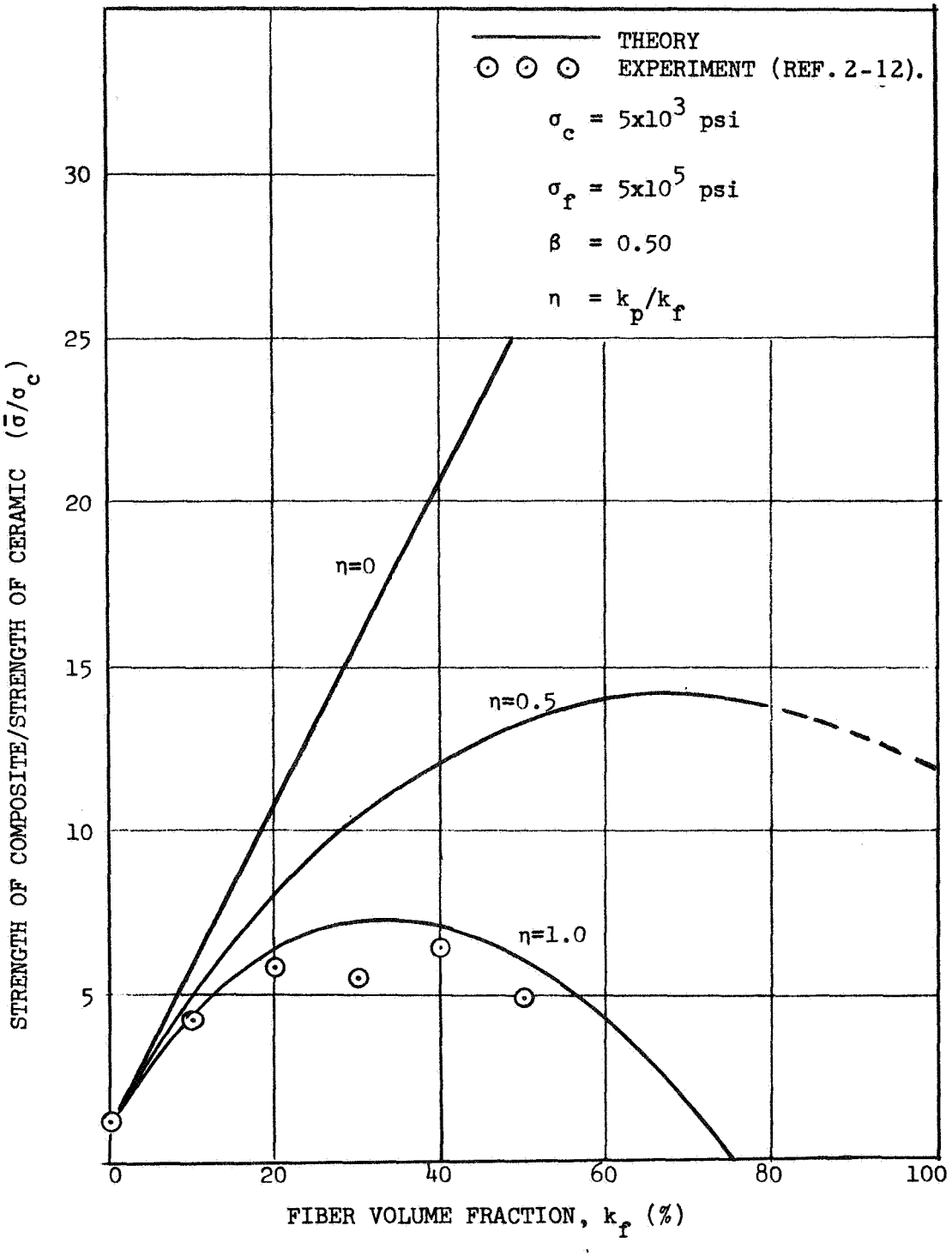

Figure 2-9. Strength of Fiber-Reinforced Porous Ceramic

the 2-mil-diameter tungsten fibers was taken as $\sigma_f = 500 \times 10^3$ psi (Reference 2-28). Strength of the ceramic was taken as $\sigma_c = 5,000$ psi (Reference 2-12), while the β-factor was assumed as $\beta = 0.5$. It is apparent from Figure 2-9 that excellent agreement is obtained between experiment and theory if one takes $\eta = 1.0$. Moreover, it is also apparent that for a given fiber volume fraction, higher increases in the composite strength can be achieved by decreasing the porosity, i.e., decreasing η.

2.3.5 Effect of Fiber Alignment on Composite Strength

When filament strength is much greater than the strength of the matrix, composite strength is strongly influenced by the direction of the filament orientation with respect to the applied load. Figure 2-10 shows the strength of tungsten-reinforced-zirconia as a function of the filament orientation angle to the applied load. These results are based on the theory given in Reference 2-30. In arriving at these results, it was assumed that the aspect ratio, ℓ/d, of the chopped fibers is sufficiently great so that the load can be transferred from the matrix to the fiber by shear. This assumption means the fiber acts as a continuous filament and the theory used for continuous filaments then applies to chopped fibers. As indicated in Figure 2-10, an angle of 5 degrees between reinforcement direction and direction of the applied load causes a reduction of over 50 percent in the allowable strength of the composite containing a 0.30-fiber-volume fraction. Therefore, for unidirectional loads, it is desirable to orient the filaments in the direction of the applied load. Also, it can be seen from Figure 2-10 that for bidirectional loading it is much better to orient a percentage of filaments in the direction of each of the applied loads, according to the ratio of the applied loads, rather than orient all the filaments at some angle to the applied loads. For multiaxial loading, a random fiber array may be desirable.

In order to estimate the strength of a composite containing a random distribution of fibers, a multilayer laminate model is considered. The fiber orientation in each layer is assumed to be the same; however, it is assumed to differ from layer to layer. If the thickness of each layer

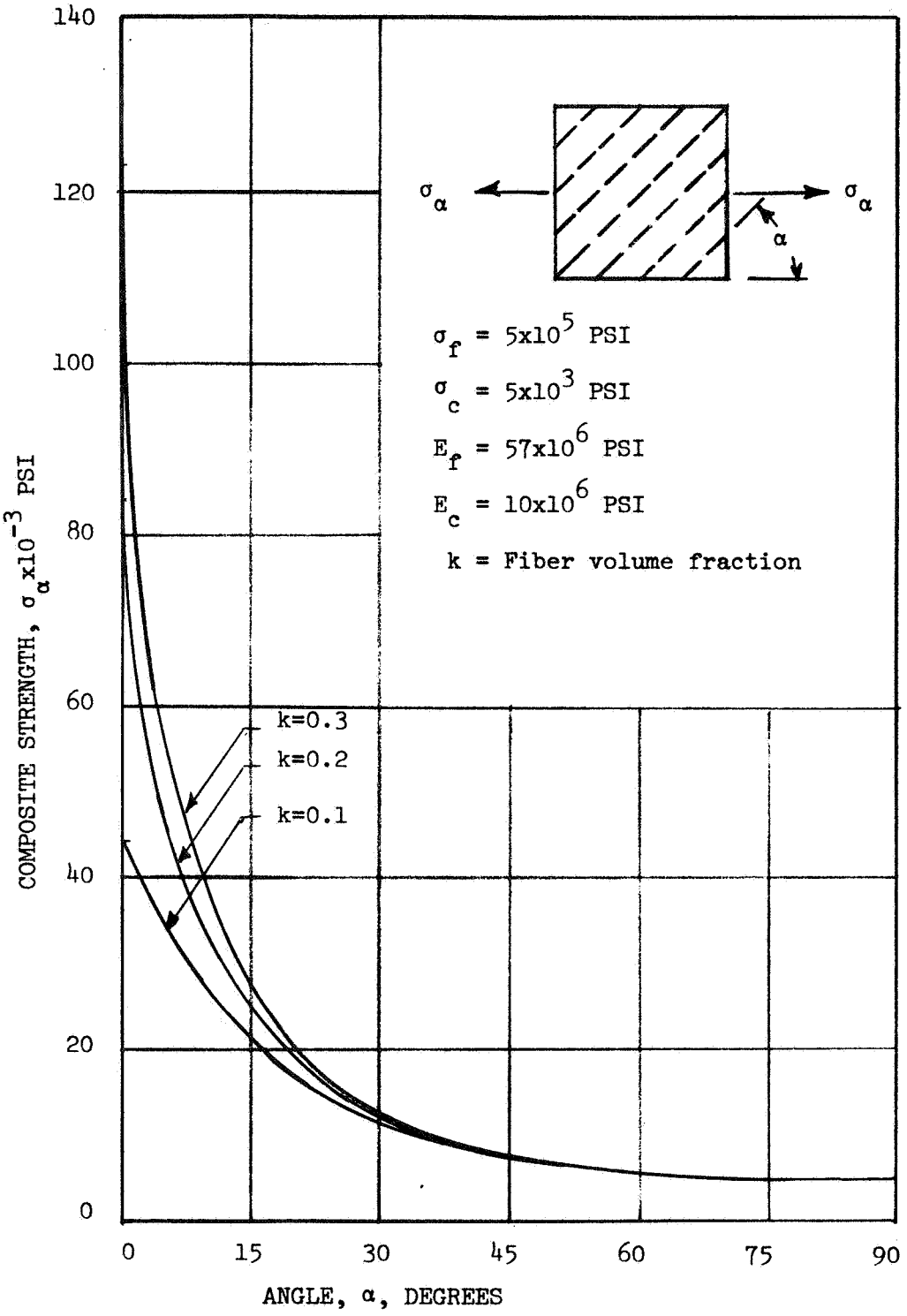

Figure 2-10. Strength of Filament Reinforced Ceramic vs Angle of Filament

is allowed to approach zero, a sheet is obtained with a variable fiber distribution in the plane of the sheet. Moreover, it is also assumed that all layers of the composite exhibit perfectly elastic behavior up to failure. When a particular layer of a composite fails, the load carried by that layer is assumed to be transferred to the remaining, unfailed layers. Figure 2-11 shows the theoretically predicted stress-strain curve for such a multi-directional composite. The encircled numbers shown in Figure 2-11 denote the composite stresses at which various layers fail. Thus, the first layer fails when the composite stress reaches a value of 5,700 psi. Once the first layer fails, failure of layers 2, 3, and 4 is caused at a somewhat lower stress. Failure of the first four layers does not cause failure in layer 5, and the applied composite stress may be increased from 5,700 psi to 6,100 psi before layer 5 fails. Similarily, layer 6 fails at a composite stress of 8,200 psi, and layer 7 at a composite stress of 17,600 psi.

Results shown in Figure 2-11 are typical to those expected for the stress-strain behavior of a composite reinforced with randomly distributed discontinuous fibers. The effect of progressive layer failures on Young's modulus of a composite is readily apparent from Figure 2-11.

2.4 REFERENCES FOR SECTION 2

2-1. C. G. Harmon. Non-Glassy Inorganic Fibers and Composites, NASA-SP-5055, p. 9, 1966.

2-2. J. N. Harris, A. T. Sales, W. J. Corbett, et al. Filament Wound Silica Randome Technique, AFAL-TR-67-65, p. 25, April 1967.

2-3. "A Review of the Air Force Materials Research and Development Program, Supplement 10," WADC-TR-53-373, p. 65 and p. 92, June 1964.

2-4. R. H. Singleton, D. G. Miller, and A. V. Wallace. Metal-Fiber Reinforced Ceramic Composites, Summary of the Tenth Refractory Composites Working Group Meeting, p. 704, August 1965.

2-5. J. N. Harris, A. T. Sales, W. J. Corbett, et al. Ibid p. 36.

2-6. M. Ebner. Stability of Refractories in Hydrogen-Fluorine Flames, Journal Amer. Ceramic Society, Vol. 44, No. 1, p. 7, 1961.

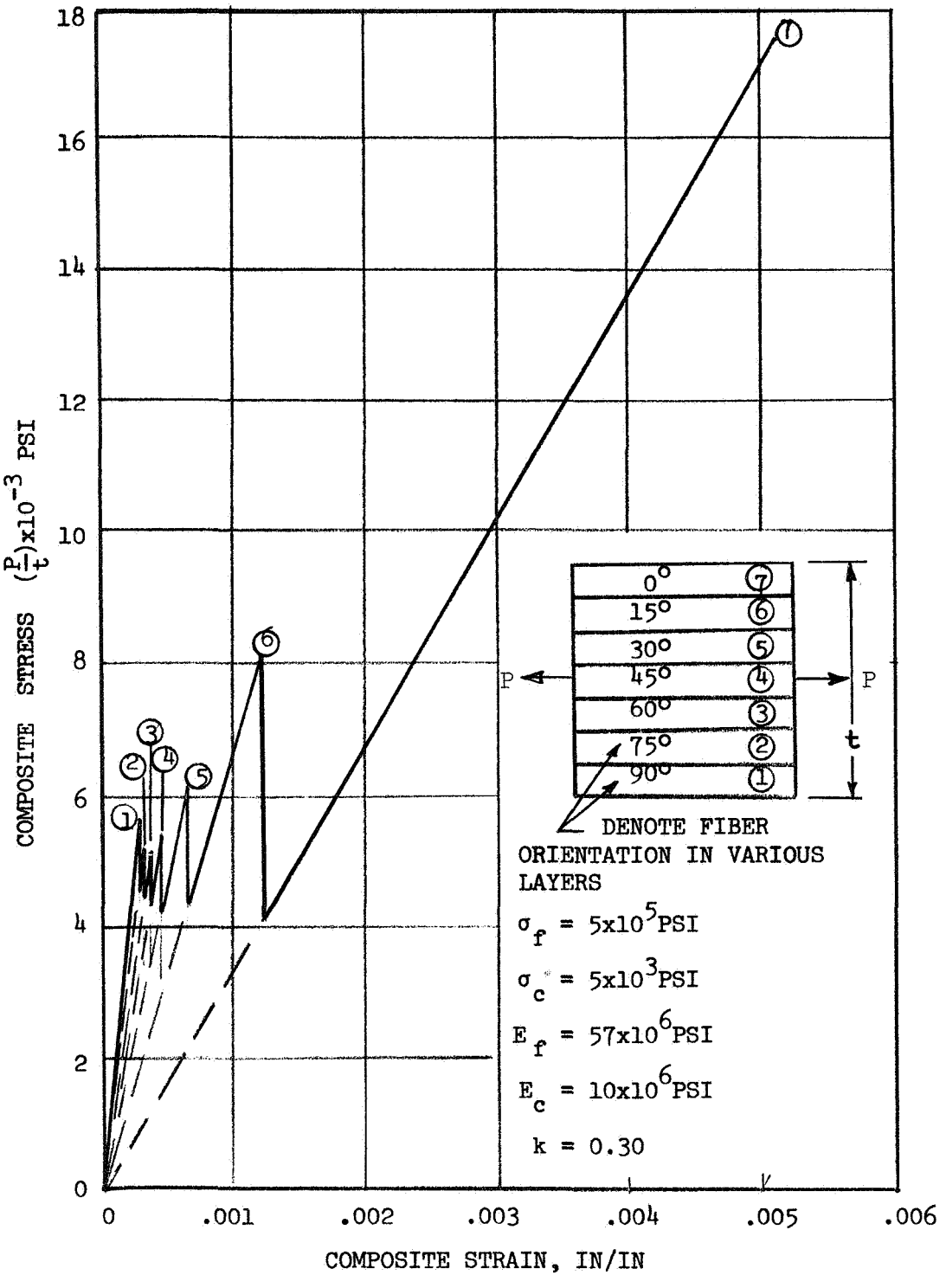

Figure 2-11. Stress-Strain Behavior of Multidirectionally Reinforced Ceramic

2-7. J. Woodburn, and R. F. Lynch. U. S. Patent 2.686, 539, August 3, 1954.

2-8. C.A. Allen. Ceramics Play Major Role in New Composites, Ceramic Industry, p. 132, April, 1967.

2-9. R. H. Singleton, D. G. Miller, and A. V. Wallace, Ibid p. 705.

2-10. J. N. Harris. Ibid, p. 95.

2-11. S. A. Bortz. A Review of Current Refractory Composite Research in Ceramics at IIT Research Institute, Summary of the Tenth Refractory Composites Working Group Meeting, AFML-TR-65-207, p. 778, August 1965.

2-12. J. R. Tinklepaugh, B. R. Goss, W. R. Hoskyns, et al. Metal-Fiber Reinforced Ceramics, WADC-TR-58-452, Part III, November 1960.

2-13. J. I. Fisher, and R. L. Hodson. Development of Metal Fiber-Ceramic Rocket Nozzles, Armour Research Foundation Report 2177-3, August 1959.

2-14. A. B. Levy. Extreme High Temperature Materials, Chapter 3, Materials for Missiles and Spacecraft, edited by E. R. Parker, McGraw-Hill Book Company, Inc., New York, 1963.

2-15. Y. Baskin, C. A. Arenburn, and J. H. Handwerk. Thoria Reinforced Metal Fibers, Am. Ceramic Soc, Bull., Vol. 38, No. 7, pp 345-48, July 1959.

2-16. J. J. Swica, W. R. Hoskyns, B. R. Goss, J. H. Connor, and J. R. Tinklepaugh. Metal Fiber Reinforced Ceramics, WADC Technical Report 58-452, Part II, January 1960.

2-17. D. W. Levinson. Fiber Reinforced Structural Materials, Materials Science and Technology for Advanced Applications edited by D. R. Nash, Prentics Hall, Inc., Englewood Cliffs, N. J., pp 559-575, 1962.

2-18. P. Boland, and J. D. Walton, Jr. Aerosapce Ceramics - Characteristics and Design Principles, Technical Report AFML-TR-65-171, June 1965.

2-19 J. E. Walton, Jr. and W. J. Corbett. Metal Fiber Reinforced Ceramics, Chapter 10, Fiber Composite Materials, Published by American Society for Metals, Metals Park, Ohio, 1964.

2-20. C. Z. Caroll-Pororynski. Advanced Materials, Astex Publishing Company Ltd., Guildford, Great Britain, 1962.

2-21. W. H. Sutton. Whisker Composite Materials - A Prospectus for the Aerospace Designer. Astronautics and Aeronautics, p. 48, August 1966.

2-22. E. Scala. Design and Performance of Fibers and Composites. Chapter 7 of Fiber Composite Materials, published by American Society of Metals, Metals Park, Ohio, 1964.

2-23. F. H. Norton. Refractories. McGraw-Hill Book Company, Inc., New York, 1949.

2-24. Anon. Materials in Design Engineering. Materials Selector Issue, p. 21, 1964.

2-25. Private Communication, Cleveland Refractory Metals, Solon, Ohio.

2-26. Anon. Technical Information Bulletin No. 465-202-DG. Published by Union Carbide Corporation, Carbon Products Division, New York, N. Y.

2-27. W. H. Sutton, and H. W. Rausch, Sr. Review of Current Developments in New Refractory Fibers and Their Utilization as High Temperature Reinforcements. Presented at 10th National SAMPE Symposium in San Diego, California, 9-11 November 1966.

2-28. L. B. Greszczuk and H. Leggett. Development of a System for Prestressing Brittle Materials, Final Report prepared under Contract No. NAS 7-429, August 1967.

2-29. L. B. Greszczuk. Effect of Voids on Strength Properties of Filamentary Composites, Proceedings of the 22nd Annual Technical and Management Conference of the Society of Plastics Industry (SPI), Washington, D. C., February 1967.

2-30. L. Fisher. How to Predict Structural Behavior of RP Laminates, Modern Plastics, pp. 120-124, June 1960.

2.5 ADDITIONAL BIBLIOGRAPHY ON FIBER STRENGTHENED AND REINFORCED CERAMICS

1. C. A. Arenberg, Y. Baskin, and J. N. Handwerk. Metal Reinforced Thoria-Based Ceramics. Paper presented at American Ceramic Society, 8 May 1957.

2. Y. Baskin, C. A. Arenberg, and J. N. Handwerk. Some Physical Properties of Thoria Reinforced by Metal Fibers. J. Am. Ceram. Soc., Vol. 43, No. 9, pp. 489-492, 1960.

3. S. W. Bradstreet. Principles Affecting High Strength to Density Composites with Fibers of Flakes. Air Force Materials Laboratory Report No. ML-TDR-64-85, May 1964.

4. F. N. Breslich, Jr. Development and Evaluation of Metal Reinforced Ceramic Systems for Radiation-Cooled Vehicles. Summary of the Eight Refractory Composites Working Group Meeting, General Dynamics, Fort Worth, Texas, 1964.

5. R. K. Francis, E. P. McNamara, and J. R. Tinklepaugh. Metal Ceramic Laminates. WADC Report 58-600, November 1958.

6. E. Glenny. Design Considerations in the Engineering Application of Brittle Materials. Trans. British Ceramic Soc. 62, pp. 565-75, July 1963.

7. B. R. Goss. Flexural Relationships of a Metal Fiber Reinforced Ceramic. M. S. Thesis, Alfred University, Alfred, N. Y., 1960.

8. T. A. Greening, S. Rovin, H. W. Levendel, and E. Bruce. Development and Evaluation of Refractory Coating for Missile and Spacecraft Applications. Lockheed Missiles and Space Company, Technical Report: Materials and Chemistry 6-90-62-88, October 1962.

9. A. D. Joseph, R. F. Riegert, K. D. Sheffer, and J. R. Tinklepaugh. The Heat Treatment, Reinforcement and Cladding of Titanium Cerments. WADC Tech. Report 55-82, December 1954.

10. C. Kallup, Jr., S. Sklarew, S. V. Castner. Application and Evaluation of Reinforced Refractory Ceramic Coatings. ASD-TDR-62-651, July 1962.

11. H. Leggett, et al. Development and Evaluation of Insulating Type Ceramic Coatings. WADC Tech. Report 59-102, Part II, April 1960.

12. A. W. Levy, S. R. Locke, and H. Legget. Composite Ceramic-Metal Systems. Astronautics, Vol. 6, No. 4, pp. 27-29, 1961.

13. M. R. Licciardello, B. Ohnysty, A. R. Stetson. Development of Frontal Section for Super- Orbital, Lifting, Re-entry Vehicle, Volume II: Materials and Composites Structural Development. FDL-TDR-64-59, May 1964.

14. D. G. Miller, R. H. Singleton, and A. V. Wallace. Metal Fiber Reinforced Composite Materials. Ceramic Bulletin, Vol. 45, No. 5, pp. 513-517, 1966.

15. R. H. Read. Fiber Metallurgy: A Progress Report. Materials Design Eng., December 1959.

16. H. H. Rice. Metal Reinforced Ceramics and Cerments. Allison Ultra-High Temperature Materials Symposium, General Motors Research, pp. 131-42, Sept. 1958.

17. S. Sklarew. Further Developments in Reinforced Refractory Coatings. Summary of the Fifth Refractory Composites Working Group Meeting, Wright-Patterson Air Force Base, Ohio, ASD-TDR-63-96. July 1961.

18. W. M. Sterry. Ceramic and Composite Ceramic-Metal Materials Systems Application to Re-Entry Structures. Presented atSAMPE National Sumposium, WADC Tech. Report 60-58, 1960.

19. J. R. Tinklepaugh, J. F. Funk, and R. M. Sullivan. A Metal Fiber-Ceramic Composite for High Temperature Use. Metals Eng. Quart., Vol. 3, pp. 56-58, 1963.

20. R. S. Truesdale, J. J. Swica, and J. R. Tinklepaugh. Metal Fiber Reinforced Ceramics. WADC Technical Report 58-452, ASTIA Document No. 207079, December 1958.

21. J. W. Vogan, J. L. Trumbull. Metal Ceramic Structural Composite Materials. Aeronautical Systems Division, Wright-Patterson Air Force Base, Ohio, Report ASD-TDR-62-784, 1962.

22. J. D. Walton, and N. E. Paulos. Slip-Cast Metal Fiber Reinforced Ceramics. Am. Ceram. Soc. Bull., Vol. 41, No. 11, pp. 778-780, 1962.

Section 3
EXPERIMENTAL STUDIES ON WHISKER-REINFORCED CERAMICS

An experimental study was conducted of the strengthening of cast, chemically consolidated zirconia by the incorporation of filamentary materials, such as whiskers and short, discontinuous fibers. The design of this study was based on the literature survey, review of candidate filamentary materials, and analysis of fiber strengthening of ceramics reported in Section 2.0. Four reinforcing materials were selected: tungsten wire, Thornel 40 fibers, silicon carbide whiskers, and sapphire whiskers.

Properties of the reinforcing materials were obtained experimentally or from vendor data. The effects of monofluorophosphoric acid on candidate reinforcing fibers were examined.

Preliminary qualitative studies indicated that the addition of filamentary materials required larger than normal quantities of liquid. The chemical reactions for consolidation and curing cycles were reviewed to determine the effects of using increased amounts of acid. It was found that the curing cycle established in Reference 3-1 could not accommodate increased evolution of product gases. An experimental program performed on flexure specimens indicated that dilution with nonpolar agents would not be successful, but that increased amounts of acid could be used to obtain castable mixes.

The formulation incorporating reinforcing fibers and whiskers into a mix of 32 parts by weight of monofluorophosphoric acid and 100 parts of zirconia was used to prepare test specimens to select one fiber type and one optimum fiber content. This selection was made from flexure strength data obtained at room temperature and at 2,000°F.

Addition of 7.4-weight-percent of silicon carbide whiskers to the ceramic was found to yield a matrix with an optimum flexure strength. A characterization of the optimum-whisker-reinforced matrix was made by determining the tensile flexure and shear properties from 70°F to 2,000°F.

3.1 PROPERTIES OF REINFORCING MATERIALS

Vendor data were utilized for work performed with graphite (Thornel 40) fibers, and silicon carbide and sapphire whiskers. The properties of the 1-mil-diameter tungsten wire were measured experimentally. In addition, the effect of the monofluorophosphoric acid on candidate reinforcing materials was investigated.

3.1.1 Description of Reinforcing Materials and their Properties

Four types of reinforcing materials were used: graphite (Thornel 40) fibers, silicon carbide whiskers, sapphire whiskers, and tungsten fibers. The matrix used was chemically bonded zirconia.

Graphite Fibers (Thornel 40)

Continuous fibers of Thornel 40 were obtained from Union Carbide Company. These were chopped into random lengths of 0.125 inch or less. The properties of Thornel 40, as given in Reference 3-2, are as follows: 250,000 psi, tensile strength (on 1-inch gage length); 40×10^6 psi modulus of elasticity; 0.7 percent elongation at failure; 0.0564 lb/in.^{3} density; all data are based on an equivalent diameter of 6.9 microns.

Silicon Carbide Whiskers

The silicon carbide whiskers were obtained from Carborundum Company, Niagara Falls, New York. The properties as given on the Carborundum Technical Data Sheet (Reference 3-3) are as follows: tensile strength of 3 to 10×10^6 psi; modulus of elasticity of approximately 70×10^6 psi; density of 0.115 lb/in.^{3}; whisker diameter range of 0.5 to 3.0 microns; and whisker length range of 10 to 300 microns. At least 50 percent of the whiskers are said to exceed the length of 40 microns, and at least 20 percent of the whiskers are said to be longer than 100 microns.

Sapphire Whiskers

Type 3B sapphire whiskers were obtained from Thermokinetic Fibers, Inc., Nutley, New Jersey. Properties of the whiskers as given on the

Thermo/kinetic Product Data Sheet are as follows: tensile strength of 0.2 to 3.5 x 10^6 psi; modulus of elasticity of 60 to 150 x 10^6 psi; density of approximately 0.146 lb/in.^{3}; whisker diameter range of 1 to 30 microns (nominal diameter of 18 microns); and a whisker length range of 180 to 2,500 microns.

Tungsten Fibers

Continuous 1-mil-diameter tungsten wire was obtained from General Electric Company, Cleveland, Ohio. The continuous tungsten fibers were cut into short lengths using the procedure outlined below.

1. A 13-inch-diameter cylindrical mandrel was cleaned and a layer of mylar film was taped to the mandrel surface.
2. The mandrel was mounted in the laboratory filament winding machine. The machine was set up to wind the filament in the circumferential mode with a carriage advance of about 0.002 inch per revolution.
3. A reel of 1-mil-diameter tungsten wire was mounted on the carriage. A teflon guide eye was mounted in close proximity to the reel in order to guide the wire to the mandrel.
4. With a spindle speed of about 30 rpm, the wire was wound continuously over a 24-inch length of the mandrel. Spacing between adjacent wires was about 0.002 inch.
5. Approximately one quart of a special water-soluble resin binder was mixed to the following formulation:

   1 part by weight Gelvatol 20-30 BP (PVA)

   1 part by weight methyl alcohol

   2 parts by weight tap water

   PVA powder was added slowly to the water and alcohol mix until the PVA was completely dissolved.
6. This resin was brush-applied to the tungsten windings.
7. The mandrel and windings received a 16-hour heating cycle at 225°F.
8. The tungsten wire laminate was cut longitudinally and removed from the mandrel.
9. A paper cutter was used to cut 1/8-inch strips approximately 24 inches in length.
10. The resin binder was dissolved from the strips with tap water. Several water rinsings were used to assure complete removal of the resin binder.

Properties of 1-Mil Tungsten Wire

Six tensile tests were performed to determine the stress-strain curve and the strength of the 1-mil tungsten filament. Average results are shown in Figure 3-1. The tests were conducted with an Instron tester. An x-y plotter was used to record load versus crosshead travel. Test lengths of 10, 15, and 20 inches were used with two determinations for each length. Elongation was determined by the head travel of the grips. To verify Young's modulus data obtained by the above method, an additional series of four tests were run in which a lightweight Instron extensometer with 1-inch gage length was attached to the wire and the deflection was recorded. These tests verified the results obtained by the previous method. Table 3-1 contains the strength and modulus of elasticity values obtained from each test. The average ultimate tensile strength and average Young's modulus were found to be 428×10^3 psi and 54.8×10^6 psi, respectively. The density of the tungsten fiber was 0.697 lb/in.^{3}.

3.1.2 Solubility of the Candidate Reinforcing Fibers in Monofluorophosphoric Acid

Acid solubility observations were made of the candidate reinforcing fibers in monofluorophosphoric acid. The acid solubility tests were performed at room temperature and at 280°F. Silicon carbide whiskers, 100 to 300 microns in length, Thornel 40, and sapphire fibers were not affected by this treatment. One-mil continuous tungsten wire dissolved slowly at the temperature of 280°F, at a rate of 0.6 percent/hour. The tungsten, after exposure, exhibited a black coating. X-ray crystallographic analysis did not reveal the composition. Microscopic observations on the reinforcement solubility are shown in Table 3-2.

3.2 PROCESSING AND PROPERTIES OF CHEMICALLY BONDED ZIRCONIA AND PRELIMINARY MATERIAL DEVELOPMENT WORK

In order to obtain a whisker-reinforced castable ceramic, studies were performed on the effect of larger than normal acid content and various nonpolar liquid agents on the strength of the matrix. Studies on the curing cycle of the resultant matrix were also performed.

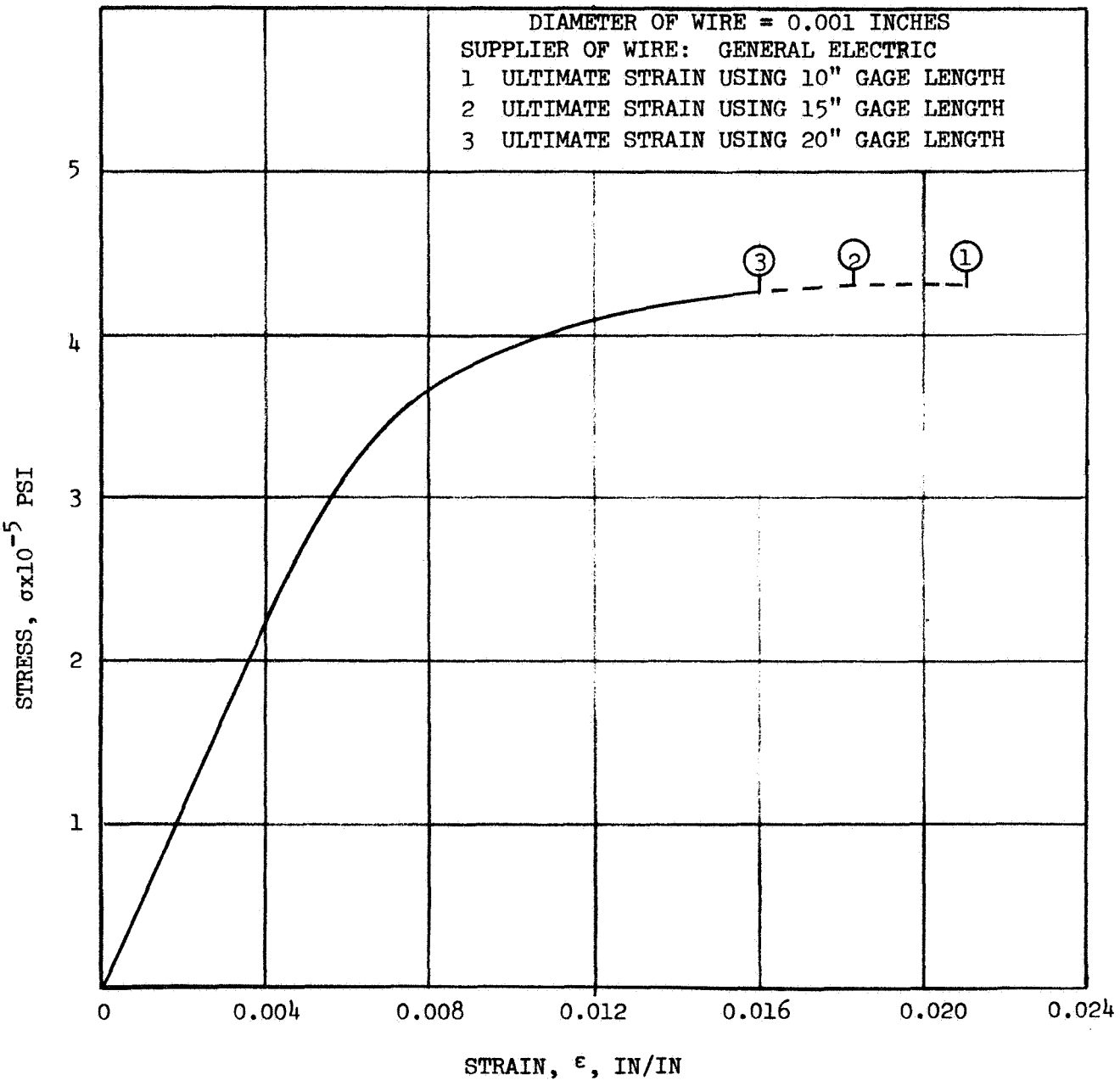

Figure 3-1. Stress-Strain Curve for Tungsten Wire

Table 3-1

EXPERIMENTAL MECHANICAL PROPERTIES OF TUNGSTEN FILAMENTS

Test Number	Gage Length (in.)	Ultimate Strength (KSI)	Young's Modulus (x 10^{-6} PSI)	Yield Strength 2% Offset (KSI)
1	15	423	58.7	370
2	15	433	57.6	376
3	10	433	52.1	377
4	10	431	53.1	375
5	20	421	55.1	375
6	20	427	56.6	370
7*	1	Not Obtained	53.6	Not Obtained
8*	1	Not Obtained	53	Not Obtained
9*	1	Not Obtained	52.7	Not Obtained
10*	1	Not Obtained	55.3	Not Obtained

*Denotes tests in which a lightweight Instron extensometer was used to record deflection instead of measuring crosshead travel as in Tests 1 through 6.

Table 3-2

FIBER SOLUBILITY INFORMATION

Filament	Producer	Name	Microscopic Observations	Observed Effect Due to Reaction with H_2PO_3F
Silicon Carbide B	Carborundum	----	100 to 300μ* long	None
Graphite	Union Carbide	Thornel 40	Yarn continuous; individual filaments average 6μ in diameter	None
Tungsten	General Electric	----	1-mil continuous wire	Partial
Sapphire	Thermokinetics	Type 2B loose fibers	1 to 10μ diameter up to 100μ long	None

* = micron = 3.94×10^{-5} inches

3.2.1 Properties of the Constituents Used in Preparing ZrO_2

The calcia-stabilized zirconia powder was obtained from Norton Company, Worcester, Massachusetts; the monofluorophosphoric acid was obtained from Ozark-Mahoning Company, Tulsa, Oklahoma. The amount of calcia present in the zirconia powder has a decided effect on the strength and expansion of sintered or chemically consolidated zirconia bodies. Calcia-stabilized zirconia, without consolidation additives, does not undergo an allotropic transformation because it has been stabilized in the cubic form. In order to help characterize the material, the weight-percent of calcia present was determined.

An x-ray spectrograph sample was prepared to determine the weight by percent of calcia present in the powder (-325 mesh powders were used for the determinations). Synthetic standards were prepared in the following manner: calculated amounts of calcium sulfate dihydrate were weighed and mixed with sufficient zirconium sulfate to produce a 1.000-gm sample. Three standards were prepared containing 1.00 percent, 3.00 percent, and 5.00 percent calcium. The standards were mixed with 1,500 mg lithium tetraborate, pelletized and analyzed.

The goniometer was positioned at 29° Bragg angle corresponding to the K.C. line of calcium, and the intensities were measured for the standard. The chromium target tube, a standard analyzing crystal (PET), and a helium patch were used during all measurements. Three, 100-second counts were taken for each standard. Intensities were plotted against calcium content. The sample was drawn from this blend for analysis. This sample was mixed with 1,500 mg lithium tetraborate, pelletized and analyzed in triplicate, as previously described. The -325-mesh ZrO_2 had a calcia content of 5.95 to 6.39 percent. The -70- to +200-mesh zirconia had a calcia content varying from 1 to 4 percent, verified by spectrographic analysis. A second sample obtained from the Norton Company had only 4-percent calcia.

3.2.2 Curing Cycle and Chemical Reactions for Consolidation of ZrO_2

In order to conduct the material development program it was necessary to review the chemical reactions involved in the consolidation of the ceramic matrix (Reference 3-1).

The chemical consolidation of ZrO_2 is produced by reaction with monofluorophosphoric acid (H_2PO_3F). The reaction, as determined by differential thermal analysis and substantiated by X-ray diffraction studies, consists essentially of two phases. Zirconium tetrafluoride (ZrF_4) is formed on the surface of each particle of ZrO_2, accompanied by a subsequent reaction with the phosphate radical to produce the bonding material, zirconium pyrophosphate (ZrP_2O_7).

Although the formula for monofluorophosphoric acid is represented as H_2PO_3F, the as-received acid consists of 70 percent by weight of H_2PO_3F and 30 percent by weight of equimolar solutions of bifluorophosphoric acid (HPO_2F_2) and orthophosphoric acid (H_3PO_4). The reaction with zirconia is shown in Equation 3-1.

$$1.4\ H_2PO_3F + 0.3\ HPO_2F_2 + 0.3\ H_3PO_4 + ZrO_2 \longrightarrow ZrP_2O_7 + 2\ HF + H_2O \qquad (3\text{-}1)$$

The stepwise reaction, as determined by differential thermal analysis, is shown in Equations 3-2 through 3-8. The initial reaction is the hydrolysis of the acid.

$$2.8\ H_2PO_3F + 2.8\ H_2O \longrightarrow 2.8\ HF + 2.8\ H_3PO_4 \qquad (3\text{-}2)$$

$$0.6\ HPO_2F_2 + 1.2\ H_2O \longrightarrow 1.2\ HF + 0.6\ H_3PO_4 \qquad (3\text{-}3)$$

$$0.6\ H_3PO_4 \longrightarrow 0.6\ H_3PO_4 \qquad (3\text{-}4)$$

$$2.8\ H_2PO_3F + 0.6\ HPO_2F_2 + 0.6\ H_3PO_4 + 4H_2O \longrightarrow 4.0\ HF + 4.0\ H_3PO_4 \qquad (3\text{-}5)$$

The H_3PO_4 dissociates to form $H_4P_2O_7$, as shown in Equation (3-6)

$$4H_3PO_4 \longrightarrow 2H_4P_2O_7 + 2H_2O \qquad (3\text{-}6)$$

The HF, formed from hydrolysis of the fluorophosphate acids, reacts with ZrO_2 to form ZrF_4, as shown in Equation (3-7)

$$4HF + ZrO_2 \longrightarrow ZrF_4 + 2H_2O \qquad (3\text{-}7)$$

Only 1 mole of the $H_4P_2O_7$ is required to react with the 1 mole of ZrF_4 formed from the reactions of zirconia with the 4 moles of HF as shown in Equation (3-8). The excess HF formed upon reaction of ZrF_4 with the $H_4P_2O_7$ is available for further reaction with ZrO_2 and, consequently, to react with the additional moles of $H_4P_2O_7$. The excess HF is vaporized during processing at 500°F to 600°F after all available $H_4P_2O_7$ is reacted.

$$ZrF_4 + H_4P_2O_7 \longrightarrow 4HF + ZrP_2O_7 \qquad (3\text{-}8)$$

A typical differential thermal analysis thermogram of a mixture of H_2PO_3F and ZrO_2 is shown in Figure 3-2. The endothermic peak initiating at 167°F is consistent with those occurring for mixtures of HF and ZrO_2. This peak is attributed to the volatilization of HF and/or water vapor. The endothermic peak occurring at approximately 212°F represents the conversion of orthophosphoric acid (H_3PO_4) to pyrophosphoric acid ($H_4P_2O_7$). The intense exothermic reaction at 302°F indicates the formation of ZrP_2O_7 and $\widehat{ZrF_4 \cdot 3H_2O}$. The presence of these compounds has been substantiated by X-ray diffraction studies, thermogravimetric analysis, and stoichiometric studies (Reference 3-1). The endothermic peak occurring at approximately 230°C (466°F) indicates conversion of $\widehat{ZrF_4 \cdot 3H_2O}$ to $\widehat{ZrF_4 \cdot H_2O}$. The endothermic peak occurring in the neighborhood of 526°F indicates decomposition of $\widehat{ZrF_4 \cdot H_2O}$.

When more acid is used, more gases (HF and H_2O) will have to be evolved, which presents curing problems. The chemical reaction as shown below

$$1.4\ H_2PO_3F + 0.3\ HPO_2F_2 + 0.3\ H_3PO_4 + ZrO_2 \longrightarrow ZrP_2O_7 + 2HF\uparrow + H_2O\uparrow$$

was used to determine the quantities of gas evolved as shown in Table 3-3.

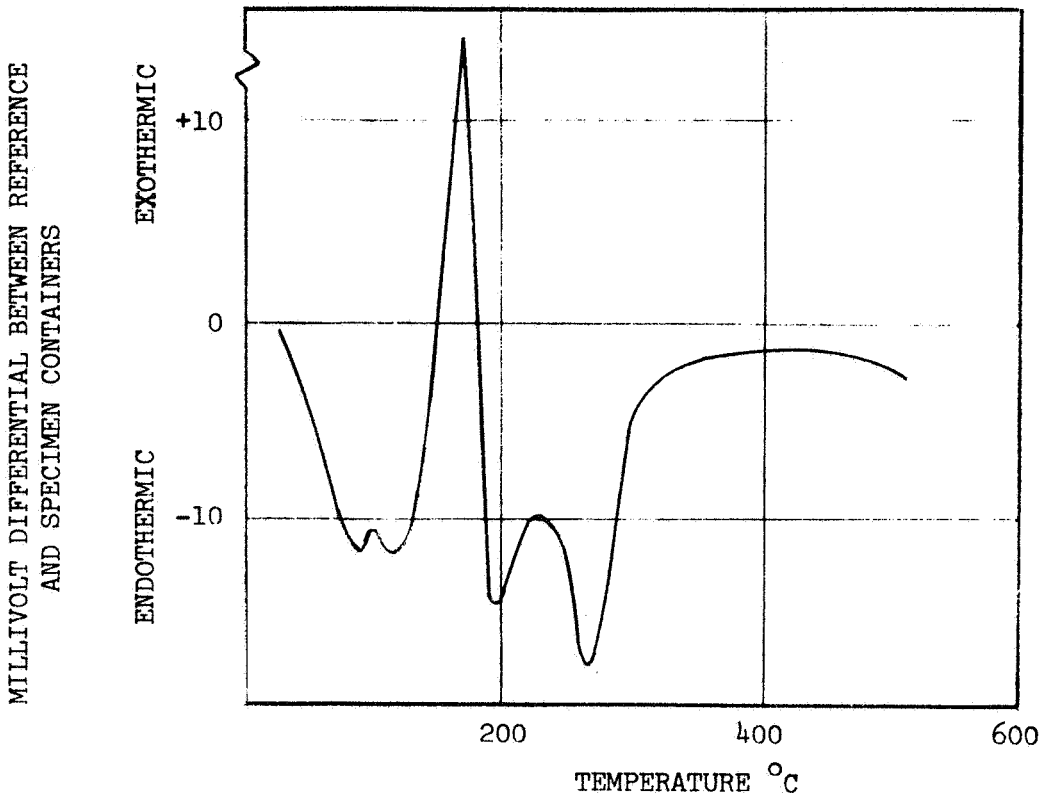

Figure 3-2. Differential Thermal Analysis of $H_2PO_3F+ZrO_2$

Table 3-3

REACTION PRODUCTS OF CHEMICALLY CONSOLIDATED ZIRCONIA

Parts H_2PO_3F/ 100 Parts ZrO_2	Combines with Parts ZrO_2	Retain Parts ZrO_2	Parts ZrP_2O_7	Forms Parts H_2O & HF
16	9.8	90.2	21.2	4.6
32	19.7	80.3	42.4	9.3
48	29.5	70.5	63.6	13.9

Two batches of monofluorphosphoric acid with specific gravities of 1.80 and 1.72 were obtained from the vendor (Ozark-Mahoning Company). The lower liquid density results from a larger amount of bifluorophosphoric acid than shown in chemical Equation 3-1. An examination of chemical Equations 3-2 and 3-3 reveals that increases in bifluorophosphoric acid result in increases of HF.

3.2.3 Preliminary Material Development

During the first year of this effort (Reference 3-1) castable, chemically consolidated zirconia was selected as the final matrix on the basis of tradeoff studies and experimental work. In that work, the strength of the matrix at room temperature was increased consistent with good casting practices. In the current work an attempt was made to further increase the strength by incorporating filamentary materials into the matrix. Preliminary qualitative studies indicated: (1) that the addition of filamentary materials required larger quantities of liquid, and (2) that the previously established curing schedules (Reference 3-1) could not accommodate increased evolution of product gases resulting from increased liquid content.

These preliminary studies were performed using inexpensive, low-grade silicon carbide whiskers, which were primarily powders rather than whiskers, with high L/D (length/diameter) ratios. Mixes made with 7.5-volume-percent silicon carbide whiskers, added to formulation No. 4 (taken from Table 4-1 of Reference 3-1, 16 parts by weight monofluorphosphoric acid to 100 parts by weight zirconia), were found not to be fluid enough for casting. In the previous effort (Reference 3-1), increased fluidity with lower acid content was gained with additions of either water or isopropyl alcohol. However, these additions lowered the original strength of the matrix. In the current effort, increased fluidity of the matrix was obtained by dilution with esters and through addition of larger than normal quantities of monofluorophosphoric acid. The effect of adding esters and larger quantities of acid on the strength of the matrix was investigated experimentally.

Effect of Nonpolar Agents and High Acid Content on the Strength of Zirconia

The study of the reactions between ZrO_2 and H_2PO_3F (see Section 3.2.2) revealed that increasing the acid content would proportionally increase the products of the reaction, ZrP_2O_7, HF and H_2O. The reaction between ZrO_2 and H_2PO_3F results, within 2 hours at normal temperature and humidity, in an increase of viscosity. Product gases are being evolved during this period and during the curing. Evolution of the gases is restricted when the viscosity of the mixture is increased, which could result in the entrapment of the gases that develop high pressures during curing. This problem was considered in the development of a castable formulation.

To minimize these problems, liquids which do not enter into reactions between ZrO_2 and H_2PO_3F were used in an effort to obtain a matrix with good casting characteristics. The use of alcohol and water achieved the desired result, but was ruled out because the addition of alcohol and water to the mix significantly lowers the strength of zirconia (as reported in Reference 3-1). This decrease in strength is apparently due to the interference of these polar additives (alcohol and water) with the ionic balance of the acid and zirconia. Therefore, in the present work, nonpolar liquids were used as diluents for the acid. On the basis of work done with tricresyl phosphate, two acids, designated as VM-6-73B5 and VM-6-73B3, were obtained from Ozark-Mahoning. Both acids had 60-weight-percent H_2PO_3F and 40-weight percent of proprietary diluents. The latter contained a phosphate ester diluent which boils at 572°F (300°C), while the former acid contained an ester diluent with a boiling point of 266°F (130°C).

An evaluation of the four acids obtained from Ozark-Mahoning and the effect of adding silicon carbide whiskers to the zirconia matrix was then conducted.

Five groups of three sets of samples (79 samples, 1.5 x 0.5 x 0.2 inches) were prepared for flexure strength testing. Each of the groups had, respectively, one set made with 16 parts by weight of acid per 100 parts ZrO_2, a second set, with 32 parts acid, and a third set with 48 parts acid. The five groups of samples differed in the type of acids which were used. Four of the acids were supplied by the vendor (Ozark-Mahoning Company) in fresh experimental lots, while the fifth group was acid remaining from the previous program. The data obtained in this testing are given in Table 3-4.

Sample groups 6, 8, and 20 were prepared using 7.5-percent volume-fraction of low-grade silicon carbide whiskers. Since these whiskers contained approximately 50-weight-percent of material with an aspect ratio (length/diameter) less than 2, the fibers were washed to obtain the longer whiskers. Whiskers which were 100 to 250 microns in length were removed by washing through screens. It was found that only high-pressure water would separate the whiskers during the screening operation; separation of the whiskers could not be accomplished by settling in water or dry screening. Plastic mixes could not be obtained with the 16 parts acid and silicon carbide whiskers, but were obtained with 32 and 48 parts acid.

Table 3-4

FLEXURE STRENGTHS* OF PHOSPHATE BONDED ZIRCONIA CONTAINING VARIOUS ADDITIVES

Sample No.	Sample Type (Parts acid/ 100 Parts ZrO_2)	Average Flexure Strength (PSI)	Range of Flexure Strength (PSI)	Number of Samples
15	16 Parts H_2PO_3F Acid (1.80 g/cc)	3,440 ± 200**	3,245 to 3,645	4
11	32 Do	2,336 ± 1,000	1,082 to 3,311	5
17	48 Do	3,852 ± 700***	3,050 to 4,800	4
16	16 Parts H_2PO_3F Acid (1.72 g/cc)	4,441 ± 340	4,012 to 5,019	6
12	32 Do	2,912 ± 800	1,500 to 3,670	7
18	48 Do	4,464 ± 300**	3,785 to 4,680	8
19	16 Parts Diluted Acid (60% H_2PO_3F Acid +40% VM-6-73B5 Ester)	1,037 ± 300	603 to 1,570	6
13	32 Do	1,058 ± 350	542 to 1,445	4
22	48 Do	1,390 ± 250	1,020 to 1,730	8
21	16 Parts Diluted Acid (60% H_2PO_3F Acid +40% VM-6-73B3 Ester)	1,381 ± 250	985 to 1,685	8
14	32 Do	1,769 ± 500	1,403 to 2,280	6
23	48 Do	980 ± 220	720 to 1,230	3
20	16 Parts H_2PO_3F Acid (+ 7.5 V/O SiC Whiskers)	3,250	2,730 to 3,770	2
6	32 Do	5,036 ± 1,000	2,730 to 6,180	4
8	48 Do	3,923 ± 600	3,315 to 4,725	4

*Flexure tests were done on 1-inch spans, using 3-point loading. The approximate sample dimensions were 0.2 x 0.4 x 1.5 inches.

**These data are given ±1 Sigma

***Samples laminated; bottom half of the sample was dense, top portion was highly porous. Only the bottom portion of the sample was tested.

The curing schedule for the 79 samples is given in Table 3-5. The schedule was similar to that utilized in the previous work, except that it was increased at the boiling point of the esters. Flexure strength test data given in Table 3-4 revealed that Sample 6, containing SiC whiskers with 32 parts of acid had strengths higher than those obtained with the formulation utilized in the first year's effort. The maximum strength of zirconia reinforced with SiC whiskers was 6,180 psi. The use of the 1.72 specific gravity acid provided bodies which were stronger than those obtained with 1.80 specific gravity (sample groups 11, 15, and 17 for 1.80 grams/cc and 12, 16, and 18 for 1.72 grams/cc). The lower strengths noted for samples containing the esters are attributed to incomplete evaporation of the diluent.

When selecting the acid for the final preparation of the specimens, consideration was given to the amount of gases that evolve during the chemical consolidation. Based on the information provided by the vendor, the lower the specific gravity of the acid, the higher is the amount of HF evolved. The explanation for this is as follows. When monofluorophosphoric acid containing 0.6 mole HPO_2F_2 is used, 4.0 moles of HF are evolved upon hydrolysis (see Equations 3-5). However, if 0.8 mole of HPO_2F_2 is used to decrease the specific gravity of the acid, 4.4 moles of HF are evolved as shown by Equation 3-9.

$$2.8H_2PO_3F + 0.8HPO_2F_2 + 0.4H_3PO_4 + 4.4H_2O \longrightarrow$$

$$4.4HF + 4H_3PO_4 \qquad (3\text{-}9)$$

The increased amount of HF that evolves when using low specific gravity acid increases the possibility of having increased porosity in the ceramic matrix. This would be especially true for large size ceramic specimens. Therefore, to avoid the possibility of having high porosity parts, the acid with specific gravity of 1.80 gm/cc was selected for the preparation of chemically consolidated ceramic.

Table 3-5

CURING CYCLE FOR CHEMICALLY CONSOLIDATED ZrO_2 UTILIZING DILUENTS

Temperature (°F)	Temperature (°C)	Time (Hr) First Year (No Diluents)	Time (Hr) Second Year (With Diluents)
100	38	2	1
130	54		1
150	66	2	1
180	82	-	1
212	100	2	2
266	130	-	16
400	204	1	1
450	232	-	1
500	260	-	1
550	288	-	1
600	316	1	2

Preliminary Evaluation of Fiber-Reinforced Zirconia

Prior to making final whisker- or fiber-strengthened specimens, preliminary studies were performed on mixing various reinforcing materials with zirconia matrix. The objectives of these studies were to develop mixing techniques, to establish problem areas, and to further evaluate the reactions between the chemically consolidated zirconia and the various reinforcing materials. The matrix used in these studies is described in Table 3-6.

Zirconia samples, reinforced with the following types of short fibers (or whiskers), were tested: graphite (Thornel 40) fibers, silicon carbide whiskers, sapphire whiskers, and tungsten fibers. In order to simplify presentation of specific strength data, it was planned that each composite contain the same weight-percent of fibers. However, because of the diverse densities (between 0.0564 to 0.697 lb/in.^{3}) of the fibers, the required volume of Thornel 40 to be added was too high for good mixing practices. The work at that point revealed that about 12-volume-percent SiC or sapphire fibers (based on 100 parts by weight of zirconia) was the maximum addition that could be made and still obtain a castable mix (using the formula given in Table 3-6). The maximum amount of tungsten or Thornel 40 that could be added was not determined. A higher fiber or whisker content in the composite would require quantities of acid greater than 32 weight-percent.

Table 3-6

ZIRCONIA MATRIX FOR FIBROUS ADDITIONS IN WEIGHT PERCENT

60 (-80 + 200 mesh calcia stabilized ZrO_2)
40 (-325 mesh calcia stabilized ZrO_2)
32 monofluorophosphoric acid (specific gravity 1.8 gm/cc)

Mixing of reinforcing material into the matrix was accomplished by screening the fibers into the wet mix and folding. This technique worked fairly well, except that the final mix still contained lumps of fibers, especially when tungsten fibers were used. Mortar and pestle were used to break up these lumps. Although this technique worked more satisfactorily, it was still inadequate for mixing of 1-mil tungsten fibers. The final mixing technique selected for the tungsten fibers consisted of screening small portions of tungsten fibers through a 10-mesh screen into the zirconia-acid mixture and folding the tungsten into the mixture. For other reinforcing materials the use of mortar and pestle was adequate.

Reactions of the tungsten fibers with constituents of the ceramic mix did not appear to be as serious as those which occurred during studies of the solubility of the fibers in monofluorophosphoric acid. Since the above-described mixing technique for tungsten fibers did not allow addition of predetermined amounts of fibers into the mix, a semi-quantitative technique was used to determine the weight-percent of fibers in the cured specimen. This was accomplished through chemical analyses of the matrices containing tungsten and the zirconia. For samples with low tungsten content, a semi-quantitative chemical analysis was conducted by emission spectroscopy, using standard ASTM electrodes and Spec Industries G-1 Standard (0.1 w/oW). The samples with high tungsten content in the zirconia matrix were determined by wet chemical analysis, as follows: The cured matrix was crushed to fine particles, dissolved overnight in 30 w/o hydrogen peroxide at room temperature; filtered, and washed with water; dried at 221^{o}F, and weighed. The loss in weight was reported as the tungsten content of the matrix.

For specimens containing other reinforcing materials, the fiber content was determined by adding predetermined amounts of fibers into a predetermined amount of zirconia-acid mix.

The specimens prepared during these preliminary mixing studies were tested in flexure at room temperature; the results are shown in Table 3-7. The results for zirconia without any fiber addition (standard specimens) are also shown in Table 3-7. Although the standard specimens (S-2) described in Table 3-7 were smaller in size than those used in the previous effort (see Reference 3-1), the flexure strength data for both sets of specimens were approximately the same. For comparison, the strength data obtained for zirconia during the first-year effort are shown in Table 3-8. It is noted here that the density of sample group S-2 is within 1 percent of the density shown in Table 3-8.

3.3 FINAL PREPARATION AND TESTING OF WHISKER-STRENGTHENED ZIRCONIA SPECIMENS

Following the preliminary exploratory material development work on whisker- and fiber-strengthened zirconia, final specimens were prepared for strength evaluation. All specimens were mixed using mortar and pestle, except for tungsten-fiber-strengthened specimens. The specimens containing tungsten fibers were mixed as previously described. Because of the poor initial performance of Thornel-fiber-strengthened specimens, this material was excluded from subsequent studies.

The three remaining reinforcing materials (silicon carbide whiskers, sapphire whiskers, and tungsten fibers) were used in the preparation of flexure specimens, which were tested at room temperature and at 2,000°F. The test results were used to select an optimum reinforcing medium, which was found to be silicon carbide whiskers. Additional specimens were then prepared for obtaining data on flexure strength, tensile strength, moduli of elasticity, and coefficients of thermal expansion.

Table 3-7 (page 1 of 2)

PRELIMINARY RESULTS ON ROOM-TEMPERATURE FLEXURE PROPERTIES OF FIBER-REINFORCED ZIRCONIA MATRIX

Sample Designation Group No.	No.	Material	Apparent Content Reinforcement Weight Percent	Apparent Content Reinforcement Volume Percent	Test Sample Dimensions (in.) Thickness	Test Sample Dimensions (in.) Width	Test Sample Dimensions (in.) Length	Weight (lb)	Bulk Density (lb/in.^{3})	Failure Load (lb)	Flexure Strength (psi)	(1) Apparent Young's Modulus (psi x 10^{-6})	Strength/ Density (in.)
27	1	Thornel - 40	6.74	14.0	0.2013	0.402	2.495	0.0156	0.0773	9.0	1655	1.86	21,410
	2	Thornel - 40	6.74	14.0	0.2000	0.403	2.496	0.0176	0.0877	7.4	1379	1.44	15,724
28	3	Thornel - 40	12.10	25.0	0.2013	0.403	2.505	0.0133	0.0653	10.0	1840	1.16	28,177
	4	Thornel - 40	12.10	25.0	0.1998	0.403	2.502	0.0112	0.0556	5.0	933	0.45	16,780
31	5	SiC Whiskers	3.3	5.5	0.2013	0.403	2.549	0.0200	0.0964	18.7	3443	3.90	35,715
	6	SiC Whiskers	3.3	5.5	0.2020	0.402	2.555	0.0199	0.0960	21.0	3840	4.55	40,000
	7	SiC Whiskers	3.3	5.5	0.2022	0.402	2.550	0.0221	0.1065	17.3	3165	3.76	29,718
32	8	Sapphire Whiskers	3.3	4.5	0.2020	0.402	2.507	0.0222	0.1090	17.3	3165	4.47	29,037
	9	Sapphire Whiskers	3.3	4.5	0.2033	0.402	2.503	0.0178	0.0870	20.4	3688	4.35	42,390
33	10	Sapphire Whiskers	6.4	8.5	0.2024	0.402	2.520	0.0221	0.1076	19.2	3490	4.32	32,435
	11	Sapphire Whiskers	6.4	8.5	0.2026	0.402	2.554	0.0220	0.1061	17.7	3218	4.50	30,330
	12	Sapphire Whiskers	6.4	8.5	0.2022	0.402	2.553	0.0243	0.1173	22.3	4080	5.23	34,783
34	13	Sapphire Whiskers	11.0	14.7	0.2035	0.402	2.504	0.0199	0.0971	20.0	3615	4.50	37,229
	14	Sapphire Whiskers	11.0	14.7	0.2045	0.403	2.505	0.0199	0.0964	21.0	3750	4.45	38,900
	15	Sapphire Whiskers	11.0	14.7	0.2040	0.403	2.504	0.0199	0.0964	17.0	3053	4.35	31,670
36	19	Tungsten Fibers	(2) 1.0	0.30	0.1915	0.498	2.865	0.0354	0.1296	27.4	4515	4.35	34,838
	20	Tungsten Fibers	(2) 1.0	0.30	0.2022	0.403	2.503	0.0244	0.1195	14.8	2690	5.22	22,510
	21	Tungsten Fibers	(2) 1.0	0.30	0.2022	0.402	2.504	0.0245	0.1199	20.7	3788	5.22	31,593
	22	Tungsten Fibers	(2) 1.0	0.30	0.2008	0.493	2.844	0.0332	0.1177	25.9	3925	3.63	33,347
37	23	Tungsten Fibers	(2) 2.0	0.56	0.2000	0.403	2.505	0.0266	0.1318	20.2	3975	5.08	30,159

Table 3-7 (page 2 of 2)

Sample Designation Group No.	No.	Material	Apparent Content Reinforcement Weight Percent	Apparent Content Reinforcement Volume Percent	Test Sample Dimensions (in.) Thickness	Test Sample Dimensions (in.) Width	Test Sample Dimensions (in.) Length	Weight (lb)	Bulk Density (lb/in.^{3})	Failure Load (lb)	Flexure Strength (psi)	(1) Apparent Young's Modulus (psi x 10^{-6})	Strength/ Density (in.)
37	24	Tungsten Fibers	(2) 2.0	0.56	0.2007	0.403	2.505	0.0287	0.1415	42.6	7888	6.79	55,746
	25	Tungsten Fibers	(2) 2.0	0.56	0.2010	0.403	2.507	0.0264	0.1313	29.4	5410	7.06	41,520
S-2	26	Standard ZrO_2	0.0	0.0	0.1980	0.403	2.504	0.0265	0.1328	17.0	3228	7.98	24,307
	27	No Reinforcement;	0.0	0.0	0.1990	0.403	2.507	0.0287	0.1426	27.6	5208	6.82	36,522
	28	100 parts ZrO_2	0.0	0.0	0.1983	0.403	2.502	0.0267	0.1332	21.3	4045	8.70	38,368
	29	16 parts Acid	0.0	0.0	0.1982	0.402	2.503	0.0265	0.1325	25.2	4272	8.69	32,242

(1) The modulus was measured with a deflectometer. Due to the deformation of the test fixture, it was necessary to multiply the measured modulus of elasticity by 1.45 to arrive at a true flexure modulus. This correction factor was arrived at by testing aluminum specimens of the same dimensions as the specimens used in this program. The flexure tests were performed on a 2-inch span using 3-point loading.

(2) Obtained by spectrographic semiquantitative analysis.

FOLDOUT FRAME 1

FOLDOUT FRAME 2

Table 3-8

PROPERTIES OF CHEMICALLY CONSOLIDATED ZIRCONIA*

Property	Range of Values	Average Value	Number of Tests
Flexure Strength (psi)	3,600 to 4,640	4,210	6
Tensile Modulus of Elasticity ($x10^{-6}$ psi)	8.6 to 12.5	10.25	8
Bulk Density ($lb/in.^3$)	----	0.137	---

*Reference 3-1, pp. 66, 105, 112 and 114)

3.3.1 Properties of Whisker- or Fiber-Strengthened ZrO_2

The properties of the final whisker- or fiber-strengthened, chemically consolidated zirconia are shown in Tables 3-9 and 3-10. Table 3-9 shows the room-temperature properties, while Table 3-10 shows the properties at 2,000°F. Also shown in these tables are: specimen geometry, specimen weight, theoretical and actual density of the material, fiber content, flexure strength, flexure modulus, and strength/density ratio. The results are also presented graphically in Figures 3-3, 3-4, 3-5, and 3-6. These figures show the variation in flexure strength with fiber content at temperatures of 70°F and 2,000°F.

Only the addition of silicon carbide whiskers has resulted in a significant increase in flexure strength at room temperature and at 2,000°F. At room temperature, the addition of 9.1-weight-percent† of silicon carbide whiskers to zirconia matrix increased the strength of zirconia by 55 percent. For the same composite, the flexure strength at 2,000°F was increased from 165 psi for unreinforced zirconia (Reference 3-1) to an average of 2,087 psi for silicon carbide reinforced zirconia. The highest flexure strength obtained at 2,000°F was 2,620 psi.

†The weight and volume fractions of whiskers are based on unreacted zirconia. For example, weight fraction of whiskers is equal to weight of whiskers, divided by weight of whiskers, plus weight of unreacted zirconia (no acid).

Table 3-9 (page 1 of 2)

ROOM TEMPERATURE FLEXURE PROPERTIES OF FIBER REINFORCED ZIRCONIA MATRIX

Sample Designation Group No.	No.	Reinforcing Material	(1) Apparent Content of Reinforcement Weight Percent	Volume Percent	Test Sample Dimensions (in.) Thickness	Width	Length	Weight (lb)	Bulk Density (lb/in^3) Estimated Theoretical	Actual	Failure Load (lb)	Flexure Strength (psi)	(2) Apparent Young's Modulus (psi x 10^{-6})	Strength/ Density (in.)	Failure Type and Location	Percent of Estimated Theoretical Density
38	30	Tungsten Fibers	(4) 11.3	3.5	0.2040	0.402	2.505	0.02932	0.1700	0.1427	33.4	6,000	7.54	42,046	Center	83.94
38	31	Tungsten Fibers	11.3	3.5	0.2033	0.403	2.502	0.02910	0.1700	0.1420	32.4	5,880	7.75	41,408	Center	83.53
38	32	Tungsten Fibers	11.3	3.5	0.2035	0.402	2.502	0.02976	0.1700	0.1454	36.3	6,560	7.97	45,117	Center	85.53
39	33	Tungsten Fibers	(4) 14.3	4.5	0.2038	0.402	2.503	0.02756	0.1738	0.1343	34.0	6,110	6.52	45,495	Center	77.27
39	34	Tungsten Fibers	14.3	4.5	0.2036	0.403	2.501	0.02711	0.1738	0.1322	32.2	5,790	(3) 7.50	43,797	Center	76.06
39	35	Tungsten Fibers	14.3	4.5	0.2030	0.402	2.505	0.02700	0.1738	0.1321	33.3	6,060	5.12	45,701	Center	76.00
41	36	SiC Whiskers	3.85	6.4	0.2018	0.403	2.502	0.02513	0.1578	0.1235	25.7	4,700	8.34	38,057	Center	78.26
41	37	SiC Whiskers	3.85	6.4	0.2030	0.403	2.503	0.02601	0.1578	0.1270	27.4	4,950	8.50	38,976	Center	80.48
41	38	SiC Whiskers	3.85	6.4	0.2028	0.403	2.507	0.02689	0.1578	0.1312	33.0	5,960	8.21	45,427	Center	83.14
40-1	39	SiC Whiskers	7.4	12.1	0.2023	0.399	2.507	0.02337	0.1555	0.1155	22.0	4,050	6.25	35,065	Center	74.28
40-1	40	SiC Whiskers	7.4	12.1	0.2023	0.400	2.502	0.02326	0.1555	0.1149	23.3	4,290	4.85	37,337	Center	73.89
40-1	41	SiC Whiskers	7.4	12.1	0.2028	0.401	2.505	0.02271	0.1555	0.1115	26.5	4,820	6.82	43,229	Center	71.70
40-2	42	SiC Whiskers	7.4	12.1	0.2020	0.401	2.507	0.02273	0.1555	0.1128	39.6	7,244	6.56	64,220	Center	72.54
40-2	43	SiC Whiskers	7.4	12.1	0.2015	0.401	2.506	0.02205	0.1555	0.1086	36.2	6,663	7.61	61,353	Center	69.84
40-2	44	SiC Whiskers	7.4	12.1	0.2013	0.401	2.505	0.02293	0.1555	0.1133	30.0	5,556	6.33	49,038	Center	72.86
42	45	SiC Whiskers	9.1	14.7	0.2030	0.402	2.508	0.02337	0.1547	0.1142	35.0	6,400	(3) 7.50	56,042	Center	73.82
42	46	SiC Whiskers	9.1	14.7	0.2038	0.402	2.504	0.02315	0.1547	0.1129	30.0	5,390	5.32	47,741	Center	72.97
42	47	SiC Whiskers	9.1	14.7	0.2038	0.402	2.502	0.02370	0.1547	0.1156	42.4	7,620	8.34	65,917	Center	74.72
43	54	Sapphire Whiskers	1.96	2.7	0.2018	0.402	2.503	0.02359	0.1588	0.1162	22.4	4,095	(3) 4.92	35,241	Center	73.17
43	55	Sapphire Whiskers	1.96	2.7	0.1805	0.389	2.035	0.01797	0.1588	0.1258	17.0	3,010	(5) 8.30	23,927	Center	79.22
43	56	Sapphire Whiskers	1.96	2.7	0.1808	0.392	1.893	0.01642	0.1588	0.1224	20.0	3,515	(5) 8.02	28,717	Center	77.08
44	57	Sapphire Whiskers	3.85	5.2	0.2020	0.393	2.555	0.02039	0.1586	0.1005	18.4	2,585	(5) 3.82	25,721	Center	63.37
44	58	Sapphire Whiskers	3.85	5.2	0.2015	0.393	2.530	0.02028	0.1586	0.1012	20.0	2,830	(5) 4.61	27,964	Center	63.81

FOLDOUT FRAME 1

FOLDOUT FRAME 2

Table 3-9 (page 2 of 2)

Sample Designation Group No.	No.	Reinforcing Material	(1) Apparent Content of Reinforcement Weight Percent	Volume Percent	Test Sample Dimensions (in.) Thickness	Width	Length	Weight (lb)	Bulk Density (lb/in^3) Estimated Theoretical	Actual	(2) Failure Load (lb)	Flexure Strength (psi)	Apparent Young's Modulus (psi x 10^{-6})	Strength/ Density (in.)	Failure Type and Location	Percent of Estimated Theoretical Density
44	59	Sapphire Whiskers	3.85	5.2	0.2008	0.512	2.085	0.02513	0.1586	0.1172	21.0	2,295	(5) 5.06	19,582	Center	73.90
45	60	Sapphire Whiskers	5.7	7.6	0.1970	0.489	2.850	0.02711	0.1583	—	21.2	2,510	(5) 5.07	25,431	Center	—
45	61	Sapphire Whiskers	5.7	7.6	0.2017	0.401	2.501	0.02513	0.1583	0.1241	22.5	4,140	(3) 4.72	33,360	Center	78.40
45	62	Sapphire Whiskers	5.7	7.6	0.2012	0.401	2.502	0.02467	0.1583	0.1214	24.2	4,480	(3) 5.36	36,903	Center	76.69
S-3	48	Standard ZrO_2 (6)	00.0	0.00	0.2020	0.402	2.504	0.02623	0.1590	0.1290	26.0	4,750	5.85	36,822	Center	81.13
S-3	49	Standard ZrO_2	00.0	0.00	0.2020	0.402	2.502	0.02667	0.1590	0.1312	20.0	3,660	5.95	27,896	Center	82.52
S-3	50	Standard ZrO_2	00.0	0.00	0.2023	0.401	2.185	0.02238	0.1590	0.1267	27.0	4,940	6.15	38,990	Center	79.69
S-5	51	Standard ZrO_2	00.0	0.00	0.2022	0.409	2.506	0.02821	0.1590	0.1388	23.7	4,335	8.56	31,232	Center	87.30
S-5	52	Standard ZrO_2	00.0	0.00	0.2018	0.407	2.507	0.02579	0.1590	0.1272	9.7	1,785	No Data Available	14,033	Center	80.00
S-5	53	Standard ZrO_2	00.0	0.00	0.2020	0.408	2.507	0.02734	0.1590	0.1344	18.0	3,293	4.89	24,501	Center	84.53

(1) Weight and volume percent based on zirconia content only - weight or volume of fibers divided by sum of fibers and zirconia.

(2) Flexure test performed on two-inch span three-point loading, except for specimen 50-55 which were tested using 1.5-inch span.

(3) Obtained from strain gage data and also deflectometer measurement.

(4) Obtained by digestion in H_2O_2.

(5) Obtained from deflectometer measurement (corrected).

(6) Standard ZrO_2 specimens contained 100 parts ZrO_2 and 32 parts acid

FOLDOUT FRAME 1

FOLDOUT FRAME 2

Table 3-10 (page 1 of 2)

FLEXURE PROPERTIES OF FIBER REINFORCED ZIRCONIA MATRIX AT TEMPERATURE OF 2, 000°F (1, 093°C) (1) (2)

Sample Designation			(1) Apparent Content of Reinforcement		Test Sample Dimensions (in.)				Bulk Density (lb/in^3)		(2)					
Group No.	No.	Reinforcing Material	Weight Percent	Volume Percent	Thickness	Width	Length	Weight (lb)	Estimated Theoretical	Actual	Failure Load (lb)	Flexure Strength (psi)	Apparent Young's Modulus (psi x 10^{-6})	Strength/ Density (in.)	Failure Type and Location	Percent of Estimated Theoretical Density
37	63	Tungsten Fibers	2.0	0.56	0.2010	0.403	2.505	0.02866	0.1613	0.1414	5.5	990	N.O.	7,001	Center	87.66
37	64	Tungsten Fibers	2.0	0.56	0.1983	0.403	2.504	0.02778	0.1613	0.1389	5.0	948	N.O.	6,825	Center	86.11
37	65	Tungsten Fibers	2.0	0.56	0.2007	0.403	2.505	0.02888	0.1613	0.1426	2.0	370	N.O.	2,595	Center	88.41
39	66	Tungsten Fibers	14.3	4.5	0.2032	0.402	2.504	0.02712	0.1738	0.1325	1.5	271	N.O.	2,045	Center	76.24
39	67	Tungsten Fibers	14.3	4.5	0.2036	0.402	2.502	0.02668	0.1738	0.1304	0.6	108	N.O.	828	Center Large Void	75.02
39	68	Tungsten Fibers	14.3	4.5	0.2027	0.402	2.500	0.02712	0.1738	0.1330	1.0	182	N.O.	1,368	Center	76.52
41	69	SiC Whiskers	3.85	6.4	0.2020	0.403	2.501	0.02425	0.1578	0.1194	5.0	915	N.O.	7,663	Near Edge	75.67
41	70	SiC Whiskers	3.85	6.4	0.2030	0.403	2.503	0.02557	0.1578	0.1250	7.8	1410	N.O.	11,280	Center	79.21
41	71	SiC Whiskers	3.85	6.4	0.2026	0.403	2.501	0.02557	0.1578	0.1254	8.0	1455	N.O.	11,603	Center	79.47
40	72	SiC Whiskers	7.4	12.1	0.2017	0.401	2.506	0.02249	0.1555	0.1110	7.9	1445	N.O.	13,018	End	71.38
40	73	SiC Whiskers	7.4	12.1	0.2020	0.401	2.506	0.02293	0.1555	0.1128	10.5	1933	N.O.	17,137	Center	72.54
40	74	SiC Whiskers	7.4	12.1	0.2023	0.401	2.501	0.02359	0.1555	0.1163	9.5	1738	N.O.	14,944	Center	74.79
42	75	SiC Whiskers	9.1	14.7	0.2035	0.403	2.502	0.02337	0.1547	0.1140	9.7	1743	2.10	15,289	Near Edge Excess Porosity	73.69
42	76	SiC Whiskers	9.1	14.7	0.2032	0.403	2.503	0.02315	0.1547	0.1130	14.5	2620	1.42	23,186	Center	73.04
42	77	SiC Whiskers	9.1	14.7	0.2022	0.402	2.502	0.02315	0.1547	0.1136	10.5	1898	1.36	16,708	Center, Excessive Porosity	73.43
43	78	Sapphire Whiskers (Type 3B)	1.96	2.7	0.2012	0.401	2.501	0.02315	0.1588	0.1145	2.0	370	N.O.	3,231	Center	72.10

FOLDOUT FRAME

FOLDOUT FRAME 2

Table 3-10 (page 2 of 2)

Sample Designation Group No.	No.	Reinforcing Material	(1) Apparent Content of Reinforcement Weight Percent	Volume Percent	Test Sample Dimensions (in.) Thickness	Width	Length	Weight (lb)	Bulk Density (lb/in^3) Estimated Theoretical	Actual	(2) Failure Load (lb)	Flexure Strength (psi)	Apparent Young's Modulus (psi x 10^{-6})	Strength/ Density (in.)	Failure Type and Location	Percent of Estimated Theoretical Density
43	79	Sapphire Whiskers (Type 3B)	1.96	2.7	0.2015	0.401	2.500	0.02381	0.1588	0.1178	2.0	370	N.O.	3,141	Center	74.18
43	80	Sapphire Whiskers (Type 3B)	1.96	2.7	0.2012	0.401	2.502	0.02370	0.1588	0.1174	2.0	370	N.O	3,152	Excessive Deformation	73.93
44	81	Sapphire Whiskers (Type 3B)	3.85	5.2	0.2015	0.401	2.503	0.02458	0.1586	0.1219	3.5	645	N.O	5,291	Center	76.86
44	82	Sapphire Whiskers (Type 3B)	3.85	5.2	0.2015	0.401	2.502	0.02403	0.1586	0.1187	3.6	660	N.O.	5,560	Center	74.84
44	83	Sapphire Whiskers (Type 3B)	3.85	5.2	0.2020	0.401	2.503	0.02436	0.1586	0.1203	2.2	395	N.O.	3,283	Center, Minute Burnout	75.85
45	84	Sapphire Whiskers (Type 3B)	5.7	7.6	0.2012	0.401	2.503	0.02480	0.1583	0.1229	2.6	480	N.O.	3,906	Center Large Voids	77.64
45	85	Sapphire Whiskers (Type 3B)	5.7	7.6	0.1992	0.401	2.501	0.02458	0.1583	0.1232	1.5	285	N.O.	2,313	Center Large Voids	77.83
45	86	Sapphire Whiskers (Type 3B)	5.7	7.6	0.2022	0.401	2.501	0.02458	0.1583	0.1213	2.0	365	N.O.	3,009	Center Large Voids	76.63

(1) Weight and volume percent based on zirconia content only - weight or volume of fibers divided by sum of fibers and zirconia.

(2) Flexure test performed on two inch span - three point loading. All elevated temperature tests were performed in Argon atmosphere.

N.O. Not obtained due to equipment problems with graphite fixture.

FOLDOUT FRAME 1

FOLDOUT FRAME 2

3.3.2 Selection of Optimum Reinforcing Material

On the basis of the data shown in Figures 3-3, 3-4, 3-5, and 3-6, silicon carbide whiskers were selected as the most desirable material for strengthening of the ceramic. From the information shown in Figures 3-3 and 3-6, a 7.4-weight-percent (approximately 12-volume-percent) whisker content has been selected as the optimum amount for preparing additional specimens for the more complete characterization of the whisker-strengthened matrix.

3.4 CHARACTERIZATION OF OPTIMUM WHISKER-REINFORCED MATRIX

To characterize more completely the properties of chemically bonded zirconia reinforced with 7.4-weight-percent of silicon carbide whiskers, specimens were prepared for obtaining flexure strength and modulus, tensile strength and modulus, shear strength, and thermal expansion.

3.4.1 Preparation of SiC-Whisker-Strengthened Zirconia Matrix

The flexure, shear, and tensile specimen blocks were fabricated in wax-coated aluminum molds, 1-1/8 x 1-1/8 x 39 inches in size. The castings were separated by spaces 13 inches apart, permitting three blanks to be obtained from each casting. The blanks were machined into flexure specimens, shear specimens, and tensile specimens. (See Section 3.4.2 for a detailed description of specimen size and geometry.)

The matrix composition that was used in further evaluation of the optimum whisker-strengthened matrix, and also throughout the remainder of the program, is given in Table 3-11. The solid material was placed in a mortar and blended manually with a pestle; acid was then added and folded manually into the solids, with continual use of the pestle.

Technical difficulties caused the loss of many tensile specimens during curing and machining. Cracking of specimens, excessive porosity, fracture during machining, and foaming during initial casting were some of the loss factors.

The loss rate was decreased by: (1) increasing air circulation during curing, and (2) pre-machining of the metal flanges to eliminate chatter during the truing operation. Allowing the mix to react to an advanced stage before casting

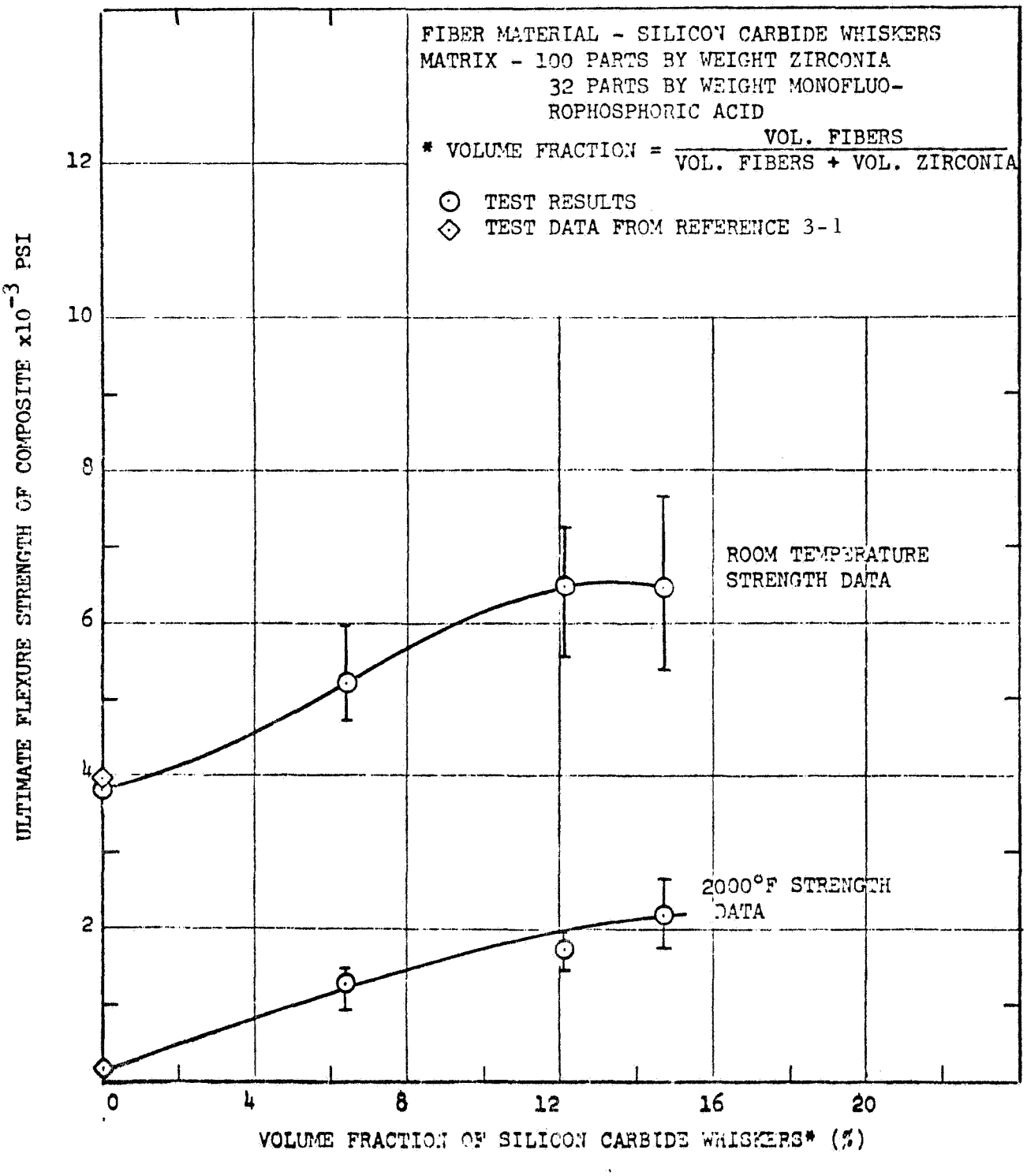

Figure 3-3. Flexure Strength of Chemically Consolidated Zirconia Strengthened with Silicon Carbide Whiskers

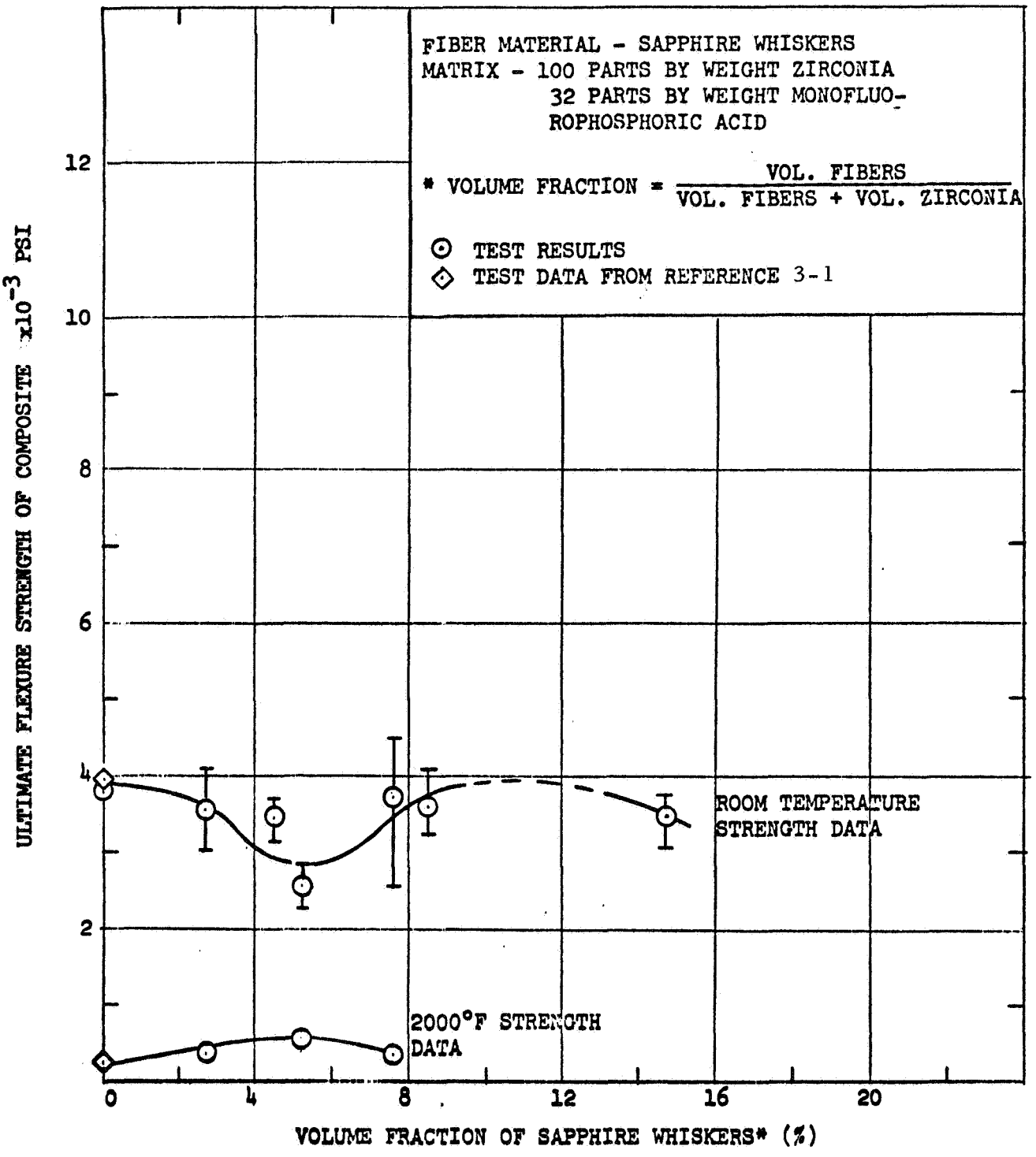

Figure 3-4. Flexure Strength of Chemically Consolidated Zirconia Strengthened With Sapphire Whiskers

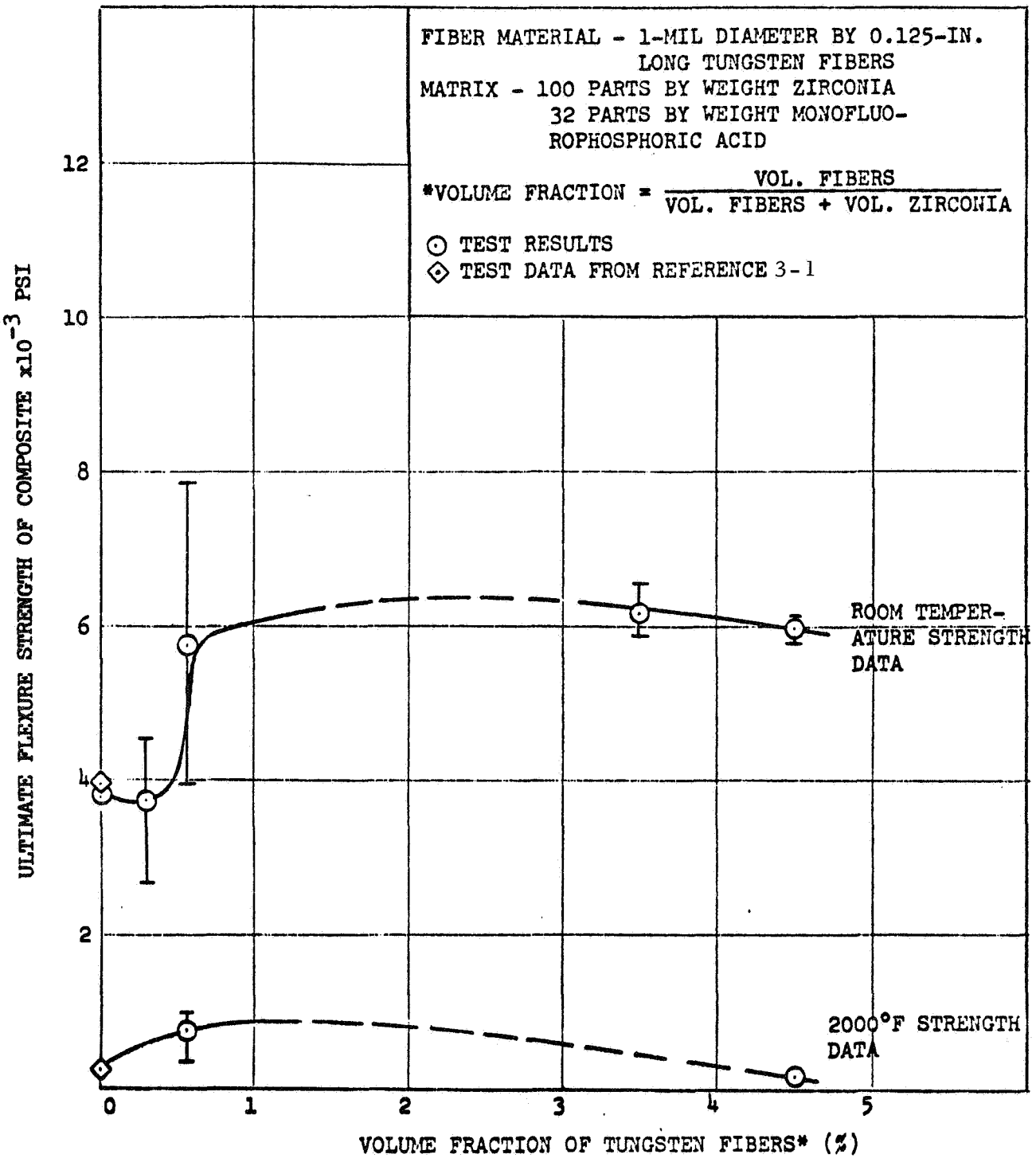

Figure 3-5. Flexure Strength of Chemically Consolidated Zirconia Strengthened with Tungsten Fibers

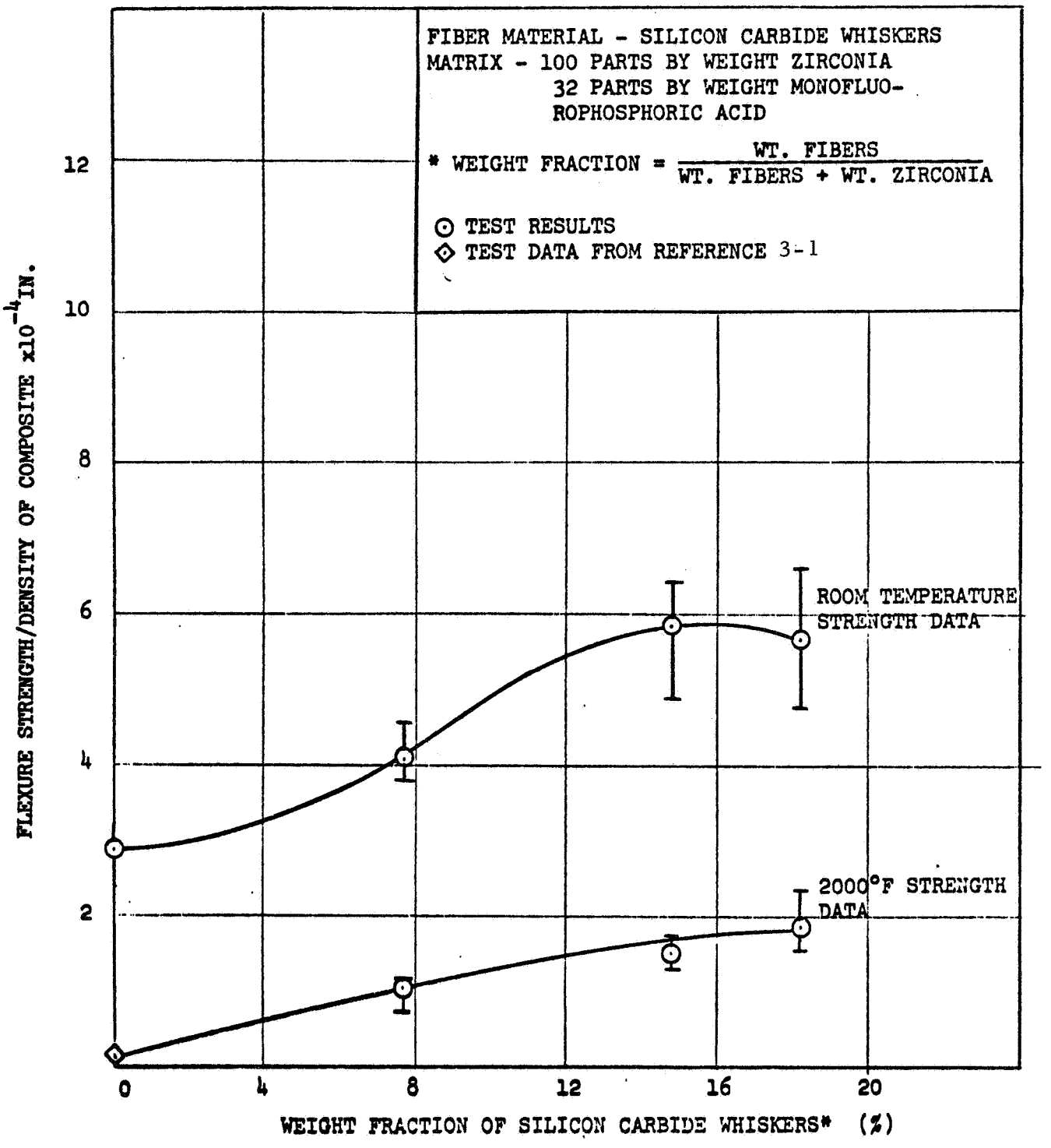

Figure 3-6. Specific Flexure Strength of Chemically Consolidated Zirconia Strengthened With Silicon Carbide Whiskers

Table 3-11

COMPOSITION OF CHEMICALLY CONSOLIDATED, WHISKER-STRENGTHENED ZIRCONIA

Material	Parts by Weight	Weight Percent
CaO Stabilized Zirconium Oxide (-70 + 200 mesh - Norton Company)	60	55.6
CaO - Stabilized Zirconium Oxide (-325 mesh - Norton Company)	40	37.0
Silicon Carbide Whiskers (Carborundum Company)	8	7.4
		100.0
Monofluorophosphoric Acid (Specific gravity of 1.80 gmcc; Ozark-Mahoning Company)	32	

reduced the number of large-size voids. The first stage in the curing process requires the evolution of H_2O and HF at room temperature before surface gelling. In this stage, vibration of the mix to a low viscosity for 30 minutes prior to casting aids in the evolution of the gases. The mix was cast into a vibrating mold. More gaseous products are formed during the curing from room temperature to 212°F. This curing period (Table 3-12) was doubled to permit more complete evolution of the gases. Fewer large voids appeared in samples processed in this manner.

3.4.2 Specimen Testing

Tension, flexure, shear, and thermal expansion tests were performed on the SiC-whisker-strengthened matrix. Test methods employed previously (Reference 3-1) were used. For completeness of the report, these are described in the following subsections.

Table 3-12

CURING SCHEDULE FOR CHEMICALLY CONSOLIDATED, SiC-WHISKER-STRENGTHENED ZIRCONIA

Temperature		
^{o}F	^{o}C	Period (Hours)
100	38	2
130	54	2
180	82	2
212	100	4
300	149	2
300-600	149 to 316	2
600	316	1

Tensile Tests

A dog-bone type of specimen (Figure 3-7), similar to that described in ASTM E3-61T, was used to test specimens at both room and elevated temperatures. Since the grips were not subjected to high temperature, it was possible to reduce fabrication costs by bonding metallic shoulders onto the specimen ends with epoxy adhesives.

Precise alignment of the specimen with the grips was possible using the gripping and alignment fixture shown in Figure 3-8. The alignment of the system was based on a completely rigid load train operating through a special die set. The grips act through aligned holes in the die set, thus minimizing lateral movement during the test.

The furnace used for heating the tensile specimens consisted of a water-cooled shell with three graphite resistance-heating elements. Fire-brick insulation was used to minimize the heat loss to the water-cooled shell. Since it was necessary to protect the graphite from oxidation, argon gas was introduced into the furnace during the tests. A chromel-alumel thermocouple was

NOTE: 1. TOL. FRACTIONS ± 1/16, DECIMALS ± .020.
2. ALL DIAMETERS CONCENTRIC TO .0005".
3. 1 1/2" COLLAR IS BONDED TO SPECIMEN

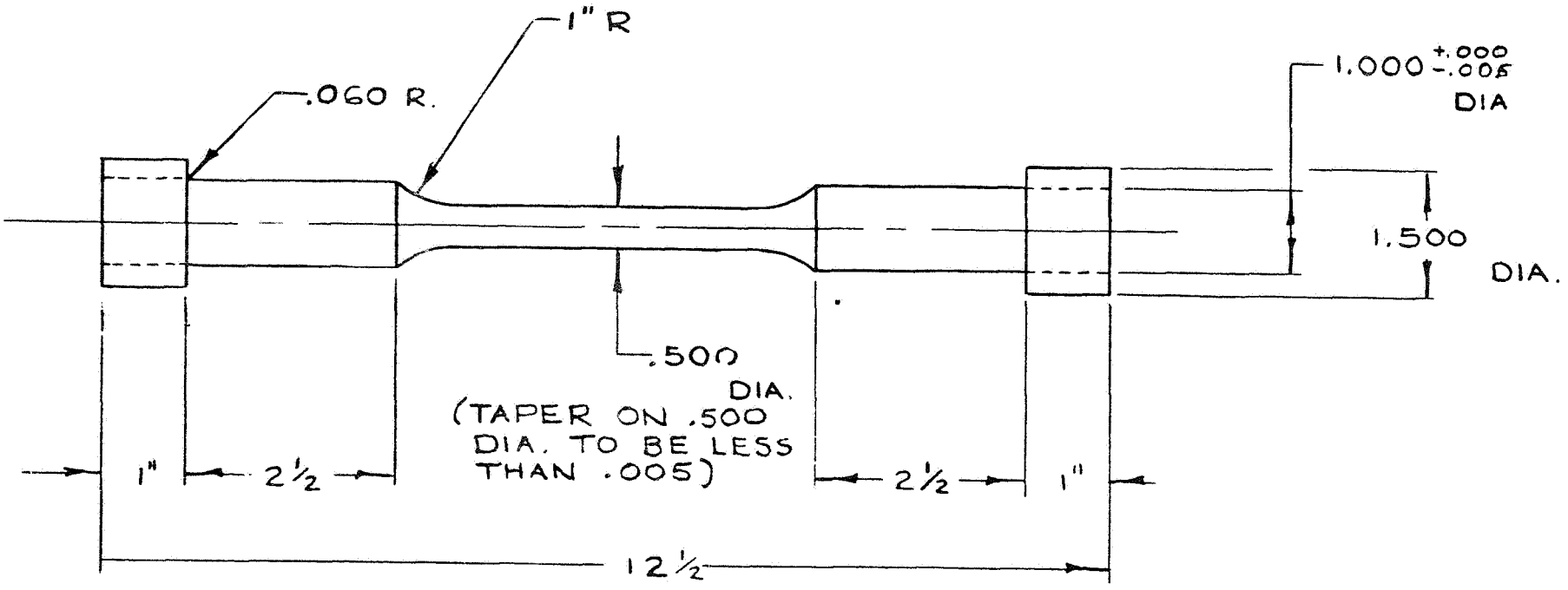

Figure 3-7. Tensile Specimen

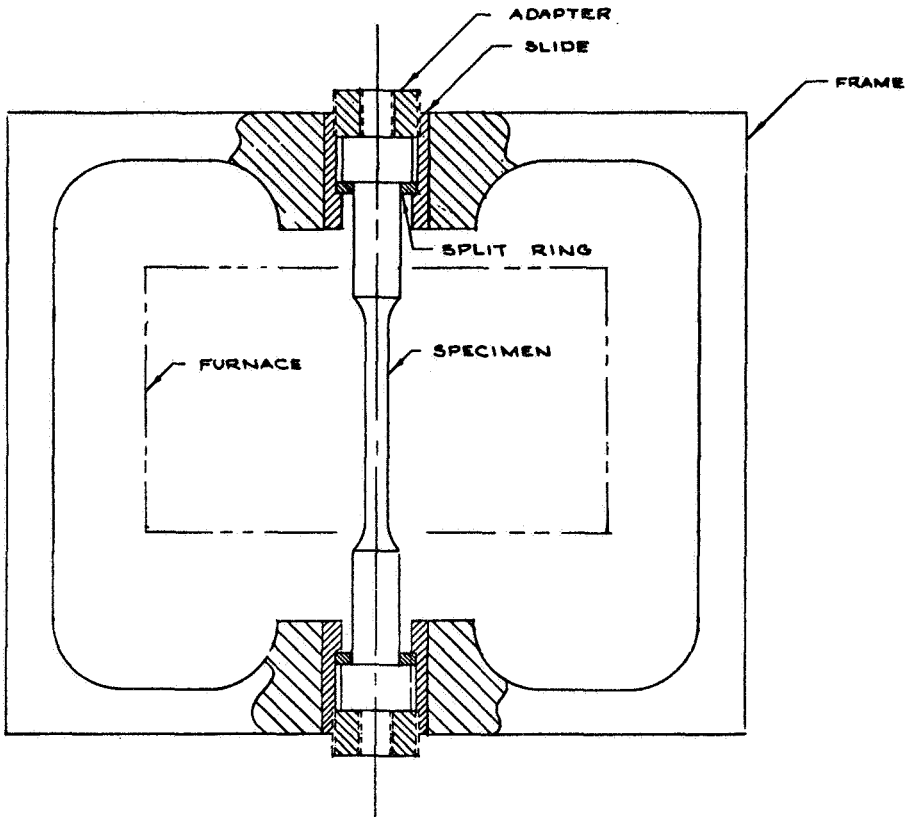

Figure 3-8. Tensile Test Alignment Fixture

cemented to the specimen to monitor the temperature. A photograph of the tensile test furnace is shown in Figure 3-9.

Strain measurements at room temperature were made using strain gages located 180° apart in the test section. Two strain gages were used to detect any misalignment caused by improper seating in the grips. The Optron optical extensometer was used for elevated-temperature tensile tests. Figure 3-10 is a photograph showing the Optron in place for a test.

Flexure Tests

Flexure tests, using three-point loading as shown in Figure 3-11, were performed on specimens measuring 4-1/2 x 1 x 1/4 inches. The distance between supports was 4 inches. A heating unit (shown in Figure 3-12) was used to perform elevated-temperature tests (70°F to 2,000°F). The specimens were radiantly heated by six graphite,. resistance-heating elements. The same temperature monitoring method as employed for the tensile tests was used. All high-temperature tests were conducted in an argon atmosphere. Autographic recordings of load as a function of beam deflection were obtained

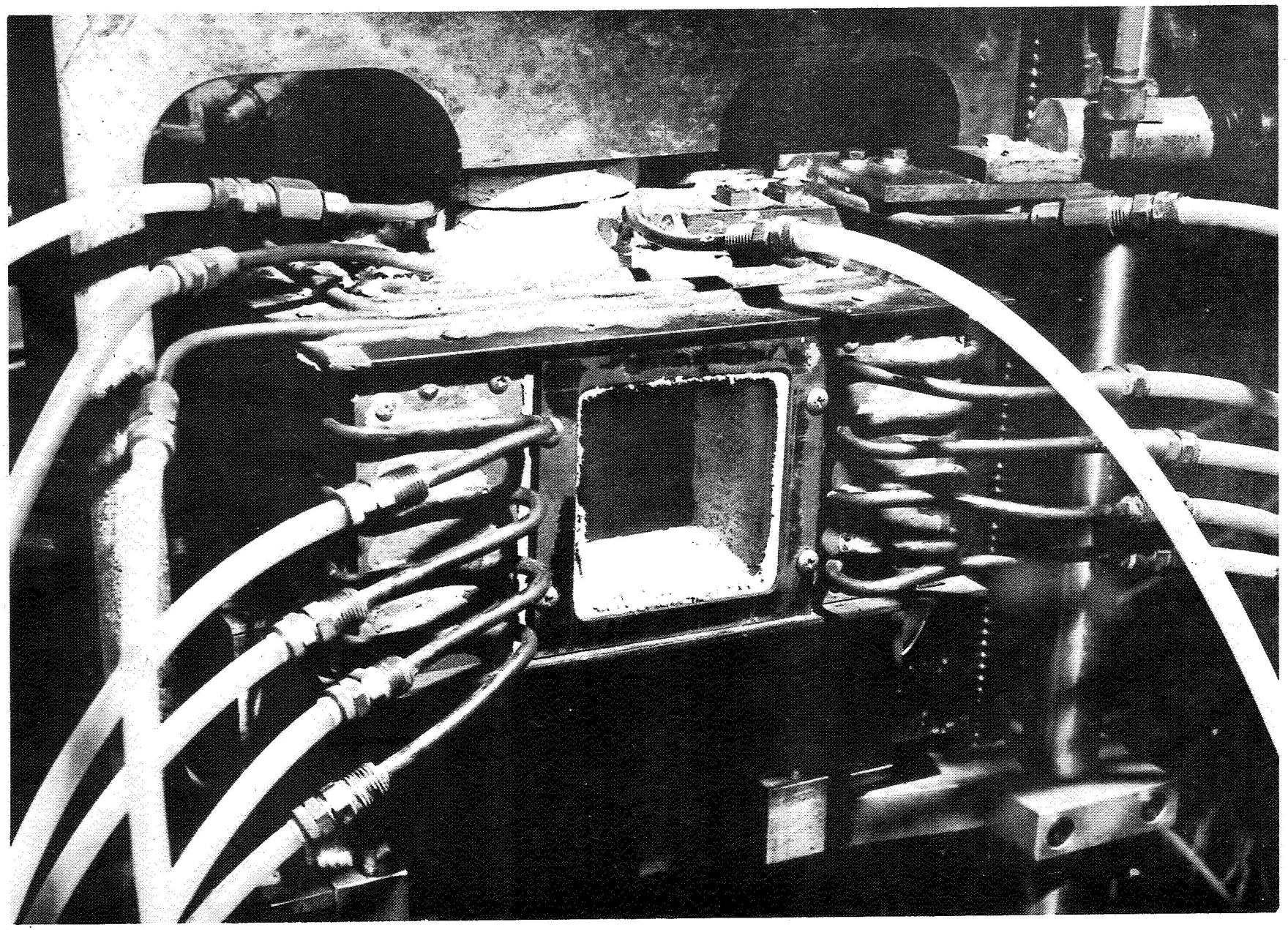

Figure 3-9. Tensile Test Furnace

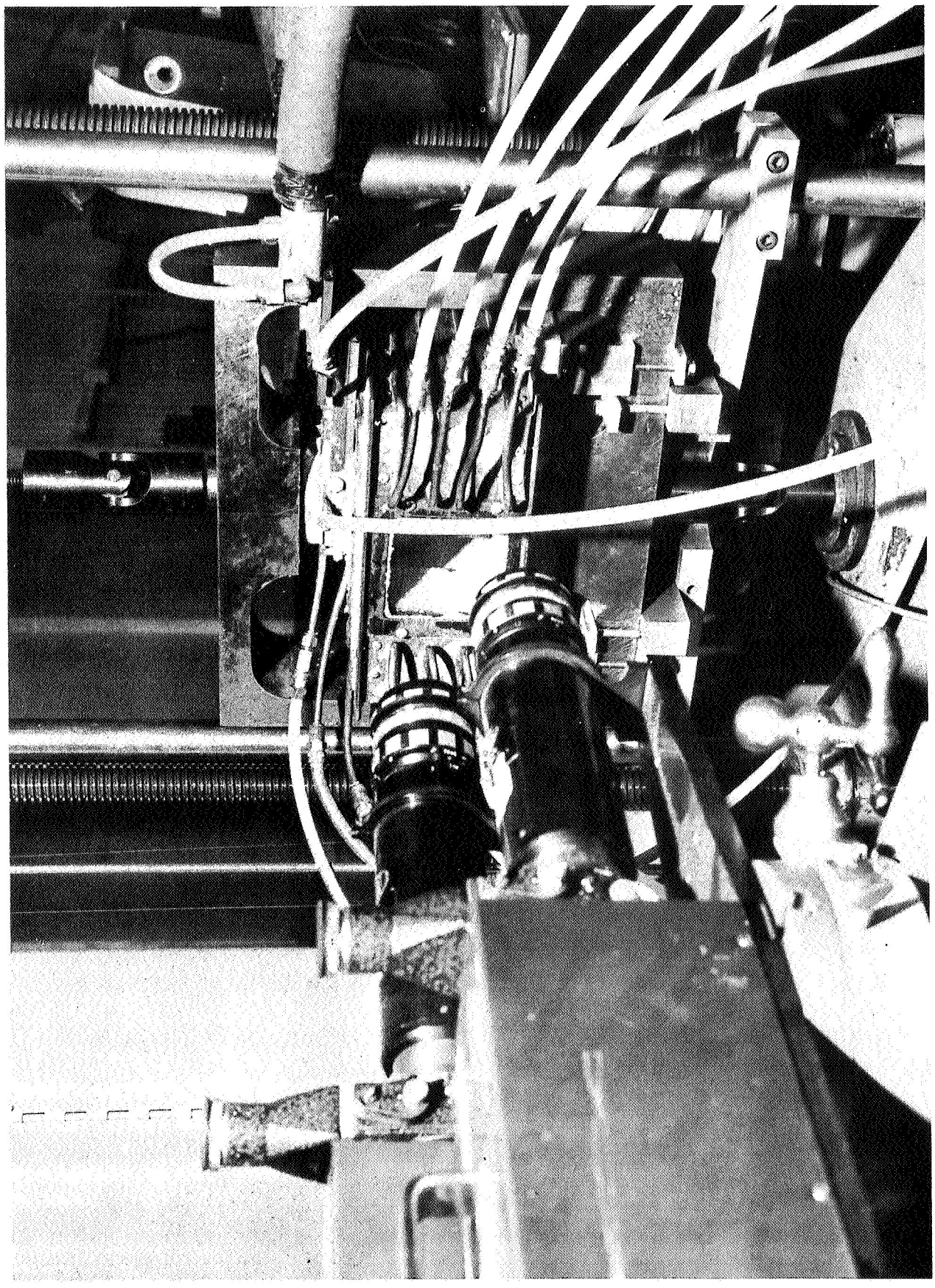

Figure 3-10. Optron Extensometer for Tensile Tests

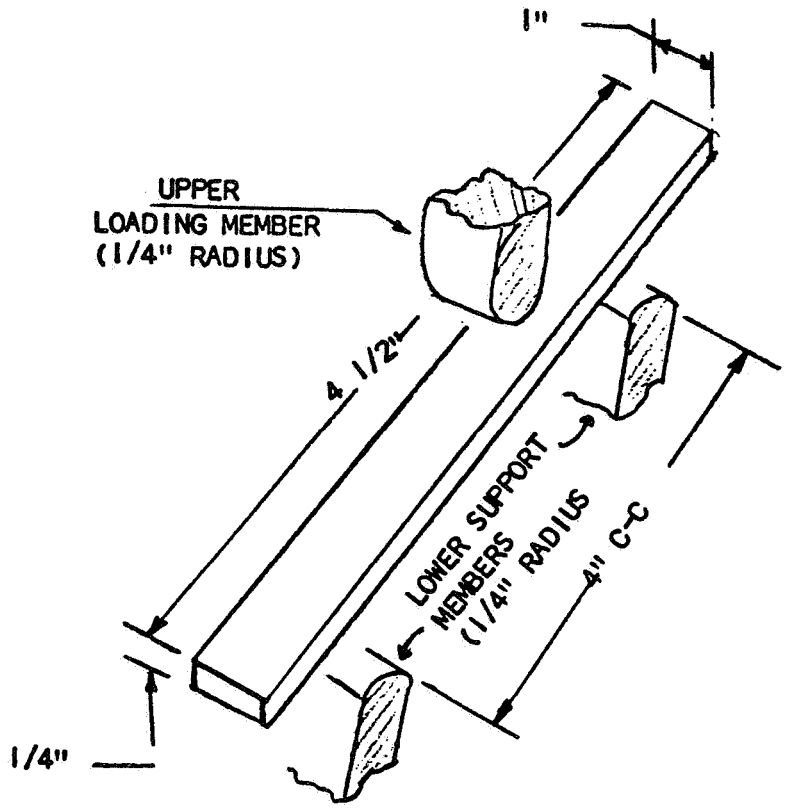

Figure 3-11. Flexural Testing of Specimens

using the Model 680 Optron optical extensometer. The load was plotted on the autographic recording by manually transmitting a signal at fixed load increments. A deflectometer was also used to obtain the load-deflection data. The measured data were used to compute stress, strain, and flexure modulus.

Shear Tests

In the shear testing, it was found that notching specimens at the shear planes was required to assure failure at the desired location (Figure 3-13). Previously it was found (Reference 3-1) that, without the notches, the specimens had a tendency to fail in bending at the midpoint between the shear planes. All shear tests were conducted with notched specimens.

The shear test fixture was composed of two pieces; the bottom, or solid piece, was 1 x 4-1/2 inches with a 1-inch cavity in the center. The top, or ram, was 1-inch square and applied the load across the entire section between the notches. The test fixture was made of graphite. The same furnace and temperature monitoring devices used for flexure tests were used for the shear tests.

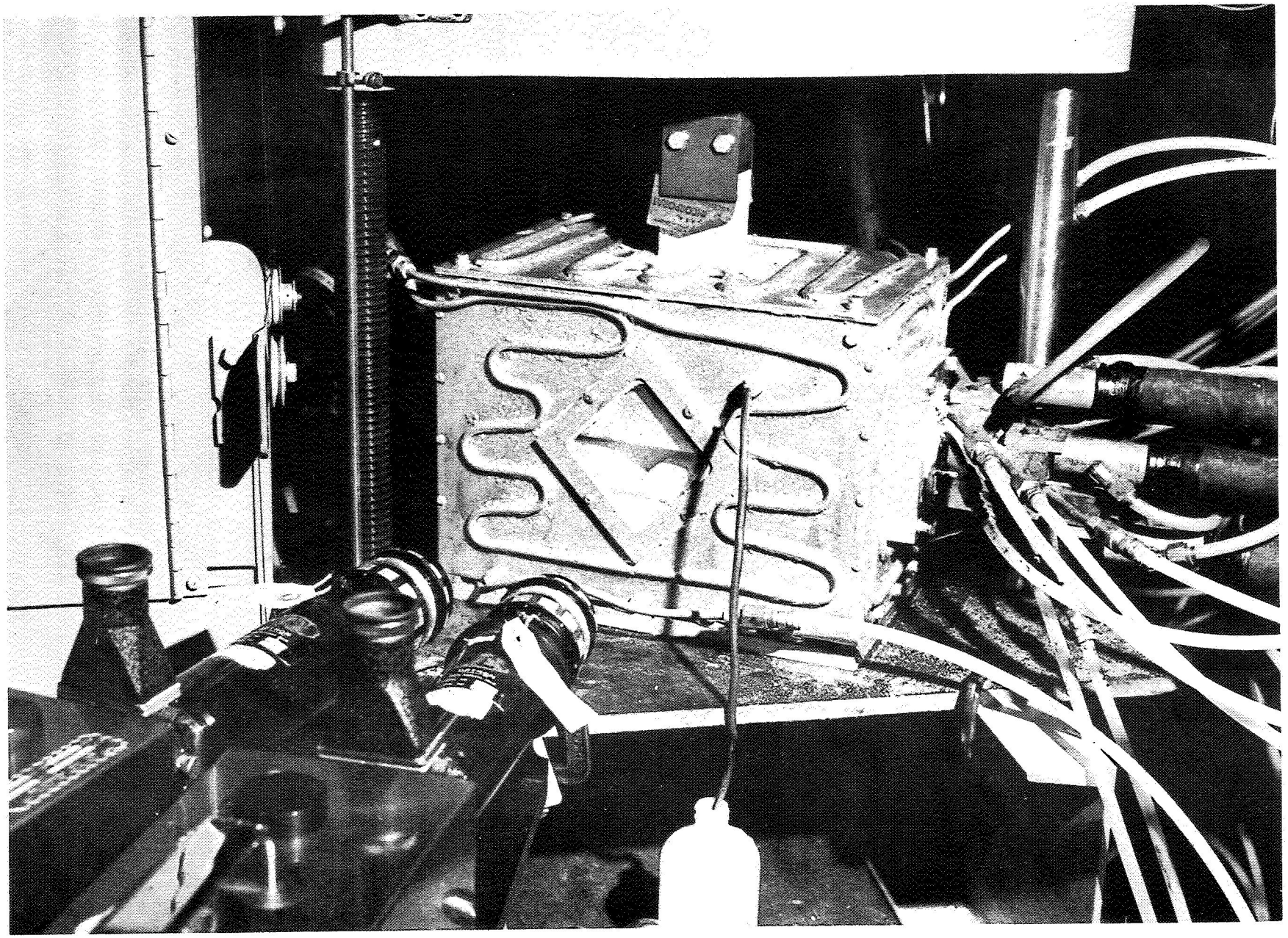

Figure 3-12. Flexure Test Furnace With Optron Extensometer

NOTE: 1. TOL. ± 1/16

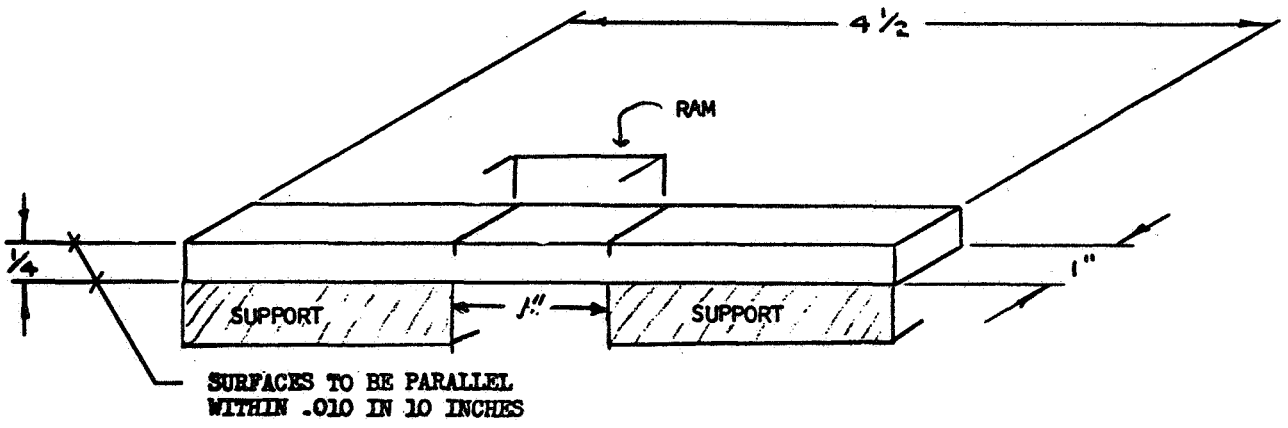

Figure 3-13. Shear Specimen

Thermal Expansion Tests

Thermal expansion of the specimens was measured using dual-image extensometers, and alumina and sapphire dilatometers. From 70°F to 1,500°F the thermal expansion was measured with a NETZSCH alumina dilatometer. Above 1,500°F thermal expansion was measured with a sapphire dilatometer and, as a rough check, with a Gaertner dual-image extensometer.

Up to 1,500°F, the test temperature was determined with a chromel alumel thermocouple attached to the specimen. Above 1,500°F, an optical pyrometer was used to determine temperature of the specimen with corrections made for emittance.

3.4.3 Properties of SiC-Whisker-Strengthened Zirconia

Using the test methods described in the previous section, tensile, flexure, shear, and thermal expansion properties at room and elevated temperatures were obtained for a zirconia matrix strengthened with 7.4-weight-percent of SiC whiskers.

Tensile Properties

Table 3-13 is a resume of the tensile test data obtained for the SiC-whisker-strengthened zirconia.

Flexure Properties

A summary of the flexure properties at room and elevated temperatures is shown in Table 3-14. The variations of flexure strength, Young's modulus, and strength-density with temperature are shown in Figures 3-14 and 3-15. Finally, Figure 3-16 shows a typical stress-strain curve for a SiC-whisker-strengthened zirconia tested at 75°F.

Shear Properties

Shear properties of the zirconia matrix, strengthened with SiC whiskers, are shown in Table 3-15. In view of the mode of failure, these data are considered questionable.

Thermal Expansion Properties

Figure 3-17 shows thermal expansion data measured with various techniques. Thermal expansion of SiC-whisker-strengthened zirconia is lower than the thermal expansion of plain ZrO_2.

3.4.4 Comments on Test Data

Flexure strengths of the SiC-whisker-strengthened, chemically consolidated zirconia with 32 parts monofluorophosphoric acid revealed during this study, are different from those of the unreinforced matrix (Reference 3-1, p. 112). At room temperature and 2,000°F, the whisker-strengthened matrix had higher flexure strength than the unreinforced ceramic; while at temperatures of 1,000°F and 1,500°F the reverse is true. There was no failure at a temperature of 1,500°F, but the samples deformed beyond the limits of the test equipment. At 2,000°F, the average flexure strength of whisker-reinforced ceramic was 1,520 psi as compared to 165 psi for a matrix without any whiskers (Reference 3-1). The presence of whiskers imparts some plasticity to the material. As shown in Figure 3-14 both the modulus and flexure strength curves show an unexplainable dip at 1,500°F.

Table 3-13

TENSILE PROPERTIES OF ZIRCONIA MATRIX CONTAINING SILICON CARBIDE WHISKERS[1]

Sample	Test Temperature (°F)	Test Temperature (°C)	Diameter of Gage Section (Inches)	Area of Gage Section (Inches)	Failure Load (lb)	Tensile Strength (lb/in.^{2})	Modulus of Elasticity[3] x 10^{-6} (lb/in.^{2})	Remarks
1	70	21	0.4980	0.1948	568.5	2,918	9.8	Dense
2	70	21	0.4097	0.1949	268.5	1,379	10.26	Broke in radius
3	70	21	0.5010	0.1971	284.5	1,433	10.5	Dense[2]
4	1,000	538	0.4984	0.1948	258.5	1,326		Large void and cracks[4]
5	1,000	538	0.4984	0.1948	373.5	1,918		Dense
6	1,000	538	0.5052	0.2003	515.5	2,573		Dense
7	1,500	815	0.4988	0.1948	368.5	1,893		Dense
8	1,500	815	0.5050	0.2003	91.5	457		One large void[5]
9	1,500	815	0.5013	0.1971	88.5	449		Dense, broke on radius
10	2,000	1,093	Furnace burned out, sample cracked[6]					Dense
11	2,000	1,093	Specimen failed at +1, 850°F (1, 010°C)[6]					Porous
12	2,000	1,093	Specimen failed at +1, 780°F (970°C)[6]					Dense

(1) The test samples contained 7.4-weight-percent of silicon carbide whiskers. The weight-percent is defined as the weight of whiskers divided by the weight of zirconia plus whiskers.

(2) This sample was made by casting new matrix onto matrix that was precured to 212°F (100°C). The sample broke normally in the gage length and did not break at the interface.

(3) Modulus data were obtained from resistance strain gages. For specimens 4 through 9, the instrumentation did not function properly and reliable strain data were not obtained.

(4) This void was about 40% of the area where the sample failed in the gage length.

(5) This void was about 50% of the area where the sample failed in the gage length.

(6) The weight of the fixture was 8.5 pounds.

Table 3-14

FLEXURE PROPERTIES OF ZIRCONIA MATRIX CONTAINING SILICON CARBIDE WHISKERS[1]

Sample Number	Test Temperature (°F)	Test Temperature (°C)	Test Sample Dimensions (in.) Thickness	Width	Length	Weight (lb)	(2) Bulk Density (lb/in.^{3}) Estimated Theoretical	Actual	Percent of Estimated Theoretical Density	Failure Load (lb)	Flexure Strength (lb/in.^{2})	(3) (4) Flexure Modulus x 10^{-6} (lb/in.^{2})	Strength/ Density (in.)	(5) Failure Type and Location
1	70	21	0.2545	1.009	4.635	0.1390	0.1555	0.1168	0.7511	59.0	5,410	(4) 8.36	46,318	Center
2	70	21	0.2560	1.004	4.560	0.1345	0.1555	0.1148	0.7383	62.0	5,780	(4) 7.57	50,348	Center
3	70	21	0.2543	1.009	4.630	0.1389	0.1555	(2a) 0.1170	0.7524	63.0	5,660	(4) 8.10	48,376	Center
4	1,000	538	0.2540	1.008	4.630	0.1325	0.1555	0.1117	0.7183	32.0	2,955	4.82	26,455	Center
5	1,000	538	0.2543	1.002	4.630	0.1345	0.1555	0.1140	0.7331	39.5	3,665	6.08	32,149	Center
6	1,000	538	0.2552	1.002	4.630	0.1367	0.1555	0.1155	0.7428	33.0	3,035	4.91	26,277	Center
7	1,500	815	0.2547	1.002	4.630	0.1345	0.1555	0.1138	0.7318	5.0	461	0.375	4,051	Excessive Deformation
8	1,500	815	0.2552	1.002	4.560	0.1367	0.1555	0.1142	0.7344	4.0	370	0.28	3,240	Excessive Deformation
9	1,500	815	0.2547	1.003	4.560	0.1280	0.1555	0.1072	0.6894	5.5	500	0.32	4,664	Excessive Deformation
10	1,500	815	0.2515	1.002	4.630	0.1281	0.1555	0.1099	0.7068	3.0	284	0.425	2,584	Excessive Deformation
11	1,500	815	0.2552	1.002	4.560	0.1323	0.1555	0.1105	0.7106	2.5	230	0.26	2,081	Excessive Deformation
12	2,000	1,093	0.2564	1.003	4.560	0.1325	0.1555	0.1130	0.7267	18.0	1,640	1.08	14,513	Center
13	2,000	1,093	0.2547	1.002	4.630	0.1345	0.1555	0.1138	0.7318	15.0	1,370	1.26	12,039	Center
14	2,000	1,093	0.2547	1.004	4.540	0.1323	0.1555	0.1140	0.7331	17.5	1,600	0.71	14,035	Center
15	2,000	1,093	0.2553	1.002	4.630	0.1389	0.1555	0.1173	0.7544	16.0	1,470	0.915	12,532	Center

(1) The test samples contained 7.4-weight-percent of silicon carbide whiskers. The weight percent is defined as the weight of whiskers divided by the weight of unbonded zirconia plus whiskers.

(2) The bulk density is the measured weight divided by the measured volume, the latter being calculated from the measured specimen dimensions.

(2a) Bulk density was also determined by ASTM C20 and found to be 0.1156 pound/cubic inch.

(3) The modulus was measured with a deflectometer, except as noted (See Note 4).
As to the deformation of the test fixture, it was necessary to multiply the measured modulus by 1.55 to arrive at a true flexure modulus. This correction factor was arrived at by testing aluminum specimens of the same dimensions as the specimens used in this program. Moreover, the same correction factor was also established by using strain gages and deflectometer on the ceramic specimens tested at room temperature.

(4) Obtained from strain gage data and also deflectometer measurement.

(5) Samples with excessive deformation did not fail - the test was aborted because of equipment limitations.

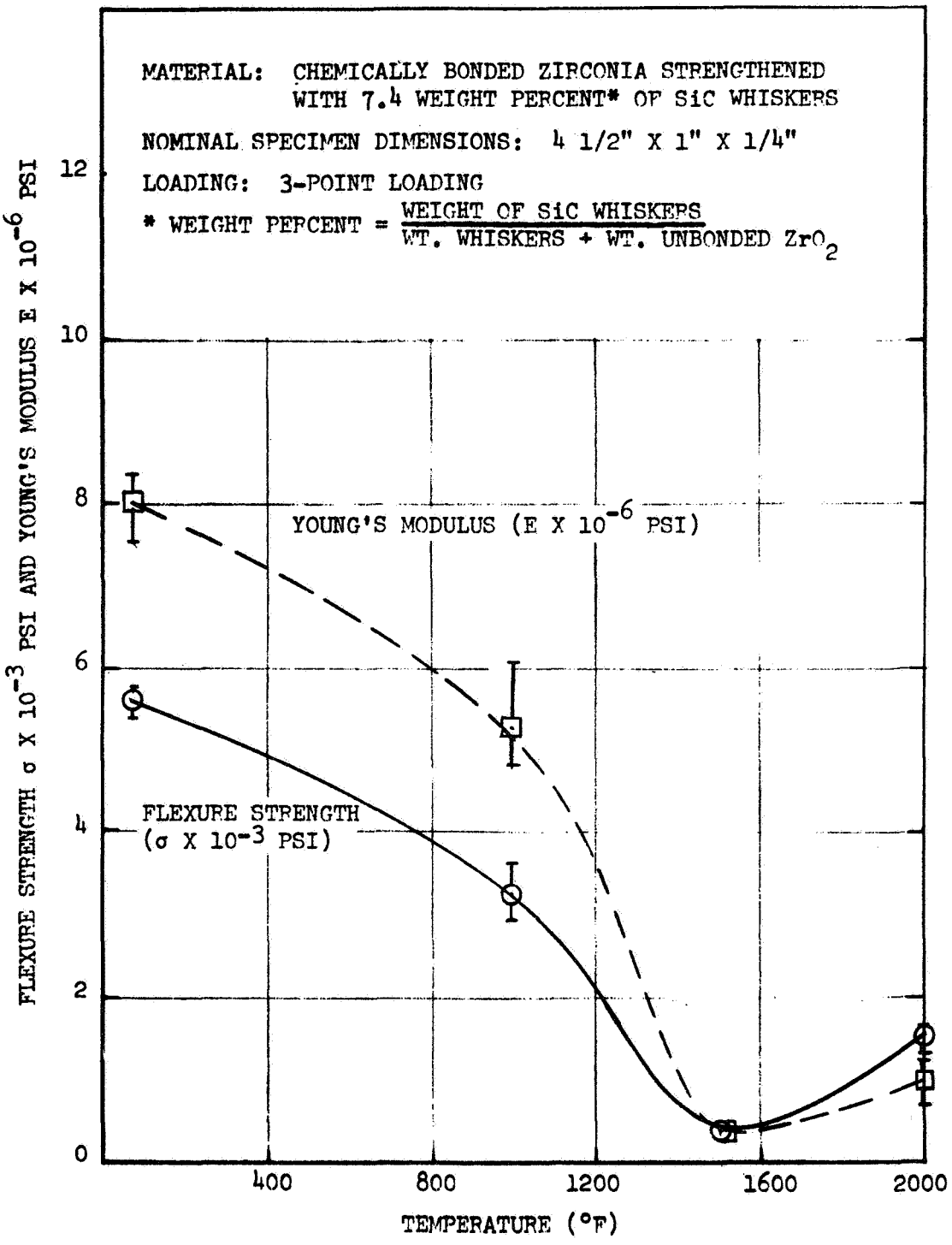

Figure 3-14. Flexure Strength and Young's Modulus of SiC-Whisker-Reinforced, Chemically Consolidated Zirconia as a Function of Temperature

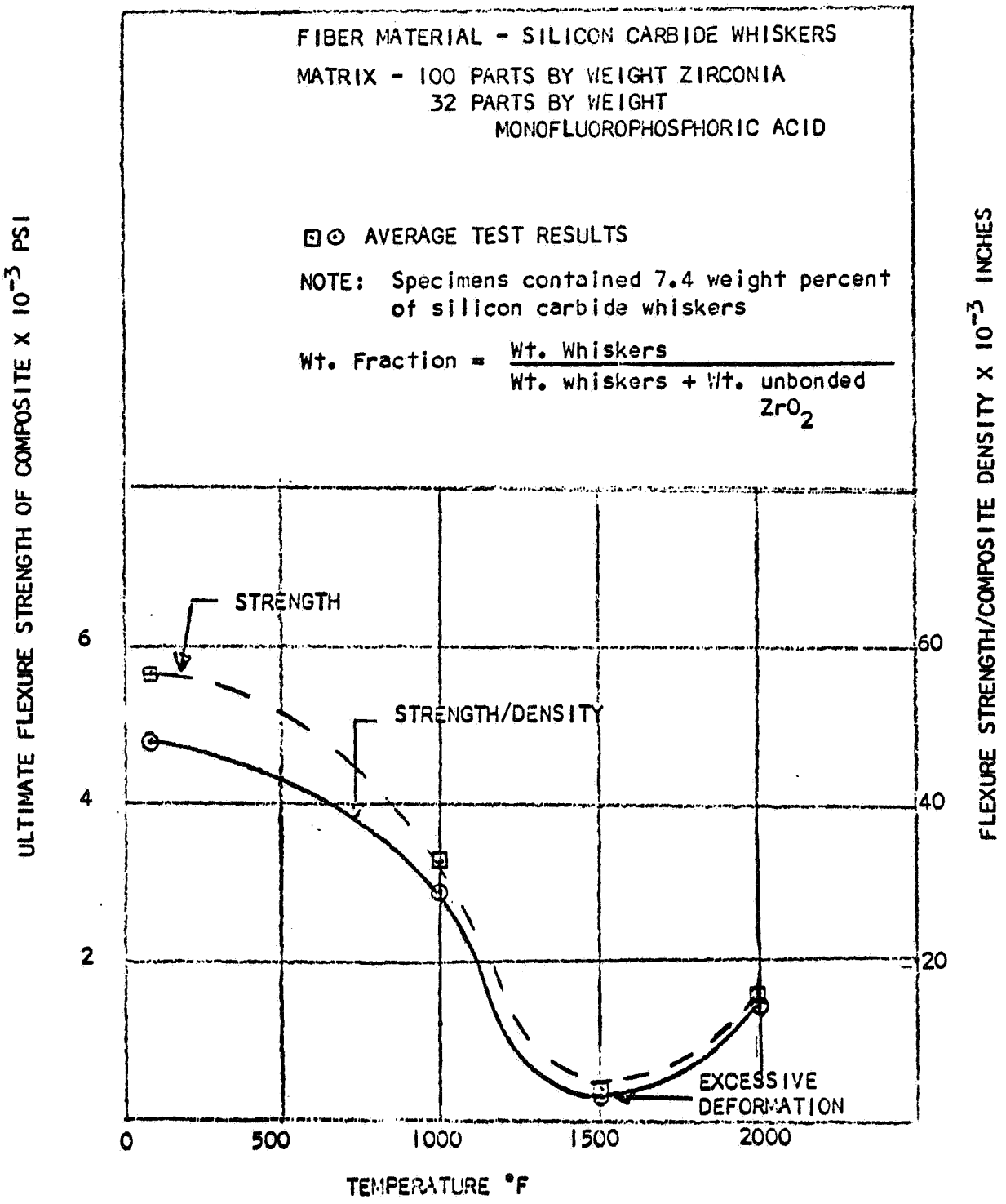

Figure 3-15. Flexure Strength of Sic-Whisker-Reinforced, Chemically Consolidated Zirconia as a Function of Temperature

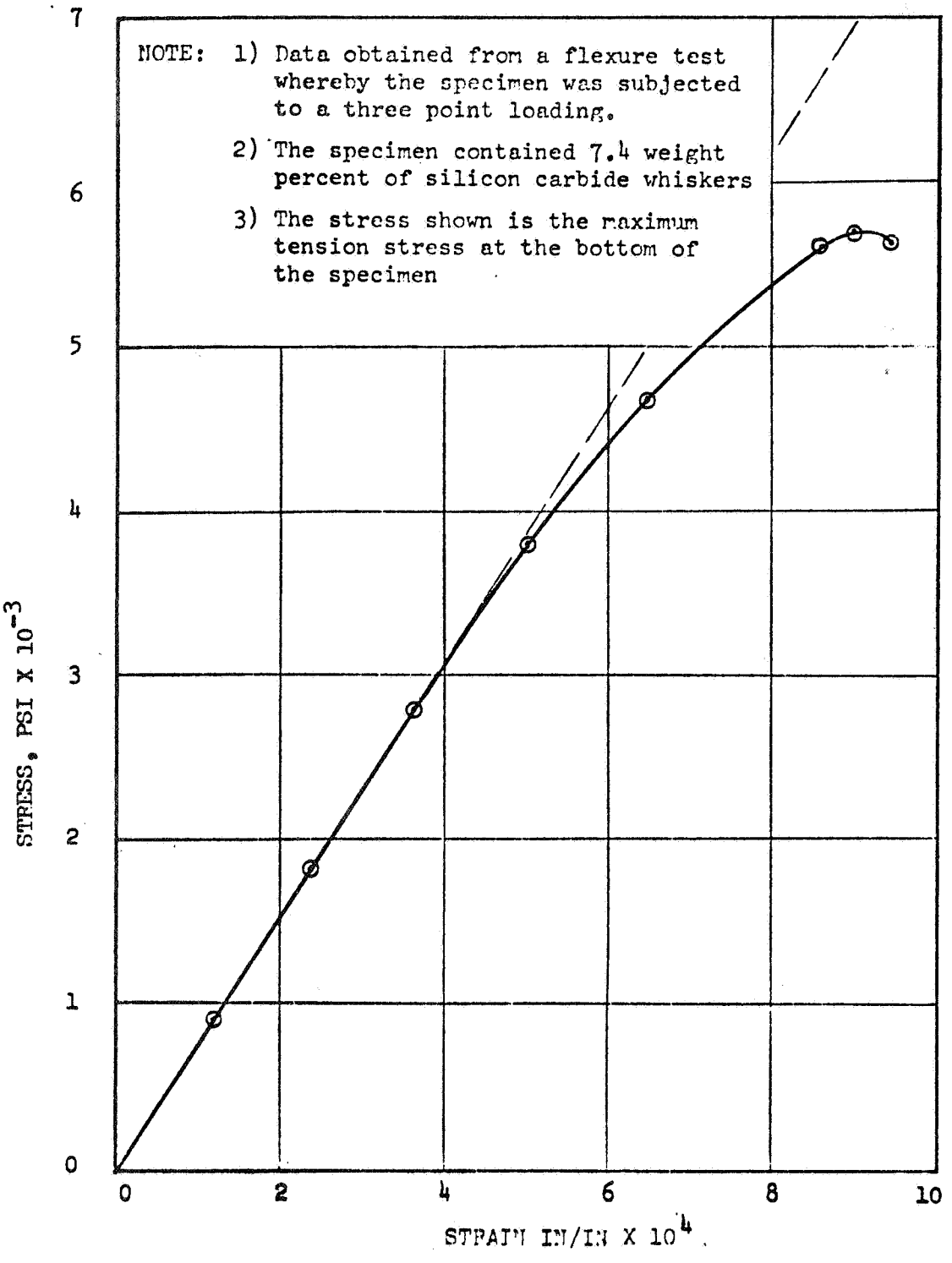

Figure 3-16. Typical Stress-Strain Curve for SiC-Whisker-Reinforced, Chemically Bonded Zirconia (Room-Temperature Data)

Table 3-15

SHEAR PROPERTIES OF ZIRCONIA MATRIX CONTAINING SILICON CARBIDE WHISKERS

Sample Number	Test Sample Dimensions: Temperature (°F)	(°C)	Thickness (In.)	Width (In.)	Area (In.^{2})	Load (Lb)	Shear Stress (PSI)	Comments
1	70	21	0.1332	1.003	0.268	110.0	410	Failed, singly
2	70	21	0.1319	1.003	0.267	105.0	393	Failed, singly
3	70	21	0.1315	1,003	0.267	116.0	434	Failed, singly
4	1,000	538	0.1306	1.002	0.267	114.0	427	Failed, singly
5	1,000	538	0.1314	1.002	0.267	72.0	270	Failed, singly
6	1,000	538	0.1333	1.003	0.272	74.0	272	Failed, singly
7	1,500	815	0.1289	1.002	0.262	86.0	328	Failed, singly
8	1,500	815	0.1322	1.002	0.263	80.0	300	Failed, singly. Plastic Deformation
9	1,500	815	0.1313	1.002	0.267	136.0	517	Failed, doubly
10	2,000	1,093	0.1324	1.003	0.266	126.0	474	Failed, singly
11	2,000	1,093	0.1324	1.002	0.265	85.0	321	Failed, doubly
12	2,000	1.093	0.1315	1.003	0.264	78.0	295	Failed, singly

NOTE: The test samples contained 7.4 weight percent of silicon carbide whiskers. The weight percent is defined as the weight of whiskers divided by the weight of unbonded zirconia plus whiskers.

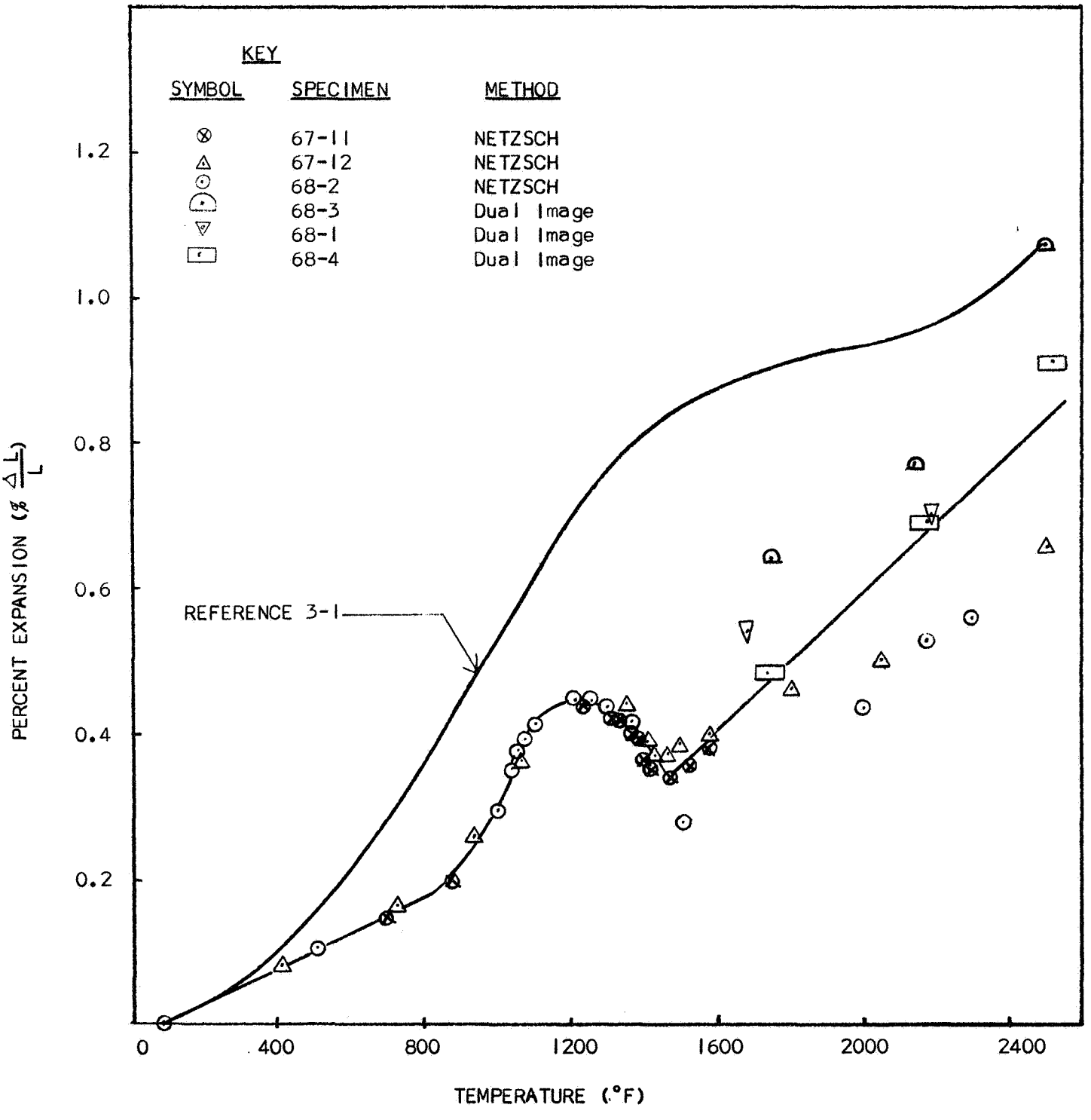

Figure 3-17. Linear Thermal Expansion of SiC-Whisker-Reinforced Chemically Consolidated Zirconia (32 Parts H_2PO_3F) Compared with Unreinforced Matrix (16 Parts H_2PO_3F)

The large scatter and relatively low strength values in the tensile test data are difficult to explain. A logical reason may be a non-uniform whisker distribution within the gage length. The flexure specimens usually have a short gage length, of the order of 0.01 inch, and the tensile specimens have a gage length of approximately 5 inches. The possibility of non-uniform whisker distribution is obviously much greater for the long gage length. Thus, if any section within the 5-inch gage length is low in whisker content, failure would take place at that point.

3.5 REFERENCES FOR SECTION 3

3-1. L. B. Greszczuk and H. Leggett. Final Report - Development of a System for Prestressing Brittle Materials. Douglas Aircraft Company Report No. DAC-49200, August 1967.

3-2. Anon. Technical Information Bulletin No. 465-202-DG. Union Carbide Corporation, Carbon Products Division, New York, New York.

3-3. Anon. Carborundum Technical Data Sheet. Carborundum Company, New Products Division, Niagara Falls, New York, July 1965.

Section 4

EXPERIMENTAL AND THEORETICAL STUDIES ON UNIAXIALLY PRESTRESSED, SiC-WHISKER-STRENGTHENED ZrO_2

Using the analyses developed in Reference 4-1, tradeoff studies were conducted on the strength of uniaxially prestressed, whisker-strengthened zirconia as affected by the volume fraction of the reinforcement, applied reinforcement prestress, temperature, and externally applied load. The results of these studies were used to design uniaxially prestressed flexure and tensile specimens. The specimens were fabricated using the previously developed setup (Reference 4-1, pp. 131-138). The flexure and tensile specimens were tested at room and elevated temperatures. In addition to these tests, the specimens were also evaluated for resistance to thermal shock and thermal cycling. Finally, a data evaluation and test-theory correlation were made for uniaxially prestressed, SiC-whisker-strengthened ZrO_2.

4.1 TRADEOFF STUDIES AND DESIGN OF UNIAXIALLY PRESTRESSED, SiC-WHISKER-STRENGTHENED ZrO_2

Calculations for the tensile strength of uniaxially prestressed composites were made using the equations in Section 3.2 of Reference 4-1, the ceramic properties indicated in Figures 3-14 and 3-17, and the tungsten cable properties given in Section 5 of Reference 4-1. The variables considered in this study were reinforcement configuration, reinforcement volume fraction, mechanical and thermal prestress of the cable, and use temperature. Variation of the properties of constituents with temperature was also considered. The volume fractions and configurations of the cables were the same as those used in the first-year effort (Reference 4-1). Figures 4-1 and 4-2 show typical results of the analytical studies. Essentially, these curves represent the envelopes for the tensile strength of prestressed, whisker-reinforced ceramics. The composite stresses shown are the stresses which would initiate failure in the ceramic or the reinforcement.

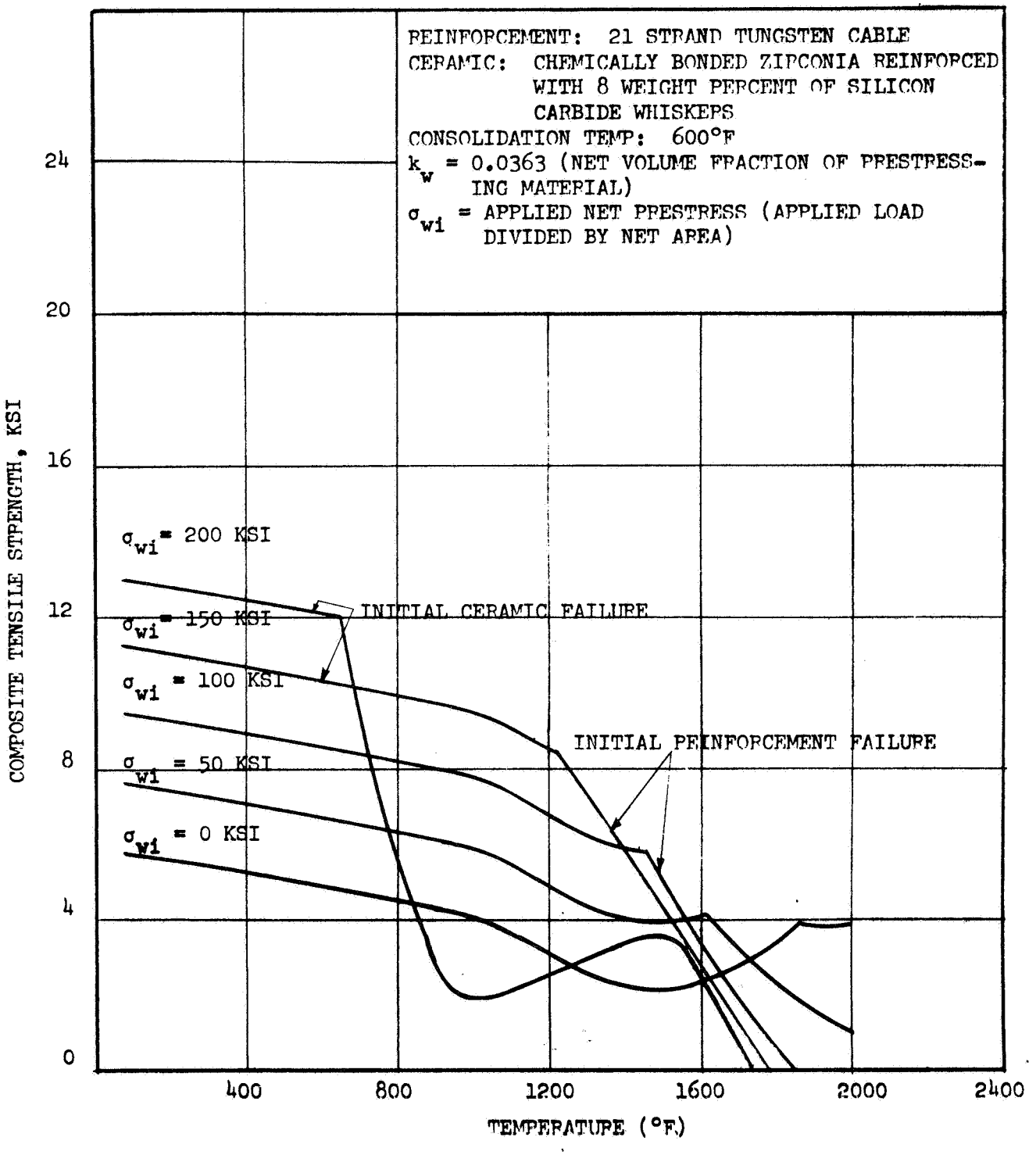

Figure 4-1. Elevated Temperature Tensile Strength of SiC-Whisker-Reinforced Zirconia Prestressed With 21-Strand Tungsten Cable (Theoretical Results)

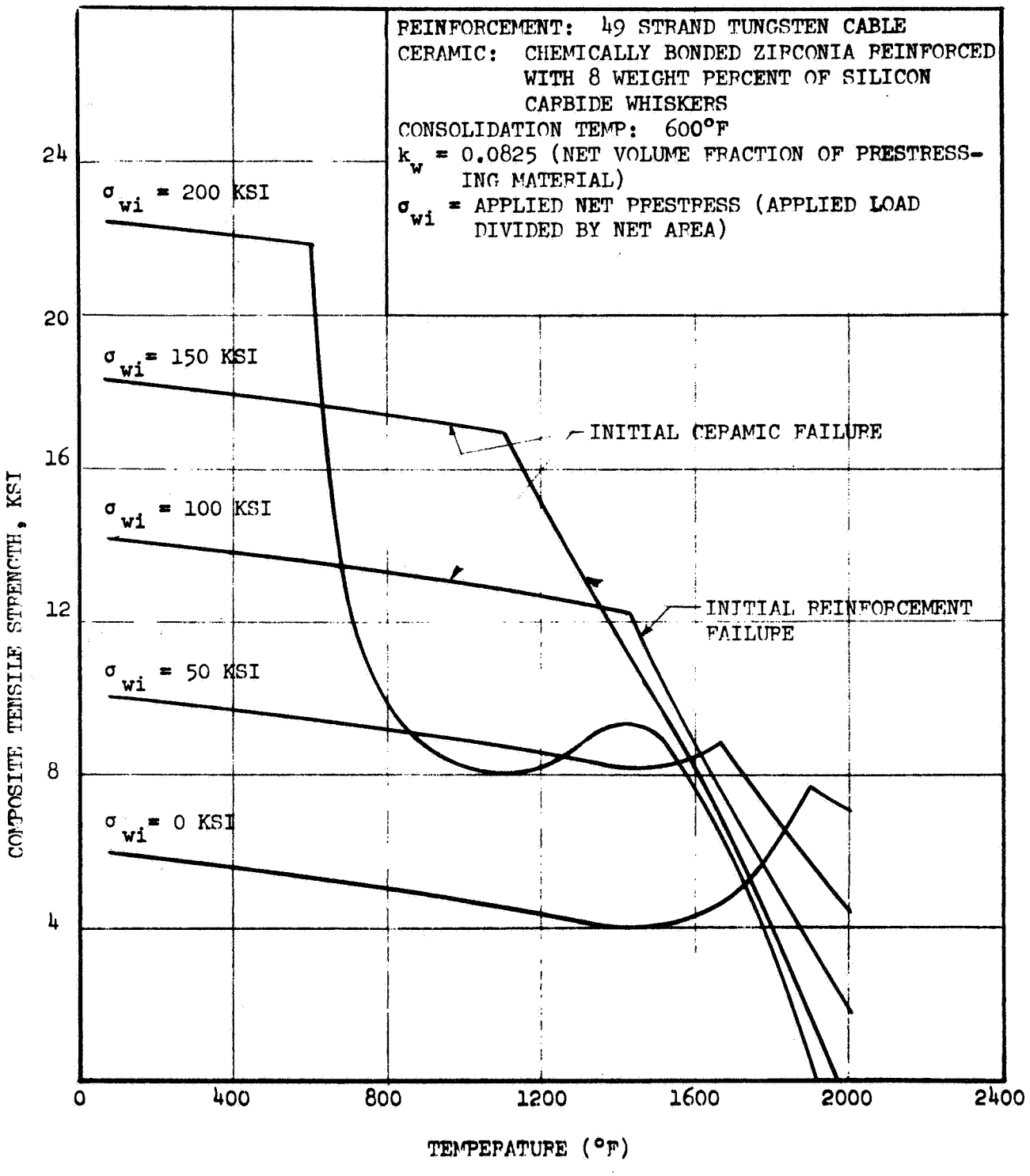

Figure 4-2. Elevated Temperature Tensile Strength of SiC-Whisker-Reinforced Zirconia Prestressed With 49-Strand Tungsten Cable (Theoretical Results)

For any given prestress, the upper horizontal portion of the curve represents the composite stress that will cause tensile failure in the ceramic (without necessarily causing reinforcement failure); the steep portion of the curve represents the composite stress required to cause failure of the reinforcement (without necessarily causing ceramic failure). On the basis of the results presented in Figures 4-1 and 4-2, a uniaxially prestressed specimen design was selected; the selected prestress level was 88,400 psi, while the prestressing material was approximately 8.25-volume-percent, 49-strand tungsten cable. The above selection was made to demonstrate high composite strength at 1,500°F, a temperature at which the unprestressed material exhibits poorest properties.

4.2 FABRICATION OF UNAXIALLY PRESTRESSED, SiC-WHISKER-REINFORCED SPECIMENS

The setup described in Reference 4-1 was used to fabricate the prestressed zirconia matrix specimens for the flexural and tensile strength tests. The flexure specimens were made with four cables, and the tensile specimen with three cables. Each cable contained 49 strands of tungsten wires. The diameter of each strand was 0.012 inch. The matrix compositions for the flexure and tensile specimens were those shown in Table 3-11. The curing schedule shown in Table 3-12 was used. The prestressing technique and fixtures used were the same as described in Reference 4-1.

The development of the SiC-whisker-reinforced zirconia body was continued during fabrication of the unaxially prestressed tensile specimens. The mortar and pestle were not used; instead, the solid materials were blended in a V-type blender. Acid was added to the solids by manual mixing. Batches were made large enough to fill two cavities of the prestressing molds which were 1-1/8 x 1-1/8 x 39 inches in size. The flexure specimens were cast after a 30-minute aging of the mix on the vibrator. The molds and the prestressing fixture were vibrated while the ceramic was cast in place. After the ceramic was cast and vibrated in place for 1 hour, it was cured in place as described in Reference 4-1.

The specimens continued to have occasional large voids. The aging period was extended to 120 minutes for the fabrication of 12 uniaxially prestressed specimens. The cure cycle was extended further by precuring at room temperature for 16 hours, followed by the cure cycle given in Section 3.2. Most of the specimens were free of large voids, indicating that the aging of the mix and the extension of the cure period reduced void size. Although the specimens occasionally had voids and cracks, in general the above-described fabrication technique appeared to work satisfactorily, and was used to prepare the flexure and tensile specimens.

4.3 CHARACTERIZATION OF UNIAXIALLY PRESTRESSED, SiC-WHISKER-STRENGTHENED ZIRCONIA

Following the preparation of uniaxially prestressed specimens, tests were performed to obtain their tensile and flexure strengths at room and elevated temperatures. In addition, thermal cycling tests were performed on prestressed flexure specimens; the specimens also were evaluated for resistance to thermal shock.

4.3.1 Testing of Uniaxially Prestressed Specimens

The flexure and tensile strength tests were conducted in the manner described in Section 3.4. The specimens were tested at the following temperatures: $70^{\circ}F$, $1,000^{\circ}F$, $1,500^{\circ}F$, and $2,000^{\circ}F$; a minimum of three specimens were tested at each temperature. No special problems were encountered while testing the flexure specimens by the previously described methods. While testing the tensile specimen, most of the ultimate failures were caused by pullout of the cables, rather than cable fracture.

Initially, all tensile specimens were made as shown in Figure 4-3a. This design was adequate for obtaining cracking stresses. However, ultimate failure was caused by pullout of the cables. Reducing the length of the shoulder or tying the cables into one unit did not prevent cable pullout. Therefore, the specimen was redesigned to the configuration shown in Figure 4-3b. This design worked satisfactorily for obtaining cracking and

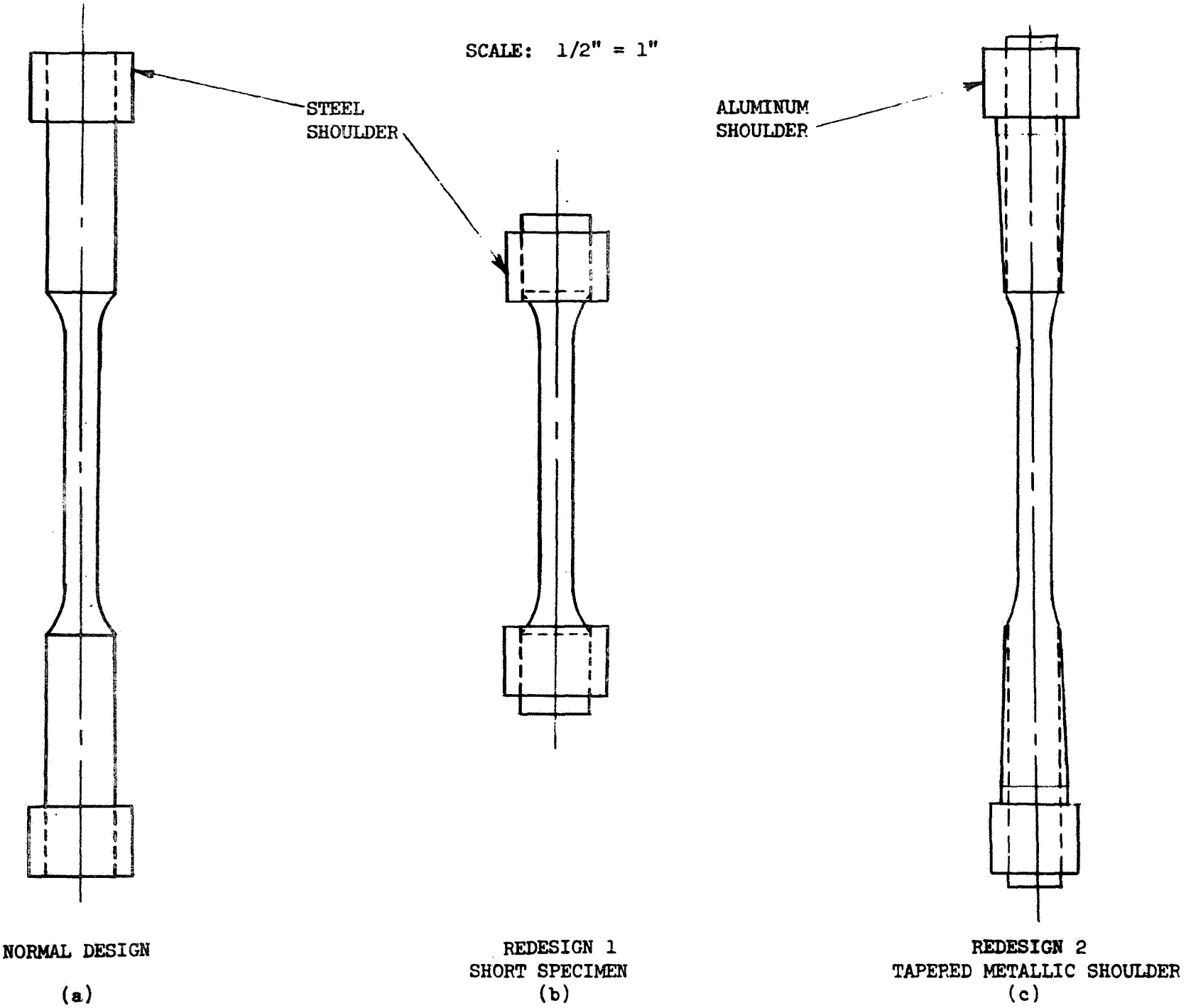

Figure 4-3. Tensile Specimen Configurations

ultimate strengths. This specimen was, however, too short for the elevated-temperature test fixture. The specimen was redesigned further to the configuration shown in Figure 4-3c. This design was found to work satisfactorily. Ultimate failures occurred in the test section.

The design shown in Figure 4-3c was used on several specimens, which were tested once, and which failed by pullout. Tapered aluminum sleeves were bonded onto the specimens; after which they were retested. Figure 4-4 shows a new tensile specimen design; Figure 4-5 shows the ultimate failure of the tensile specimen tested in the new manner.

4.3.2 Flexure Strength of Uniaxially Prestressed, SiC-Whisker-Strengthened Zirconia

Complete descriptions of flexure specimens, and of the flexure test results, are given in Table 4-1. A description of the specimen quality and failure mode is also given in Table 4-1. Most of the specimens failed by cracking on the bottom surface of the specimen (tensile side of the flexure specimen). This initial failure, referred to as the cracking stress, was followed by compressive failure on the top surface, denoted as the ultimate strength. A typical flexure stress-strain curve for a prestressed flexure specimen tested at 1,000°F is shown in Figure 4-6. After the specimens were tested and fractured as described in Table 4-1, several specimens were tested a second time. During the second test, the specimens were turned over and tested in flexure. The results are shown in Table 4-2. It is repeated here that the second test was conducted on pre-cracked specimens. Even so, the ultimate strengths obtained during the second test were significantly higher than during the first test, as can be seen by comparing the results shown in Tables 4-1 and 4-2.

4.3.3 Tensile Strength of Uniaxially Prestressed, SiC-Whisker-Strengthened Zirconia

A complete description of the results of tensile testing is shown in Table 4-3. While tensile tests were being conducted, some problems were encountered using the Optron to measure Young's modulus. Therefore, in several instances, a high-temperature extensometer was used to obtain the modulus data.

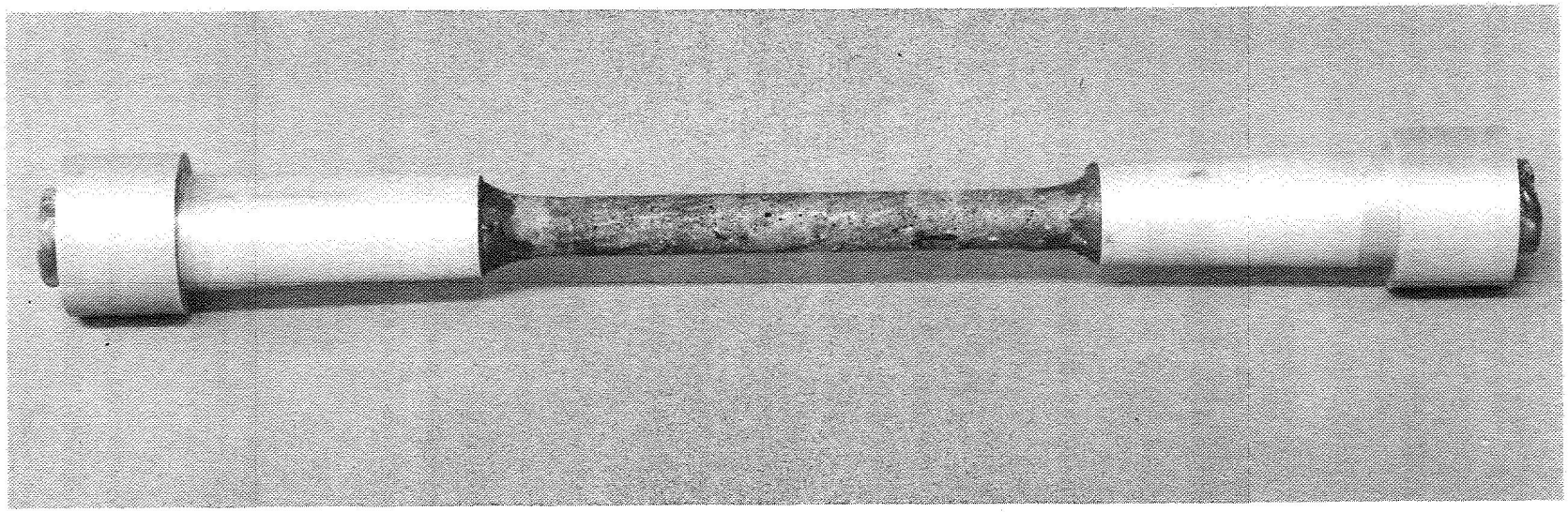

Figure 4-4. New Tensile Specimen Design

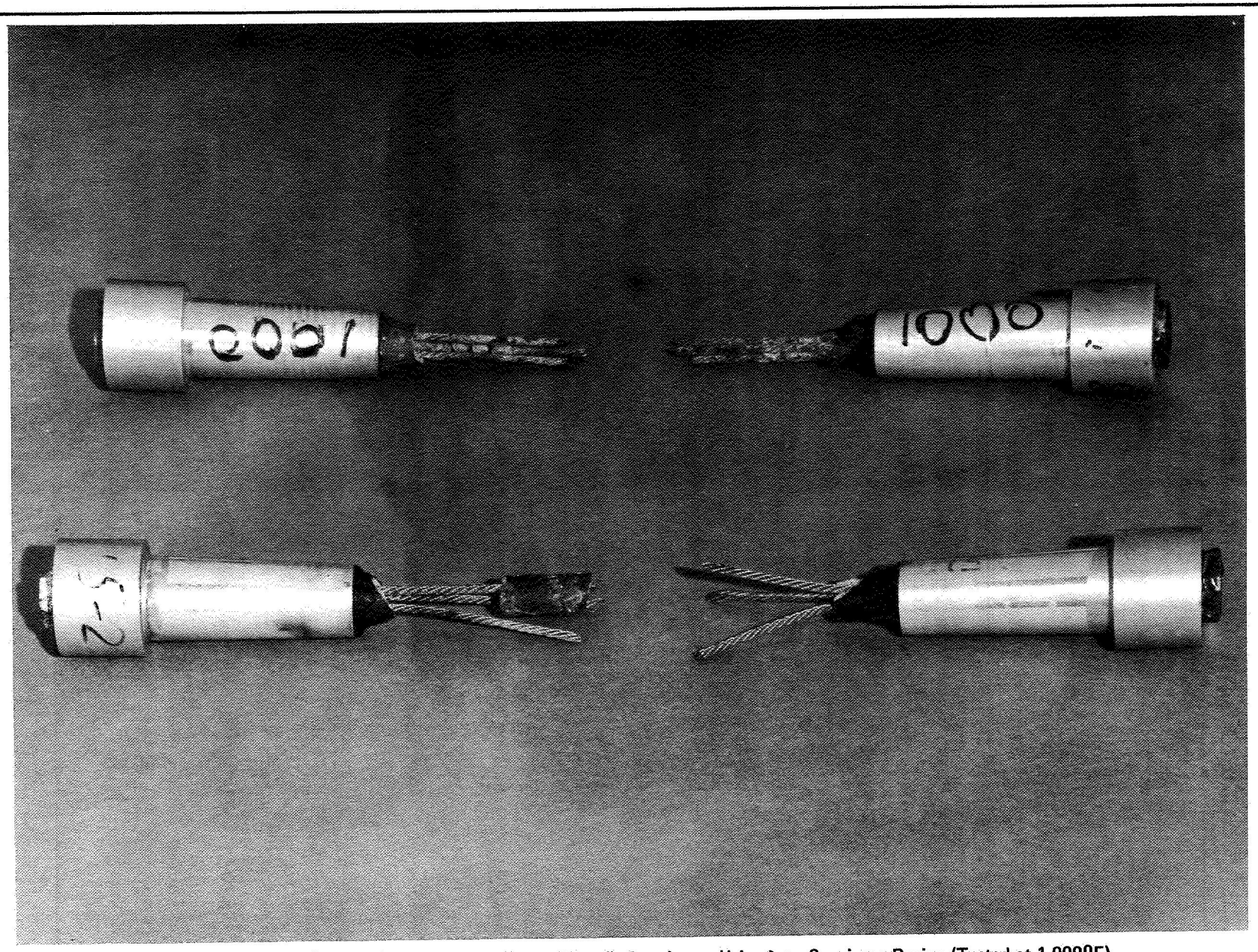

Figure 4-5. Ultimate Failure of Tensile Specimens Using New Specimen Design (Tested at 1,000°F)

Table 4-1 (Page 1 of 2)

FLEXURAL STRENGTH OF TUNGSTEN-REINFORCED, PRESTRESSED ZIRCONIA, STRENGTHENED WITH SiC WHISKERS[1, 2]

Sample Number	Test Temperature °F	Test Temperature °C	Test Sample Dimensions (in.) Thickness	Width	Length	(4) Distance of Wire From Bottom of Sample (in.) End 1	End 2	(5) Sample Weight Composite (lb) Before Test	After Test	(6) Ultimate Load at Failure (lb)	Ultimate Composite Stress at Failure (psi)	Cracking Load (lb)	Composite Stress for Cracking Load (psi)	Modulus of Elasticity of Composites (psi x 10^{-6})	Specimen Quality	Failure Type
1	70	21	0.2517	1.011	4.500	0.121	0.129	---	---	155	14,510	86	8,050	9.5[7]	Low Prosity; crack 3/4 inch in from the end	Cracking on tensile side followed by compressive failure
2	70	21	0.2515	1.011	4.500	0.153	0.145	---	---	80	7,500	49	4,600	6.5[7]	Medium Porosity: lot of cracks and spalling on top surface	Compressive failure at top surface
3	70	21	0.2484	1.011	4.500	0.129	0.129	---	---	149	14,525	64	6,150	7.9[7]	Low Porosity	Cracking on bottom, followed by compressive failure
13	70	21	0.2490	1.011	4.500	0.121	0.129	0.187	---	135	12,900	75	7,160	6.4[7]	Low Porosity; crack in the plane of the reinforcement	Interlaminar shear in the plane of reinforcement
4	1,000	538	0.2517	1.011	4.500	0.153	0.137	---	---	218	20,405	93.8	8,800	6.6	Low Porosity	Cracking on bottom surface, followed by compressive failure at top
5	1,000	538	0.2517	1.011	4.500	0.153	0.121	---	---	110	10,300	92.7	4,000	6.2	Low Porosity	Cracking on bottom surface, followed by compressive failure at top
6	1,000	538	0.2487	1.011	4.500	0.129	0.145	---	---	135	13,000	62.3	6,000	5.9	Low Porosity; crack at the end of the plane of reinforcement	Cracking on bottom surface, followed by compressive failure at top
7	1,500	815	0.2517	1.011	4.500	0.137	0.145	0.205	---	21.8	2,040	6.1	570	---[8]	Low Porosity	Failure by excessive deformation; few cracks on tension side
8	1,500	815	0.2515	1.011	4.500	0.137	0.137	0.198	0.193	19.8	1,855	6.1	570	1.2	Low Porosity	Failure by excessive deformation; cracks on bottom surface
9	1,400	760	0.2504	1.011	4.460	0.137	0.145	0.190	0.183	34.0	3,240	18.9	1,800	4.3	Low Porosity; some cracks visible at the ends	Interlaminar shear failure; no cracking

FOLDOUT FRAME 1

FOLDOUT FRAME 2

Table 4-1 (Page 2 of 2)

Sample Number	Test Temperature °F	Test Temperature °C	Test Sample Dimensions (in.) Thickness	Width	Length	(4) Distance of Wire From Bottom of Sample (in.) End 1	End 2	(5) Sample Weight Composite (lb) Before Test	After Test	(6) Ultimate Load at Failure (lb)	Ultimate Composite Stress at Failure (psi)	Cracking Load (lb)	(7) (8) Composite Stress for Cracking Load (psi)	Modulus of Elasticity of Composites (psi x 10^{-6})	Specimen Quality	Failure Type
10	2,000	1,093	0.2510	1.011	4.500	0.145	0.137	0.190	0.182	46.0	4,330(6)	18.1	1,700	5.0	Low Porosity	Cracking on tensile side, followed by compressive failure at the top
11	2,000	1,093	0.2490	1.010	4.500	0.137	0.129	0.198	---	47.0	4,495	15.7	1,500	1.8	Medium Porosity. Crack at the end in the plane of reinforcement	Cracking on the tensile side only
12	2,000	1,093	0.2488	1.011	4.500	0.145	0.145	0.192	0.185	21.0	2,010	10.5	1,000	1.2	Low Porosity	Cracking on the tensile side only, followed by deformation.

(1) The matrix of the test samples contained 7.4 weight-percent of silicon carbide whiskers. The weight-percent is defined as the weight of the whiskers divided by the weight of unbonded zirconia plus whiskers. The volume-fraction of prestressing material (four 49-strand tungsten cables) was 8.7%.

(2) The average applied reinforcement prestress (σ_{wi}) psi was 90,000 psi with a range of 81,000 to 100,000 psi. All tests were conducted in an argon atmosphere.

(3) The samples were tested as soon as the specimen was at temperature, except as is noted above.

(4) The measurement was taken to the centroid of the wire. The sample ends were chosen at random.

(5) The weight of tungsten cables in each specimen was 0.0507 pound.

(6) Specimen held at 2,000°F for 65 minutes before testing.

(7) The modulus of elasticity was determined using two different types of instrumentation; strain gages and optron. The values shown are the average of the two. The modulus of Specimens 4 through 13 was determined from optron data.

(8) The modulus of elasticity could not be determined because of insufficient data.

FOLDOUT FRAME 1

FOLDOUT FRAME 2

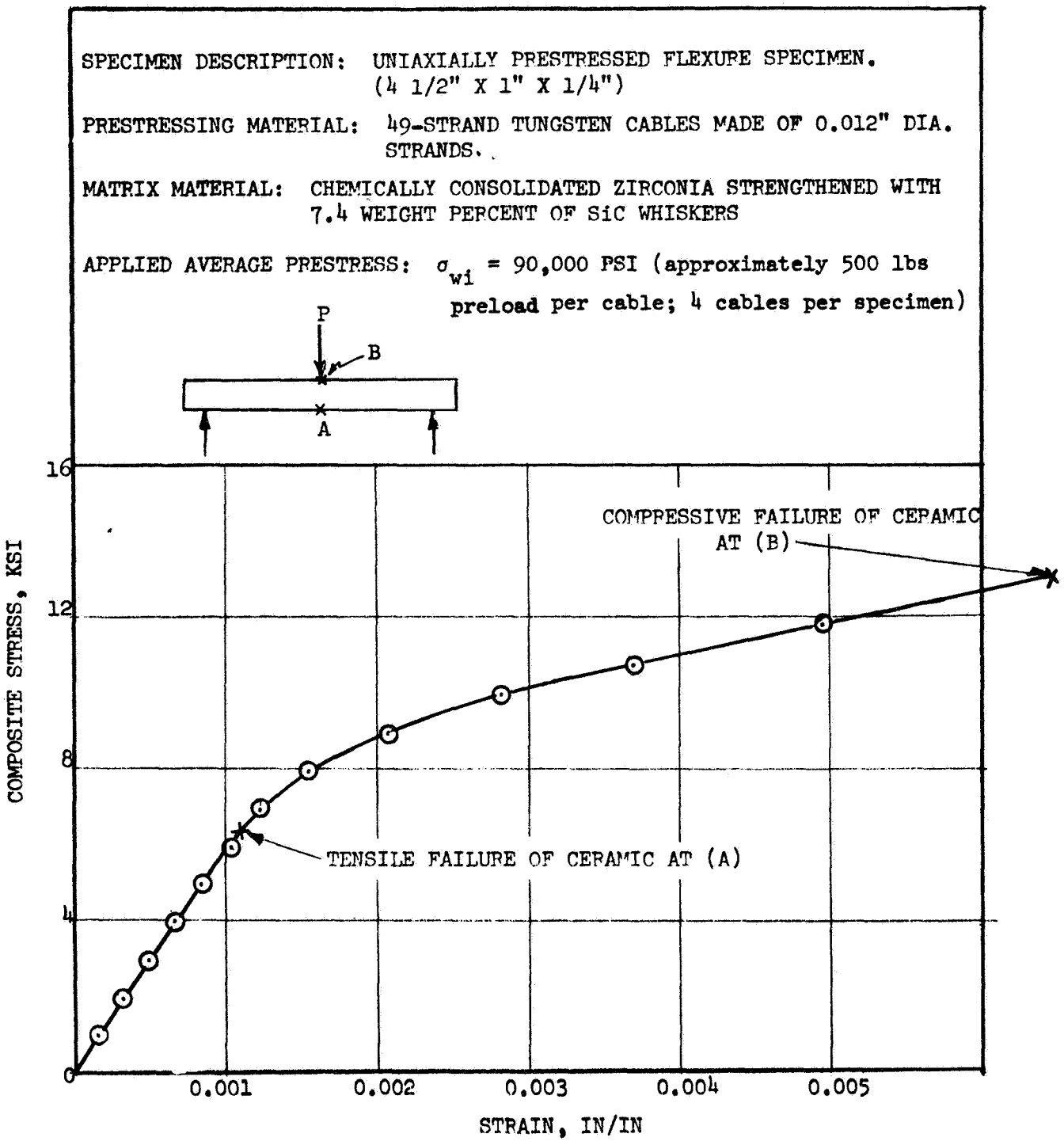

Figure 4-6. Typical Stress Strain Curve for a Uniaxially Prestressed Flexure Specimen Tested at 1000°F

Table 4-2

FLEXURE STRENGTH OF PRE-CRACKED SPECIMEN[1]

(2) Sample No.	Test Temperature °F	Test Temperature °C	Cracking Load (lb)	Ultimate Load (lb)	Composite Cracking Stress (psi)	Ultimate Composite Stress at Failure (psi)	Comments
1-2	70	21	---	265	---	24, 850	Top surface cracked from first test; compressive failure on top due to second loading.
2-2	70	21	---	359	---	34, 750	Bottom surface cracked from first test; compressive failure on top during second test.
3-2	70	21	---	283	---	27, 200	Top surface cracked from first test; compressive failure on top surfaces due to second test.
7-2	1,500	815	145	145	13, 580	13, 580	Specimen heat-treated.
12-2	1,500	815	70	70	6, 700	6, 700	Initially, specimen was bent; to straighten it up it was subjected to 70 lb at 1,500°F, it failed after about 10 minutes.
11-2	2,000	1, 043	86	92	8, 230	8, 800	Cracking on bottom surface; compressive failure on top surface; top surface pre-cracked.

(1) The strength data given here are for the specimens which were tested and failed as described in Table 4-1. After the first failure, the specimans were turned over and retested.

(2) The first number refers to the specimen described in Table 4-1; the second number denotes that the specimen was retested.

Table 4-3

TENSILE STRENGTH OF SiC WHISKER[1] REINFORCED ZIRCONIA PRESTRESSED WITH 49-STRAND TUNGSTEN CABLES

Specimen Designation No.	Specimen Designation Code	Test Temperature (°F)	Test Temperature (°C)	(2) (3) Applied Reinforcement Prestress σ_{wi} (psi)	(4) Variation in σ_{wi} ±(%)	(5) Composite Cracking Stress (psi)	(6) Ultimate Strength of Composite (psi)	(7) Young's Modulus x 10^{-6} (psi)	Failure Type and Location	Porosity Observations	Remarks
1	10R	70	21	61, 100	10	12, 500	(18, 840)	---	Pull out of 3 cables.	Low porosity; longitudinal cracks.	Short specimen; specimen repaired
2	15-2	70	21	102, 400	21	N/A	(23, 200)	---	1 cable broke; 2 pulled out.	Medium; few large pores.	Short specimen. Room temperature retest of Specimen 15 which was tested at 1, 500°F.
3	14	70	21	102, 400	21	12, 300	(12, 300)	3. 02 (E)	Pull out of 3 cables.	Medium porosity; few large voids.	
4	16	70	21	112, 300	26	N/A	(8, 180)	9. 65 (E)	Pull out of 3 cables.	Low porosity; few large pores; longitudinal cracks in specimen.	
5	8	70	21	---	---	N/A	(7, 580)	10. 00 (E)	Pull out of 3 cables.	Low porosity.	Short Specimen.
6	12	1, 000	538	61, 100	10	8, 880	(15, 475)	(I. D)	Pull out of cable end.	Low porosity; 1/4 inch longitudinal cracks.	
7	13	1, 000	538	102, 400	21	N/A	(12, 080)	8. 72 (E)	Pull out of 3 cables.	Medium porosity on half the circumference.	
8	18	1, 000	538	112, 300	26	8, 840	20, 800	5. 66 (E)	Center.	High porosity.	Specimen redesigned and retested (see Fig 4-3c and Fig 4-4)
9	15	1, 500	815	102, 400	21	N/A	15, 400	1. 65 (E)	Center.	Medium porosity, few large voids.	Specimen redesigned and retested (see Fig 4-3c and Fig 4-4)
10	11	1, 500	815	61, 100	10	6, 300	(7, 650)	2. 62 (O)	Pull out of 3 cables.	Low porosity, 1/4 to 3/4 inch, longitudinal cracks along test length; 1 inch cracks in shoulder.	
11	7R	1, 500	815	78, 000	10	N/A	(6, 535)	2. 00 (O)	Pull out of 3 cables.		Specimen had cracks; was repaired. Heated twice.
12	3	1, 500	815	75, 600	9	6, 830	(10, 700)	0. 90 (E)	Pull out of 3 cables.	Medium porosity.	Heated to 800°F. Thermocouple burned out. Reheated to 1, 500°F and tested.
13	2	2, 000	1, 093	75, 600	9	3, 650	(8, 260)	1. 69 (E)	Pull out of 3 cables; also failure in gage length.	High porosity, large pores (one of 0. 2 inch diameter) one longitudinal crack 3/4 of test length.	Heated to 2, 000°F three times
14	1	2, 000	1, 093	75, 600	9	4, 590	(8, 270)	(I. D)	Pull out of 3 cables.	Medium to high; three longitudinal cracks about 1 inch long.	
15	17	2, 000	1, 093	112, 300	26	4, 310	(9, 420)	1. 47 (E)	Pull out of 3 cables.	Medium porosity.	Heated to 2, 000°F two times.
16	4	2, 000	1, 093	52, 500		4, 250	(9, 020)	0. 72 (E)	Pull out of 3 cables.	Low porosity; crack in shoulder.	

(1) The test specimens contained 7. 4-weight-percent of silicon carbide wiskers. The weight-percent is defined as the weight of whiskers divided by the weight of zirconia plus whiskers.
(2) The specimens contained 8. 74 volume percent of reinforcement (49-strand tungsten cables of 0. 012-inch-diameter strands).
(3) σ_{wi} is the mechanically applied prestress (average of the stresses in three cables).
(4) This column represents the variation in prestress from cable to cable in any given specimen. If no number is given, the variation was less than 5%.
(5) Cracking not apparent (N/A)
(6) Numbers in parentheses denote that the ultimate failure was by pullout of the reinforcement.
(7) (I.D.) -- The load-deflection curve was inadequate for determining Young's modulus.
(E) -- Young's modulus determined using extensometer.
(O) -- Young's modulus determined using optron.

4.3.4 Resistance to Thermal Shock of Prestressed and Non-Prestressed Ceramic

Thermal shock tests were conducted on three SiC-whisker-strengthened zirconia specimens and three SiC-whisker-strengthened, prestressed specimens.

The shock test consisted of inserting a specimen into a furnace pre-heated to 2,000°F. The specimen was left in the furnace, in an argon atmosphere for 10 minutes, then removed, placed on a thick steel plate, and allowed to cool. The approximate cooling time was 10 minutes. The prestressed specimens were subjected to ten thermal shock cycles without any apparent failure. In two instances, small pieces of ceramic chipped off the sharp edges when the ceramic was subjected to the first cycle. No further chipping occurred during cycles 2 to 10. For all practical purposes, the prestressed specimens were intact. Following thermal shock cycling, the specimens were tested in flexure at room temperature. Three-point loading was used, with a 4-inch span between supports, and a load applied at the midspan.

Similar tests were performed on three non-prestressed, whisker-strengthened specimens. The non-prestressed specimens exhibited failure during the first cycle. They failed by cracking normal to the major axis of the specimen. Several cracks were visible on both flat surfaces of the specimen. These cracks appeared to penetrate through the thickness of the specimen and through approximately 75 percent of the specimen width. Although each specimen remained in one piece after the first cycle, each crumbled completely when subjected to subsequent cycles. Since the non-prestressed specimens failed in the first thermal shock cycle, they could not be tested in flexure.

The results of the thermal shock testing are shown in Table 4-4. The benefit of prestressing on thermal shock resistance is quite obvious from the results presented therein. The non-prestressed specimens failed during the first cycle, while the prestressed specimens withstood ten thermal shock cycles without failure. Moreover, after ten thermal shock cycles, the average

Table 4-4

THERMAL SHOCK DATA ON PRESTRESSED AND NON-PRESTRESSED, WHISKER STRENGTHENED FLEXURE SPECIMEN (1)

Specimen Type	(2) Specimen Dimensions (In.) Length	Width	Thickness	Maximum Thermal Shock Temperature °F	°C	(3) Cycles to Failure	(4) Ultimate Failure Load at 70°F After 10 Thermal Shock Cycles (Lb)	Ultimate Composite Failure Stress at 70°F after 10 Thermal Shock Cycles (PSI)
Non-Prestressed	4.50	0.999	0.252	2,000	1,093	1 (3)	0	0
Non-Prestressed	4.50	0.996	0.246	2,000	1,093	1	0	0
Non-Prestressed	4.50	0.998	0.247	2,000	1,093	1	0	0
Prestressed	4.50	0.815 (2)	0.284	2,000	1,093	>10 (3)	123	11,200 (4)
Prestressed	4.50	1.037	0.280	2,000	1,093	>10	212	15,600
Prestressed	4.50	1.037	0.282	2,000	1,093	>10	235	17,200

(1) All specimen contained 7.4 weight-percent of SiC whiskers. The prestressed specimen were prestressed with 49-strand tungsten cables which constituted 7.65% volume fraction of the composite. The average applied reinforcement prestress (σ_{wi}) was 90,000 psi.

(2) Specimen cracked longitudinally during shock testing at 235°F; one cable was removed and testing continued at 2,000°F.

(3) Non-prestressed specimen failed during first cycle; prestressed specimens withstood 10 thermal shock cycles without failure.

(4) The average ultimate room temperature flexure strength of prestressed, SiC whisker reinforced zirconia which was not shock tested was 12,309 psi.

flexure strength of these specimens at room temperature was significantly higher than the average flexure strength of specimens which were not thermal shock cycled. The specimens which were thermal shock cycled had an average flexure strength of 14,667 psi, while those which were not shocked had an average flexure strength of 12,309 psi.

4.3.5 Thermal Cycling Tests on Prestressed and Non-Prestressed Ceramic

Thermal cycling tests were conducted on three, SiC-whisker-strengthened zirconia specimens and three, SiC-whisker-strengthened, prestressed specimens. The thermal cycling tests consisted of inserting the specimens in the furnace in an argon gas atmosphere at room temperature, and slowly heating the furnace to 2,000°F (about one-half hour); the furnace was held at 2,000°F for 5 minutes, and then allowed to cool slowly to room temperature (about one-half hour); the furnace was again heated slowly to 2,000°F (about one-half hour) and held at 2,000°F for ten minutes. The specimen was then cooled, while still in the furnace, and flexure tested at room temperature. The results of thermal cycling tests are shown in Table 4-5. After thermal cycling, the flexure strength of prestressed specimens was an order of magnitude higher than that of the non-prestressed ones. The average composite strength of prestressed specimens which have been cycled was 5,263 psi, as compared to 434 psi for the non-prestressed specimens. The reduction in composite strength for prestressed specimens, as compared to that discussed in the previous section, is attributed to prolonged exposure to high temperatures. By using a slow heating rate, high relaxation of prestress would be expected.

4.4 DATA EVALUATION AND TEST-THEORY CORRELATION FOR UNIAXIALLY PRESTRESSED, SiC-WHISKER-STRENGTHENED ZIRCONIA

The experimental results obtained from flexure and tensile tests were compared with the theoretically predicted results. Moreover, a comparison was also made between the strength of zirconia, prestressed zirconia, SiC-whisker-strengthened zirconia, and prestressed, whisker-strengthened zirconia.

Table 4-5

THERMAL CYCLING DATA ON PRESTRESSED AND NON-PRESTRESSED, WHISKER-STRENGTHENED FLEXURE SPECIMEN (1)

Specimen	(2) Specimen Dimensions (In.) Length	Width	Thickness	(3) Ultimate Load at Failure at 70°F (Lb)	(4) Ultimate Composite Stress at Failure at 70°F (PSI)	Comments
Non-Prestressed	4.50	0.999	0.252	3.4	321	Specimens were slightly bent after thermal cycling.
Non-Prestressed	4.50	0.999	0.252	4.0	378	
Non-Prestressed	4.50	0.999	0.252	6.4	604	
Prestressed	4.50	1.038	0.284	90	6,450	Specimens were warped after thermal cycling.
Prestressed	4.50	1.038	0.284	60	4,300	
Prestressed	4.50	1.037	0.274	70	5,020	

(1) All specimens contained 7.4 weight-percent of SiC whiskers. The prestressed specimens were prestressed with 49-strand tungsten cables which constituted 7.65% volume fraction of the composite. The average applied reinforcement prestress (σ_{wi}) was 90,000 psi.

(2) The average ultimate room temperature flexure strength of prestressed, SiC whisker reinforced zirconia was 12,309 psi.

4.4.1 Test-Theory Correlation for the Strength of Prestressed, SiC-Whisker-Strengthened Flexure Specimens

Using the theory developed in Reference 4-1, the stresses causing cracking and ultimate failures of prestressed, SiC-whisker-strengthened flexure specimens were predicted. Table 4-6 shows a comparison between experimental and theoretical results. The correlation between experiment and theory is much poorer than the correlation obtained previously (Reference 4-1) for the case of zirconia without any SiC whiskers. This stems apparently from the poor quality of the specimens that were obtained when using SiC whiskers and 32 parts acid content (twice the amount used in the first-year effort).

4.4.2 Test-Theory Correlation for the Strength of Prestressed, SiC-Whisker-Strengthened Tensile Specimens

The test data shown in Table 4-5 were compared with theoretical results based on the equations given in Reference 4-1. Table 4-7 shows test-theory correlation for the cracking and ultimate strengths of prestressed zirconia strengthened with SiC whiskers. The theory appears to predict the cracking stress with a reasonable degree of accuracy. The greatest difference between experimental and theoretical results occurs in specimens having large variations in applied prestress, σ_{wi}; that is, the variation in σ_{wi} from cable to cable within any given specimen.

Since most of the specimens failed ultimately by pullout of the three cables, the experimental results given in the column entitled "Ultimate Tensile Strength of Composite" do not represent true ultimate strength. The theoretical results are, however, based on the assumption that the ultimate failure would be by a tensile failure of the reinforcement. The inability to experimentally achieve the correct failure mode in most of the cases (i.e., ultimate failure in the test section), accounts for the discrepancy between the experimental and theoretical results for the ultimate tensile strength. Only specimens 2, 8, 9, and 13 had correct ultimate failure modes, that is, reinforcement failure.

Table 4-6

FLEXURAL STRENGTH OF TUNGSTEN-REINFORCED, PRESTRESSED ZIRCONIA (TEST VS THEORY)

(1) Sample Number	Test Temperature (°F)	(2) Distance of Wire From Bottom (in.)	Cracking Load (lb)		Ultimate Load (lb)			Stress in Ceramic at Cracking Experiment (psi)	Ultimate Composite Strength Experiment (psi)
			Experiment	Theory	Experiment	Theory Upper Bound	Theory Lower Bound		
1	70	0.125	86	129	155	444	215	3,750	14,510
2	70	0.149	49	89.4	80	426	145	3,080	7,500
3	70	0.129	64	116	149	427	192	3,100	14,324
13	70	0.125	75	124	135	433	206	3,400	12,900
4	1,000	0.145	93.8	74.1	218	199	73.5	4,070	20,405
5	1,000	0.137	42.7	88.2	110	207	86.9	4,840	10,300
6	1,000	0.137	63.2	83.1	135	201	82.2	2,450	13,000
7	1,500	0.141	6.1	20.3	21.8	23.1	12.9	111	2,040
8	1,500	0.137	6.1	22	19.8	23.4	13.8	103	1,855
9	1,400	0.141	18.9	33.5	34.0	14.2	6.4	406	3,240
10	2,000	0.141	18.1	63	46	62	27.2	437	4,330
11	2,000	0.133	15.7	74	47	68.1	33.9	323	4,495
12	2,000	0.145	10.5	53.5	21	57.4	23.1	298	2,010

(1) Applied reinforcement prestress (σ_{wi}) was 90,000 psi.

(2) Average of distance at both ends

Table 4-7

TENSILE STRENGTH OF SiC WHISKER REINFORCED ZIRCONIA PRESTRESSED WITH 49-STRAND TUNGSTEN CABLES (EXPERIMENT AND THEORY) (1)

(2) Specimen Designation	Test Temperature (°F)	(3) Applied Reinforcement Prestress (σ_{wi}) (psi)	(4) Variation in ± (%)σ_{wi}	(5) Composite Cracking Stress (psi) Experiment	Theory	(6) Ultimate Tensile Strength of Composite (psi) Experiment	Theory	Ultimate Failure Types And Location
1	70	61,100	10	12,500	11,340	(18,840)	25,100	a
2	70	102,400	21	N/A	14,950	*23,200	25,100	b
3	70	102,400	21	12,300	14,950	(12,300)	25,100	a
4	70	112,300	26	N/A	15,820	(8,180)	25,100	a
5	70	-	--	N/A	-	(7,480)	25,100	a
6	1,000	61,100	10	8,800	10,230	(15,475)	15,600	a
7	1,000	102,400	21	N/A	13,840	(12,080)	15,600	a
8	1,000	112,300	26	8,840	14,710	20,800	15,600	d
9	1,500	102,400	21	N/A	11,260	15,400	11,260	d
10	1,500	61,100	10	6,300	9,518	(7,650)	11,200	a
11	1,500	78,000	10	N/A	11,000	(6,535)	11,200	a
12	1,500	75,600	9	6,830	10,790	(10,700)	11,200	a
13	2,000	75,600	9	3,650	3,488	* 8,260	3,488(7)	c
14	2,000	75,600	9	4,590	3,488	(8,270)	3,488(7)	a
15	2,000	112,300	26	4,310	1,552	(9,420)	1,552(7)	a
16	2,000	52,500	4	4,250	4,706	(9,020)	4,706(7)	a

(1) For further details, see Table 4-6.
(2) Specimens contained 7.4 weight percent of SiC whiskers, and were prestressed with 49-strand tungsten cables made of 0.012 in. dia strands. The specimens contained 8.74 volume percent of tungsten cables.
(3) Mechanically applied prestress (average for three cables).
(4) Variation in σ_{wi} from cable to cable.
(5) N/A denotes that cracking was not apparent; this column represents the composite stress (load/area) at which ceramic cracks.
(6) The numbers with asterisks indicate that failure stress is near ultimate; numbers in parentheses denote ultimate failure by pull out of the reinforcement. Numbers without asterisks or parentheses denotes ultimate failure.
(7) Assuming no initial prestress in the reinforcement the predicted ultimate strength would be 7,475 psi. For these specimens, the theory predicts that the reinforcement would fail first, followed by ceramic failure. The experimental findings contradict this.

(a) Pull out of three cables. (b) One cable broke, two pulled out. (c) Failure by pull out and also in gage section.
(d) After these specimens failed by pull out of the cables, they were redesigned (see Fig. 4-3c) and retested. The failure was a three-cable failure in the center of the specimens.

For several of the specimens, the predicted ultimate strengths were considerably lower than the experimental values (see, for example, specimens 13, 14, 15 and 16). Assuming a lower prestress for these specimens, a much better correlation can be obtained between experiment and theory. This indicates that perhaps the true prestress levels were lower than those indicated in Table 4-7.

4.4.3 Comparison of Prestressed and Non-Prestressed Ceramics With and Without SiC Whiskers

To establish the influence of SiC whiskers and prestressing on the strength of ceramics, a comparison was made between the strength of plain ceramic, SiC-whisker-strengthened ceramic, prestressed ceramic, and SiC-whisker-reinforced, prestressed ceramic. Since the location of the prestressing material and the prestress level varied from specimen to specimen, the experimental results were normalized to a given prestress level, and a given reinforcement location.

Failure Load Normalization

Since variations existed in the prestress level and location of the reinforcement from specimen to specimen, it would be rather meaningless to compare the raw test data. Therefore, the data were normalized for a constant configuration.

In the case of the flexure specimens, the experimental data were normalized for a constant prestress of 90,000 psi and zero reinforcement eccentricity (the reinforcement was assumed to be at the centroid of the specimen).

The first step in the normalization procedure was to predict the theoretical strengths of the specimens for the actual applied preload and the actual wire location for each specimen. This predicted load was designated as F_t. The normalized theoretical load was then determined by using the reference prestress of 90,000 psi; i.e., the prestress to which everything would be normalized, and assuming that the reinforcement was located at the centroid, thus predicting a theoretical failure load, designated F_t^n. The normalized

experimental failure load was then obtained by multiplying the actual failure load, F_e, by the ratio of normalized load (F_t^n) to predicted load (F_t) as shown in Equation (4-1)

$$F_e^n = F_e \frac{F_t^n}{F_t} \tag{4-1}$$

In the case of tensile specimens, the reinforcement was concentric; therefore, the data were normalized with respect to the prestress only. In this case, all the data were normalized to a 100,000-psi prestress.

The experimental data were normalized to a constant prestress of 100 KSI by first predicting, theoretically, the cracking load for actual prestress in the specimen, T_t, then predicting, theoretically, the cracking load corresponding to a prestress of 100 KSI, T_t^n. The normalized experimental cracking load, T_e^n, was determined from the following equation.

$$T_e^n = T_e \left(\frac{T_t^n}{T_t} \right) \tag{4-2}$$

Comparison of Flexure Strengths for ZrO_2 Specimens, Prestressed ZrO_2 Specimens, Whisker-Strengthened ZrO_2 Specimens, and Prestressed, Whisker-Strengthened ZrO_2 Specimens

A comparison of normalized flexure strengths of various specimens is shown in Figures 4-7 and 4-8. Figure 4-7 shows a comparison between the flexure strength of plain ZrO_2, flexure strength of SiC-whisker-reinforced ZrO_2, cracking stress of prestressed ZrO_2, and cracking stress for SiC-whisker-strengthened and prestressed ZrO_2. The data for plain and prestressed ZrO_2 were obtained during the first-year effort (Reference 4-1). However, for use in Figure 4-7, it was normalized for zero reinforcement eccentricity and a prestress of 90,000 psi. The data for SiC-whisker-strengthened ZrO_2 were obtained during the present effort. These data, too, were normalized.

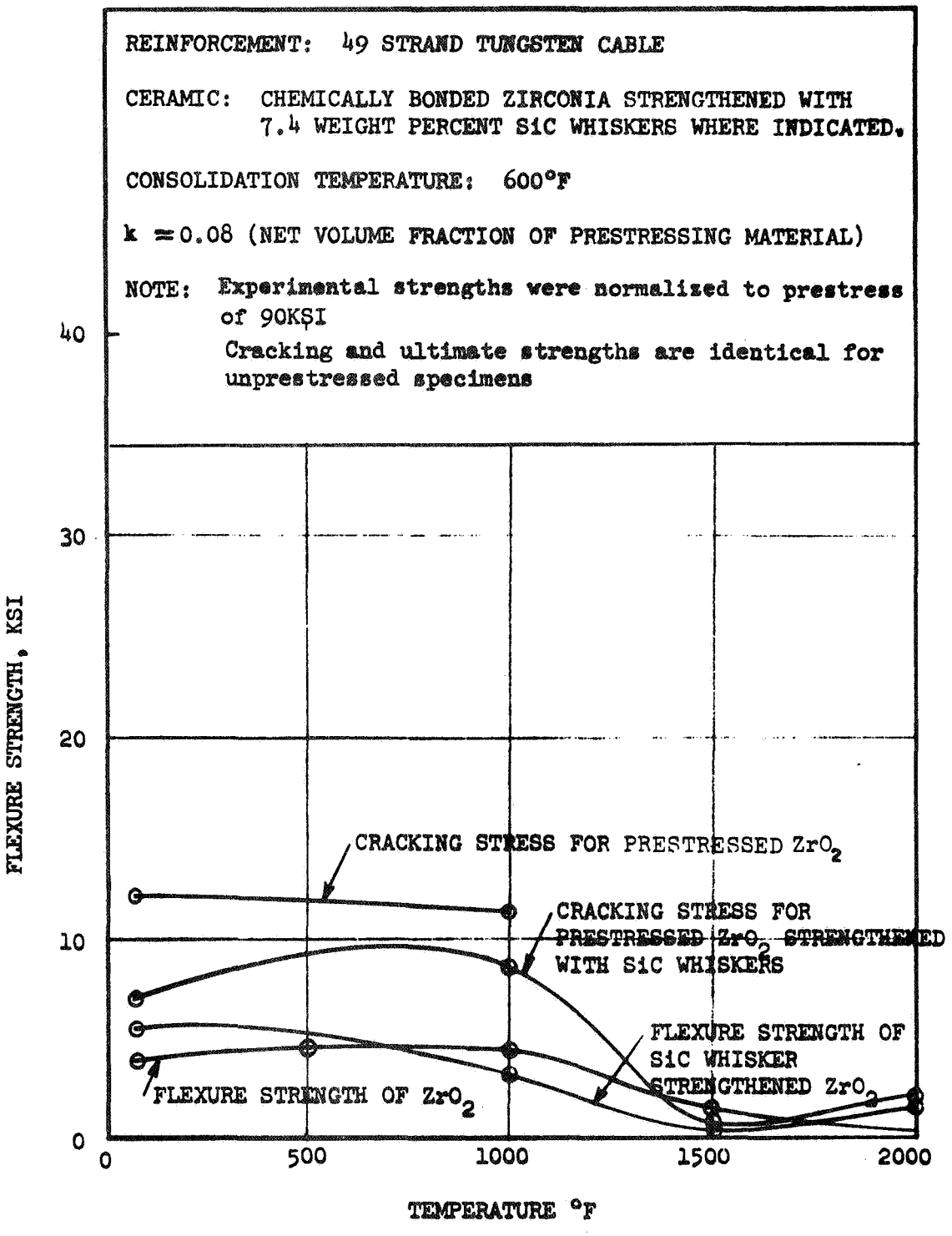

Figure 4-7. Normalized Experimental Cracking Stresses for Flexure Specimens

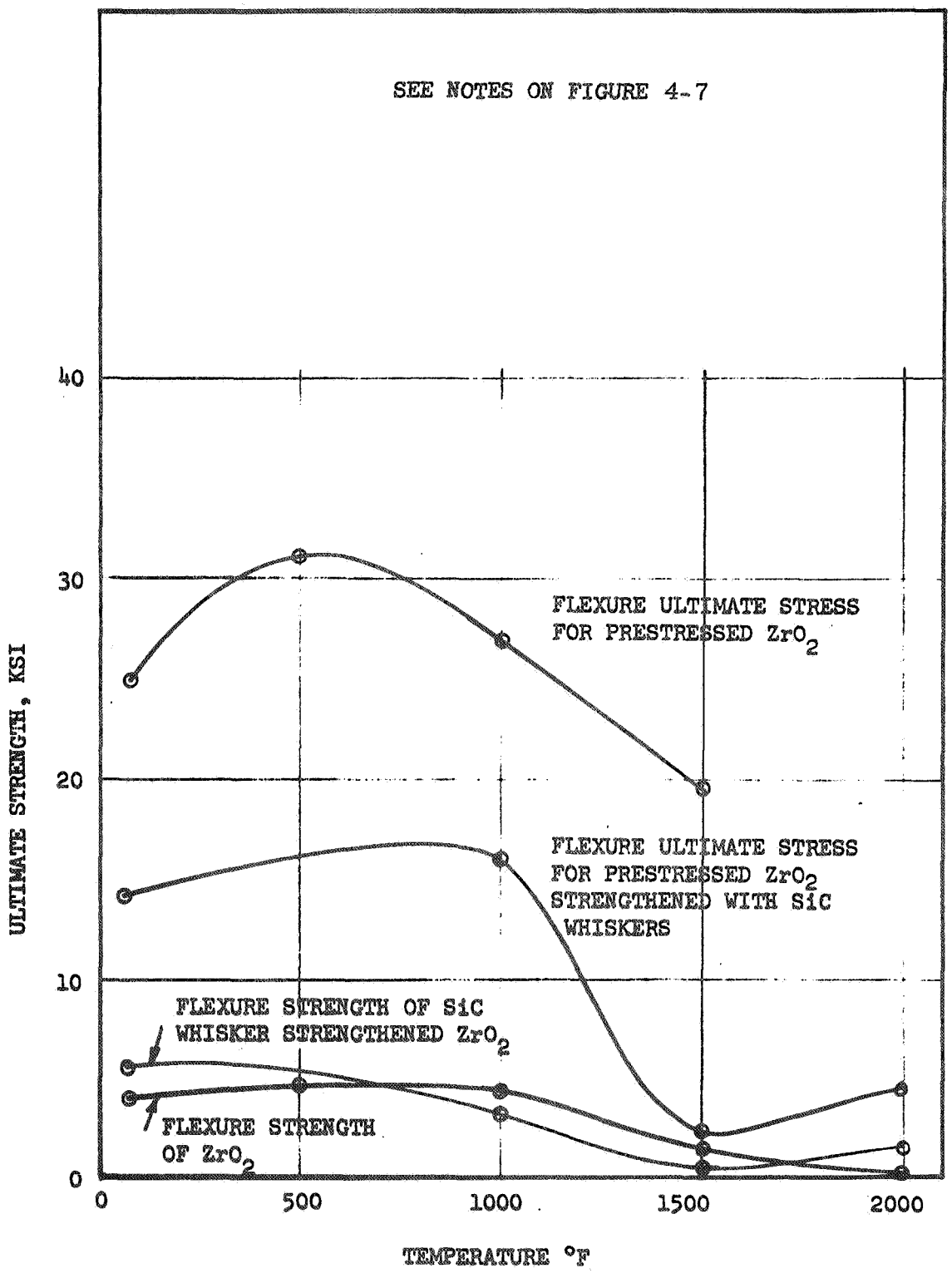

Figure 4-8. Normalized Experimental Ultimate Strength for Flexure Specimens

Figure 4-8 compares the flexure strengths of ZrO_2, and SiC-whisker-strengthened ZrO_2 to the ultimate strengths of prestressed ZrO_2 and SiC-whisker-strengthened ZrO_2. It is noted here that, for non-prestressed ceramics, the cracking stress and the ultimate strengths coincide.

The results shown in Figure 4-7 indicate that SiC whiskers increase the flexure strength of ZrO_2 at low temperatures (70°F to ≈ 700°F) and at high temperatures (≈ 1,700°F to 2,000°F, and above). In the intermediate temperature region (700°F to 1,700°F), plain ZrO_2 shows somewhat better strength than whisker-reinforced ZrO_2. A significant increase in strength was obtained at 2,000°F through addition of SiC whiskers.

For prestressed systems, the data indicate that the stress at which ceramic cracking occurs is higher for ZrO_2 than for SiC-whisker-strengthened and prestressed ZrO_2. This holds true up to 1,000°F. No data could be obtained for prestressed ZrO_2 above 1,000°F. Above that temperature the prestressed ZrO_2 failed by excessive deformation. On the other hand, the SiC-whisker-strengthened and prestressed ZrO_2 retained its strength to 2,000°F. A reduction in strength occurred at 1,500°F. Thus, for prestressed systems, the SiC-whisker-strengthened, prestressed ZrO_2 appears to be superior to prestressed ZrO_2 at temperatures of 1,000°F and above.

For ultimate strengths (Figure 4-8), prestressed ZrO_2 appears to be superior to prestressed, whisker-strengthened ZrO_2, up to a temperature of 1,500°F. No data were obtained for the ultimate strength of prestressed ZrO_2 above 1,500°F. Above that temperature, the material failed by excessive deformation.

Comparison of Tensile Strengths for ZrO_2 Specimens, Prestressed ZrO_2 Specimens, SiC-Whisker-Strengthened Specimens, and Prestressed, SiC-Whisker-Strengthened Specimens

Comparison of the tensile strength of various specimens, similar to the data shown in Figures 4-7 and 4-8, is made in Figures 4-9 and 4-10. Figure 4-9 shows the comparison between the tensile strength of plain ZrO_2 and SiC-whisker-reinforced ZrO_2, and the cracking stress for prestressed ZrO_2 and

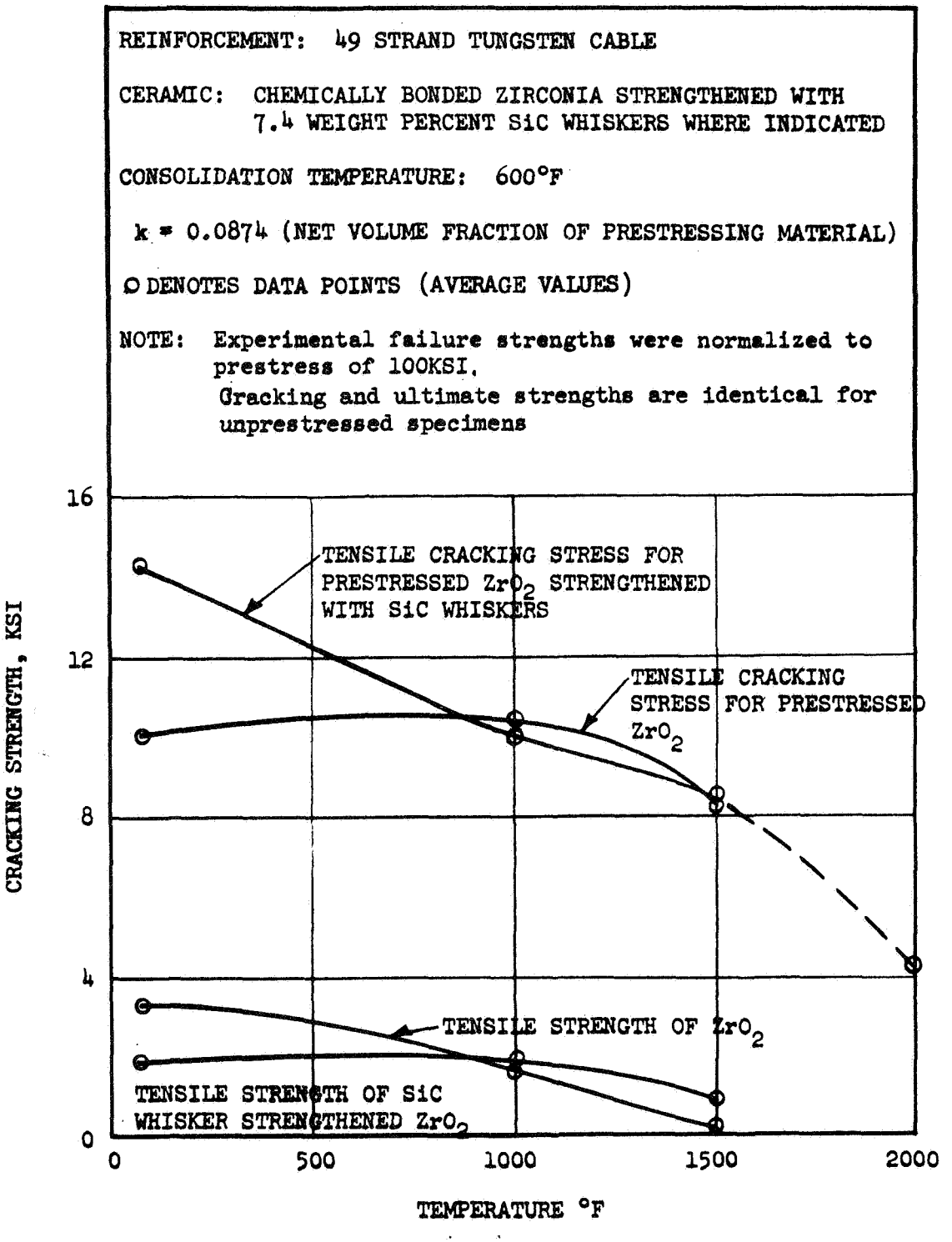

Figure 4-9. Normalized Experimental Cracking Strength for Tension Specimens

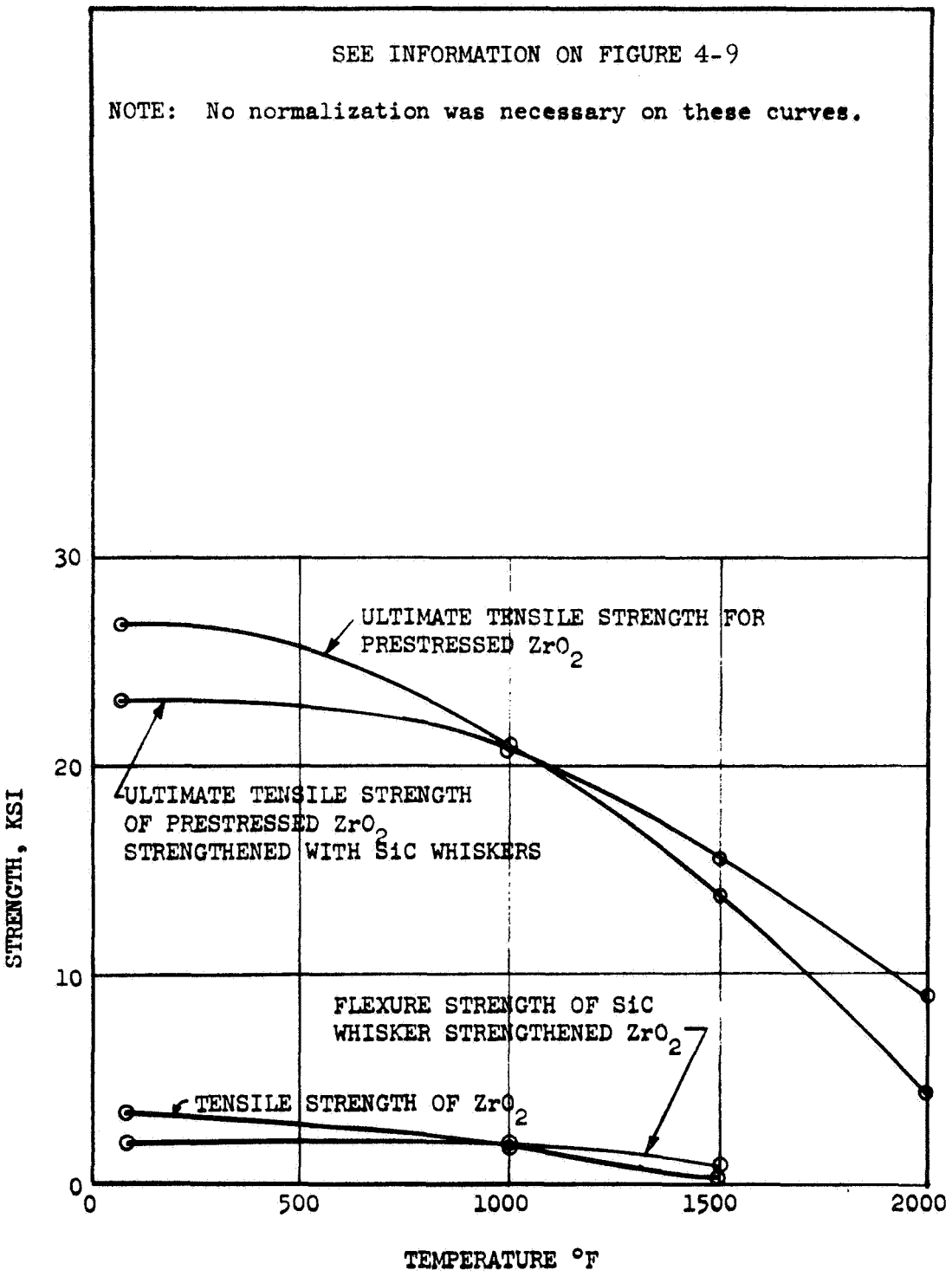

Figure 4-10. Experimental Ultimate Strength for Tension Specimens

prestressed, whisker-reinforced ZrO_2. In Figure 4-10, the ultimate strengths are shown for the case of prestressed specimens. In the latter case, only the results where the specimen failed completely (tensile failure of wire and ceramic) are shown. Ultimate failures where the wires failed by pullout were ignored in this comparison.

The results illustrated in Figure 4-9 show that, at low temperatures, the tensile strength of ZrO_2 is higher than the tensile strength of whisker-strengthened ZrO_2. At high temperatures, the opposite is true. As was mentioned previously, the low strength of whisker-reinforced ceramic is attributed not so much to the ineffectiveness of whiskers, but to poor whisker distribution within the specimens.

At temperatures above 1,000°F, the SiC-whisker-strengthened specimens exhibited higher tensile strengths than the ZrO_2 specimens.

Figure 4-9 shows that the addition of whiskers significantly increases cracking stresses for prestressed tensile specimens, both at low temperatures (70°F to 800°F), and at higher temperatures (1,500°F and above). Results for the ultimate tensile strength (see Figure 4-10) are self-explanatory.

4.5 RESULTS AND CONCLUSIONS

Experimental results obtained to date indicate that, in all cases, the addition of SiC whiskers increased the elevated-temperature strength (tensile and flexure) of the ceramic. In general, the quality of specimens containing SiC whiskers and twice the normal acid content, was not as good as that of specimens without any whiskers. Improvement of the quality of whisker-strengthened specimens is expected to yield higher strength values than those obtained to date. It appears that a reduction in acid content is desirable. The use of high acid content to achieve a castable mix resulted in specimens with higher than normal porosity.

The addition of SiC whiskers to ZrO_2 resulted in an increase of room-temperature flexure strength, and a decrease in the room-temperature tensile strength. This inconsistency in behavior is attributed to the

nonuniform whisker distribution within the gage length of the tensile specimen. Improved mixing techniques for achieving a more uniform whisker distribution appear highly desirable. Furthermore, to insure the reliability of the test data, more extensive testing than that conducted to date is desirable.

4.6 REFERENCES FOR SECTION 4

4-1. L. B. Greszczuk, and H. Leggett, Final Report-Development of a System for Prestressing Brittle Materials, Douglas Aircraft Company Report DAC 49200, August 1967.

Section 5

EXPERIMENTAL AND THEORETICAL STUDIES ON BIAXIALLY PRESTRESSED CERAMICS

Phase II of the program involved experimental and theoretical studies on biaxially prestressed cylindrical configurations. Initially, a literature survey was conducted on biaxial prestressing of brittle materials. Analysis methods were then developed and used to investigate the factors governing the strength of biaxially prestressed ceramic cylinders. Parallel with the theoretical effort, experimental techniques were investigated for fabricating biaxially prestressed specimens. This included an investigation of the feasibility of achieving a desirable reinforcement orientation through variation of winding mode, proper positioning of the reinforcement, design of the mandrel to minimize reinforcement slippage, and means of achieving desirable fiber pretension. Since it was found that ceramic strips had to be placed between the mandrel and the reinforcement to prevent the reinforcement from resting on the mandrel, studies were also performed on the ability of freshly cast ceramic to adhere to precast, precured parts. Finally, using the results of the theoretical and experimental efforts, biaxially prestressed cylinders were designed.

5.1 LITERATURE SURVEY ON BIAXIAL PRESTRESSING OF BRITTLE MATERIALS

A literature survey was conducted on biaxial prestressing of brittle materials. This survey concentrated primarily on various publications regarding prestressed concrete. Examination of various publications regarding ceramics has not produced any significant information on the work in the field of prestressed cylindrical structures. As to the work on prestressed concrete, L. Feeser and J. Chinn (Reference 5-1) conducted experimental studies on the strength and stiffness of spirally prestressed

concrete cylinders. They tested 34, 3-inch-diameter by 12-inch-long solid concrete cylinders. The cylinders were spirally overwound with two sizes of wire: 0.054-inch-diameter steel wire with an ultimate strength of 251 KSI, and 0.0595-inch-diameter steel wire with an ultimate strength of 302 KSI. The cylinders were wrapped with the wires at pitches of 1/16, 1/10, 1/6 and 1/4 inch, with initial tensions of 10, 100, 200, or 300 pounds per wire. Failure in all the prestressed cylinders occurred when the wire ruptured at a necked-down section because of excessive hoop stress. The author's concluded that the increase in strength due to spiral action was independent of the initial tension in the wire. Willis B. Johnson had reached a similar conclusion in his thesis at the University of Colorado in 1950. Figure 5-1 shows the increase in stiffness that was obtained by increasing the prestress.

Chi and Biberstein (Reference 5-2), and also Leonhardt (Reference 5-3) discuss a method of prestressing circular concrete structures which relies on a cold drawing process to give the desired tension. A die is mounted on a track which moves with a constant speed along the axial direction of the cylindrical structure, while the structure rotates on a lathe. The prestressing wire is fed from the shipping reel through the die, and anchored at one end of the cylinder. While the wire is being wound on the cylinder it is drawn through the die, acquiring its final diameter and high strength only as a result of the winding operation. The prestressing force, therefore, corresponds to the drawing resistance. The angle of wrap can be varied by changing the ratio of rotational speed of the lathe to the axial speed of the die.

Leonhardt (Reference 5-3) describes a hoop prestressing method for cylinders whereby a driving wheel, or pulley, rotates around the circumference of the cylinder. The prestress is produced when the wire to be tensioned is unwound from a pulley. The circumference of the pulley is smaller than the circumference of the drive wheel by an amount equal to the wire extension, corresponding to the desired prestress. A method similar to that described earlier may also be used, whereby the pulley or driving wheel moves only in the axial direction and the cylinder rotates on a lathe.

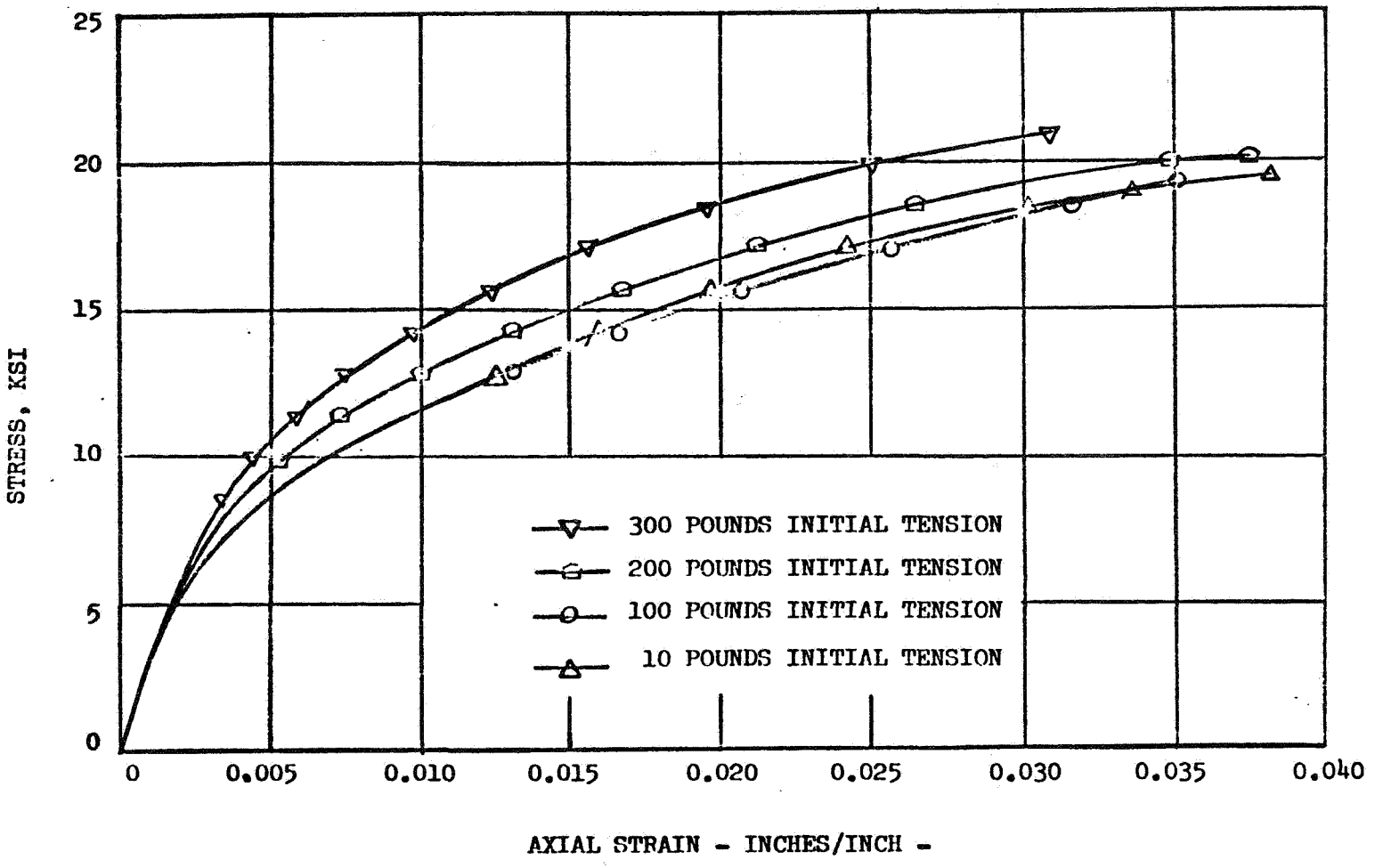

Figure 5-1. Axial Stress vs Strain for Concrete Cylinders Helically Overwound With Steel Wires (Reference 5-1.)

References 5-4 and 5-5 have short discussions on reinforced cylindrical prestressed concrete structures, or pipes, in which the reinforcement is either hoop or helically wound.

5.2 ANALYTICAL STUDIES ON BIAXIALLY PRESTRESSED CYLINDERS

Methods were developed to analyze the magnitude of biaxial prestress in cylinders, and the strength of final composite configurations. The analysis established ceramic precompression influences by such variables as reinforcement winding tension and its orientation (helix angle), volume of the reinforcement, thermal and elastic properties of the ceramic and reinforcement, and fabrication techniques. Moreover, analyses of cylinder strengths were made. The level of sophistication in this analytical effort was similar to that for predicting the strength of flat specimens, which was developed during the first-year effort. The strength of the cylinder was expressed in terms of the variables cited above, as well as temperature and the external loads acting on the cylinder. The analyses were used to perform tradeoff studies on the factors governing strength of prestressed cylinders. The results of the tradeoff studies were, in turn, used to select a cylinder design for experimental studies.

5.2.1 Theory for Internal Prestress and Strength of Biaxially Prestressed Cylinders

Knowledge of internal stresses in the ceramic, as well as the reinforcement, is required to estimate the strength of biaxially prestressed cylinders. Included in this estimate are stresses caused from externally applied loading, thermal stresses, and stresses caused from mechanical and thermal prestress. To determine these stresses, a two-dimensional stress analysis of the problem was undertaken for a multilayer anisotropic cylindrical structure, consisting of a matrix and filaments, subjected to any combination of the following loads: applied external, normal, or shear forces; internal prestress; and thermal effects. The analysis applies for the general case when the material properties of the matrix and reinforcement are different, including different values for the coefficients of thermal expansion. The

detailed description of the theoretical analysis is given in the Appendix. In brief, the analysis presented therein allows determination of the stresses in the constituents caused from pretension of the reinforcement; stresses in the constituents caused from an external load acting on a composite; and stresses in the constituents when the composite is subjected to elevated temperature. The variables in the analysis are: reinforcement volume fraction, reinforcement orientation (helix angle), reinforcement prestress, temperature, elastic properties of constituents (ceramic and reinforcement), and strength properties of constituents.

5.2.2 Theoretical Tradeoff Studies on Biaxially Prestressed Cylinders

Using the analyses presented in the Appendix, tradeoff studies were conducted to determine the optimum wrap angle for a given reinforcement prestress and a given use temperature. The constituent properties used in these studies were those which were obtained experimentally (see Section 3). The prestressing material was a 21-strand tungsten cable, while the matrix was a chemically consolidated zirconia strengthened with 7.4-weight-percent of SiC whiskers. The first step in the optimization studies was to determine the stresses in the constituents as a function of the reinforcement orientation, reinforcement prestress, temperature, and externally applied loading. Figures 5-2, 5-3 and 5-4 show some typical results for the stresses in the constituents of a biaxially prestressed, internally pressurized, cylinder. The results shown are for a 2-inch internal radius by 0.25-inch thick cylinder subjected to an internal pressure of 1,250 psi. A balanced helix wrap was assumed. The reinforcement volume fraction was assumed to be $k = 0.0363$.

Figure 5-2 shows the stress in the reinforcement, as a function of the reinforcement wrap angle, for four values of initial prestress and two values of temperature. Figures 5-3 and 5-4 show the stresses in the ceramic in both circumferential and longitudinal directions of the cylinder as a function of reinforcement wrap angle. The results shown there are for the same loading conditions and temperatures as those shown in Figure 5-2.

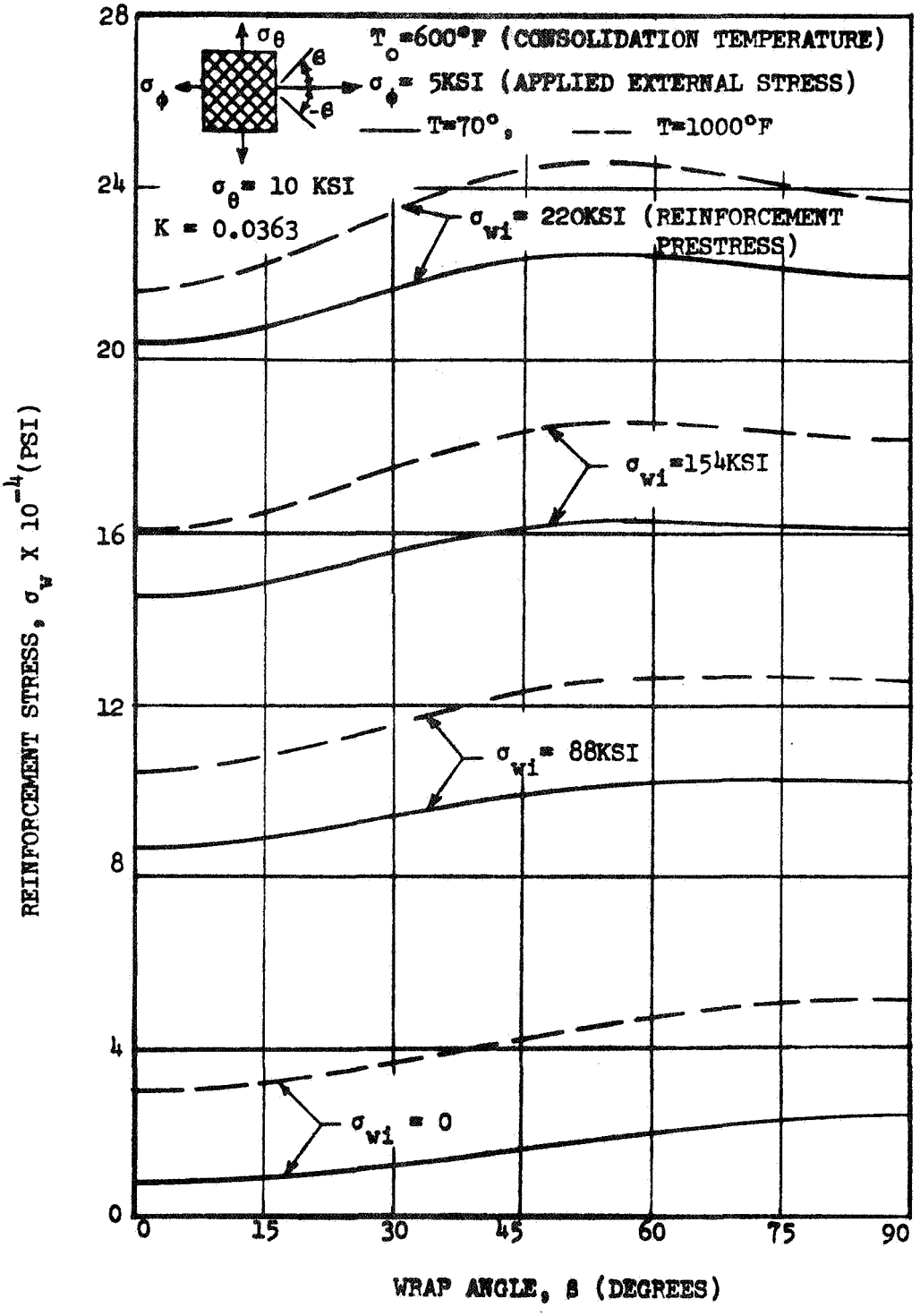

Figure 5-2. Reinforcement Stress for Various Prestresses as a Function of Reinforcement Wrap Angle

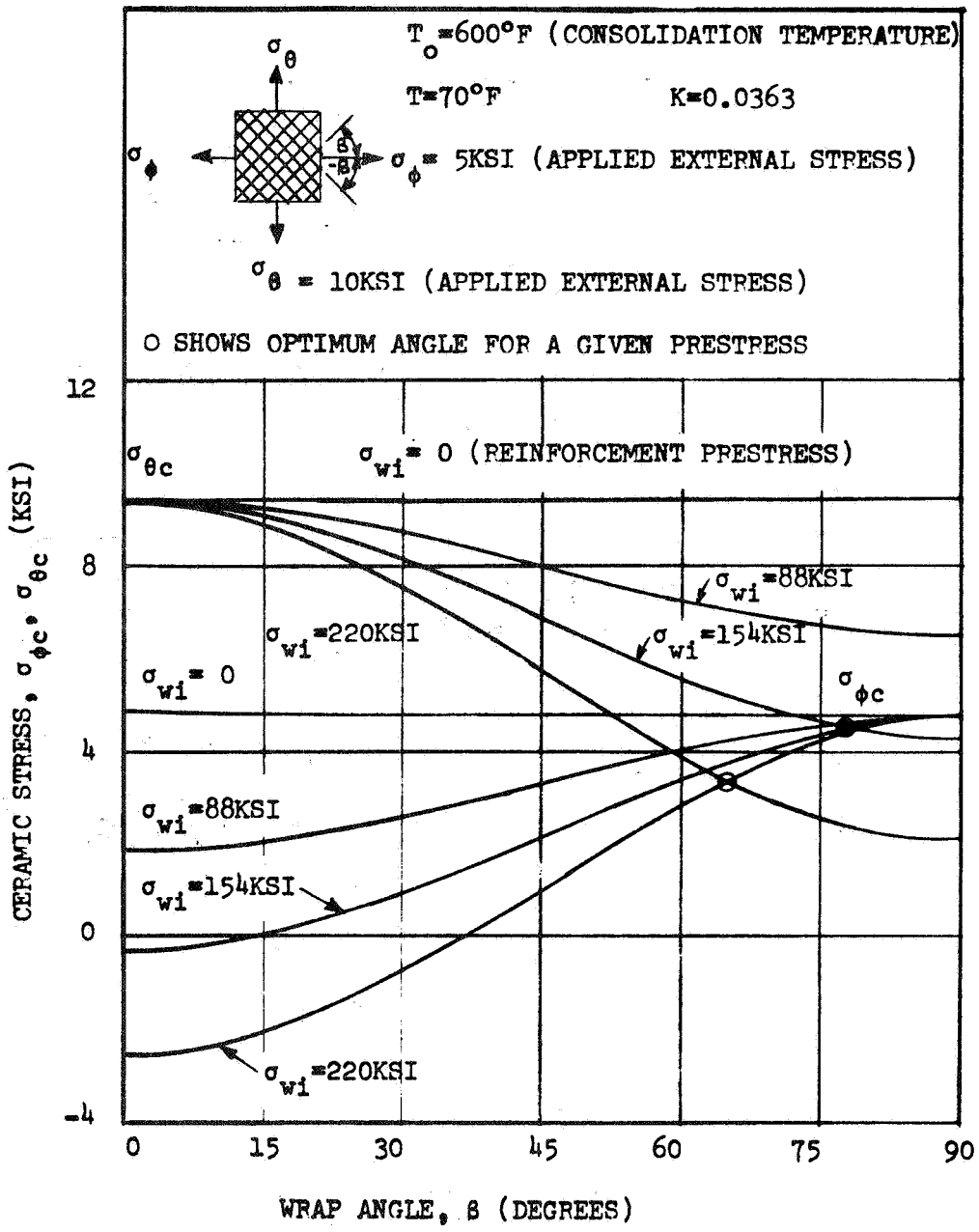

Figure 5-3. Ceramic Stress for Various Reinforcement Preloads as a Function of Reinforcement Wrap Angle (Use Temperature, T=70°F)

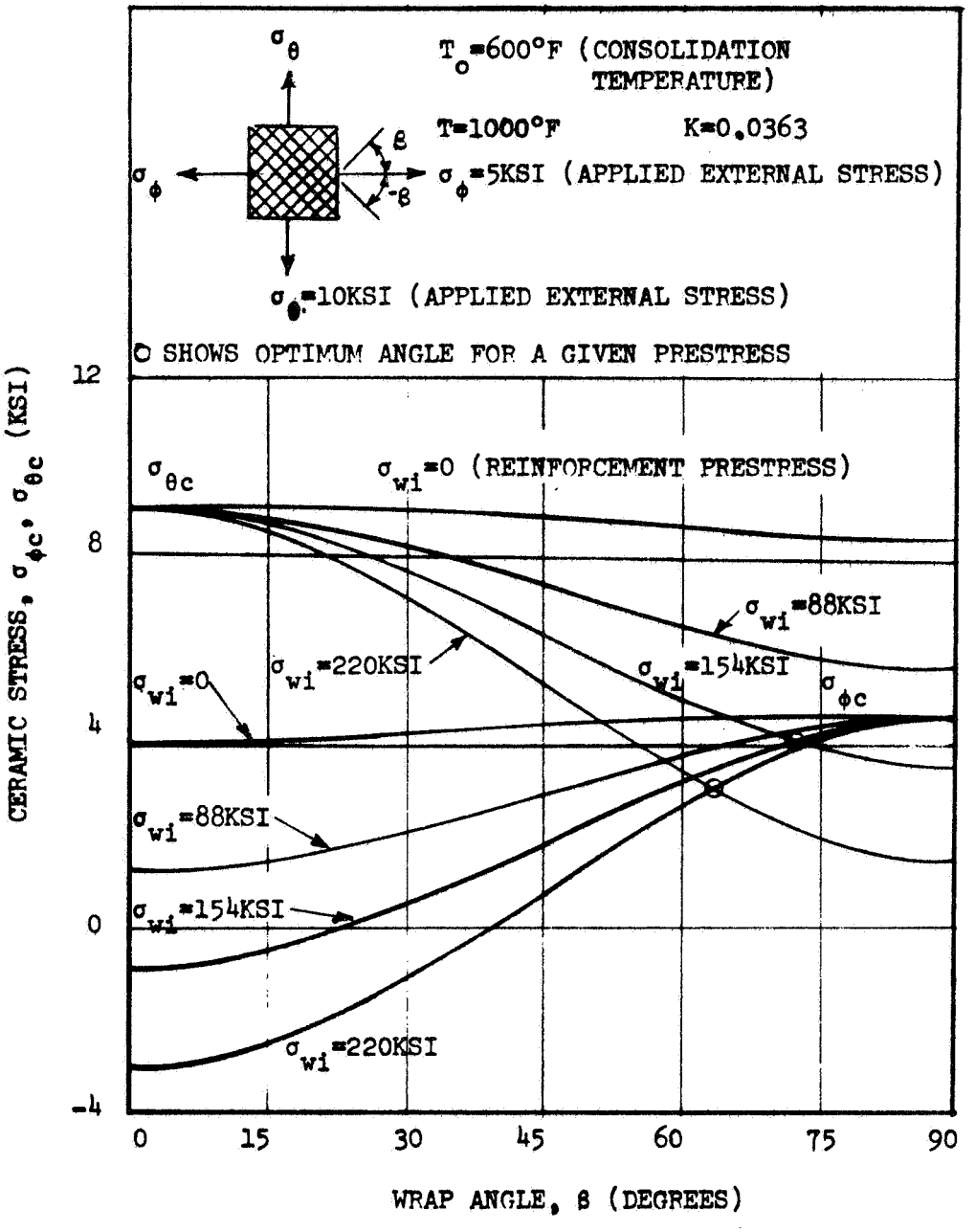

Figure 5-4. Ceramic Stress for Various Reinforcement Preloads as a Function of Reinforcement Wrap Angle (Use Temperature, t=1000°F)

The circles in Figures 5-3 and 5-4 show the optimum reinforcement wrap angles, for a given temperature and prestress, if failure is caused by excessive stress in the ceramic in the circumferential or longitudinal directions of the cylinder. The optimum wrap angle varies with temperature.

Using the information shown in Figures 5-2, 5-3 and 5-4, and the allowable strength values for the constituent (reinforcement and matrix) failure envelopes were generated for the biaxially prestressed specimens. These are shown in Figures 5-5 through 5-9.

When calculating the failure envelopes for the cylinders, the following three failure modes were considered: (1) when the tension stress in the ceramic, in either the hoop or axial direction of the cylinder, caused from the combined effects of internal prestressing, thermal stress, and applied external loading, exceeds the allowable tensile strength of the ceramic at a given temperature; and (2) when the tensile stress in the reinforcement caused from prestressing, thermal effects, and applied external loading exceeds the allowable tensile strength of the reinforcement. The strength of the cylinder was taken as the minimum of the three failure modes. Figure 5-5 illustrates the three modes of failure for a cylinder subjected to a temperature of 2,000°F. For a cylinder having $\sigma_{wi} = 0$, with a wrap angle between 0 and 50 degrees, tension failure would occur in the ceramic in the hoop direction. Between 50 and 77 degrees, tensile failure of the reinforcement would occur; and for wrap angles greater than 77 degrees, tensile failure would occur in the ceramic in the longitudinal direction.

The optimum reinforcement wrap angle for a given temperature and prestress can be obtained from Figures 5-5 through 5-9. For example, Figure 5-5 shows that the optimum reinforcement angle for zero prestress and a temperature of 2,000°F is 77 degrees. However, there is very little variation in strength between the helix angles of 50 to 77 degrees. The optimum prestress varies with temperature and, in general, high prestress is desirable for structures to be used at low temperatures; for prestressed structures to be used at high temperatures, a low prestress is the most desirable. For example, comparing the two curves shown in Figure 5-5

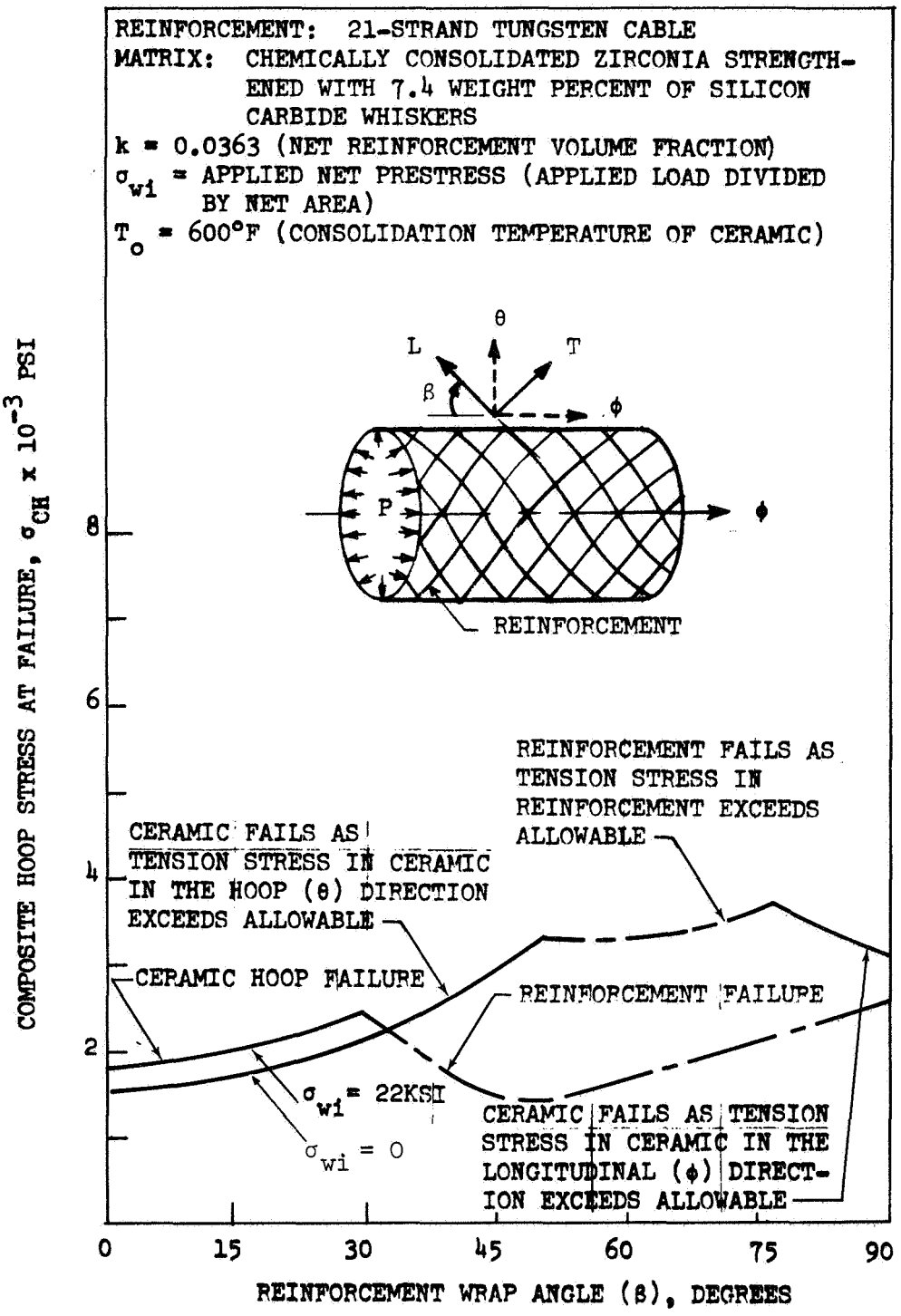

Figure 5-5. Strength of Internally Pressurized, Biaxially Prestressed Ceramic Cylinder Subjected to 2000°F

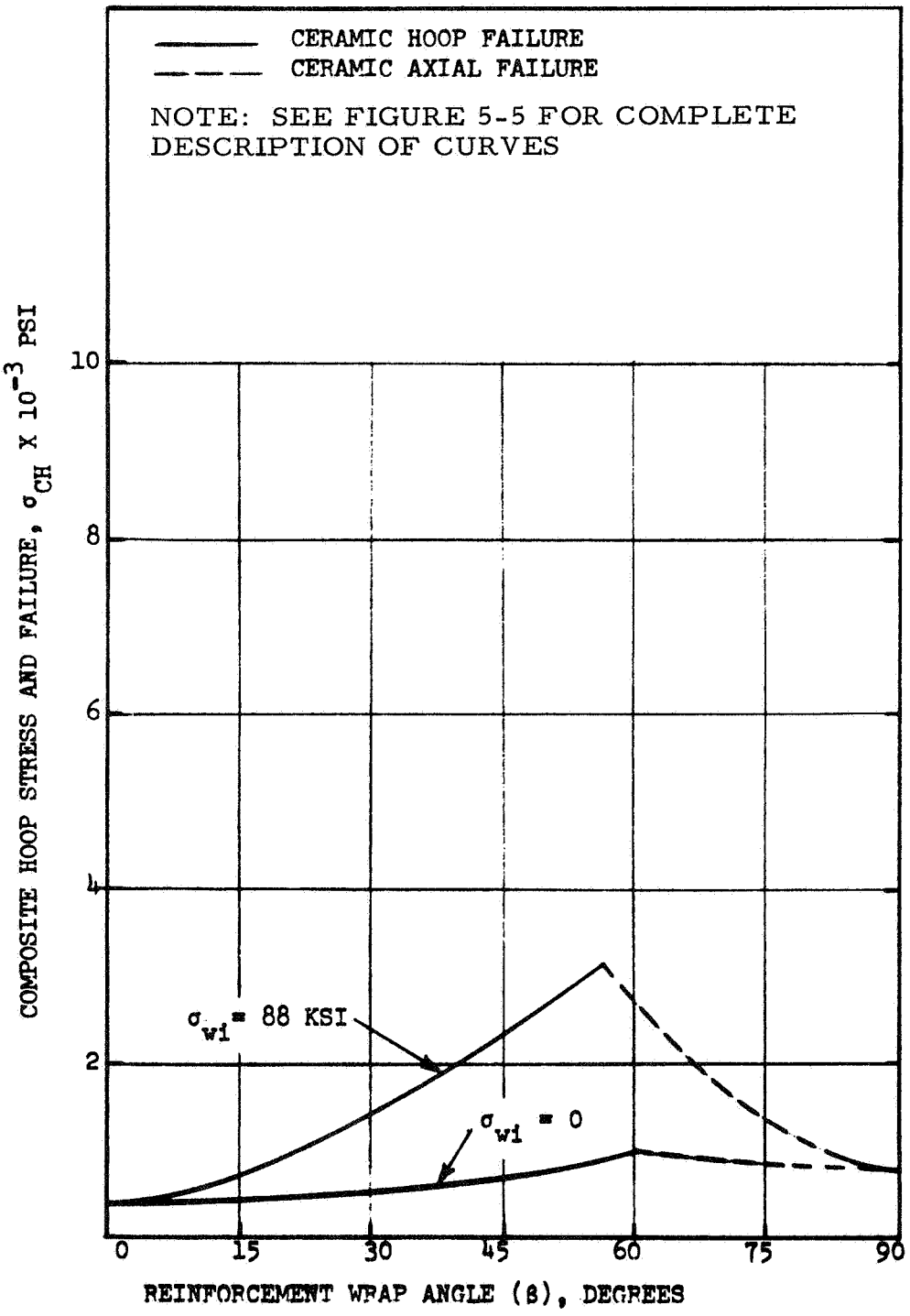

Figure 5-6. Strength of Internally Pressurized, Biaxially Prestressed Ceramic Cylinder Subjected to 1500°F

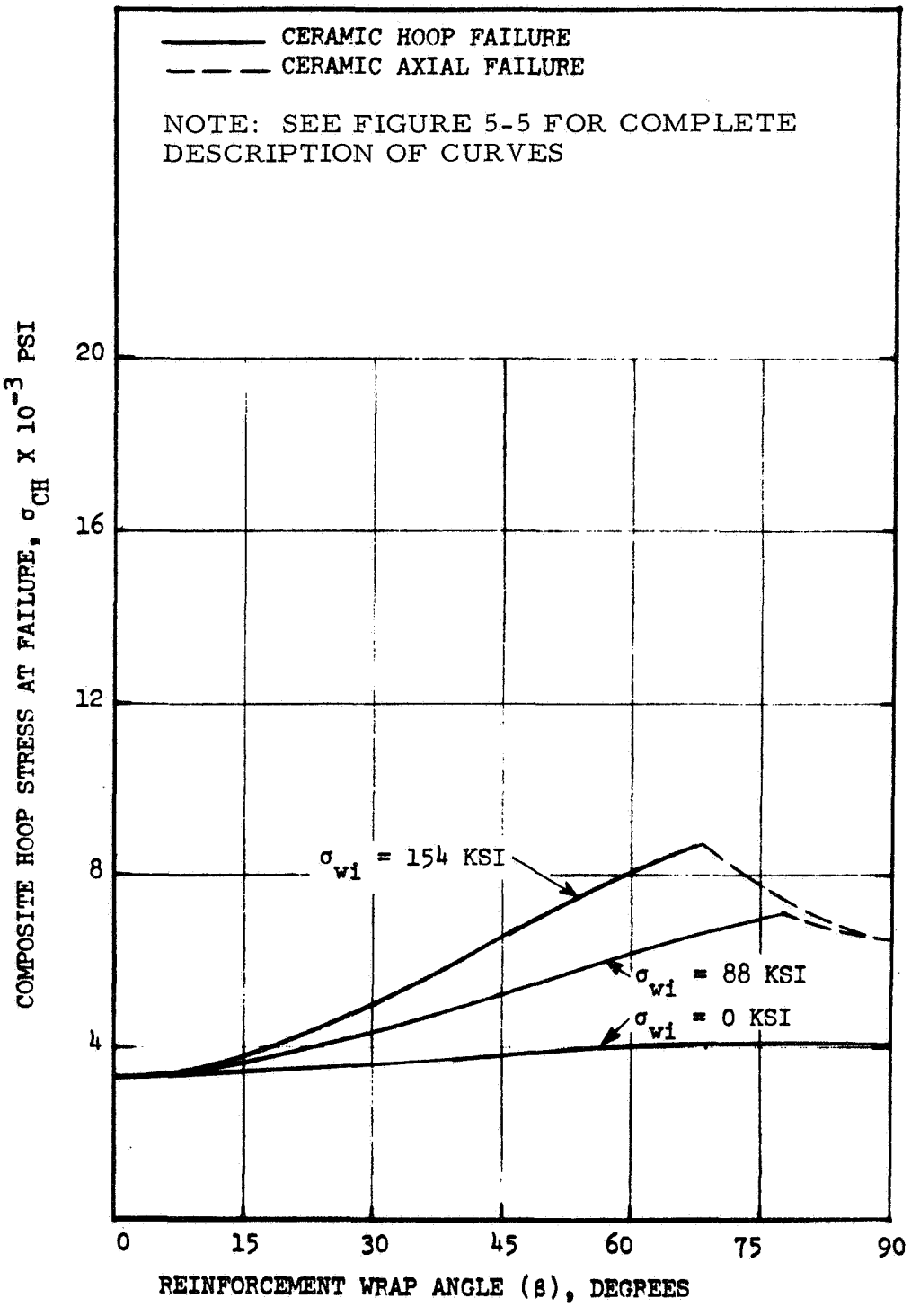

Figure 5-7. Strength of Internally Pressurized, Biaxially Prestressed Ceramic Cylinder Subjected to 1000°F

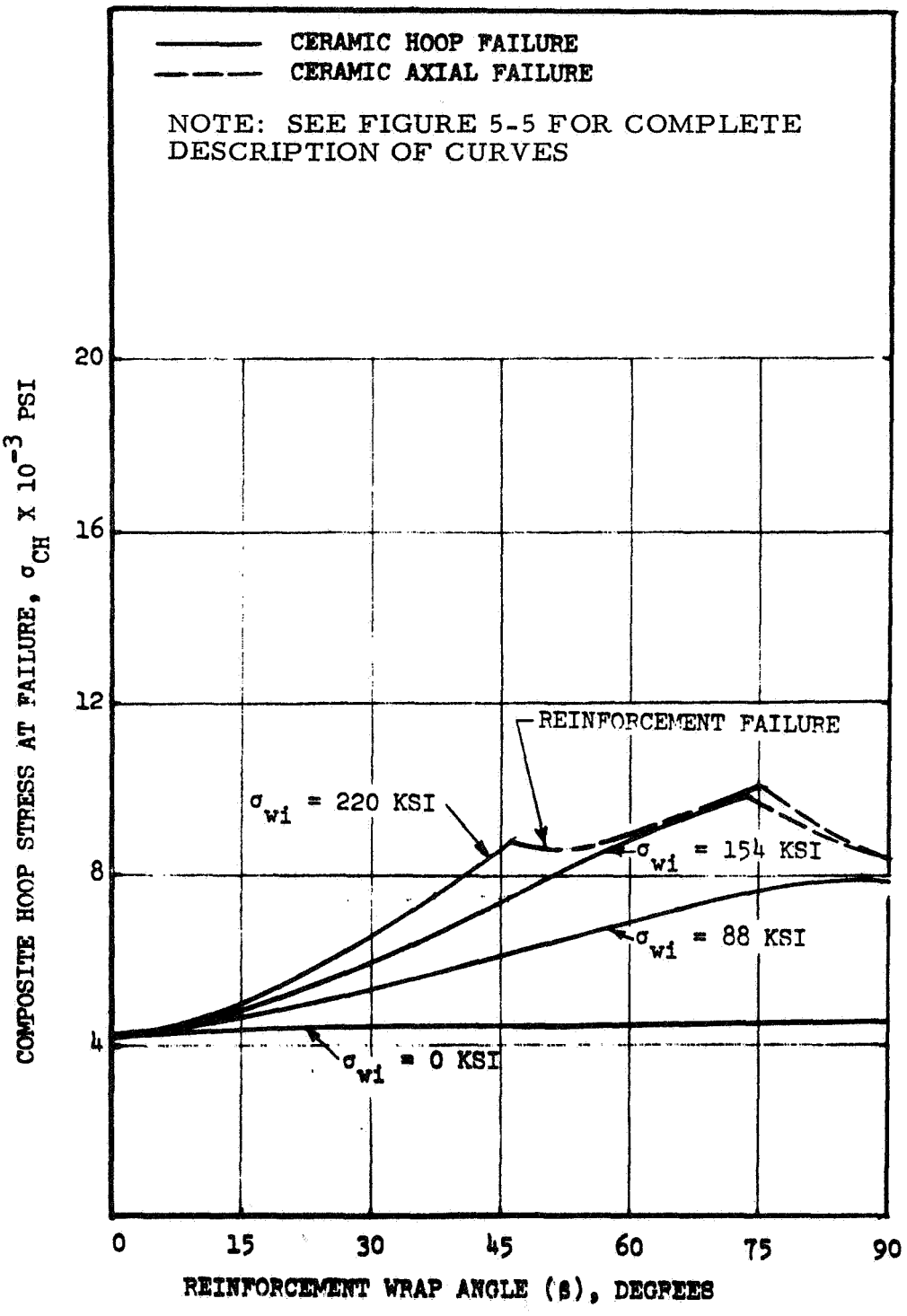

Figure 5-8. Strength of Internally Pressurized, Biaxially Prestressed Ceramic Cylinder Subjected to 600°F

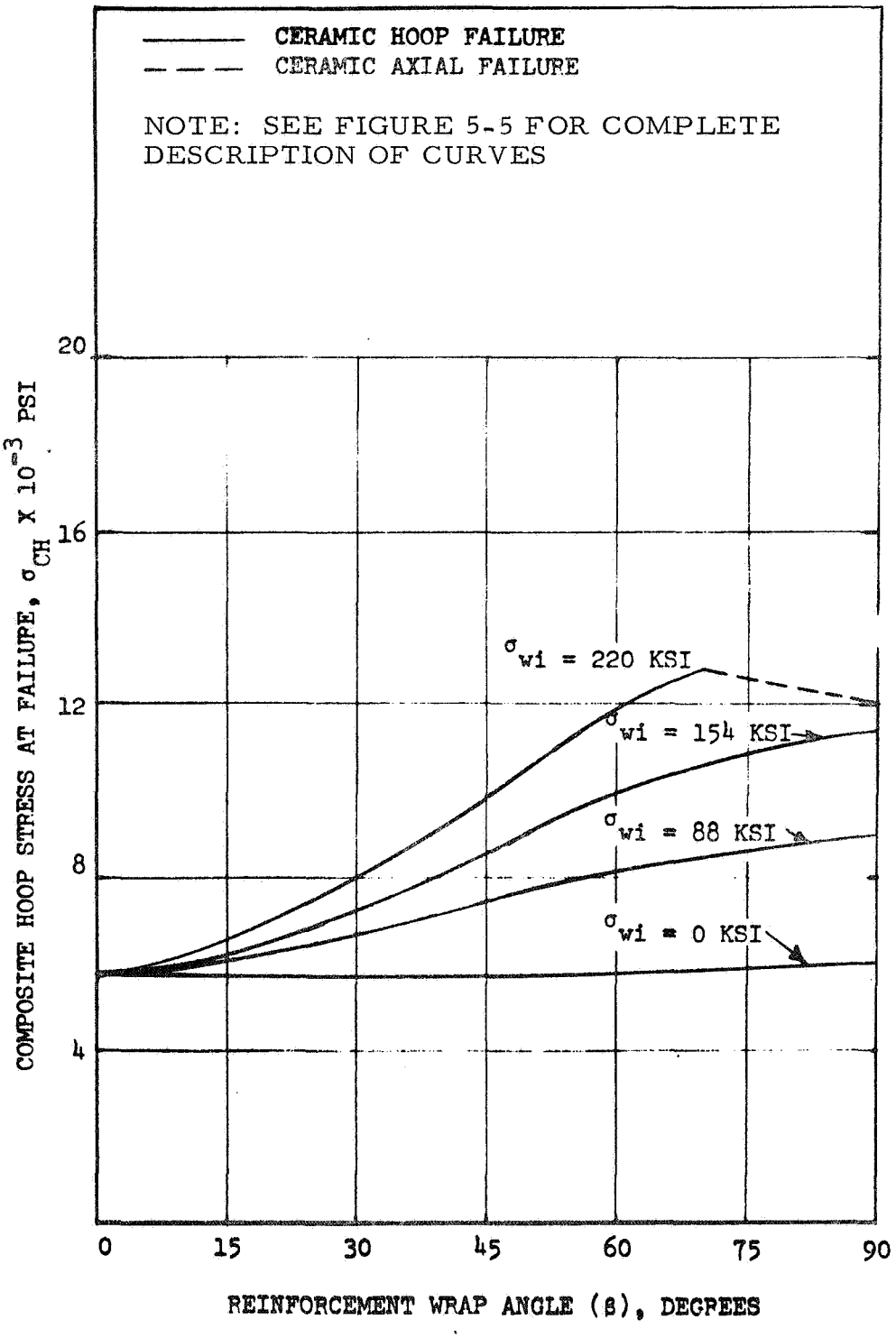

Figure 5-9. Strength of Internally Pressurized, Biaxially Prestressed Ceramic Cylinder Subjected to 70°F

(one for $\sigma_{wi} = 0$ and one for $\sigma_{wi} = 22,000$ psi) shows that the allowable applied external hoop stress causing failure at 2,000°F decreased from approximately 3,700 psi for zero internal prestress to 2,600 psi for 22,000 psi internal prestress. Figure 5-9 shows that the allowable applied external hoop stress at 70°F increases from approximately 6,000 psi for zero internal prestress to 13,000 psi for 220,000 psi internal prestress.

5.3 INVESTIGATION OF EXPERIMENTAL METHODS FOR INDUCING BIAXIAL PRESTRESS

Although there exist several techniques for prestressing cylindrical structures, only a few are of practical importance. The results of the literature survey presented in Section 5.1 summarize some of the more important work in this area.

One of the techniques considered initially involved shrink fitting of metal bands onto ceramic cylinders. This technique was abandoned because it induces only a undirectional prestress. The two techniques that were tried involved bidirectional winding and helical winding.

5.3.1 Polar Winding Mode

The results of a trial winding in the polar mode are shown in Figure 5-10. The mandrel was made of sand PVA. The end rings with radial pins were made of aluminum. The purpose of the radial pins was to prevent the reinforcement from slipping. The highest angle that could be obtained while winding in the polar mode was 15 degrees. One problem encountered initially was that the reinforcement rested directly on the sand mandrel. Since this was highly undesirable, it was then decided to place a layer of circumferential windings on the mandrel prior to winding in the polar mode. The circumferential windings raised the polar windings above the mandrel surface so that the ceramic could penetrate and encapsulate the reinforcement.

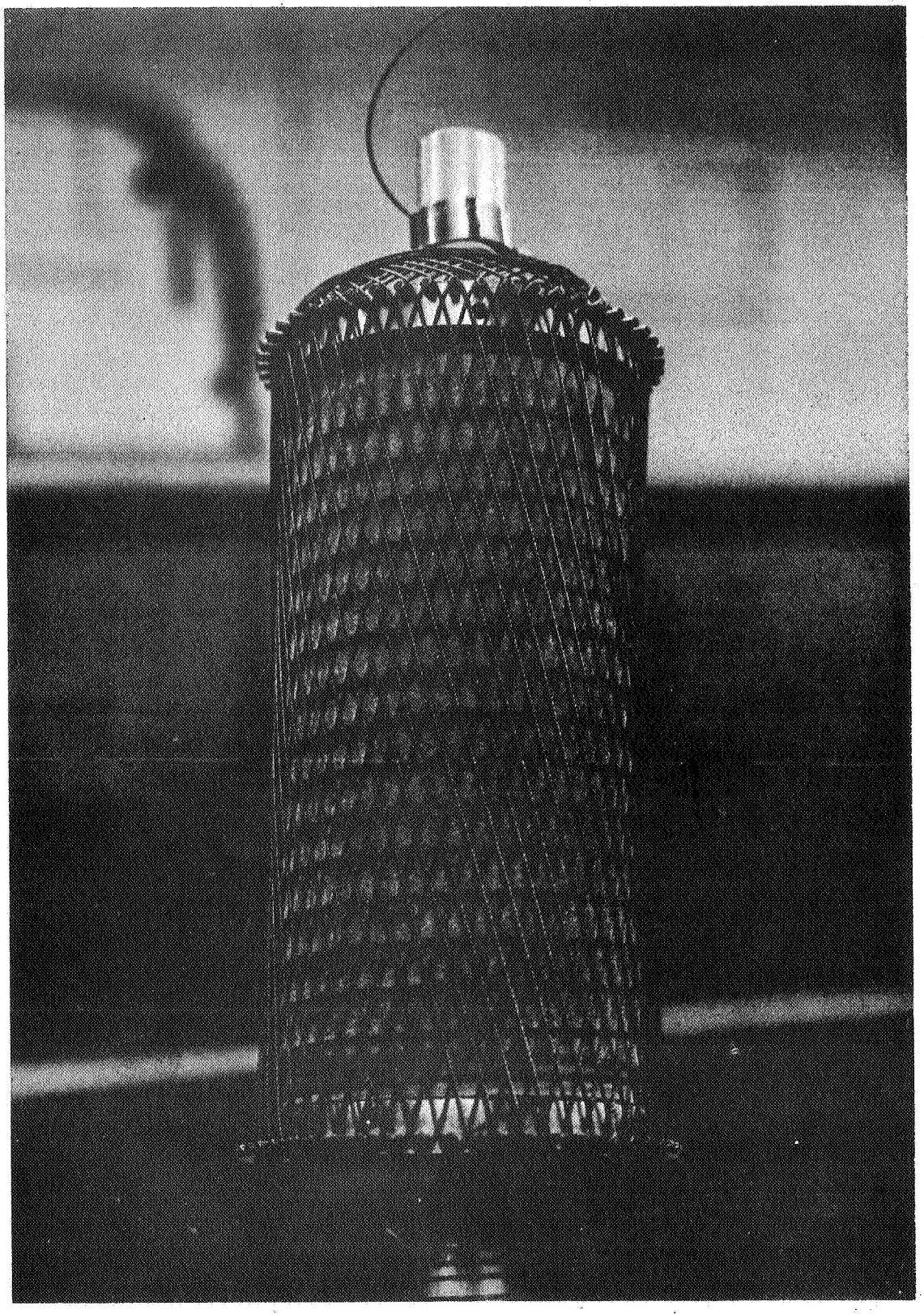

Figure 5-10. Mandrel Overwound with 7-Strand Tungsten Cables (15-Degree Helix Angle)

5.3.2 Helical Winding Mode

Since the theoretical studies indicated that reinforcement orientation angles higher than 15 degrees were required, a helical winding mode was tried next. Figure 5-11 shows a cylinder overwound with a 21-strand tungsten cable. The helix angle is about 57 degrees. Rather than using the hoop wrap to raise the helical windings above the mandrel surface, as shown in Figure 5-10, strips running in the direction of the cylinder axis were used. These would ordinarily be made of ceramic. Studies on the adhesion between the newly cast ceramic and a preformed, precast ceramic indicated that a good bond could be formed between the two. The main reason for using the ceramic strips was to ensure the complete encapsulation of the reinforcement in the ceramic. If the reinforcement were left exposed on the inner surface of the cylinder, as would be the case if the fabrication technique depicted in Figure 5-10 were used, rapid oxidization of the reinforcement would occur when the structure was exposed to elevated temperatures.

5.3.3 Preliminary Fabrication Studies

Two biaxially prestressed cylinders were fabricated using the filament winding technique described in Sections 5.3.1 and 5.3.2. The first trial cylinder was fabricated using the polar winding technique. First, teflon tape was wrapped on the sand mandrel, then, a layer of 21-strand tungsten cables. The overwound unit was placed in a cylindrical container and the surrounding space was infiltrated with a ceramic. Since this was a practice run to uncover problems in preparing biaxially prestressed specimens, the ceramic used did not contain any SiC whiskers--it was a conventional chemically consolidated ZrO_2 developed during the first-year effort (Reference 5-6).

Figure 5-12 shows an internal view of the first trial cylinder. One of the serious problems encountered was the presence of abnormally high porosity, as is obvious from Figure 5-12. Apparently, the reason for this was that when the cylinders were cast vertically in aluminum molds, the gases could not readily evolve through the 12-inch height of the ceramic.

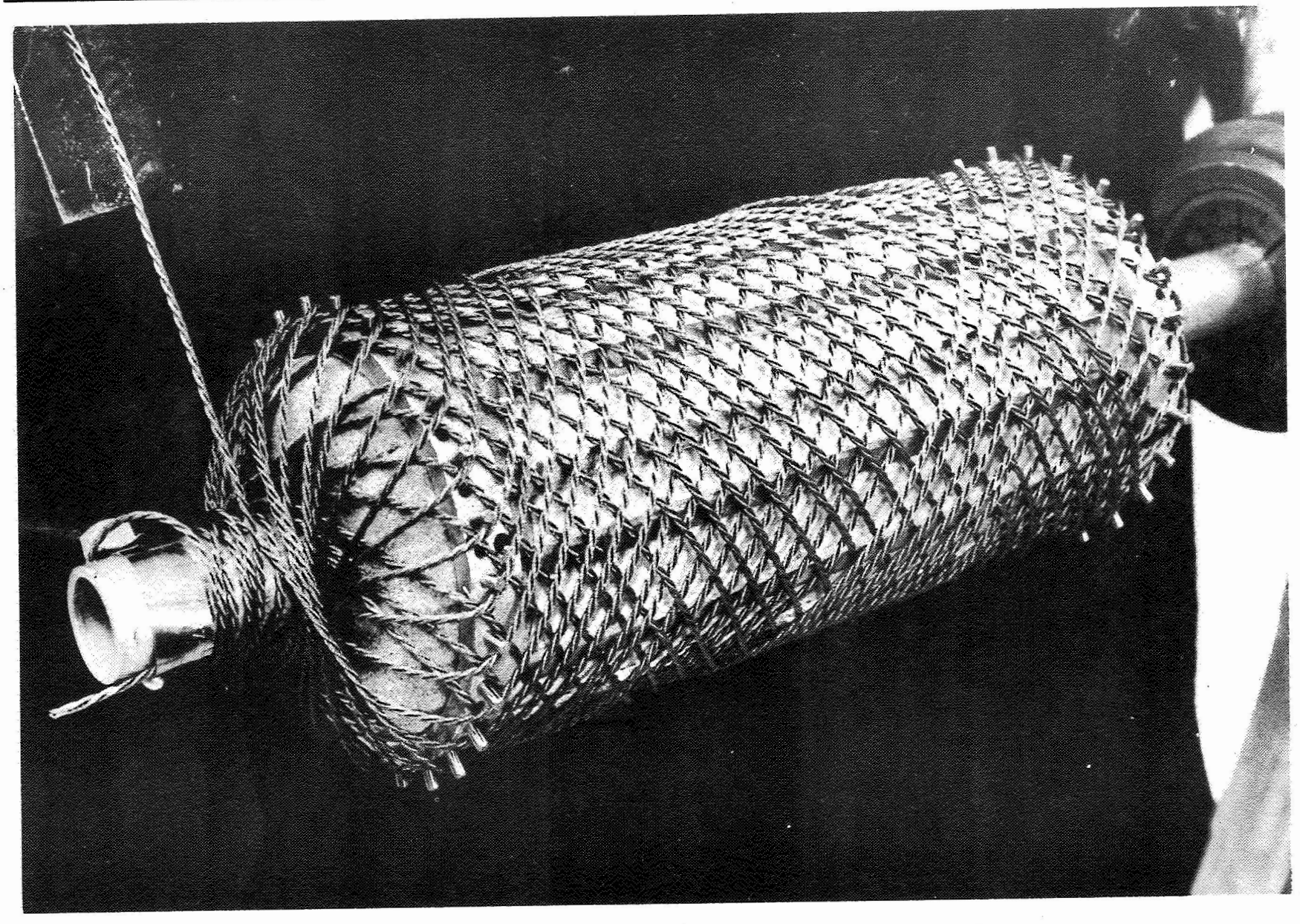

Figure 5-11. Helically Wound Cylinder (57-Degree Helix Angle, 21-Strand Tungsten Cable)

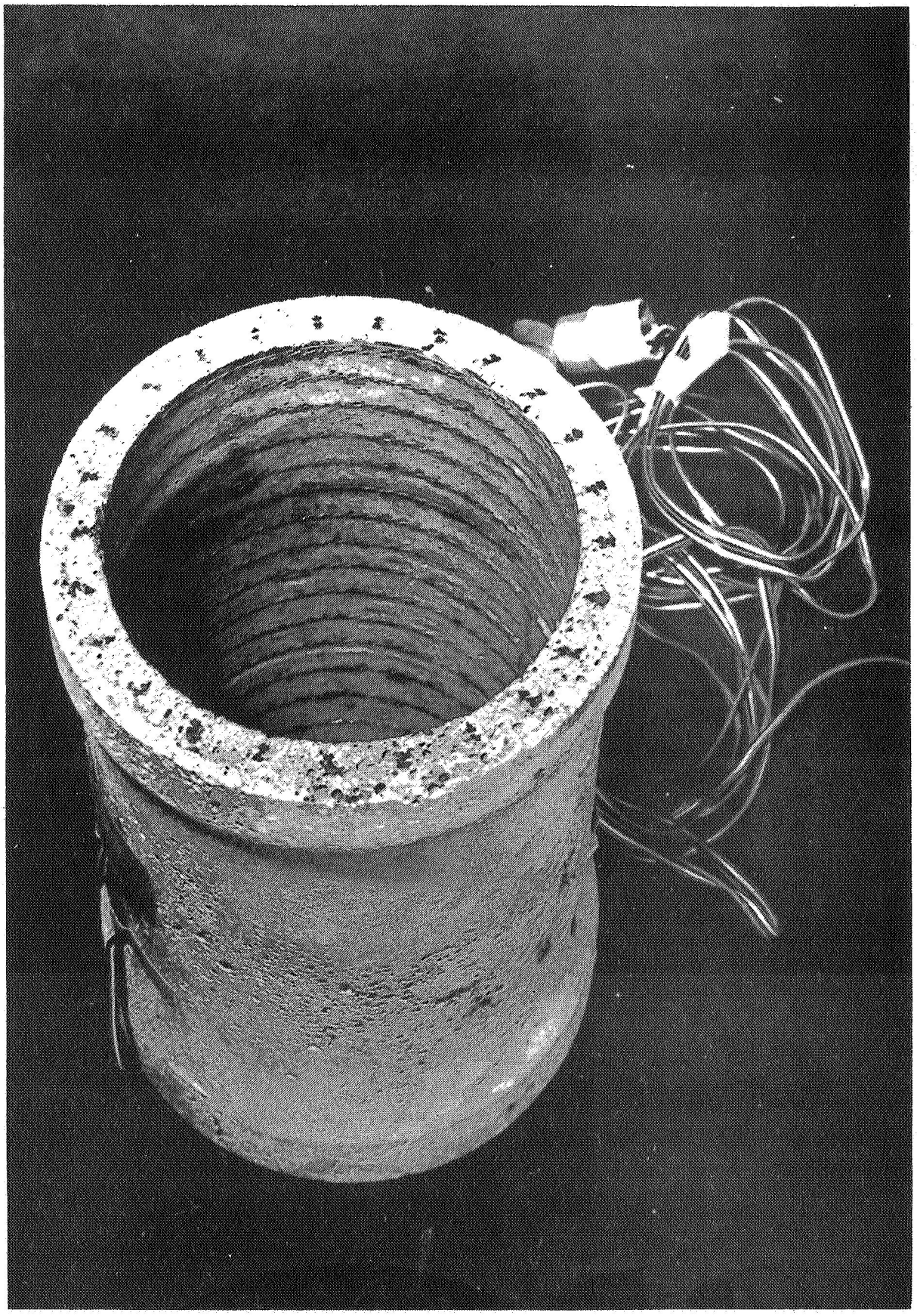

Figure 5-12. Interior View of a Biaxially Prestressed Cylinder

The second trial cylinder was made by first placing longitudinal ceramic strips (0.10 x 0.40 x 7.0 inches) on the sand mandrel, and winding the reinforcement over the strips, as described in Section 5.3.2. The assembly was then placed in a cylindrical aluminum mold and infiltrated with a ceramic slurry. Use of this fabrication technique prevented exposure of the reinforcing material. For the second cylinder, the reinforcement was wound at approximately a 45-degree helix angle. Although the second cylinder also exhibited abnormal porosity, the information obtained from this work was sufficient to establish the best mandrel design for making the final test specimen.

5.4 DESIGN OF BIAXIALLY PRESTRESSED CYLINDERS

On the basis of the work described in Sections 5.2 and 5.3, a biaxially prestressed cylinder design was selected for the experimental effort. The design selected was used to demonstrate the superior, high-temperature, strength-to-weight characteristics of biaxially prestressed ceramic, and to verify validity of the theory. The fabrication procedure described in Section 5.3 also had an influence on the final design.

In the final cylinder design, a 21-strand tungsten cable was used. A 57-degree helix angle was selected. The cable pretension was chosen as σ_{wi} = 21,000 psi. Even though it would be desirable to have $\sigma_{wi} = 0$ to achieve optimum strength at high temperature (see Figure 5-5), winding with zero cable tension was considered to be impractical.

5.5 REFERENCES FOR SECTION 5

5-1. L. J. Feeser, and J. Chinn. Strength and Stiffness of Spirally Prestressed Concrete Cylinders. Prestressed Concrete Institute Journal, Volume 7, June 1962.

5-2. M. Chi, and F. A. Biberstein. Theory of Prestressed Concrete, Prentice-Hall Inc., New Jersey, 1963.

5-3. F. Leonhardt. Prestressed Concrete Design and Construction. Wilhelm Ernst and Sohn, Berlin-Munich, 1964.

5-4. H. J. Cowan. The Theory of Prestressed Concrete Design. Macmillan and Company, Ltd, London, 1956.

5-5. T. Y. Lin. Prestressed Concrete Structures. John Wiley and Sons, Inc., New York-London, 1963.

5-6. L. B. Greszczuk, and H. Leggett. Final Report-Development of a System for Prestressing Brittle Materials. Douglas Aircraft Company Report DAC-49200, August 1967.

Section 6
FABRICATION OF BIAXIALLY PRESTRESSED CYLINDERS

Following the preliminary fabrication studies and optimum cylinder configuration design, two steel mandrels were built for fabricating the final cylindrical test specimen. Biaxially prestressed ceramic cylinders, strengthened with SiC whiskers, were then fabricated.

6.1 FINAL MANDREL CONFIGURATION

Two metal mandrels were fabricated for making the final test specimens. Figure 6-1 is a photograph of an assembled and disassembled mandrel showing the various components. The mandrels were made of steel coated with a permanent teflon coating to prevent adherence of the cast ceramic to the mandrel. The pins in the end rings were for the purpose of achieving uniform spacing between the prestressing cables, and to prevent cable slippage.

The mandrels had an outside diameter of 3.75 inches for a distance of 7.0 inches. There were 24 pins in the end plugs. These were used to achieve uniform spacing of 0.49 inch between the helically wound, prestressed cables.

6.2 FABRICATION OF FINAL TEST SPECIMEN

To fabricate the final test specimen, additional filament winding work was performed to finalize the winding setup. Appropriate modifications were made in casting the ceramic and also in the cure cycle to obtain good quality specimens. Finally, the cylinders were ground to the size required for testing.

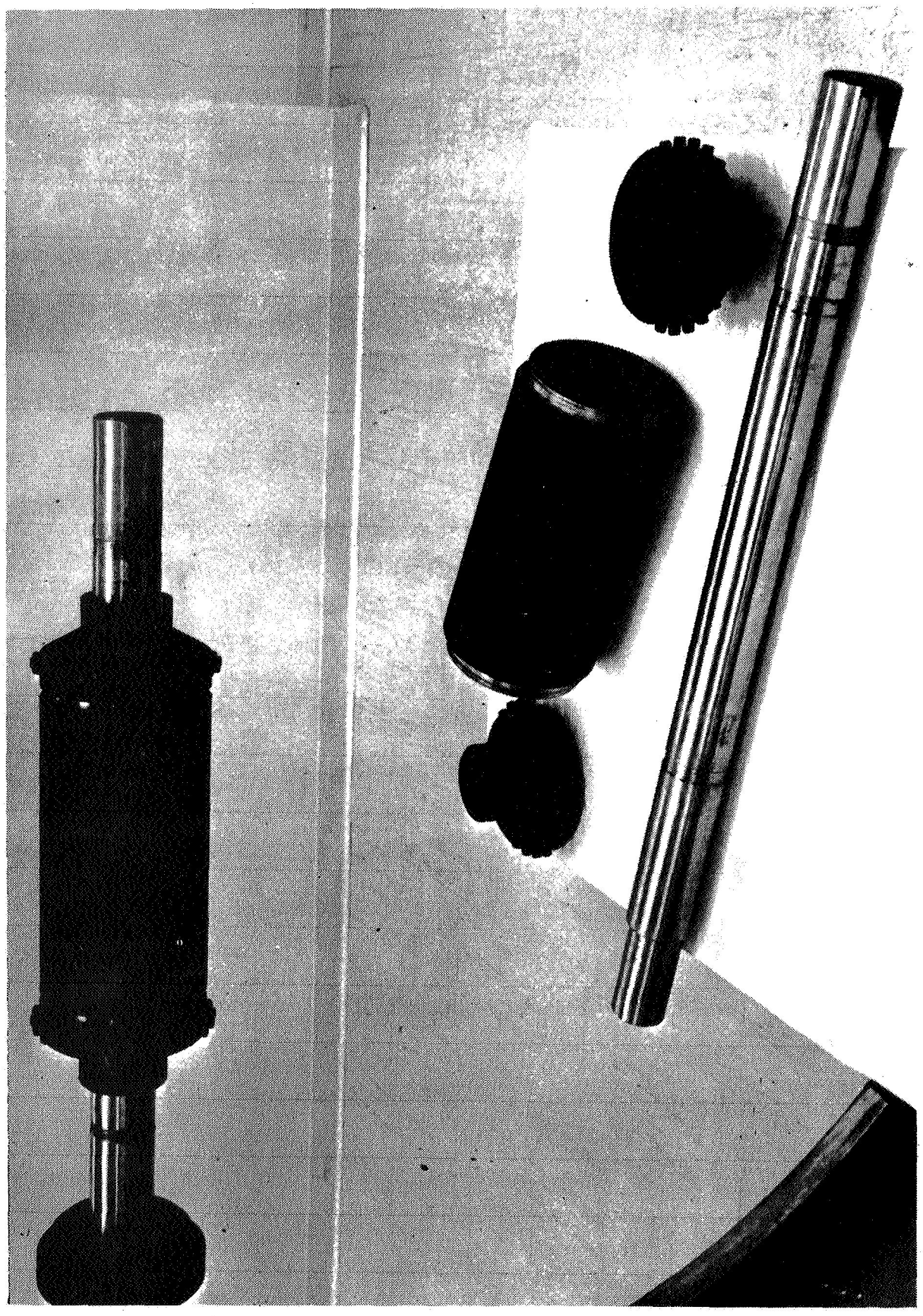

Figure 6-1. Teflon-Coated Steel Mandrels for Fabricating Biaxially Prestressed Cylinders

6.2.1 Filament Winding of Pretensioned Reinforcement

The mandrels and guide-eye tooling were fabricated, inspected and set up preparatory to tool trial winding. Several trial windings were performed before a proper interrelationship was obtained between the following:

1. Lathe crosshead rate, that is, the axial movement of the mandrel.
2. Axial speed rate of the mandrel in relation to its circumferential speed (coarse adjustment).
3. Vernier adjustment for the angular rotation of the mandrel by means of the variable speed reducer.
4. Control of mandrel axial travel by setting the reversing limit stops in order to develop the proper dwell time while maintaining cable tension.
5. Horizontal and vertical positioning of the guide eye in relation to the mandrel axis. This setting has an effect on the amount of cable bending as well as the location of the axial travel reversing stops.

The proper interrelation of the above settings was necessary to establish the desired winding pattern. Determination of the proper setting was accomplished by trial and error as the axial travel stops and variable speed reducer lack vernier precision control. In addition, it was necessary to establish control methods, or account for, the following nonadjustable variables inherent to winding the specimen configuration: stability of cable crossover; height of the ceramic strips; constantly changing effective specimen diameter; precise repeatability of each winding pass or cycle; repeatability of assembling the mandrel (specimen to specimen); and uncontrolled deflection of the mandrel at the guide eye caused from cable diameter discontinuities against the guide-eye surface. The small individual errors introduced by the nonadjustable variables almost precluded winding a perfect pattern. Therefore, manual machine adjustments were made intermittantly as necessary during specimen winding to compensate for these variables.

After several more trials, and introduction of several corrective procedures during the filament winding operation, the following fabrication procedure was established and used to helically wind the pretensioned reinforcement:

1. Clean mandrel detail parts.
2. Spray and sinter teflon dispersion onto all mandrel surfaces.

3. Apply colloidal copper to all slip-fit and threaded joints.
4. Assemble mandrel and locate per re-established indexing.
5. Install the mandrel assembly into the filament winding machine.
6. Melt beeswax into mandrel faying surfaces.
7. Sweep-in plaster into the groove adjacent to the mandrel end caps (see Figure 6-1).
8. Apply double-back tape to the cylindrical surface of the mandrel.
9. Mount ceramic strips to the double-back tape (12 axial locations).
10. Check winding machine and tension settings.
11. Anchor the 21-strand tungsten cable to outboard end of the mandrel shaft.
12. Take up slack in systems and manually adjust mandrel position in preparation for winding.
13. Commence winding first helical pass.
14. Check the winding angle of the first helical pass with a template during the winding operation, making manual machine adjustments as necessary.
15. Continue with subsequent winding passes.
16. Check cable-to-cable spacing during subsequent winding passes.
17. Make a template check of the helix angle at the sixth, twelfth, and eighteenth pass.
18. Anchor the tungsten wire cable to the outboard end of the mandrel shaft upon completion of the twenty-fourth pass.
19. Cut the tungsten wire cable.
20. Wrap the dome ends of the mandrel assembly with teflon film tape.
21. Remove the tungsten-wire-wound mandrel assembly from the filament winding machine.

The above sequence, with minor variations in technique, was utilized to filament wind the required final specimens prior to ceramic matrix casting operations. To ensure the accuracy of the cable tensioning device that was used, it was calibrated prior to winding. The calibration was made by winding a 21-strand tungsten cable onto a thin aluminum cylinder which was strain gaged on the inner surface. The strain gage readings were related to the tensionmeter settings to obtain a precise tension in the cable.

Figure 6-2 shows a cylinder during the winding operation. The final over-wound cylinders were similar in appearance to that shown in Figure 5-11; except that they were fabricated on the steel mandrel rather than the sand mandrel.

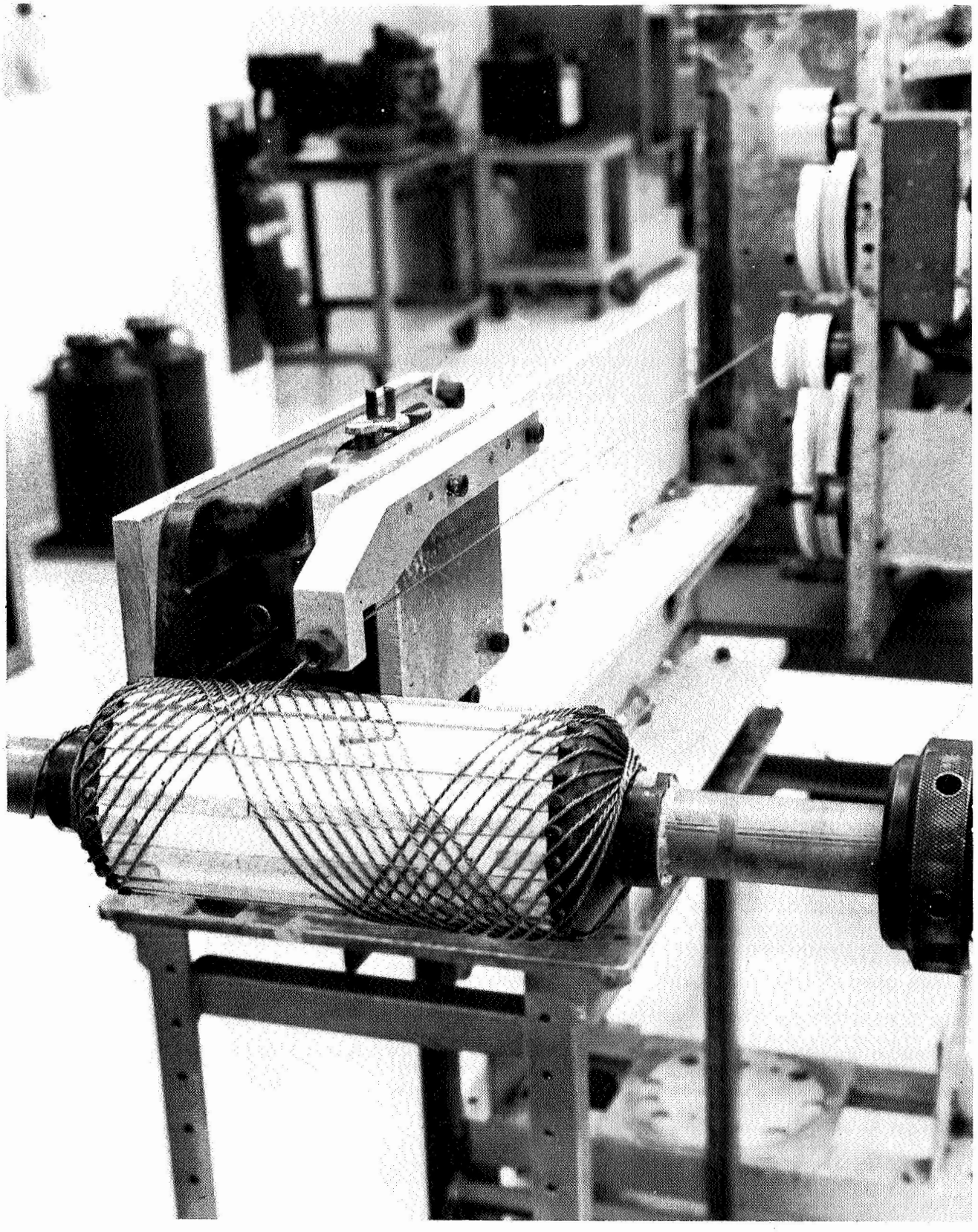

Figure 6-2. Mandrel Partially Overwound With 21-Strand Tungsten Cable

6.2.2 Application of Ceramic to Cylinders

The ceramic matrix, reinforced with 8 parts SiC whiskers, was blended in a V-blender for a minimum of 30 minutes. The material was then removed from the blender, and screened through a 35-mesh screen to eliminate agglomerated SiC whiskers. The blended powders were placed into a porcelain dish and 32 parts H_2PO_3F acid was added. After hand blending the powder and binder for 15 minutes the mix was placed on a Syntron vibrator and agitated for 30 minutes. The mandrel, with the prestressed cable wound on it, was suspended between supports and part of the mix was troweled onto the mandrel and forced between the wires. When the coating covered and surrounded all wires, the mandrel was placed into an oversized casting mold, which consisted of two half-cylinders held together with hose clamps. The inside of the cylindrical mold was lined with cotton, to wick the gases. On top of the cotton lining was placed a perforated teflon tape to act as a release agent. The mold was then mounted on a Syntron vibrator. The shaft of the mandrel rested on a removable support which raised the wound portion of the mandrel above the bottom of the external mold as shown in Figure 6-3. The ceramic was then infiltrated into the space between the overwound cylinder and the external mold, as shown in Figure 6-3. The support was then removed, which caused the mandrel to drop down and force the ceramic up the sides of the external molds. The whole assembly was vibrated during the entire operation. This semi-extrusion process appeared to work quite satisfactorily, and yielded specimens with low porosity.

6.2.3 Curing of Cylinders

After the casting was completed, the whole assembly (shown in Figure 6-3) was placed into a Blue M Oven for curing. The specimen was cured according to the schedule shown in Table 6-1. The extended cure schedule was used to assure a better evolution of the gaseous by-products of the reactions. The specimens remained in the mold until cured to 600°F, and cooled again to room temperature.

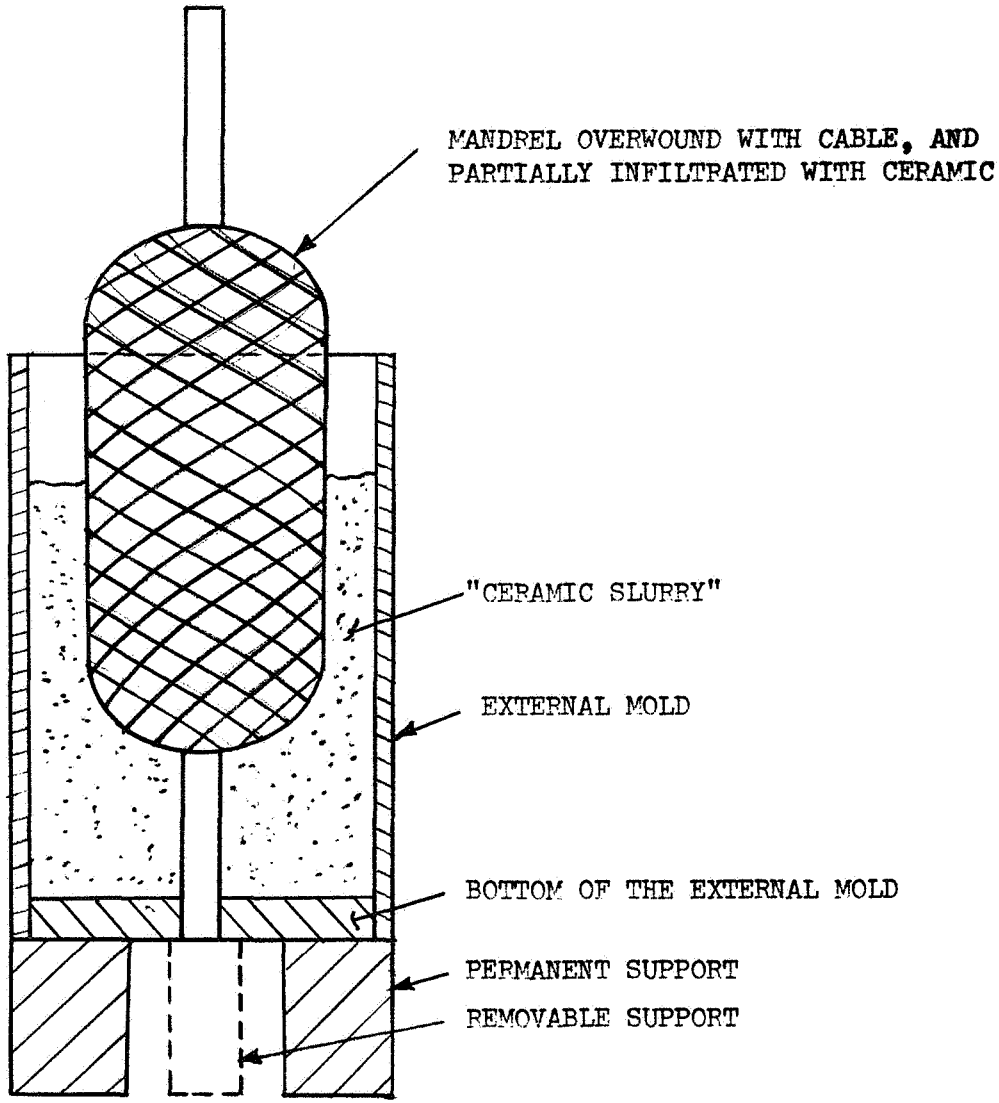

Figure 6-3. Procedure for Fabricating Cylinder

Table 6-1

CURING SCHEDULE OF BIAXIALLY PRESTRESSED CYLINDERS

Temperature °F	Temperature °C	Period (hours)
77 ± 9	20 ± 5	16
150 ± 18°	66 ± 10	4
180 ± 9	82 ± 5	2
212	100	16
300	149	2
300-600	149-316	3
600	316	1

6.2.4 Machining and Instrumentation of Biaxially Prestressed Cylinders

The machining of specimens to final dimensions (see Figure 6-4) consisted of three operations. For the first operation, the specimen was mounted in a Brown and Sharp grinder. Using a diamond wheel, the O. D. and gage length were roughed in. The second operation was accomplished on a Landis grinder using a silicon carbide wheel with a 4-inch-radius pre-cut on the wheel. With this equipment, the 4-inch radius was blended into the gage length and final finish was obtained. After this operation, two hoop and two axial strain gages were placed within the 3-inch test section of the specimen and strain readings were taken. The gages were located 180° apart. It is noted here that during the whole grinding operation the specimen remained on the steel mandrel. Finally, after the instrumentation, the specimen was transferred to another Landis grinder to cut off the two ends. The specimen was then removed from the mandrel and the final strain reading was taken. The two strain readings were used to obtain the precompression of the ceramic which occurred when the cables were cut off and the specimen was removed from the mandrel.

Figures 6-5 and 6-6 show two of the completed specimens ready for testing.

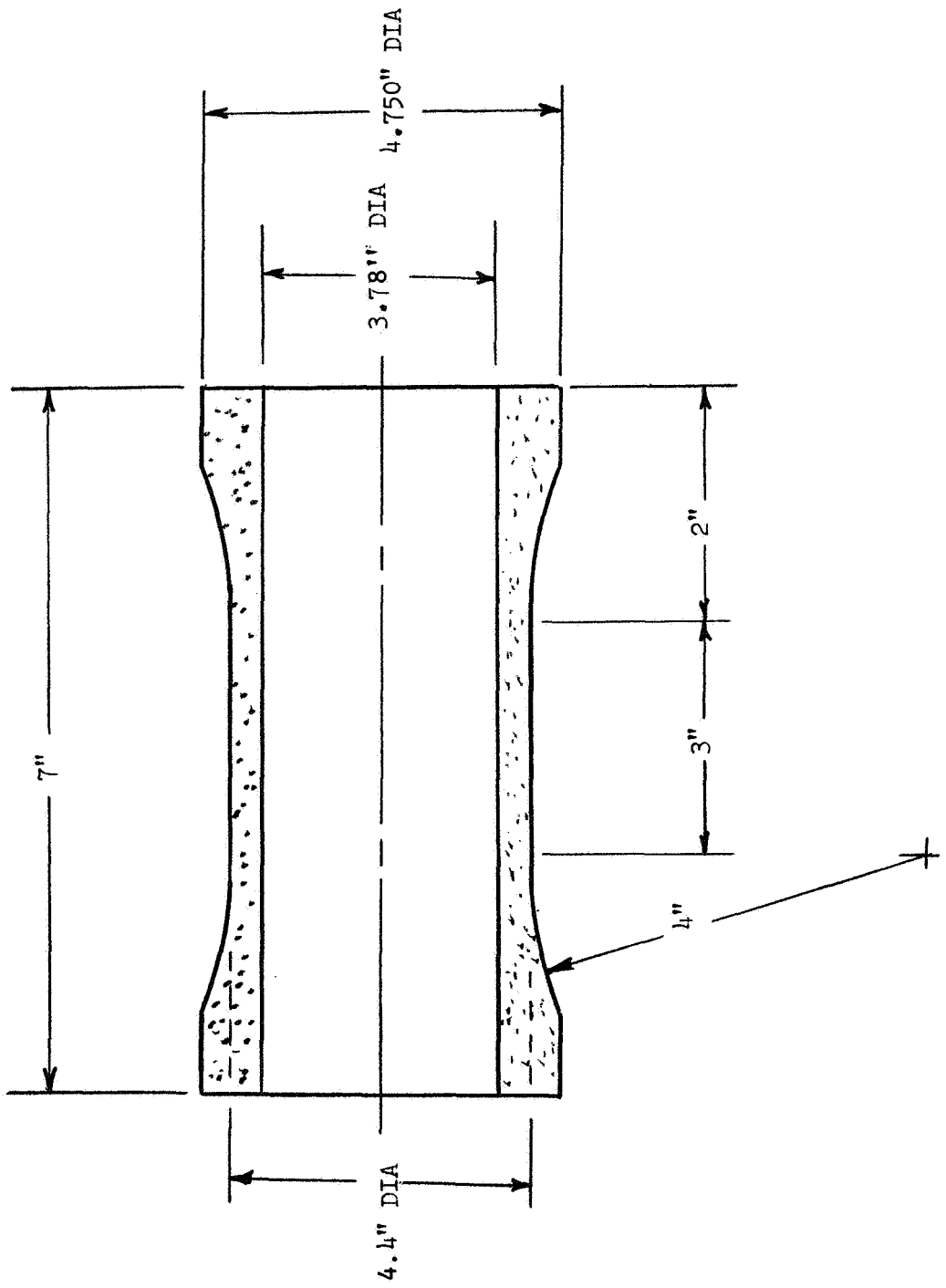

Figure 6-4. Hoop Tensile and Biaxial Tension-Tension Prestressed Ceramic Specimen

Figure 6-5. Biaxially Prestressed Cylinder BC-5

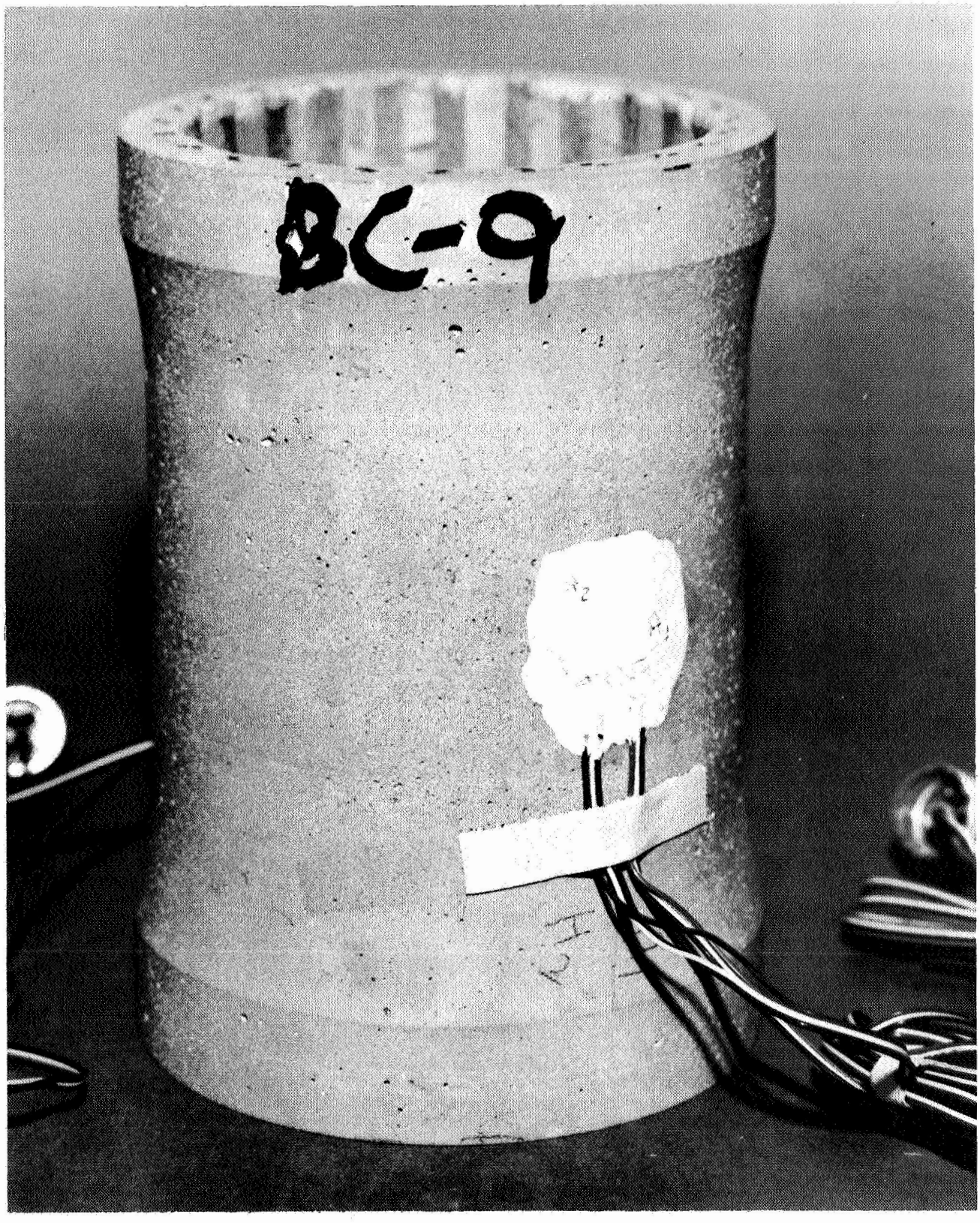

Figure 6-6. Biaxially Prestressed Cylinder BC9

Section 7

TESTING OF BIAXIALLY PRESTRESSED CYLINDERS

Four types of tests were performed on the biaxially prestressed cylindrical specimens: room-temperature, hoop-tension tests (1:0 stress ratio), room-temperature, biaxial-tension tests (2:1 stress ratio), elevated-temperature, hoop-tension tests (1:0 stress ratio), and high velocity ballistic impact tests. To perform these tests, appropriate test fixtures were designed, fabricated and checked out.

7.1 HOOP TESTING AT ROOM TEMPERATURE

Prior to performing the actual tests, the test setup was checked out. Trial cylinders made during the preliminary fabrication studies were used to checkout the test setup. Since there were no standard techniques for performing the desired tests, the results of the preliminary testing were used to modify, whenever necessary, the developed testing procedure.

7.1.1 Description of Test Fixture and Instrumentation

To conduct the uniaxial and biaxial tests on the biaxially prestressed cylinders, special end plugs were designed and fabricated. A sketch of the final test setup is shown in Figure 7-1. The actual components used in pressure testing of cylinders are shown in Figure 7-2.

As noted in Figure 7-1, the end plugs were unbonded and clamped externally when conducting hoop-tension test; they were bonded to the ceramic cylinder with an epoxy resin when performing the biaxial test.

The test section on the inside of the ceramic cylinder was first coated with a rubberized paint. Next, a thick, rubber cylinder was inserted. Finally, a double rubber balloon bladder was inserted as shown in Figure 7-1 and the end plugs were placed in position. The end plugs were restrained against axial movement with external C-clamps. The final test setup is shown in

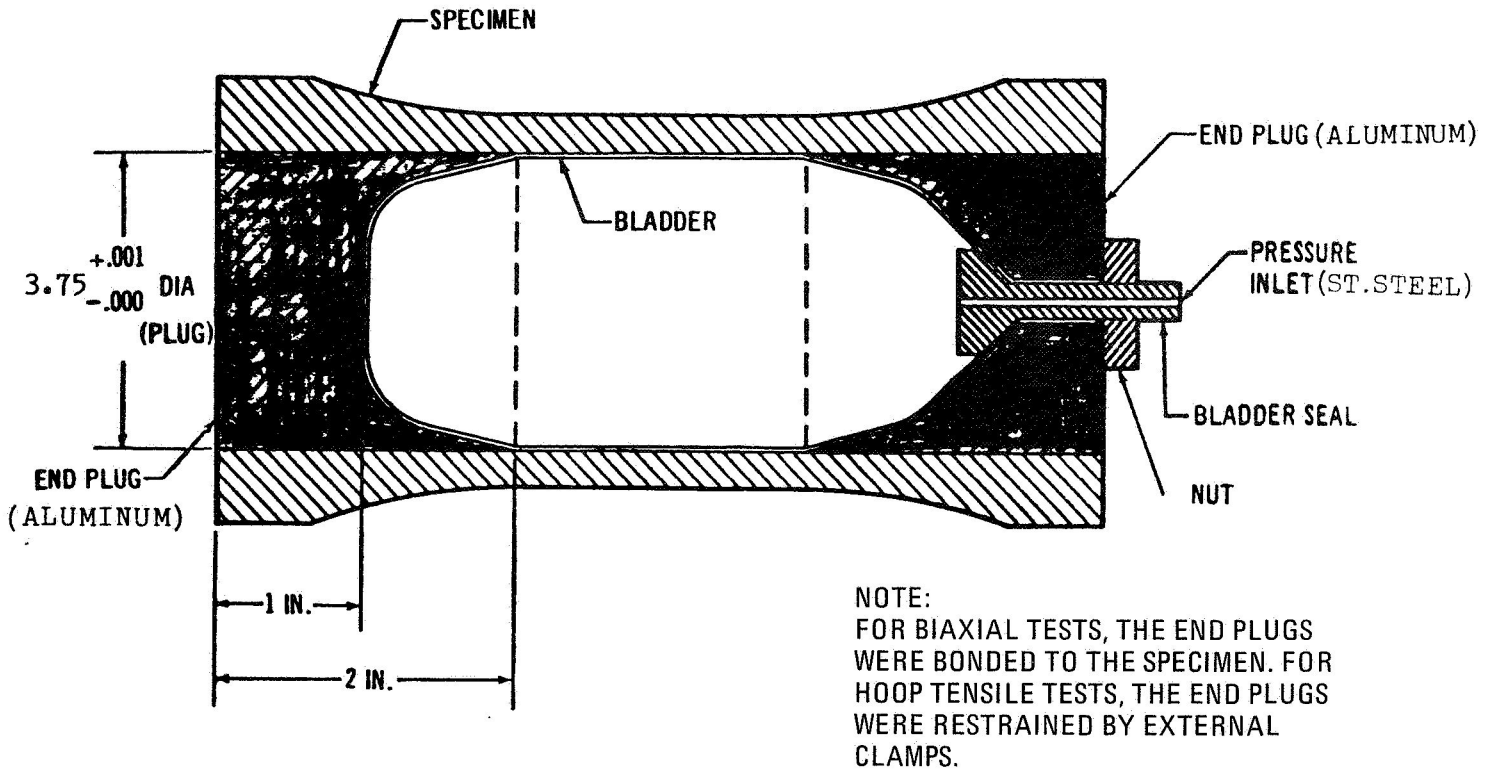

Figure 7-1. Hoop Tensile and Biaxial Tension – Tension Test Setup for Room Temperature Testing

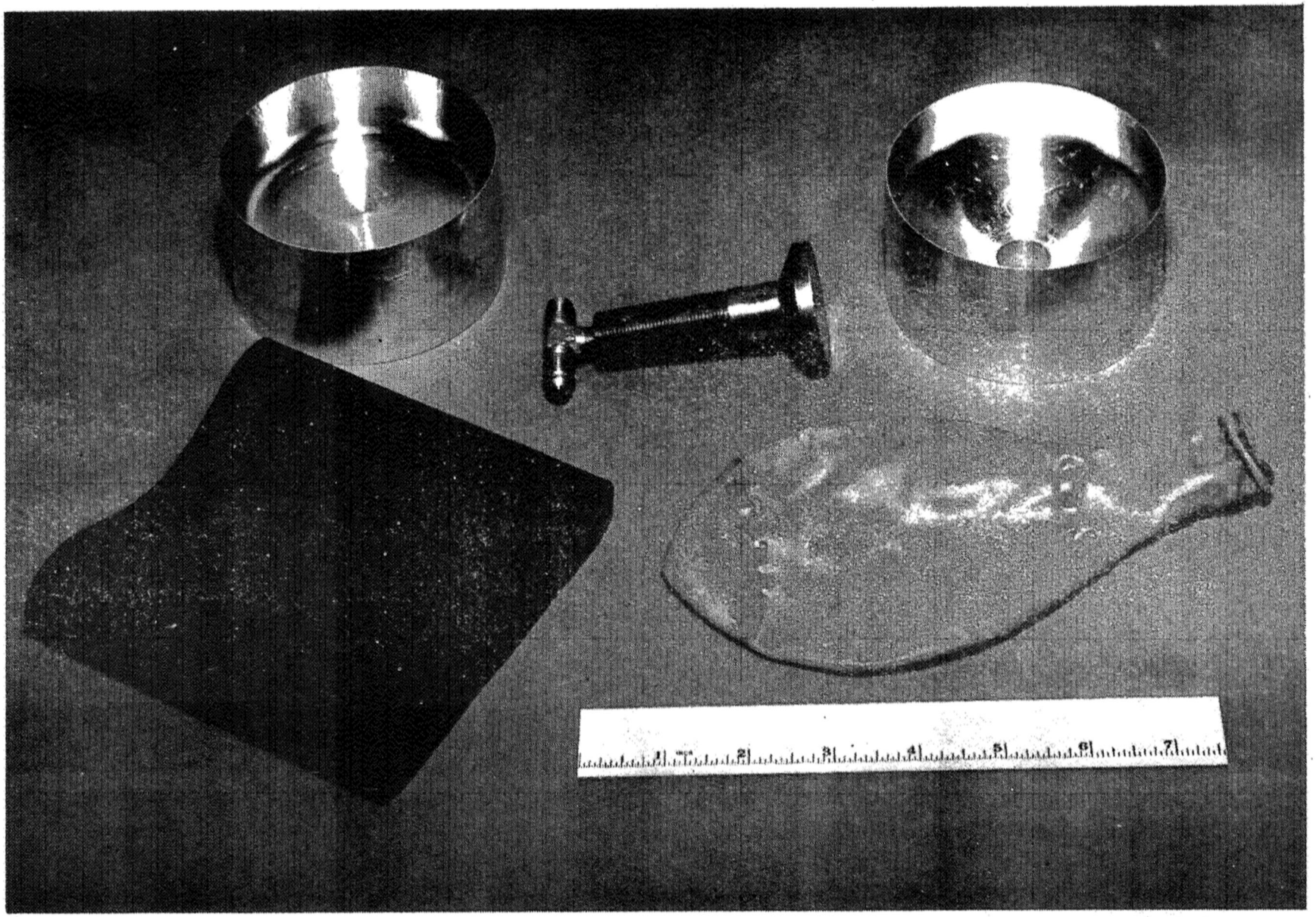

Figure 7-2. Components for Internal Pressure Testing of Cylinders

Figure 7-3. Water-oil solution was used to pressurize the cylinders. A pressure transducer was used to monitor pressure during the test. Axial and circumferential strains were also monitored on the x-y recorder during the test. Each test cylinder was instrumented with two axial and two hoop gages placed 180 degrees apart at the midsection of the cylinder.

7.1.2 Test Results for Room-Temperature Hoop Testing

Three hoop tests were performed, one on a trial cylinder to checkout the test setup, and two on final cylinders. The test results are shown in Table 7-1, which also gives other pertinent data for the final test specimens. To prevent blowing out of the plugs, and ensure that there was no leakage between the plugs and the ceramic cylinder, the test setup shown in Figure 7-3 was slightly modified. Rubber gaskets were placed on the two ends of the cylinder. The cylinder was then clamped between aluminum plates. The latter test setup worked satisfactorily. At failure, longitudinal cracks were noted in the test section, as was expected. Figure 7-4 shows a failed specimen that was tested in hoop tension.

7.2 BIAXIAL TESTING AT ROOM TEMPERATURE

Biaxial tension tests were performed on prestressed cylinders. The cylinders were provided with end closures so that a 2:1 stress ratio existed in the cylinder upon pressurization.

7.2.1 Description of Test Fixture and Instrumentation

The test setup used in biaxial testing was similar to that used in uniaxial testing, except as is noted in Figure 7-1, the end closures were bonded to the ceramic cylinder. Moreover, to obtain a 2:1 stress ratio in the cylinder, no external clamps were used.

To ensure that the ceramic cylinder would not fail due to stress concentration at the end of the taper of the end plugs, slots were made in the tapered portion of the plugs. The slots were approximately 0.3-inch long and were spaced at approximately 0.7 inch around the circumference. Also, instead of coating the inside of the specimens with a rubberized paint, a cylindrical rubber sleeve

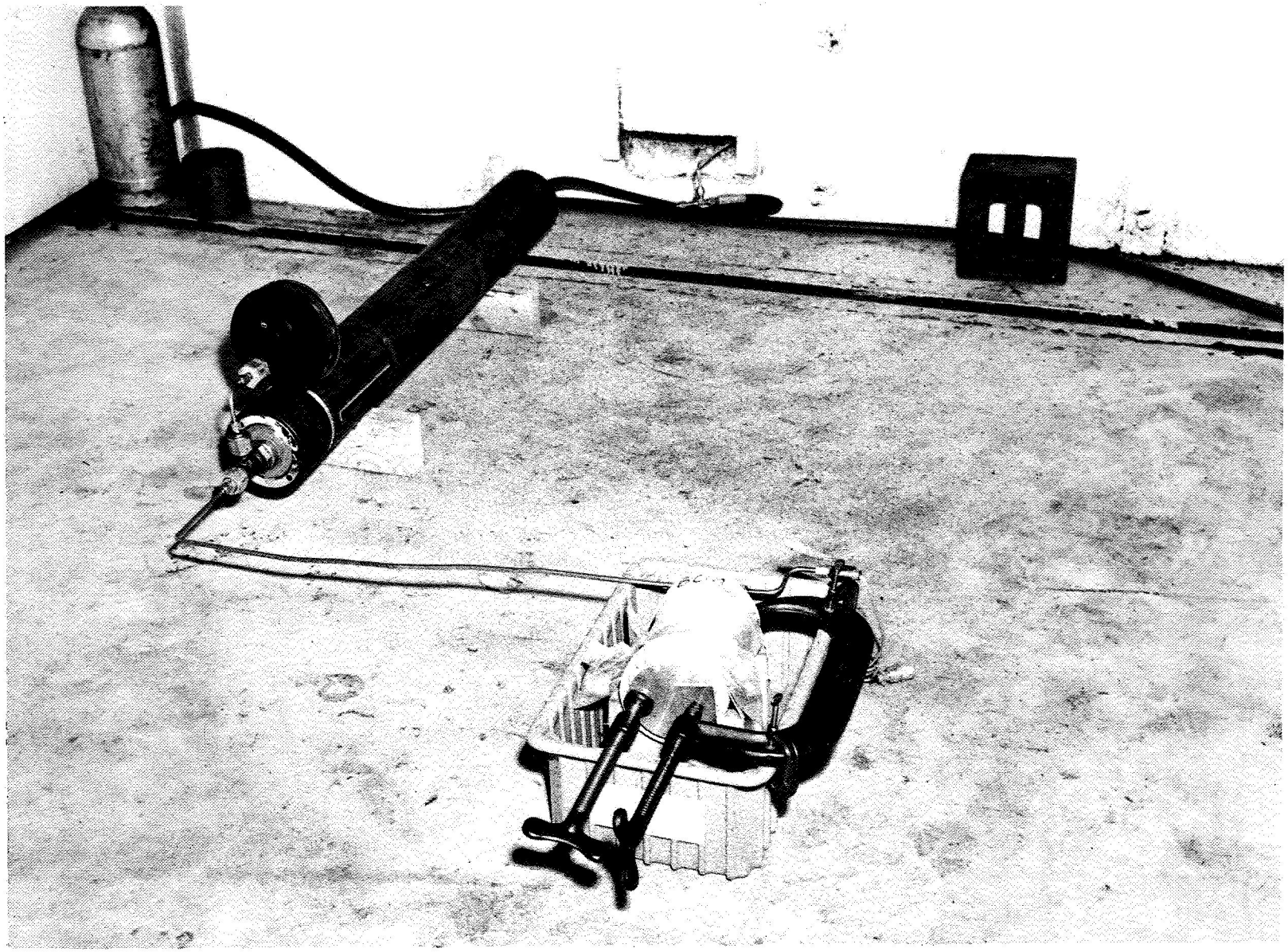

Figure 7-3. Test Set-Up for Testing in Uniaxial Hoop Tension

Table 7-1

ROOM TEMPERATURE TENSILE STRENGTH OF BIAXIALLY PRESTRESSED, SiC WHISKER STRENGTHENED ZrO_2 CYLINDERS SUBJECTED TO INTERNAL RADIAL PRESSURE[1]

Specimen Designation	Applied Wire Prestress σ_{wi} (PSI)	Cylinder Diameter (I.D.) (in.)	Cylinder Thickness (in.)	Internal Radial Pressure at Failure (PSI)	Hoop Stress at Failure (PSI)	Comments
BC-4	21,000	3.78	0.31	1,420	9,360	Cylinder pressurized twice; first to 850 psi and end plugs blew out. It was then reassembled and retested. At failure, longitudinal cracks were present in the test section. Failure at the end also took place.
BC-5	21,000	3.78	0.31	1,415	9,330	Cylinder pressurized twice; first time to 1,415 psi and the bladder fractured, causing leakage. One longitudinal crack, extending to the end of the cylinder, was noted. Cylinder was then reassembled and retested. It failed at 1,270 psi in the end section, in the area of the crack.

[1] Cylinders contained 7.4-weight percent of SiC whiskers, and were prestressed with 3.4-volume-percent of 21-strand tungsten cables, helically wound at a 57° helix angle with respect to cylinder axis. The strands were 0.012-inch diameter.

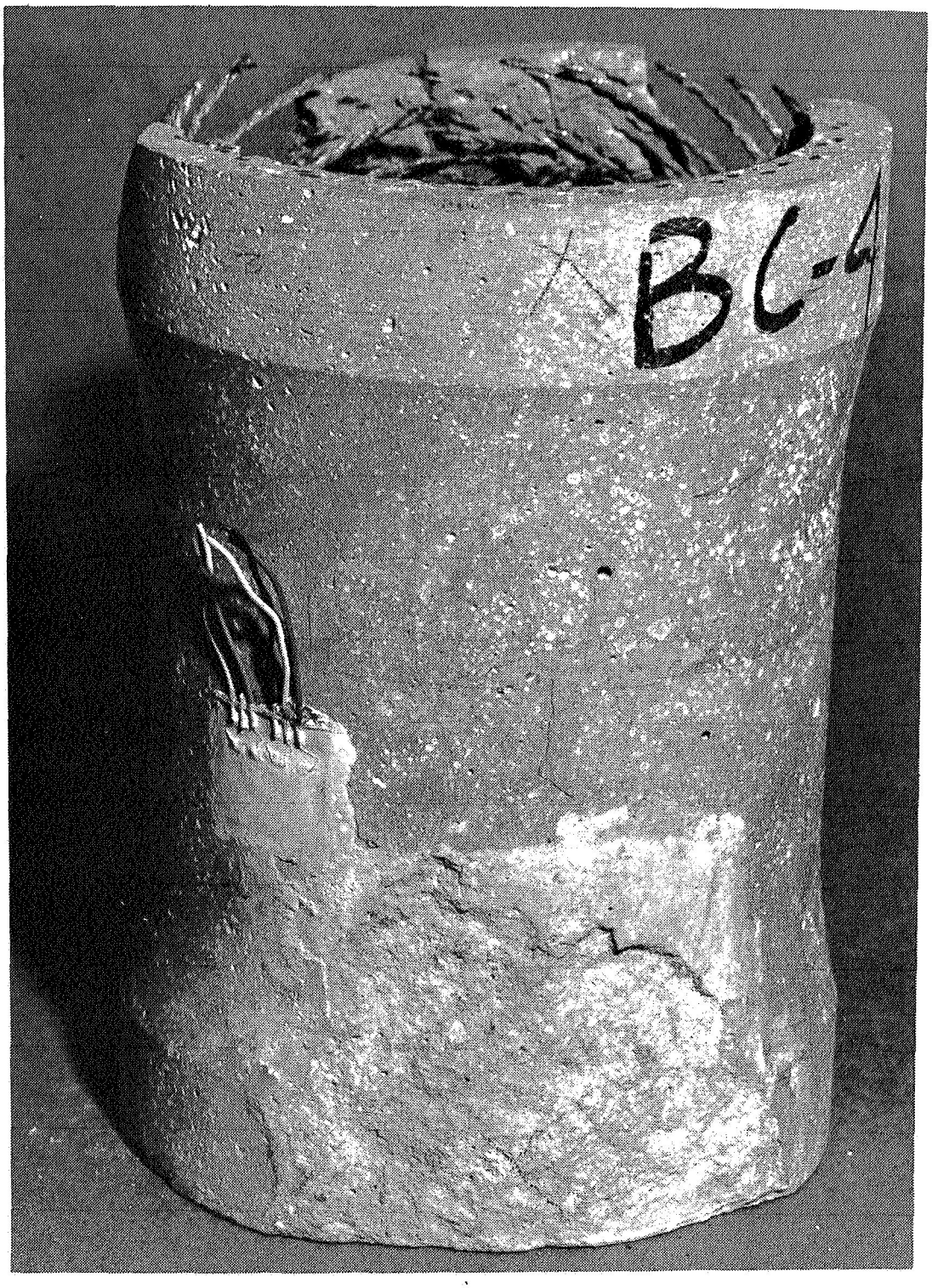

Figure 7-4. Hoop Failure of Cylinder BC-4

was bonded on the inside of the ceramic cylinder. Otherwise, the components and instrumentation used for biaxial testing were identical to those used for hoop testing.

7.2.2 Test Results of Room-Temperature Biaxial Testing

The biaxial test setup worked satisfactorily and excellent results were obtained. Both cylinders failed in the test section. No failures such as cracking, were noted in the ends. The test results for the cylinders subjected to biaxial tension are shown in Table 7-2. Figures 7-5 and 7-6 show two specimens after failure. As is readily seen, specimen BC-6 failed by overall failure, that is failure of the ceramic and the reinforcement.

7.3 HOOP TESTING AT ELEVATED TEMPERATURE

Elevated temperature uniaxial hoop tension tests were performed on biaxially prestressed cylinders. In order to perform these tests, it was necessary to design and fabricate the test setup and test fixtures. The elevated temperature tests were performed at $\approx 2,000°F$.

7.3.1 Description of Test Setup and Instrumentation

For safety reasons, the elevated temperature hoop tensile tests were performed in a bomb shelter. A schematic diagram of the test setup is shown in Figure 7-7. The test cylinder and fixture are shown in Figure 7-8. As shown, a stainless steel bladder was welded onto a stainless steel mandrel. Nitrogen gas from a bottle was metered into the mandrel to pressurize the bladder. At 2,000°F the stainless steel bladder is quite soft, and contributed practically nothing to the load-carrying ability of the ceramic cylinder.*

Heating was accomplished through the use of four ceramic-backed wire-wound heating elements. These were rectangular plates arranged in a square box around the specimen. Power to the heating elements was manually controlled through the use of a powerstat. Two chromel-alumel thermocouples were attached to the test section of the cylinder to monitor the temperature. Fire bricks were placed around the heating elements for

*See note (2) in Table 7-3 for the numerical estimate of the effect of bladder.

Table 7-2

ROOM TEMPERATURE TENSILE STRENGTH OF BIAXIALLY PRESTRESSED, SiC WHISKER STRENGTHENED ZrO_2 CYLINDERS SUBJECTED TO BIAXIAL LOADING (INTERNAL HYDROSTATIC PRESSURE)[1]

Specimen Designation	Applied Wire Prestress (PSI)	Cylinder Diameter (I.D.) (PSI)	Cylinder Thickness (in.)	Internal Pressure at Failure (PSI)	Hoop Stress at Failure (PSI)	Axial Stress at Failure (PSI)	Comments
BC-7	21,000	3.78	0.31	1,560	10,290	5,145	Longitudinal and hoop cracking in the test section at failure.
BC-7	21,000	3.78	0.31	1,660	10,940	5,470	Overall failure of the ceramic and reinforcement in the test section.

[1] Cylinders contained 7.4-weight-percent SiC whiskers, and were prestressed with 3.4-volume-percent of 21-strand tungsten cables, helically wound at a 57° helix angle with respect to cylinder axis. The strands were 0.012-inch diameter.

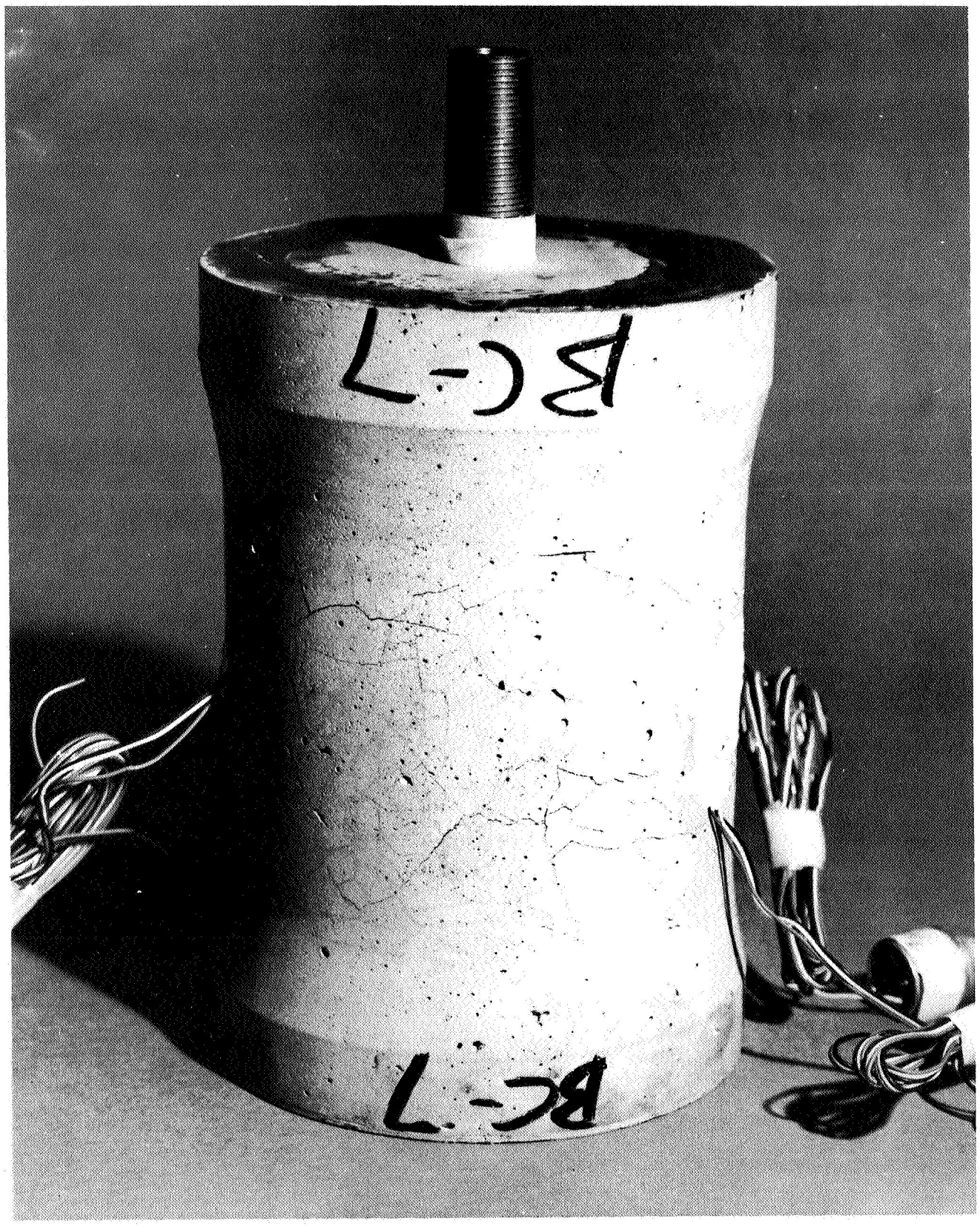

Figure 7-5. Biaxial Failure of Specimen BC-7 Subjected to Internal Hydrostatic Pressure (at 70° F)

Figure 7-6. Biaxial Failure of Specimen BC-6 Subjected to Internal Hydrostatic Pressure (at 70^{0} F)

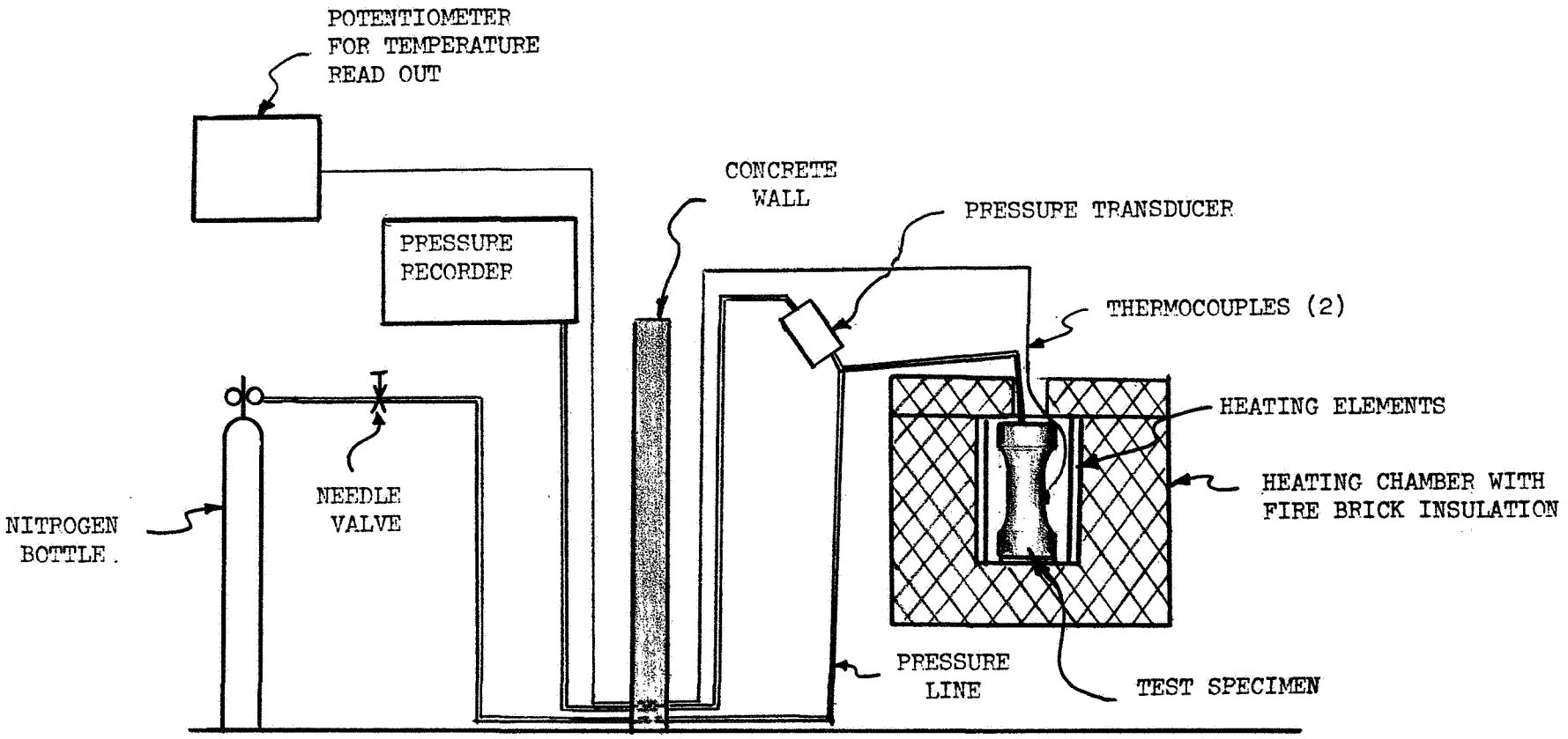

Figure 7-7. Schematic Diagram of Hoop Tensile Test Set-up for Elevated Temperature Testing

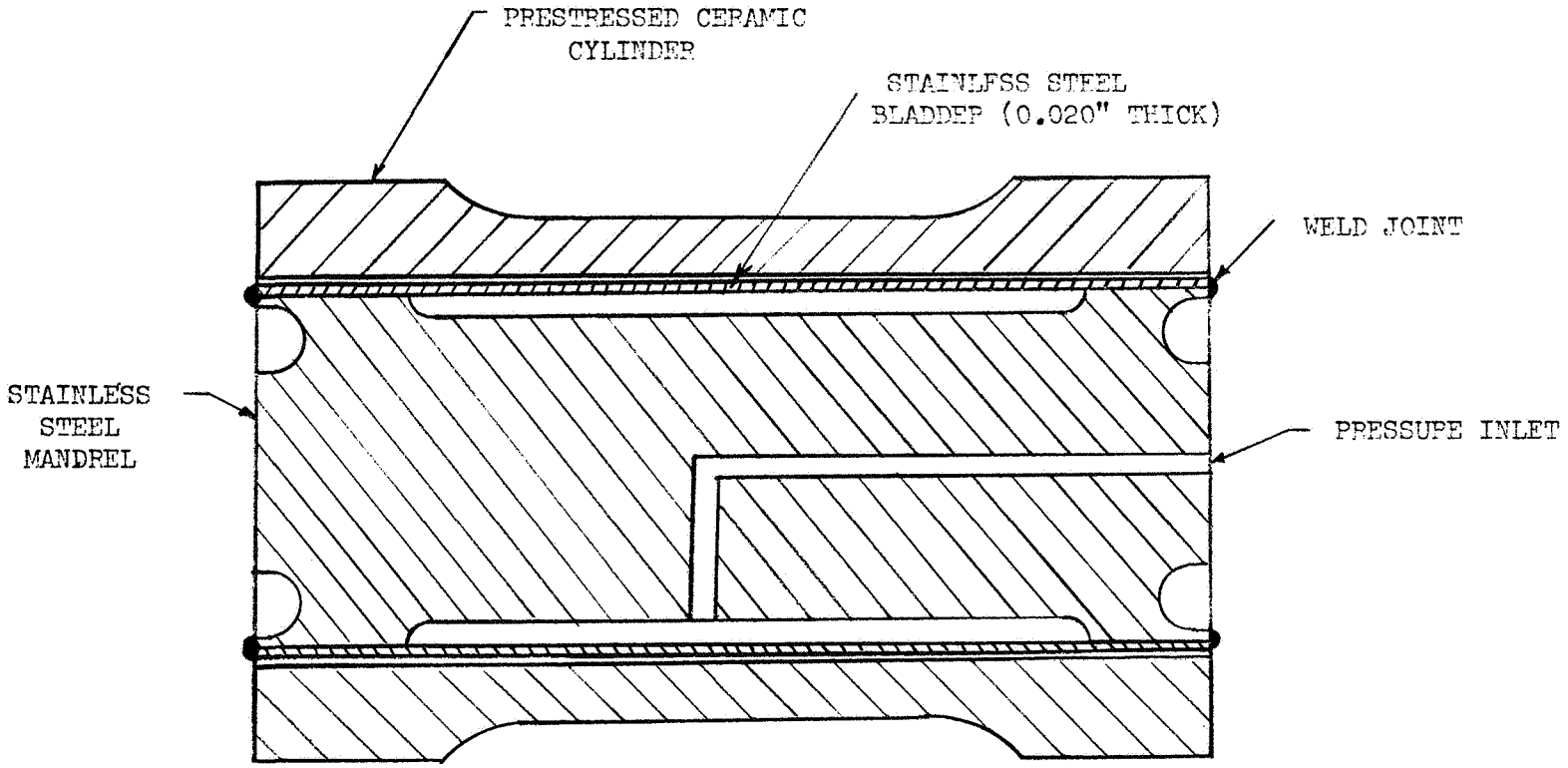

Figure 7-8. Cross Section of Test Fixture and Specimen for Elevated Temperature Hoop Tensile Test

insulation. The furnace was sealed with Sauereisen cement to prevent air from entering the furnace. Argon gas was pumped into the furnace during heating and testing.

Pressure was monitored by a pressure transducer placed in the line between the metering valve and the test sample. The transducer was located about 2 feet from the test specimen. The pressure indicating signal from the transducer was recorded on a Moseley x-y recorder.

7.3.2 Test Results for Elevated-Temperature Hoop Testing

One of the trial cylinders made during the preliminary fabrication studies was used to check out the test setup. Following this, tests were performed on final specimens. The test results are shown in Table 7-3.

Cylinder BC-10 was tested first. The heating time from 70°F to 2,000°F was 2 hours. Near the end of the heating time, both thermocouples were lost. When the new ones were inserted into the heating furnace, the specimen temperature had gone up to about 2,300°F. Altogether, the specimen remained for 1 hour at a temperature of 2,000 to 2,300°F. After installation of the new thermocouples, the temperature was decreased to 2,000°F and the cylinder was tested using nitrogen gas. The cylinder failed at a pressure of 300 psi (hoop stress of 1,980 psi).

The failed specimen (BC-10) contained numerous cracks in the built-up ends, and also several longitudinal cracks in the test section. Examination of the stainless steel bladder showed severe oxidation. In several spots the bladder appeared to have oxidized through the wall thickness. It was not obvious if the oxidation was caused by the gases given off by the ceramic specimen when it was heated up, or by air which might somehow have entered the test furnace (it is noted here that the test was conducted in an argon atmosphere).

To avoid problems encountered during testing of cylinder BC-10, certain modifications were made when testing cylinder BC-9 at 2,000°F. The thickness of the stainless steel bladder was increased from 0.020 inch to 0.035 inch. Moreover, a thin layer (approximately 0.001-inch thick) of hard chromium plating was electro-deposited on the outer surface of the bladder.

Table 7-3

ELEVATED-TEMPERATURE TENSILE-STRENGTH OF BIAXIALLY PRESTRESSED, SiC-WHISKER-STRENGTHENED ZrO_2 CYLINDERS SUBJECTED TO INTERNAL RADIAL PRESSURE (1)

Specimen Designation	Applied Wire Prestress σ_{wi} (psi)	Test Temperature °F	Cylinder Diameter (I. D.) (in.)	Cylinder Thickness (in.)	Internal Radial Pressure at Failure (psi)	Hoop Stress at Failure (psi)	Comments
BC-10	21,000	2,000	3.78	0.310	300	1,980	Thermocouple lost during test. Temperature overshot to 2,300°F. Cylinder held at temperature of 2,000 to 2,300°F for 1 hour and tested. Cracking in the ends and in test section.
BC-9	21,000	1,860	3.80	0.300	840	5,740	Specimen heated twice, once to 400°F and once to 1,220°F. Heating elements lost both times. It was then heated to 1,860°F and tested. Failure was a typical hoop failure-longitudinal cracks in the test section, spaced about 1 in. apart.

(1) Cylinders contained 7.4 weight-percent of SiC whiskers, and were prestressed with 3.4-volume-percent of 21-strand tungsten cables, helically wound at a 57° helix angle with respect to the cylinder axis. The strands were 0.12-inch in diameter.

(2) Based on extrapolated properties of stainless steel at 1860°F, the load-carrying ability (in terms of internal pressure) of the stainless steel bladder was calculated to be 9 psi, or 1 percent of the failure pressure of 840 psi.

The ends of the ceramic specimen (flat portion) were overwound with two layers of 7-strand tungsten cable to prevent cracking at the ends. The required amount of end overwrap was determined from analysis. Finally, the heating furnace was resealed to prevent entrance of air into the test chamber.

The modified, elevated-temperature, test setup worked satisfactorily. The thermocouples were lost at 1,860°F when the cylinder was heated; therefore, the cylinder was held at that temperature for about 10 minutes and tested. The hoop burst pressure was 840 psi. Figure 7-9 shows a photograph of a failed specimen, BC-9, which was tested at 1,860°F. Longitudinal cracks are present in the test section, which is typical for this type of loading. The stainless steel bladder had several longitudinal cracks at failure. Table 7-3 shows the test results of the elevated-temperature testing.

7.4 BALLISTIC-IMPACT TESTING

Ballistic-impact tests were performed on biaxially prestressed cylinders. The main purpose of these tests was to establish the failure mode, and failure progression, including the ability of prestressing material to stop a catastrophic failure of the ceramic.

The tests were performed using a 30-06 rifle (approximately 30 caliber). Both armor-piercing and ball-type ammunition were used. The weight of the projectiles was 150 grains, while their impact velocity was 2,860 feet per second. The target was located 30 feet from the rifle. The test was completely automated and was performed at the MDAC-WD ballistic impact facility.

The failure area of a specimen subjected to armor-piercing projectile is shown in Figure 7-10, while Figure 7-11 shows the failure area caused by the ball-type projectile. In both cases the projectiles penetrated through the cylinder walls. No catastrophic failure of the ceramic took place. The reinforcement did prevent crack propagation. Local failures occurred where the projectiles entered and exited the specimens.

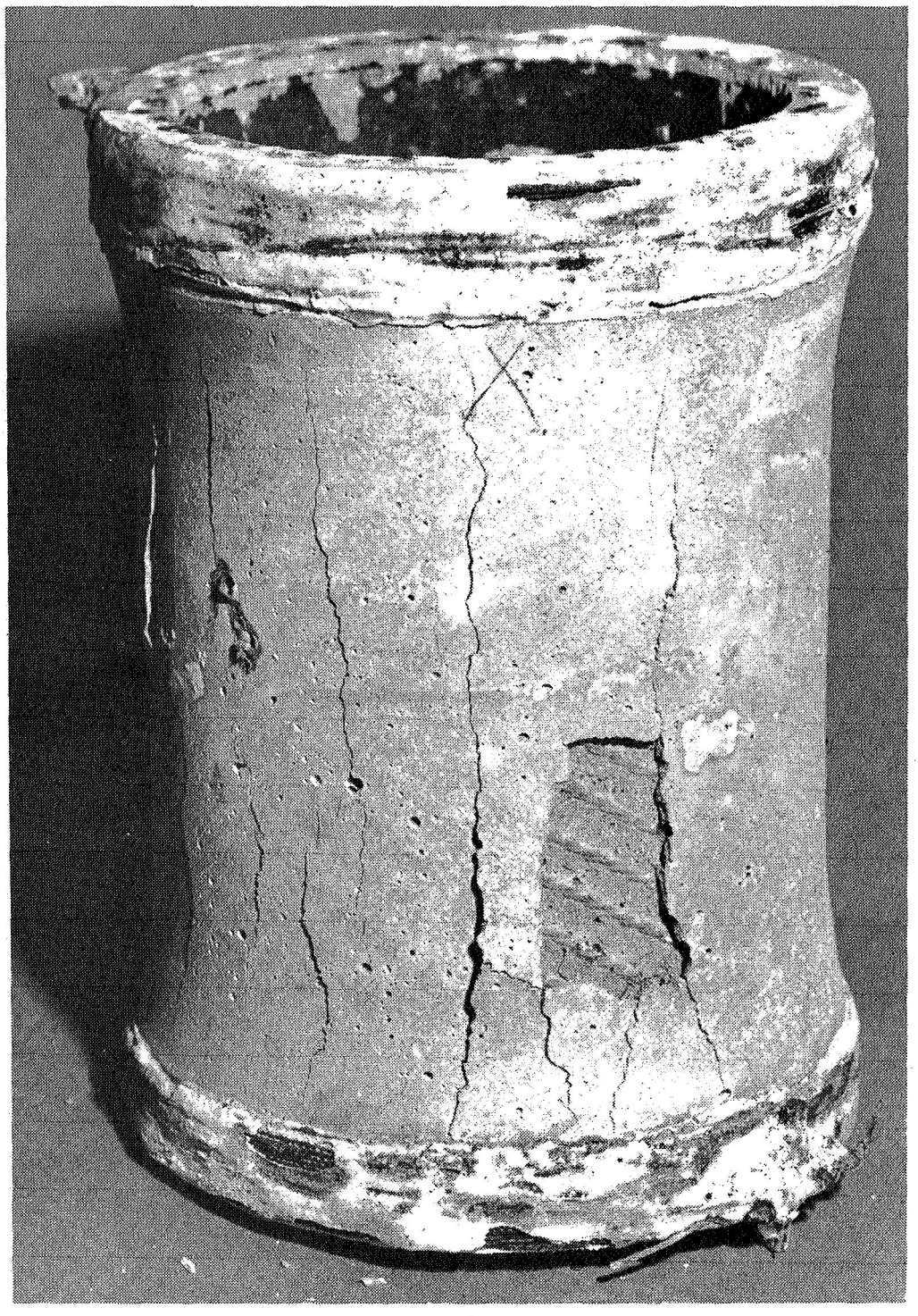

Figure 7-9. Failed Specimen BC-9 Tested in Hoop Tension at 1860°F

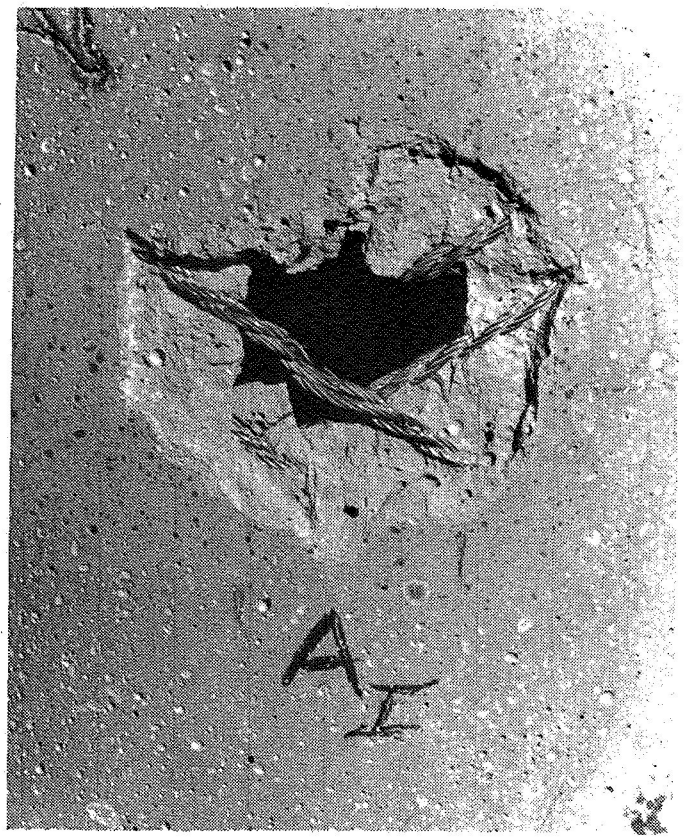

FAILURE AT THE IMPACT SURFACE

FAILURE AT THE EXIT SURFACE

Figure 7-10. Failure Area in a Biaxially Prestressed Cylinder Subjected to Armor Piercing Projectile

FAILURE AT THE IMPACT SURFACE

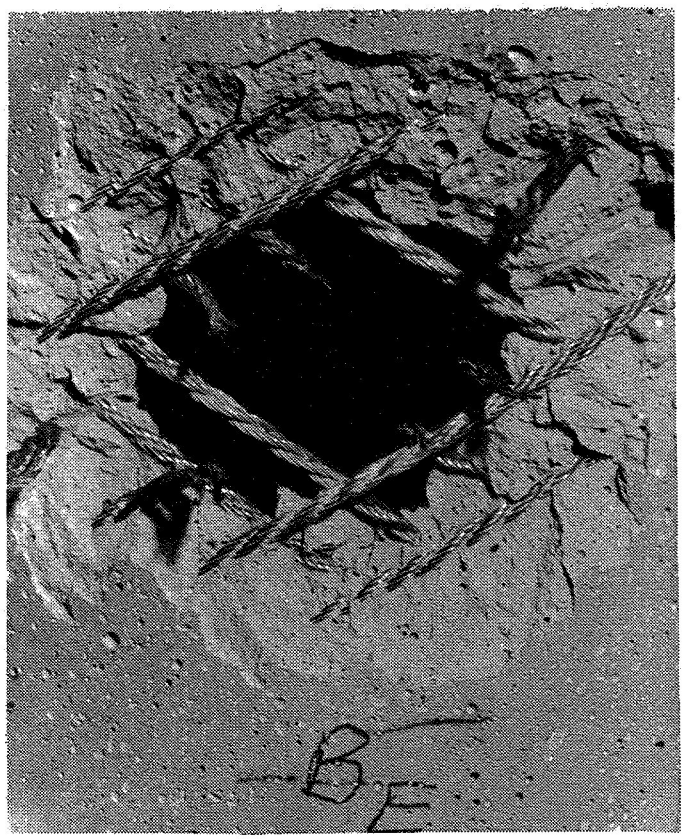

FAILURE AT THE EXIT SURFACE

Figure 7-11. Failure Area in a Biaxially Prestressed Cylinder Subjected to Ball-Type Projectile

Section 8

EVALUATION OF TEST RESULTS AND TEST THEORY CORRELATION FOR BIAXIALLY PRESTRESSED CYLINDERS

The experimental results reported in Section 7 for biaxially prestressed cylinders subjected to biaxial stress at room temperature, as well as uniaxial hoop stress at room and elevated temperatures, were compared with the theoretically predicted results. The comparison between experiment and theory is shown in Table 8-1.

The theoretical results shown in Table 8-1 were predicted using the theory given in the Appendix. Since the cylinders were cured while still on a steel mandrel, it was necessary to consider not only the mechanical prestress of σ_{wi} = 21,000 psi applied during the filament winding, but also the thermal prestress induced in the cables because of thermal expansion of the mandrel. At cure temperature of 600°F, the difference in the coefficients of thermal expansion between the steel mandrel and the tungsten cables gave rise to a 57,400 psi thermal pretension in the helically wound, 21-strand tungsten cables. The ceramic consolidated at 600°F; therefore, upon cooling to 70°F, the precompression induced in the ceramic was caused from mechanical as well as thermal prestress in the cables. Thus, the total equivalent initial pretension in the cables, inducing precompression in the ceramic, was 78,400 psi. The strength of the cylinders subjected to various types of loading was based on the latter value of the prestress.

The mechanical properties of the prestressing cables and of SiC-whisker-strengthened ZrO_2 that were used in the analysis were those measured experimentally, and are discussed in Section 3. These properties as well as cylinder dimensions and other pertinent data are summarized in Table 8-2.

Table 8-1

TEST-THEORY COMPARISON FOR THE STRENGTH OF BIAXIALLY PRESTRESSED CYLINDERS SUBJECTED TO UNIAXIAL AND BIAXIAL STRESSES AT ROOM AND ELEVATED TEMPERATURES[1]

Specimen Designation	Loading Condition	Test Temperature (°F)	Internal Pressure at Failure (psi)			Comments
			Experiment	Theory		
				Cracking	Ultimate	
BC-4	Hoop stress due to internal radial pressure (1:0 stress ratio)	70	1,420	1,150[2]	1,966[3]	Ceramic Cracking
BC-5		70	1,415	1,150[2]	1,966[3]	Ceramic Cracking
BC-7	Biaxial stress due to internal hydrostatic pressure (2:1 stress ratio)	70	1,560	1,150[2]	1,966[3]	Ceramic Cracking
BC-6		70	1,660	1,150[2]	1,966[3]	Failure of Ceramic and Reinforcement.
BC-10	Hoop stress due to internal radial pressure (1:0 stress ratio)	2,000	300	580[4]	580[3]	Poor test; see comments in Table 7-3.
BC-9		1,860	840	620[4]	620[3]	Ceramic Cracking

(1) See Tables 7-1, 7-2, 7-3, and 8-2 for description of test specimens and their geometry.

(2) Pressure required to cause cracking of the ceramic, without necessarily failing the prestressing cables (elastic analysis).

(3) Pressure required to cause simultaneous failure of ceramic and cable (based on assumption that the prestress is such that both materials fail simultaneously when an external load is applied to composite).

(4) Pressure required to cause cracking of ceramic (approximate elasto-plastic analysis). Yielding of reinforcement was assumed to take place.

Table 8-2

PROPERTIES OF CONSTITUENTS AND OTHER PERTINENT DATA USED IN THE ANALYSIS OF BIAXIALLY PRESTRESSED CYLINDERS

Item	Property	Temperature		
		70°F	1,860°F	2,000°F
Zirconia strengthened with 7.4 weight percent of SiC whiskers.	Youngs Modulus, $E_c \times 10^{-6}$ psi	8.01	0.80	1.00
	Poissons Ratio, ν_c	0.25	0.25	0.25
	Flexure strength, psi	5620	1520	1520
	Coefficient of thermal expansion, $\alpha_c \times 10^6$ psi	3.0	5.45	5.97
21-strand tungsten cables made with 0.012" dia. strands	Youngs Modulus, $E_w \times 10^{-6}$ psi	27.1	19.0	16.6
	Poissons Ratio, ν_w	0.25	0.25	0.25
	Tensile strength, psi	315,000(1)	109,000(1)	95,000(1)
	Coefficient of thermal expansion, $\alpha_w \times 10^6$ psi	2.45	2.54	2.60
Biaxially Prestressed Cylinder	Cylinder radius (average), in.	2.045	2.050	2.045
	Cylinder thickness, in.	0.310	0.30	0.310
	Mechanical Prestress, σ_{wi}, psi	21,000	21,000	21,000
	Thermal Prestress, psi	57,400(2)	57,400(2)	57,400(2)
	Total Prestress, σ_{wi}, psi	78,400	78,400	78,400
	Volume fraction of Prestressing material	0.0342	0.0353	0.0342
	Helix angle, β, Degrees	57	57	57
	Consolidation temp. of ceramic, °F	600	600	600

(1) This is the strength of cable restrained against untwisting, which is somewhat higher than the strength of cable tested by itself. The reported values were obtained from Reference 8-1.

(2) The thermal prestress was induced in the wire due to the expansion of the steel mandrel during curing of the specimen.

In general, the agreement between experimental and theoretical results is quite good. Some of the most likely reasons for the discrepancy between experiment and theory are:

1. The allowable strength of the ceramic was higher than the values used in the calculations.
2. The total prestress, σ_{wi}, was higher than 78,400 psi.
3. The modulus of elasticity of tungsten cable was higher than 27.1×10^6 psi.

In conjunction with item 1, it was noted that the quality of the ceramic in biaxially prestressed cylinders was much better than of the flexure specimens which were used to obtain the ceramic properties data used in the calculations. Thus it is quite possible that the strength of the ceramic at room and elevated temperatures was higher than the values shown in Table 8-2. As to the modulus of elasticity of the 21-strand tungsten cable, it was noted in Reference 8-1 that the strength of the wire imbedded in the ceramic, and thus restrained against untwisting, was much higher than the strength of the cable tested by itself. A similar effect would also be expected in the modulus of elasticity, that is, the modulus of elasticity of a cable restrained against untwisting would be expected to be higher than that of a cable free to untwist.

Although the room temperature strength of the biaxially prestressed cylinders could have been increased significantly by increasing the prestress, this would have resulted in low strength values at 2,000°F, as was discussed in Section 5. The strength values obtained at 1,860°F and at 2,000°F do indeed demonstrate a significant improvement over the strength of unreinforced, unprestressed zirconia.

REFERENCES FOR SECTION 8

8-1. L. B. Greszczuk and H. Leggett. Final Report--Development of a System for Prestressing Brittle Materials. Douglas Aircraft Company Report DAC-49200, August 1967.

Section 9
SUMMARY, CONCLUSIONS AND RECOMMENDATIONS

On the basis of studies performed to date, it has been shown that significant increases in the room and elevated temperature strength of zirconia can be achieved through addition of SiC whiskers. A 7.4-weight-percent of SiC whiskers increased the average room temperature flexure strength of zirconia from 4,000 psi to 5,620 psi. The highest strength obtained was 7,620 psi. At 2,000°F, the addition of whiskers increased the average flexure strength of zirconia from 165 psi to 1,520 psi. Highest strength obtained at 2,000°F was 2,620 psi. Further improvements in the tensile load carrying ability of the whisker-strengthened zirconia were obtained by prestressing the matrix with high-strength, high-modulus, tungsten cables. The prestressing material not only increased the tensile load carrying ability of the ceramic, but also imparted some ductility to the brittle ceramic material.

In addition to the uniaxially prestressed specimens that were fabricated and evaluated, a concept of biaxially prestressing cylindrical shells has been developed, demonstrated and evaluated. In conjunction with this work, a theory has been developed for predicting the strength of biaxially prestressed ceramic cylinders subjected to external loading and thermal environment. To verify the theory and demonstrate the efficiency of biaxially prestressed cylinders, a number of biaxially prestressed cylinders were designed, fabricated and tested. The following types of tests were conducted: internal radial pressure at room temperature, internal hydrostatic pressure at room temperature, internal radial pressure at 2,000°F and high-velocity ballistic-impact tests. To conduct the above tests, test methods were developed for uniaxial and biaxial testing of ceramic cylinders at room temperature and also for uniaxial testing of cylinders at 2,000°F. These test methods were highly successful and yielded excellent data.

For a cylinder prestressed with 3.4 volume percent of 21-strand tungsten cable, the highest hoop strength obtained at room temperature was 10,940 psi. At 1860°F the highest hoop strength obtained was 5,740 psi. For biaxially prestressed cylinders subjected to high velocity impact loading (2, 860 ft/sec) using an armor piercing projectile, the failure area was localized and non-catastrophic. The prestressing material stopped completely any crack propagation.

For the biaxially prestressed, internally pressurized cylinders, a fair agreement was obtained between experiment and theory for the failure pressure. The theory predicted lower failure pressures than the experimental values. It appeared that the strength of ceramic in the cylinders was higher than the strength of ceramic obtained from the flexure tests, on which data the theoretical predictions for the cylinder strength were based. The quality of the cylindrical specimens was much better than the quality of the flexure specimens.

The thermal shock and thermal cycling tests performed on uniaxially prestressed specimens have conclusively demonstrated the ability of the prestressing material to prevent thermal shock failure. Some unusual behavior of the SiC whisker-strengthened zirconia was noted at ≈ 1, 500°F. At that temperature the strength and modulus dipped to their lowest values. The specimens also exhibited high ductility. When testing the specimens above 1,500°F the strength and modulus increased, and the specimens failed in a brittle manner. Additional studies are recommended on this phenomenon, and also on how to eliminate it. Preliminary studies involving heat treating of the ceramics indicate that it may be possible to eliminate the temperature region of low strength.

After thermal shock testing of the prestressed specimens, it was noted that when they were tested at room temperature, their flexure strength was significantly higher (~20%) than the flexure strength of prestressed specimens which were not thermal shock tested. These specimens had also much higher flexure strengths than the specimens which were thermal cycled slowly under similar [illegible] ment. Thus it appears that the rate of heating does

affect the strength of prestressed ceramic. The reason for this behavior is not apparent and deserves further investigation.

Investigation of the test data on uniaxially and biaxially prestressed specimens indicates that significant amount of yielding takes place in the reinforcing material, especially at high test temperatures. It appears desirable, therefore, to extend the existing elastic analysis to the case where the prestressing material does undergo elasto-plastic deformations. Other areas on which studies are recommended include:

1. Additional fabrication and testing of biaxially prestressed cylinders incorporating various types of prestressing materials, different prestress levels, and different contents of prestressing material.
2. Studies on mixing techniques to achieve better, more uniform dispersion of whiskers in the ceramic matrix.
3. Studies on fabrication of prestressed complex shapes other than cylinders, leading to a development of a prototype hardware component.
4. Further characterization of the matrix, especially its compressive strength and its properties above 2, 000 °F.

APPENDIX

ANALYTICAL STUDIES ON BIAXIALLY PRESTRESSED CERAMIC

To estimate the strength of biaxially prestressed cylindrical configurations, the knowledge of the internal stresses in the ceramic as well as the reinforcement is required. This includes the stresses due to an externally applied loading, as well as those due to mechanical and thermal prestress. The analysis presented herein permits one to calculate the required quantities. This analysis is a generalization of the results presented in Reference [1] where the problem of predicting the strength and internal stresses in a ceramic uniaxially prestressed with continuous filaments was considered. In the present analysis the problem of a multilayer anisotropic structure is investigated. The stresses that are analyzed are the internal stresses in the constituents due to pretension in the reinforcement, the stresses in the constituents due to an externally applied loading and also the thermal stresses arising in the constituents when the composite is subjected to elevated temperature. The analysis is also applicable, by superposition, to various combinations of loading. In the present analysis it is assumed that the matrix is cast around pretensioned fibers, and that the end restraints, by means of which the pretension is applied, are removed after the consolidation of the matrix has taken place.

1.0 DETERMINATION OF STRAINS AND STRESSES IN PRESTRESSED CERAMIC

Assume the initial preload per reinforcement is f and there are n reinforcements per inch. Throughout the report tension stresses will be positive and compressive stresses are negative.*

*The nomenclature is given at the end of the Appendix.

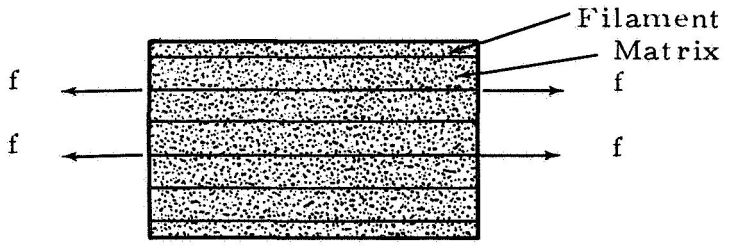

Figure 1. Applied Preload

Equation (1) is obtained from the requirement of equilibrium of internal forces, where N_c is the force in the ceramic and N_w is the force in the reinforcement. Also strain compatibility requires that the strain in the longitudinal direction, i.e., the direction of the reinforcement, must be the same for the reinforcement and ceramic as given in equation (2). The total applied preload is given by equation (3).

$$N_c^p + N_w^p = 0 \tag{1}$$

$$\epsilon_{cL} = \epsilon_{wL} = \epsilon_{LP} \tag{2}$$

$$p_w = nf \tag{3}$$

The longitudinal strains in the ceramic and reinforcement are given by equations (4) and (5), respectively.

$$\epsilon_{cL} = \frac{N_c^p}{A_c E_c} \tag{4}$$

$$\epsilon_{wL} = \frac{-\Delta p_w}{A_w E_w} \tag{5}$$

Where Δp_w represents the loss in preload in the reinforcement during compression of the ceramic. The remaining preload in the reinforcement is given by equation (6).

$$N_w^p = p_w - \Delta p_w \tag{6}$$

Solving equations (1), (4), (5) and (6) simultaneously for N_c^p yields equation (7).

$$N_c^p = \frac{-p_w}{\left(1 + \frac{A_w E_w}{A_c E_c}\right)} \tag{7}$$

The longitudinal strain is obtained by simultaneous solution of equations (4) and (7). Using equation (8) and Maxwell's reciprocity theorem the transverse strain is obtained.

$$\epsilon_{Lp} = \frac{-p_w}{A_c E_c + A_w E_w} \tag{8}$$

$$\epsilon_{Tp} = \frac{\mu_{LT}\, p_w}{A_c E_c + A_w E_w} \tag{9}$$

The stresses in the ceramic and reinforcement in the direction of the reinforcement are given by equations (10) and (11), respectively.

$$\sigma^p_{cL} = \frac{N_c^p}{A_c} \tag{10}$$

$$\sigma^p_{wL} = \frac{N_w^p}{A_w} \tag{11}$$

2.0 DETERMINATION OF COEFFICIENTS OF THERMAL EXPANSION

Strain compatibility requires that the strain in the reinforcement and ceramic must be equal, therefore if the coefficients of thermal expansion of the constituents are not equal, thermal stress is introduced and the strain compatibility equation can be written as follows:

$$\epsilon_L^T = \alpha_w \Delta T + \frac{\sigma_{wL}^T}{E_w} = \alpha_c \Delta T + \frac{\sigma_{cL}^T}{E_c} \tag{12}$$

Equilibrium requires that the sum of the forces in the ceramic and reinforcement equal zero as given by equation (13).

$$\sigma_{wL}^T A_w + \sigma_{cL}^T A_c = 0 \tag{13}$$

Solving equations (12) and (13) simultaneously for the longitudinal thermal strain yields equation (14).

$$\epsilon_L^T = \alpha_c \Delta T + \frac{(\alpha_w - \alpha_c)\,\Delta T}{\left(1 + \frac{E_c A_c}{E_w A_w}\right)} \tag{14}$$

The coefficient of thermal expansion in the direction of the reinforcement is given as follows:

$$\alpha_L = \frac{\epsilon_L^T}{\Delta T} \tag{15}$$

Substituting for the strain yields:

$$\alpha_L = \alpha_c + \frac{(\alpha_w - \alpha_c)\,E_w A_w}{E_w A_w + E_c A_c} \tag{16}$$

For composites incorporating low volume fractions of reinforcement, the approximate expression for the coefficient of thermal expansion in the transverse direction is:

$$\alpha_T = \frac{\alpha_c A_c + \alpha_w A_w}{A} \tag{17}$$

Therefore,

$$\epsilon_T^T = \alpha_c \Delta T \tag{18}$$

The strains in any direction may be obtained from the principal strains using the following relations (Ford [2]). The coordinate axes are shown in Figure 2.

$$\begin{bmatrix} \epsilon_\phi \\ \epsilon_\theta \\ \gamma_{\phi\theta} \end{bmatrix} = \begin{bmatrix} \cos^2\beta & \sin^2\beta & \cos\beta\sin\beta \\ \sin^2\beta & \cos^2\beta & -\cos\beta\sin\beta \\ -2\cos\beta\sin\beta & 2\sin\beta\cos\beta & \cos^2\beta - \sin^2\beta \end{bmatrix} \begin{bmatrix} \epsilon_L \\ \epsilon_T \\ \gamma_{LT} \end{bmatrix} \tag{19}$$

Similarly, the coefficients of thermal expansion are obtained from:

$$\begin{bmatrix} \alpha_\phi \\ \alpha_\theta \\ \alpha_{\phi\theta} \end{bmatrix} = \begin{bmatrix} \cos^2\beta & \sin^2\beta & \cos\beta\sin\beta \\ \sin^2\beta & \cos^2\beta & -\cos\beta\sin\beta \\ -2\cos\beta\sin\beta & 2\cos\beta\sin\beta & \cos^2\beta - \sin^2\beta \end{bmatrix} \begin{bmatrix} \alpha_L \\ \alpha_T \\ 0 \end{bmatrix} \tag{20}$$

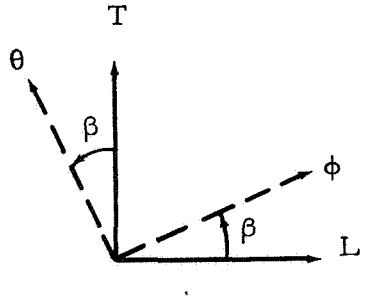

Figure 2. Coordinate Transformation

3.0 STRESS-STRAIN RELATIONS

The strains in a single layer may be expressed in terms of stresses as follows where the equations given by Chao [3] or MIL-HDBK-17 [5] have been modified to include thermal effects.

$$\begin{bmatrix} e^i_\phi \\ e^i_\theta \\ e^i_{\phi\theta} \end{bmatrix} = \begin{bmatrix} A^i_{11} & A^i_{12} & A^i_{13} \\ A^i_{21} & A^i_{22} & A^i_{23} \\ A^i_{31} & A^i_{32} & A^i_{33} \end{bmatrix} \begin{bmatrix} \sigma^i_\phi \\ \sigma^i_\theta \\ \tau^i_{\phi\theta} \end{bmatrix} \tag{21}$$

Where:

$$e^i_\phi = \epsilon_\phi - \alpha^i_\phi \Delta T$$

$$e^i_\theta = \epsilon_\theta - \alpha^i_\theta \Delta T \tag{22}$$

$$e^i_{\phi\theta} = \gamma_{\phi\theta} - \alpha^i_{\phi\theta} \Delta T$$

$$A_{11} \quad \frac{\sin^4\beta}{E_T} + \frac{\cos^4\beta}{E_L} + \left[\frac{1}{G_{LT}} - \frac{2\mu_{LT}}{E_L}\right] \sin^2\beta \cos^2\beta$$

$$A_{22} \quad \frac{\sin^4\beta}{E_L} + \frac{\cos^4\beta}{E_T} + \left[\frac{1}{G_{LT}} - \frac{2\mu_{LT}}{E_L}\right] \sin^2\beta \cos^2\beta$$

$$A_{33} \quad 4\left[\frac{1}{E_L} + \frac{1}{E_T} + \frac{2\mu_{LT}}{E_{LT}}\right] \sin^2\beta \cos^2\beta + \frac{1}{G_{LT}} \left[\cos^2\beta - \sin^2\beta\right]^2$$

$$A_{12} \quad A_{21} \quad \left[\frac{1}{E_L} + \frac{1}{E_T} - \frac{1}{G_{LT}}\right] \sin^2\beta \cos^2\beta - \frac{\mu_{LT}}{E_L} \left[\sin^4\beta + \cos^4\beta\right]$$

$$A_{13} = A_{31} = \left[\frac{1}{G_{LT}} - \frac{2\mu_{LT}}{E_L} - \frac{2}{E_L}\right]\sin\beta\cos^3\beta - \left[\frac{1}{G_{LT}} - \frac{2\mu_{LT}}{E_L} - \frac{2}{E_T}\right]\sin^3\beta\cos\beta$$

$$A_{23} = A_{32} = \left[\frac{1}{G_{LT}} - \frac{2\mu_{LT}}{E_L} - \frac{2}{E_L}\right]\sin^3\beta\cos\beta - \left[\frac{1}{G_{LT}} - \frac{2\mu_{LT}}{E_L} - \frac{2}{E_T}\right]\sin\beta\cos^3\beta$$

The stresses in a single layer may be expressed in terms of strains by equations (23) (See Chao [3] or MIL-HDBK-17 [5]).

$$\begin{bmatrix} \sigma^i_\phi \\ \sigma^i_\theta \\ \tau^i_{\phi\theta} \end{bmatrix} = \begin{bmatrix} B^i_{11} & B^i_{12} & B^i_{13} \\ B^i_{21} & B^i_{22} & B^i_{23} \\ B^i_{31} & B^i_{32} & B^i_{33} \end{bmatrix} \begin{bmatrix} e^i_\phi \\ e^i_\theta \\ e^i_{\phi\theta} \end{bmatrix} \qquad (23)$$

For any given layer i,

$$B_{11} = \frac{1}{1 - \mu_{LT}\mu_{TL}}\left\{E_L\cos^4\beta + E_T\sin^4\beta + \left(2E_L\mu_{LT} + 4G_{LT}\left[1 - \mu_{LT}\mu_{TL}\right]\right)\sin^2\beta\cos^2\beta\right\}$$

$$B_{22} = \frac{1}{1 - \mu_{LT}\mu_{TL}}\left\{E_T\cos^4\beta + E_L\sin^4\beta + \left(2E_L\mu_{TL} + 4G_{LT}\left[1 - \mu_{LT}\mu_{TL}\right]\right)\sin^2\beta\cos^2\beta\right\}$$

$$B_{33} = \frac{1}{1 - \mu_{LT}\,\mu_{TL}}\left\{\left(E_L + E_T - 2E_L\,\mu_{TL}\right)\sin^2\beta\cos^2\beta\right.$$

$$\left. + G_{LT}\left(1 - \mu_{LT}\,\mu_{TL}\right)\left(\cos^2\beta - \sin^2\beta\right)^2\right\}$$

$$B_{12} = B_{21} = \frac{1}{1 - \mu_{TL}\,\mu_{LT}}\left\{\left(E_L + E_T - 4G_{LT}\left[1 - \mu_{LT}\,\mu_{TL}\right]\right)\sin^2\beta\cos^2\beta\right.$$

$$\left. + E_L\,\mu_{TL}\left(\cos^4\beta + \sin^4\beta\right)\right\}$$

$$B_{13} = B_{31} = \frac{1}{1 - \mu_{TL}\,\mu_{LT}}\left\{\left(E_T - E_L\,\mu_{TL} - 2G_{LT}\left[1 - \mu_{LT}\,\mu_{TL}\right]\right)\sin^3\beta\cos\beta\right.$$

$$\left. - \left(E_L\left(1 - \mu_{TL}\right) - 2G_{LT}\left[1 - \mu_{TL}\,\mu_{LT}\right]\right)\sin\beta\cos^3\beta\right\}$$

$$B_{23} = B_{32} = \frac{1}{1 - \mu_{TL}\,\mu_{LT}}\left\{\left(E_T - E_L\,\mu_{TL} - 2G_{LT}\left[1 - \mu_{LT}\,\mu_{TL}\right]\right)\sin\beta\cos^3\beta\right.$$

$$\left. - \left(E_L\left[1 - \mu_{TL}\right] - 2G_{LT}\left[1 - \mu_{TL}\,\mu_{LT}\right]\right)\sin^3\beta\cos\beta\right\}$$

The equivalent external force on the total laminate can be expressed in terms of the total strain of the laminate by equation (24).

$$\begin{bmatrix} N_\phi \\ N_\theta \\ S_{\phi\theta} \end{bmatrix} = \begin{bmatrix} C_{11} & C_{12} & C_{13} \\ C_{21} & C_{22} & C_{23} \\ C_{31} & C_{32} & C_{33} \end{bmatrix} \begin{bmatrix} \epsilon_\phi \\ \epsilon_\theta \\ \gamma_{\phi\theta} \end{bmatrix} \tag{24}$$

Where:

$$N_\phi = N_\phi^T - N_\phi^p + N_\phi^F$$

$$N_\theta = N_\theta^T - N_\theta^p + N_\theta^F \tag{25}$$

$$S_{\phi\theta} = S_{\phi\theta}^T - S_{\phi\theta}^p + S_{\phi\theta}^F$$

Where N_ϕ^T, N_θ^T and $S_{\phi\theta}^T$ represent the equivalent direct and shear force required to resist strain due to thermal effects and are given by equations (26).

$$N_\phi^T = \Delta T \sum_{i=1}^{n} \left(B_{11}^i \alpha_\phi^i t_i + B_{12}^i \alpha_\theta^i t_i + B_{13}^i \alpha_{\phi\theta}^i t_i \right)$$

$$N_\theta^T = \Delta T \sum_{i=1}^{n} \left(B_{22}^i \alpha_\theta^i t_i + B_{21}^i \alpha_\phi^i t_i + B_{23}^i \alpha_{\phi\theta}^i t_i \right) \tag{26}$$

$$S_{\phi\theta}^T = \Delta T \sum_{i=1}^{n} \left(B_{33}^i \alpha_{\phi\theta}^i t_i + B_{31}^i \alpha_\phi^i t_i + B_{32}^i \alpha_\theta^i t_i \right)$$

The forces N_ϕ^p, N_θ^p and $S_{\phi\theta}^p$ represent the forces due to preloads and are given by equations (27), where the effects of Poisson's ratio is ignored.

$$N_{\phi}^{p} = \sum_{i=1}^{n} \cos^2 \beta^i p_w^i$$

$$N_{\theta}^{p} = \sum_{i=1}^{n} \sin^2 \beta^i p_w^i \tag{27}$$

$$S_{\phi\theta}^{p} = -1/2 \sum_{i=1}^{n} \sin 2\beta^i \, p_w^i$$

The forces N_{ϕ}^{F}, N_{θ}^{F} and $S_{\phi\theta}^{F}$ represent the applied external force. The coefficients C_{ij} are given by equation (28) (Ambartsumyan [4]).

$$C_{ij} = \int_{-t/2}^{t/2} B_{ij} \, dz \tag{28}$$

where t is the thickness of the multilayer laminate. The values of C_{ij} are obtained by numerically integrating through the thickness.

The resultant strains due to internal stresses are given by equations (29).

$$\begin{bmatrix} \epsilon_{\phi} \\ \epsilon_{\theta} \\ \gamma_{\phi\theta} \end{bmatrix} = \begin{bmatrix} C_{11} & C_{12} & C_{13} \\ C_{21} & C_{22} & C_{23} \\ C_{31} & C_{32} & C_{33} \end{bmatrix}^{-1} \begin{bmatrix} N_{\phi} \\ N_{\theta} \\ S_{\phi\theta} \end{bmatrix} \tag{29}$$

The stresses in each layer of the laminate are now obtained by substituting equations (29) into equations (22) and substituting the resulting equations into equations (23). The stresses in any given layer direction (x, y) can now be obtained from equations (30) (Ford [2]).

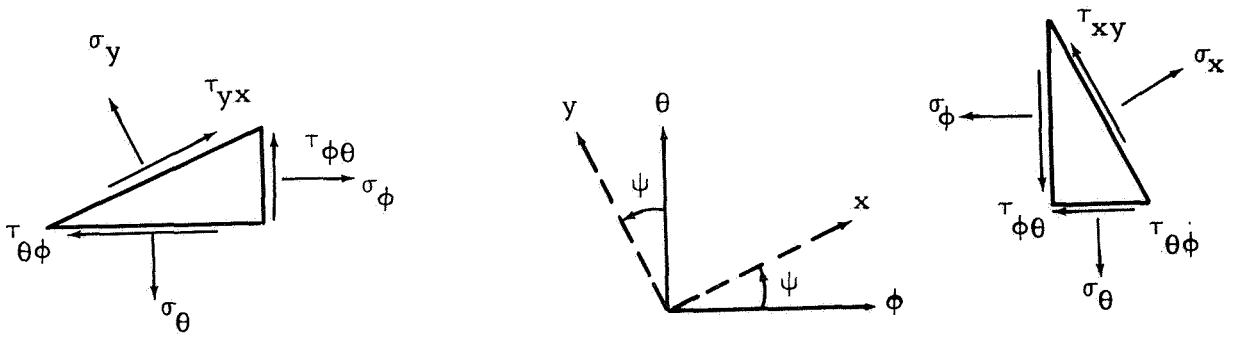

Figure 3. Stress Transformation

$$\begin{bmatrix} \sigma^i_x \\ \sigma^i_y \\ \tau^i_{xy} \end{bmatrix} = \begin{bmatrix} \cos^2\psi^i & \sin^2\psi^i & \sin 2\psi^i \\ \sin^2\psi^i & \cos^2\psi^i & -\sin 2\psi^i \\ -1/2\ \sin 2\psi^i & 1/2\ \sin 2\psi^i & \left(\cos^2\psi^i - \sin^2\psi^i\right) \end{bmatrix} \begin{bmatrix} \sigma^i_\phi \\ \sigma^i_\theta \\ \tau^i_{\phi\theta} \end{bmatrix} \tag{30}$$

The composite stresses in the filament direction, L, and transverse to the filament, T, resulting from the stresses given in equation (23) can be obtained using the transformation equations (30) where $\psi = -\alpha$. The resultant stresses in the filament direction in the filament and matrix are given by equations (31) and (32), respectively.

$$\sigma^i_{wL} = \frac{E^i_{wL}}{E^i_L} \cdot \sigma^i_L + \frac{p^i_w}{A^i_w} + \sigma^{Ti}_{wL} \tag{31}$$

$$\sigma^i_{cL} = \frac{E^i_c}{E^i_L} \cdot \sigma^i_L + \sigma^{Ti}_{cL} \tag{32}$$

The matrix shear stress in the T direction in the plane normal to the L direction is given by equation (33).

$$\tau^{i}_{cLT} = \tau^{i}_{LT} \frac{G^{i}_{c}}{G^{i}_{LT}} \tag{33}$$

The stress in the matrix transverse to the filament direction is σ^{i}_{T}.

The total matrix stresses in the ϕ and θ directions are given by equations (34) and (35), respectively. The total matrix shear stress in the θ direction in the plane normal to the ϕ direction is given by equation (36).

$$\sigma^{i}_{c\phi} = \sigma^{i}_{\phi} \frac{E^{i}_{c}}{E^{i}_{x}} + \sigma^{Ti}_{cL} \cos^{2} \beta \tag{34}$$

$$\sigma^{i}_{c\theta} = \sigma^{i}_{\theta} \frac{E^{i}_{c}}{E^{i}_{y}} + \sigma^{Ti}_{cL} \sin^{2} \beta \tag{35}$$

$$\tau^{i}_{\phi\theta c} = \tau^{i}_{\phi\theta} \frac{G^{i}_{c}}{G^{i}_{xy}} - \frac{1}{2} \sigma^{Ti}_{cL} \sin 2\beta \tag{36}$$

Failure occurs when one of the following conditions exist.

$$\sigma^{i}_{wL} > \sigma^{a}_{w}$$

$$\sigma^{i}_{cL} > \sigma^{a}_{c}$$

$$\sigma^{i}_{cT} > \sigma^{a}_{c}$$

Or the total stresses in any direction (x, y) can be found using the transformation equations and if the allowable strengths are known failure occurs when the following conditions exist.

$$\sigma_x^i > \sigma_x^a$$

$$\sigma_y^i > \sigma_y^a$$

$$\tau_{xy}^i > \tau_{xy}^a$$

REFERENCES FOR THE APPENDIX

1. Greszczuk, L. B., and Leggett, H., "Final Report — Development of a System for Prestressing Brittle Materials," Douglas Aircraft Company Report, DAC-49200, August, 1967.

2. Ford, H., and Alexander, J. M., Advanced Mechanics of Materials, John Wiley and Sons, 1963.

3. Chao, H., Equations and Computing Program for Elastic Constants and Membrane Stresses In Fiberglas Shells, Douglas Aircraft Company, Report SM-44593, September 1963.

4. Ambartsumyan, S. A., Theory of Anisotropic Shells, NASA Technical Translation, May 1964.

5. MIL-HDBK-17, Plastics for Flight Vehicles, Armed Forces Supply Center, Washington, D. C., June 1965.

NOMENCLATURE FOR THE APPENDIX

A_c	Area of matrix
A_w	Area of reinforcement
E_c	Modulus of elasticity of matrix
E_L	Modulus of elasticity of a single layer in the reinforcement direction
E_T	Modulus of elasticity of a single layer transverse to the reinforcement direction
E_w	Modulus of elasticity of reinforcement
G_{LT}	Shear modulus of a single layer in the plane in which the reinforcements lie
n	Denotes number of layers in a laminate
N	Normal force
S	Shear force
ΔT	Difference between initial and final temperatures
α_c	Coefficient of thermal expansion of matrix
α_w	Coefficient of thermal expansion of reinforcement
μ_{LT}	Poisson's ratio relating strain in the transverse direction to stress in the reinforcement direction
μ_{TL}	Poisson's ratio relating strain in the reinforcement direction to stress in the transverse direction
ϵ	Strain
σ	Stress
	Subscripts and Superscripts
a	Denotes allowable stress
c	Denotes matrix

i	Denotes i^{th} layer of laminate
L	Denotes direction of reinforcement
p	Denotes preload
T	Denotes direction transverse to reinforcement when used as subscript and denotes temperature when used as a superscript
w	Denotes reinforcement

DISTRIBUTION LIST

Addressee	No. Copies
Mr. G. P. Dix Chief, Safety Branch Space Electrical Office United States Atomic Energy Commission Washington, D. C. 20545	1
Mr. W. R. Graner Code 634C Bureau of Ships Department of the Navy Washington, D. C.	1
Dr. A. V. Illyn Research and Development Division The Babcock and Wilcox Company Alliance, Ohio 44601	1
Scientific and Technical Information Facility Attn: NASA Representative P. O. Box 33 College Park, Maryland 20740	2
Mr. Richard R. Heldenfels Code 23000, Mail Stop 108 NASA Langley Research Center Langley Station Hampton, Virginia 23365	1
Mr. Paul R. Hill Code 61000, Mail Stop 213 NASA Langley Research Center Langley Station Hampton, Virginia 23365	1
Mr. Jack B. Esgar Code 2320, Mail Stop 49-1 NASA Lewis Research Center 21000 Brookpark Road Cleveland, Ohio 44135	1
Mr. Donald L. Nored Code 9522, Mail Stop 500-209 NASA Lewis Research Center 21000 Brookpark Road Cleveland, Ohio 44135	1

Addressee	No. Copies
Library NASA Lewis Research Center 21000 Brookpark Road Cleveland, Ohio 44135	1
Mr. Norman J. Mayer, Code RV-2 NASA Headquarters Washington, D. C. 20546	2
Mr. William H. Gayman Section 353, Mail Stop 156-119 Jet Propulsion Laboratory 4800 Oak Grove Drive Pasadena, California 91103	1
Dr. Stephen W. Tsai Philco Corporation Aeronutronic Division Ford Road Newport Beach, California	1
Prof. Francis R. Shanley Department of Engineering University of California Los Angeles, California 90024	1
Mr. Ralph L. Barnett IITRI 10 West 35th Street Chicago, Illinois 60616	1
Dr. Hans U. Schuerch Astro Research Corporation P.O. Box 4128 Santa Barbara, California	1
Mr. William J. Eakins DeBell & Richardson, Inc. Hazardville, Connecticut 06036	1
Mr. James C. Withers General Technologies Corporation 708 North West Street Alexandria, Virginia	1
Mr. B. Walter Rosen General Electric Company P.O. Box 8555 Philadelphia, Pennsylvania	1

Addressee	No. Copies
Dr. Anthony M. Schwartz Harris Research Laboratories, Inc. 6220 Kansas Avenue, NE. Washington, D.C. 20011	1
Mr. J. M. Whitney Code MANC Wright-Patterson Air Force Base, Ohio 45433	1
Mr. George Peterson Code MAC Wright-Patterson Air Force Base, Ohio 45433	1
Mr. J. A. Kies Naval Research Laboratories Washington, D.C.	1
Mr. Paul Stone Materials Division RRMA Bureau of Weapons Department of the Navy Washington, D.C.	1
Dr. Julian H. Lauch Dean, School of Technology Southern Illinois University Carbondale, Illinois 62903	1
Dr. Ralph Cook Department of Ceramic Engineering 209 Ceramics Building University of Illinois Urbana, Illinois 61801	1
Mr. Robert H. Bragg Dept. 52-30, Bldg. 201 Lockheed Palo Alto Research Laboratory 3251 Hanover Street Palo Alto, California 94304	1
Mr. Robert T. Niehoft Information Specialist Defense Metals Information Center c/o Battelle Memorial Institute 505 King Avenue Columbus, Ohio 43201	1

Addressee	No. Copies
Mr. J. Jacobs Dept. 9333 Sandia Corporation Albuquerque, New Mexico 87115	1
Library NASA Langley Research Center Langley Station Hampton, Virginia 23365	1
Mr. J. B. Blumrich R-P&VE-SA NASA Marshall Space Flight Center Huntsville, Alabama 35812	1
Dr. William R. Lucas R-P&VE-DIR NASA Marshall Space Flight Center Huntsville, Alabama 35812	1
Mr. Albert L. Erickson Mail Stop N-218-1 NASA Ames Research Center Moffett Field, California 94035	1
Mr. Joseph N. Kotanchik Code ES NASA Manned Spacecraft Center Houston, Texas 77058	1
Library NASA Manned Spacecraft Center Houston, Texas 77058	1
Library NASA Goddard Space Flight Center Greenbelt, Maryland 20771	1
Mr. Edward J. Kirchman, Code 321 NASA Goddard Space Flight Center Greenbelt, Maryland 20771	1
Mr. Jack H. Ross Code ASRCN-3 Wright-Patterson Air Force Base, Ohio 45433	1
Mr. R. F. Hoener Structures Division, Code FDT Wright-Patterson Air Force Base, Ohio 45433	1

Addressee	No. Copies
Mr. Eldon E. Mathauser Code 23600 Mail Stop 188 NASA Langley Research Center Hampton, Virginia 23365	1
Mr. Edward F. Baehr Mail Stop 500-116 NASA Lewis Research Center 21000 Brookpark Road Cleveland, Ohio 44135	1
Mr. N. E. Promisel Materials Division RRMA Bureau of Weapons Department of the Navy Washington, D.C.	1